FACULTAD DE CIENCIAS

Departamento de Química Física Aplicada

"NUEVOS PROCESOS CATALÍTICOS PARA LA OBTENCIÓN DE FURFURAL"

TESIS DOCTORAL

Maria José Campos Molina

MADRID, 2015

FACULTAD DE CIENCIAS
Departamento de Química Física Aplicada

NUEVOS PROCESOS CATALÍTICOS PARA LA OBTENCIÓN DE FURFURAL

Memoria para aspirar al grado de

DOCTOR

Maria José Campos Molina

Instituto de Catálisis y Petroleoquímica (CSIC)

Madrid, 2015

Maria José Campos Molina

NUEVOS PROCESOS CATALÍTICOS PARA LA OBTENCIÓN DE FURFURAL

Memoria para aspirar al grado de
DOCTOR

Director:
Dr. D. Manuel López Granados
Investigador Científico
Instituto de Catálisis y Petroleoquímica (CSIC)

UNIVERSIDAD AUTÓNOMA DE MADRID
FACULTAD DE CIENCIAS
Dpto. Química Física Aplicada

Madrid, 2015

AGRADECIMIENTOS

Como todo en esta vida, las cosas tienen un inicio y un final y es hora de poner fin a esta etapa de mi vida. Sin embargo, no me gustaría despedirme de ella sin antes agradecer a todas aquellas personas que me han acompañado, ayudado y apoyado durante este camino, especialmente en aquellos momentos más duros en los que sólo se te ocurre huir y abandonarlo todo.

En primer lugar, quiero agradecer a mi director de tesis, Dr. Manuel López Granados, por su dedicación y entusiasmo que siempre ha mostrado para que el trabajo que realizara fuera un trabajo bien hecho. Sin duda su motivación, ilusión y su apoyo ha sido un pilar esencial durante estos cuatro años y si alguien ha conseguido sacar de mí lo mejor y que terminara realmente amando lo que hacía, ése sin duda ha sido él.

Tampoco puedo olvidar al Dr. Rafael Mariscal López, por su ayuda y contribución en la discusión de los resultados obtenidos para que fuera posible finalmente desarrollar esta tesis.

Quiero también agradecer muy especialmente al Dr. José Luis García Fierro, por la oportunidad de formar parte de su grupo de trabajo y su atención y ayuda prestada en todo momento en que lo he necesitado.

Igualmente, quiero expresar mi gratitud al Prof. Paolo Carniti y a la Profesora Antonella Gervasini de la Universidad Degli Studi de Milán por haberme permitido realizar una estancia predoctoral en su departamento y por su inestimable ayuda en la investigación allí desarrollada. Creo que mi

experiencia allí fue muy enriquecedora, tanto a nivel personal como profesional y les estaré siempre agradecidos.

Agradezco también a la Dra. Pilar Ocón Esteban de la Universidad Autónoma de Madrid por haber aceptado ser tutora de este trabajo. También a la Profesora Antonella Gervasini y al Profesor Paolo Carniti de la Universidad Degli Studi de Milán por aceptar evaluar esta tesis para permitirme optar a la mención Internacional del grado de doctor.

Quiero dar las gracias también al Ministerio de Economía y Competitividad por la financiación recibida todos estos años sin la cual no habría podido desarrollar esta Tesis Doctoral, así como las ayudas ofrecidas para realizar estancias en otros centros de investigación.

También quiero agradecer a todo el personal técnico de la unidad del SIDI de la Universidad Autónoma de Madrid por su eficiencia en las medidas realizadas y, por supuesto a todo el personal del Instituto de Catálisis y Petroleoquímica por su labor y ayuda siempre que lo he necesitado. En especial me gustaría agradecer a la dirección del ICP, el personal de secretaría y administrativo, el personal de servicios, tanto de la unidad de apoyo a la investigación (por su eficiencia y rapidez en las medidas realizadas) como de los diferentes talleres (vidrio, mecánico) y el de mantenimiento. Y por supuesto, y no por ello menos importante, a todos y cada uno de los integrantes del grupo de investigación de "*Energía y Química Sostenibles"* al que he pertenecido todos estos años y que me han mostrado tanta confianza y cariño. Muy especialmente me gustaría mostrar mi gratitud a Gema, Noelia Fernando. Gracias por vuestros buenos ratos, vuestro apoyo en los malos momentos y

vuestras risas en los buenos. Si algo bueno me llevo de todos estos años es el haberos conocido y el saber que sois y seréis personas que nunca olvidaré a pesar de la distancia y del camino.

Finalmente, aunque no por ello menos importante, me gustaría mencionar a todas aquellas personas que me han apoyado y animado en el transcurso de este tiempo: familia, pareja y amigos.

En primer lugar, a mis amigos Cristi, Héctor, Sarita, Javi e Imelda de mi Málaga querida, porque aunque desde hace un tiempo nos separan bastantes Kilómetros, sé que siempre estáis ahí y que sóis y seréis mi pequeña gran familia de mi tierra. Por supuesto, no puedo olvidarme tampoco de todos aquellos amigos que encontré durante mi paso por Madrid y que han hecho que siempre me sintiera como en casa. Alba, Adolfo, Raqueliña, Sara, Jorgiño, Juan, Pedro, Javi y Mateo: mil gracias por vuestros encuentros madrileños tan divertidos y por los buenos ratos que hemos compartido y que estoy segura que seguiremos haciendo.

A toda mi familia, y muy especialmente, a mi madre y a mis dos hermanas, Rocío y Belén, por estar siempre ahí y por animarme, apoyarme y comprenderme en los peores momentos. A ti mamá quería agradecerte que siempre me orientes en el camino de la paz, la armonía y la felicidad y que me hayas ayudado tantísimo a quererme a mí misma y a valorarme como soy. Gracias, gracias y gracias por ser mi bastón y darme todo el cariño que sólo una madre como tú sabe dar. Son muchas más las cosas que os querría agradecer y poco el espacio que tengo pero sobre todo quiero que sepáis que si de verdad he podido llegar hasta aquí ha sido por vosotras: sois el motor de mi vida y os quiero con locura.

Y a ti Manuel, un millón de gracias por todo: por tu cariño, tu apoyo y tu comprensión y sobre todo por estar tan pendiente de mí y cuidarme y mimarme tanto en todo momento. Jamás pensé que después de tantos años me llevaría de aquí un regalo tan preciado. Has despertado en mí lo que hace años pensé que no podría volver a sentir y sólo por esta razón mereció la pena todo este esfuerzo. Gracias mi amor.

A todos los que me quieren

"El mundo está en manos de aquellos que tienen el coraje de soñar y de correr el riesgo de vivir sus sueños".

Paulo Coelho

CONTENIDO

0. SUMMARY

Aiming at obtaining the European Doctorate, some of the sections of this PhD thesis manuscript have been written in English. These sections are summary section, conclusions section and all the chapters devoted to the discussion of the results. The rest of chapters are written in Spanish.

The production of non-petroleum derived energy, fuels and chemicals is nowadays a global concern, principally due to oil depletion and the increase of the price of the petroleum feedstock in the near future. Thus, the demanding of sustainable processes is increasing in chemical industry. In this context, a new concept is being developed, the biorefinery, in which biomass is treated like feedstock as in traditional refineries. However, in these processes, the type of catalyst used results of crucial importance in the sustainability of the process. Concretly, in furfural production from lignocellulosic pentose monosaccharides, acid aqueous solutions are used as catalysts. However, the election of heterogeneous catalysts are preferred in order to avoid the corrosion and negative environmental problems that are associated to homogeneous catalysis.

This thesis aims at finding a sustainable catalytic technology for furfural production. The investigation had two main research lines: (i) identifying a green solvent that allows very selective transformation of xylose to furfural and (ii) developing active, selective and reusable acid catalyst for this reaction.

The results of this thesis are presented in four chapters. The text of these chapters correspond literally to that of articles either already published in SCI journals or manuscripts that at the time the manuscript of the thesis was finished had already been submitted for publication to SCI journals.

Thus Chapter 4 covers the research for finding a green solvent for the pentoses to furfural reaction. The investigation was conducted using sulfuric acid as catalyst and ciclopentyl methyl ether (CPME) as green solvent. The processing of both aqueous solutions of xylose and aqueous dispersion of Cynara Cardunculus lignocellulosic biomass was investigated. The study was also applied to aqueous solutions containing NaCl because it has been previously reported that the presence of inorganic salts results in a considerable increase of reaction rate. The results revealed that the incorporation of CPME brings about the close to full conversion of the pentoses to furfural, inhibiting the formation of undesirable products as resins, condensation products and humins.

Chapter 5 and 6 deal with the optimization of the synthesis of SiO_2-PSSA nanocomposites as catalysts for the xylose to furfural reaction. CPME was used as co-solvent. A sol-gel methodology was used for preparing these nanohybrids and the research was devoted to investigate the effect of different variables of synthesis on the textural, chemical and catalytic properties: temperature of sol-gel formation, molar ratio between SiO_2 precursors and PSSA, molar ratio between PSSA and N containing SiO_2 precursors, type of solvent and gel aging protocol. Irrespective the methodology used, the nanocomposite catalysts deactivated mostly by leaching of polymer derived from the harsh hydrothermal reaction environment but also, very likely, by deposition of heavy organics formed during the reaction. Deactivation was very intense during the first reutilization cycles but, once the leaching is over, catalyst display a residual activity derived from the acid sites present in the polymer molecules remained after the leaching.

Taking into account the results obtained with the very demanding xylose to furfural reaction, we decided also to explore these nanocomposites as catalysts in another acid driven reaction: esterification of free fatty acids with methanol for the synthesis of biodiesel. This reaction is conducted in organic medium (methanol and oil) and at lower temperatures. In this case leaching was not relevant and catalysts kept their catalytic properties for longer number of runs.

Finally, other type of acid catalysts different from nanocomposites was tested in the xylose to furfural reaction and results presented in Chapter 7. With this purpose, the activity of solid acid catalysts based on niobium oxide (Nb_2O_5), both supported and massive (NBO) was tested. Silica-zirconia (SZ) has been utilized as support of the NbO_x active phase and two different preparation methods were selected: wet impregnation and sol-gel routes. Acidity features-activity relationships were established. Additionally the stability and durability of the catalysts both in batch and in a fix-bed continuous reactor in different reaction solvents was also investigated. This last chapter covers the research of adequate monophasic or biphasic solvent systems that decrease the deactivation of the catalysts and increase its stability and durability. It is showed that dispersing the active phase on a support and using a mixture water-solvent are two key strategies to increase stability of the niobium catalysts.

1. INTRODUCCIÓN

ÍNDICE

1.1. Contexto energético

Antes de comenzar con la introducción de la tesis, es importante enmarcarla globalmente en un contexto de sustitución de materias primas procedentes del petróleo por otras procedentes de la biomasa.

El uso del petróleo y de otras fuentes de C no renovables (carbón y gas natural) para obtener combustibles y productos químicos ha generado dos tipos de problemas: por un lado, los impactos ambientales asociados y, en especial, sus efectos en el cambio climático; por otro, la limitación de reservas y su futuro agotamiento. Las emisiones de CO_2 debido al empleo de combustibles fósiles y el uso masivo de recursos no renovables y muy limitados son dos aspectos ambientales que han preocupado a nivel internacional desde que se toma conciencia de ello. Como consecuencia de esta preocupación internacional, a lo largo de los años se han ido adoptando numerosos acuerdos y medidas tanto nacionales como internacionales con objeto de reducir el empleo masivo de combustibles fósiles, siendo el más reciente a nivel nacional el *Plan de energías renovables 2011-2020* (PER 2011-2020) elaborado por el Ministerio de Industria, Turismo y Comercio (MITyC) junto con el Instituto de Diversificación y Ahorro de la Energía (IDAE) de España, en el que se recogen datos actualizados hasta la fecha en materia de política energética y objetivos marcados para el periodo 2011-2020, así como medidas para la consecución de los mismos, entre otros [1].

Sin embargo, a pesar de todos estos incentivos y políticas medioambientales, los biocombustibles siguen sin ser económicamente competitivos. No obstante, en un futuro a medio-largo plazo parece evidente que debido a la disminución de las reservas de petróleo, los precios del crudo subirán hasta límites que hagan cada vez más favorables nuevas tecnologías. Es

aquí donde entrarían en juego el papel de las energías renovables, entendiéndose por renovables a aquellas fuentes energéticas basadas en la utilización del sol, el viento, el agua o la biomasa vegetal o animal que no utilizan, pues, como las convencionales, combustibles fósiles, sino recursos capaces de renovarse ilimitadamente. Por lo tanto, su impacto ambiental en comparación con aquellas es muy escaso, pues además de no emplear esos recursos finitos, no generan tantos problemas medioambientales relacionados con la emisión de contaminantes. Estas formas de energía renovables habían cubierto la práctica totalidad de las necesidades energéticas del hombre hasta bien entrado el siglo XIX. Sólo en los últimos cien años han sido superadas, primero por el empleo del carbón, y a partir de 1950 por el petróleo y en menor medida por el gas natural. Sin embargo, ya que en los próximos cincuenta años, los mejores recursos petrolíferos y de gas natural estarán casi totalmente agotados, encareciendo y agravando la crisis energética y ambiental, se hace necesario emprender acciones que promuevan de nuevo su utilización a través de un mayor conocimiento de su situación actual y sus perspectivas de futuro en el ámbito político y social. En este sentido, la utilización efectiva de la biomasa para producir productos químicos de alto valor añadido podría contribuir y, subsecuentemente, acelerar tal cambio hacia una economía sostenible, con bioproductos, bioenergía y biocombustibles como sus principales pilares [2].

1.2. Biorrefinería lignocelulósica: concepto, materia prima y principales procesos

Para tratar de solventar estos problemas anteriores, se ha planteado un nuevo concepto, el de la biorrefinería, que se explica a continuación. La materia

prima que se emplea en este caso no es petróleo fósil sino biomasa, y mediante su transformación permite obtener biocombustibles y productos químicos.

1.2.1 Concepto de biorrefinería

El concepto de *biorrefinería* va adquiriendo cada vez un mayor protagonismo en el área de las nuevas tecnologías sostenibles. Existen diversas definiciones de biorrefinería, siendo relevante la formulada por la IEA, asociada al tratamiento sostenible de la biomasa para la obtención de bioproductos y bioenergía. Según IEA, una *biorrefinería* se define como una instalación industrial que emplea un amplio rango de procesos tecnológicos (mecánicos, físicos y bio- o termoquímicos) capaces de separar las fuentes biológicas o materias primas renovables en sus constituyentes principales (carbohidratos, proteínas, triglicéridos, etc…). Estos constituyentes a su vez pueden ser convertidos en productos de alto valor añadido (químicos y/o materiales) y vectores energéticos (carburantes, gases energéticos, electricidad o calor), de manera que la cantidad de residuos sea mínima. Al mismo tiempo, cada componente del proceso se convierte o utiliza de forma que incremente su valor, mejorando así la sostenibilidad de la planta. Por lo tanto, la definición de biorrefinería es análoga a la de una refinería de petróleo convencional, con la diferencia de que se utiliza biomasa como materia prima en lugar de petróleo [3, 4].

El concepto de biorrefinería ha evolucionado con el paso del tiempo, ya que inicialmente solamente existían biorrefinerías muy primarias que procesaban un determinado tipo de biomasa (aceite, caña de azúcar, maíz, etc…) a un determinado tipo de producto (biodiésel, bioetanol, etc…)

(biorrefinerías de 1ª generación).Posteriormente, se comenzaron a desarrollar biorrefinerías similares a las anteriores, pero que permitían la obtención de distintos productos (biorrefinerías de 2ª generación). Actualmente, aunque se encuentran en investigación y desarrollo, la tendencia se dirige a la implantación de biorrefinerías que sean capaces de procesar diferentes tipos de biomasa con distintos procesos de transformación y que generen una variedad de productos (biorrefinerías de 3ª generación) en función de diferentes factores externos, como pueden ser la demanda o el precio. En definitiva se trata de que puedan llegar a ser equiparables a las refinerías convencionales [5]. De esta forma, lo ideal sería que desarrollar una única instalación, denominada *biorrefinería integrada*, en la que se aprovecharán todas las fracciones y subproductos de la biomasa para producir energía (electricidad, calor), biocombustibles, bioproductos químicos y biomateriales, incluso productos dirigidos a la alimentación humana y/o animal. Así, aumentará la rentabilidad del empleo de la biomasa como materia prima y se logrará una mayor flexibilidad frente a posibles fluctuaciones de mercado (tal como sucede en una refinería convencional petroquímica).

El uso de biomasa en sustitución del petróleo está generando un importante debate internacional debido a los costes de producción, viabilidad del proceso y la competencia con los alimentos. Es por esto que de todas las biorrefinerías industriales, la que tiene mayores perspectivas de éxito es la basada en lignocelulosa. Algunas de las principales fuentes de biomasa lignocelulósica son la madera, maderas de crecimiento rápido, residuos forestales y residuos de la industria del papel y la paja. Esta materia prima presenta la ventaja de su abundancia, su bajo coste y no introduce excesivas tensiones en la industria agroalimentaria como otros tipos de biomasa (maíz,

oleaginosas, caña de azúcar, cereales y remolacha azucarera) por lo que se considera potencialmente más sostenible [6]. Además desarrollar tecnologías de aprovechamiento de la lignocelulosa permitiría también integrar la biorrefinería con la producción de alimentos mediante el aprovechamiento de los residuos generados por la industria alimentaria.

1.2.2 Lignocelulosa

Los principales recursos de la biomasa de interés en biorrefinería son fundamentalmente: la *sacarosa* (azúcar común), que es un disacárido constituido por unidades de glucosa y fructosa; el *almidón* (harina), que es un polisacárido constituido por unidades de D-glucosa unidas mediante enlaces α-1,4 y α-1,6-glicosídicos; los *triglicéridos,* que son ésteres de glicerina y ácidos grasos y se extraen de las semillas oleaginosas (girasol, colza, soja, cardo, palma, etc…), aunque también están presentes en los tejidos grasos animales (sebo); los *terpenos,* formalmente oligómeros de isopreno $(C_5H_8)_n$, y finalmente la *lignocelulosa*, constituida por celulosa, hemicelulosa y lignina.

La **lignocelulosa** es un complejo macromolecular consistente principalmente de una combinación compleja de dos polisacáridos (celulosa y hemicelulosa), y de lignina, un polímero de naturaleza aromática estructuralmente formado a partir de alcoholes fenilpropilénicos (Figura 1.1) [6-8].

La **celulosa** (40-50%) es el componente principal de las paredes celulares de las plantas y, junto con la hemicelulosa, actúan como sustancias de soporte y armazón. Es un polisacárido no ramificado e insoluble en agua constituido por varios cientos de moléculas de β-glucosa $(C_6H_{10}O_5)_n$; más

específicamente, la celulosa es un β-1,4-poliacetal de celobiosaisotáctico (4-O-β-D-glucopiranosil-D-glucosa). La celulosa es el biopolímero más abundante sintetizado por la naturaleza.

Las **hemicelulosas** (también llamadas poliosas) representan aproximadamente el 25-30% en peso de la biomasa. El nombre de hemicelulosa abarca todos los polisacáridos basados en hexosanos (polímeros formados por hexosas, fundamentalmente glucosa, manosa y galactosa) y petonsanos (polímeros basados en pentosas, fundamentalmente la xilosa o arabinosa, siendo la D-xilosa el más abundante de todos ellos). La hemicelulosa se encuentran altamente sustituidos con ácido acético.

La lignocelulosa contiene además entre un 15-20% de **lignina** y otros compuestos extractables [2]. La lignina es una red polimérica amorfa, tridimensional y termoplástica basada en subunidades de fenilpropileno (monómeros aromáticos), concretamente alcoholes cumarílico, coniferílico y sinapílico, conectados mediante diferentes tipos de enlaces para formar una red final tridimensional que constituye las paredes de las células vegetales. Dependiendo del tipo de monómeros estructurales se obtienen diferentes tipos de lignina. La lignina se asocia normalmente con la celulosa y hemicelulosa para formar la lignocelulosa, y se encuentra recubriendo todo el conjunto, siendo muy inerte químicamente por lo que otorga al material una alta resistencia a los ataques químicos y/o biológicos. Esto explica que para el aprovechamiento de los azúcares contenidos en la lignocelulosa sean necesarios pretratamientos físicos-químicos que permitan romper la barrera que supone el recubrimiento de lignina alrededor de la celulosa y hemicelulosa para facilitar así el acceso a estos compuestos. Éstos se describirán más en detalle a continuación.

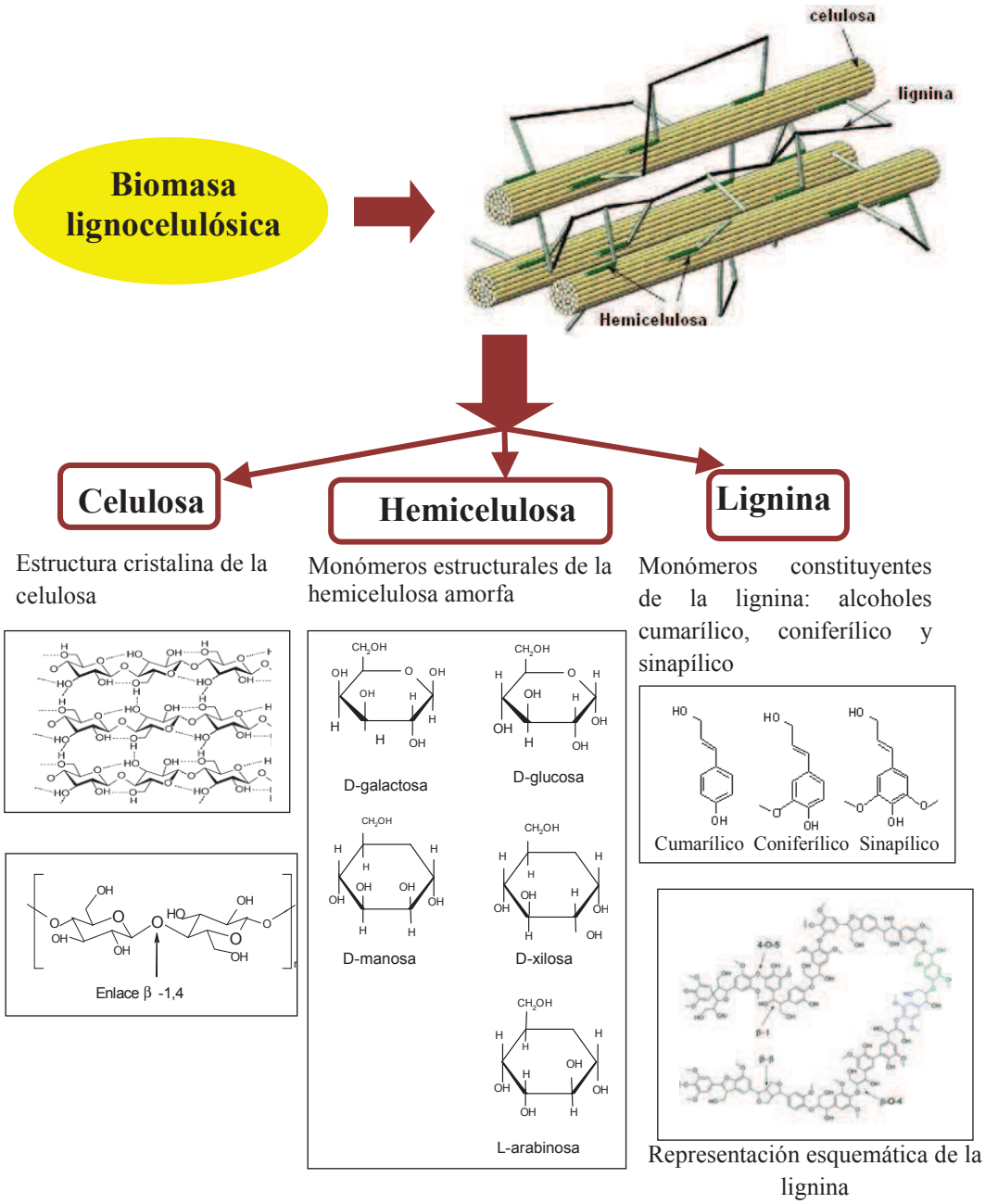

Figura 1.1. Estructura de las diferentes fracciones de la biomasa lignocelulósica (celulosa, hemicelulosa y lignina) [6, 7]

1.2.3 Procesos y productos en la biorrefinería de lignocelulosa

Un paso crucial en muchos procesos de transformación de la biomasa lignocelulósica es la etapa de pre-tratamiento que ayuda a la digestibilidad o procesado posterior del material lignocelulósico [7]. A la hora de seleccionar el tipo de pre-tratamiento se debería considerar la compatibilidad de materias primas, enzimas y organismos involucrados en el proceso global. Esta etapa no solamente es costosa sino que además tiene un impacto severo en el coste de otros procesos que le suceden tales como el manejo de las corrientes líquidas generadas, el procesado de los sólidos derivados de este pre-tratamiento o el propio tratamiento de los residuos generados. Durante varias décadas se han empleado diferentes alternativas para desarrollar pre-tratamientos de bajo coste que eliminen eficientemente el sello protector lignina y generen corrientes de azúcares derivados de la celulosa y hemicelulosa. Estos métodos incluyen procesos biológicos, mecánicos o físicos y químicos, o una combinación de los mismos [9]. Entre ellos destacan los siguientes:

- Pre-tratamientos físicos: Consiste en el procesado mecánico de la biomasa lignocelulósica para reducir su tamaño. Se emplean métodos tales como la molienda, irradiación (empleando rayos gamma, haz de electrones, radiaciones microondas, etc…) y extrusión con objeto de mejorar la hidrólisis enzimática o la biodegradabilidad de los materiales lignocelulósicos.
- Pre-tratamientos físico-químicos: Dentro de estos pre-tratamientos que combinan tanto los procesos físicos como químicos, los más importantes son: explosión con vapor (autohidrólisis) y explosión de vapor catalizada (SO_2 o CO_2), explosión de fibras por amoniaco

(AmmoniaFiberExplosion, AFEX), agua líquida caliente y pre-tratamiento líquido con microondas.

- Explosión con vapor: Es la es la técnica más ampliamente usada ya que parece ser el método más simple y efectivo. Se suele llevar a cabo en un reactor discontinuo, introduciendo la biomasa previamente pulverizada y calentándolo a alta temperatura y presión. A continuación la presión se baja bien de forma rápida para descargar el contenido del reactor en un tanque receptor de forma que se produce una explosión de vapor que rompe la lignina (*steam explosion*) o bien de forma paulatina disminuyendo la presión de vapor hasta presión atmosférica (sin explosión). Estos pretratamientos dan lugar a un material marrón oscuro que contiene hemicelulosa parcialmente hidrolizada y que se recupera fácilmente por un tratamiento de lavado. Diversos procesos industriales emplean este pretratamiento, en algunos casos con alguna variante (Masonite, Iotech, Siropulper, Stake II, Oxidación húmeda, RASH "Rapid SteamHydrolysis"). Cuando se emplea la explosión de vapor en presencia de H_2SO_4, SO_2se recupera completamente la hemicelulosa. En caso contrario, se denomina autohidrólisis y son los ácidos liberados en la descomposición de la materia de partida, tales como el ácido acético y el fórmico, los que catalizan el proceso. El papel de estos ácidos no es probablemente catalizar la solubilización de la hemicelulosa sino catalizar la hidrólisis de los oligómeros de hemicelulosa solubles. En el caso en que la explosión sea catalizada por CO_2, el proceso es similar a los dos anteriores,

pero en este caso se emplea CO_2 que forma ácido carbónico mejorando de este modo la velocidad de hidrólisis.

- Explosión de fibras por amoniaco (Ammonia Fiber Explosion, AFEX): al igual que en el caso anterior ocurre una explosión, pero en atmósfera de amoniaco, que debe ser reciclado.
- Procesos Organosolv: en este proceso se emplean disolventes orgánicos (o mezcla de estos con agua) para romper los enlaces estructurales entre la lignina y la hemicelulosa. Normalmente se emplean metanol, etanol, acetona, etilenglicol, etc. Puede añadirse ácido para mejorar el rendimiento, y es de vital importancia la recuperación del disolvente para hacer este proceso competitivo.
- Agua líquida caliente (Liquid hot water LHW): Este método se emplea para mantener el agua en estado líquido a elevadas temperaturas. De esta manera, la biomasa experimenta una cocción en agua con alta presión. Se ha demostrado que este pre-tratamiento es muy adecuado para aumentar la digestibilidad de la celulosa, la extracción de azúcares y la recuperación de las pentosas.
- Pre-tratamiento líquido con microondas: Emplea calentamiento microondas y se ha demostrado que es más efectivo que el pre-tratamiento químico de calentamiento convencional ya que acelera las reacciones durante el proceso.

- Pre-tratamientos químicos: Estos pre-tratamientos se han usado extensamente para romper la cubierta protectora alrededor de la celulosa y hacer las hemicelulosas más accesibles a la hidrólisis ya que éstas tienen una estructura amorfa con pequeña fortaleza que es fácilmente

hidrolizable por ácido o bases comparada con la estructura cristalina fuerte y rígida resistente a la hidrólisis que presenta la celulosa. Estos pre-tratamientos se pueden clasificar en tratamientos ácidos (que emplean el uso de ácidos concentrados o diluidos, siendo el más común el H_2SO_4), tratamientos alcalinos (que involucran el empleo de bases tales como hidróxido de sodio, potasio, calcio y amonio), tratamientos con disolventes (líquidos iónicos).

- Tratamientos biológicos: Estos tratamientos, que emplean microorganimos degradantes de la madera tales como hongos y bacterias, modifican la composición química y/o estructura de la biomasa lignocelulósica permitiendo la digestión enzimática más fácilmente.

Una vez que la lignocelulosa ha sido tratada mediante algunos de los procedimientos termoquímicos anteriores y se tiene un mejor acceso a los azúcares de la lignocelulosa, se procesan selectivamente mediante alguno de los siguientes medios:

- Rutas químicas: utilización de diferentes catalizadores en medio acuoso para despolimerizar los polisacáridos en los azúcares que los componen y transformarlos en productos químicos denominados plataformas químicas, a partir de los cuales se obtienen los biocombustibles y otros productos químicos de utilidad.
- Rutas biológicas (fermentación): Procesado bioquímico utilizando microorganismos y/o reacciones enzimáticas para convertir el sustrato fermentable en plataformas químicas.

Existen otras estrategias **termoquímicas** para el procesado de la biomasa lignocelulósica que no necesitan separar la lignina de los polisacáridos [8]. Estas **rutas termoquímicas** procesan la lignocelulosa a altas temperaturas y/o presiones y se obtiene un producto líquido y/o gaseoso en función de las condiciones de procesado. Estos tratamientos son:

- Gasificación. Se trata de una combustión parcial de la biomasa a altas temperaturas (>1000 K) en ausencia de oxígeno con adición de vapor.
- Pirólisis. Consiste en un tratamiento a temperaturas moderadas (650-800 K) en ausencia de oxígeno que permite la descomposición anaerobia de la biomasa.
- Licuefacción. Es un proceso alternativo a la pirolisis en el que la biomasa se mezcla con agua y catalizadores básicos (como carbonato sódico) y se lleva a cabo a temperaturas algo menores que la pirolisis (525-725 K), pero empleando presiones más elevadas (5-20 atm) y mayores tiempos de residencia.

El primero de los tratamientos, la gasificación, da lugar a gas de síntesis (mezcla de CO y H_2) que se puede emplear posteriormente en procesos hoy día comerciales y bien desarrollados que utilizan el gas de síntesis (procedente del carbón o gas natural) como materia prima para obtener diferentes productos químicos y combustibles (síntesis de Fischer-Tropsch, síntesis de metanol o síntesis de DME). La pirolisis y la licuefacción dan lugar a lo que se denomina biocrudos (o "bio-oils") que son una mezcla líquida con más de 350 compuestos orgánicos, como ácidos, aldehídos, alcoholes, azúcares, ésteres, cetonas o aromáticos. Esta mezcla puede utilizarse como fuente de productos orgánicos o como combustible, aunque se necesitan procedimientos de pretratamiento para estabilizar esta compleja mezcla de productos orgánicos.

En la Figura 1.2 se presenta de manera resumida un ejemplo de algunos de los productos potenciales que pueden obtenerse a partir de lignocelulosa y mediante las transformaciones químicas y biotecnológicas descritas hasta ahora [1]. Es una de las múltiples propuestas que existen que ejemplifica la importancia del aprovechamiento integral de la lignocelulosa en una biorrefinería.

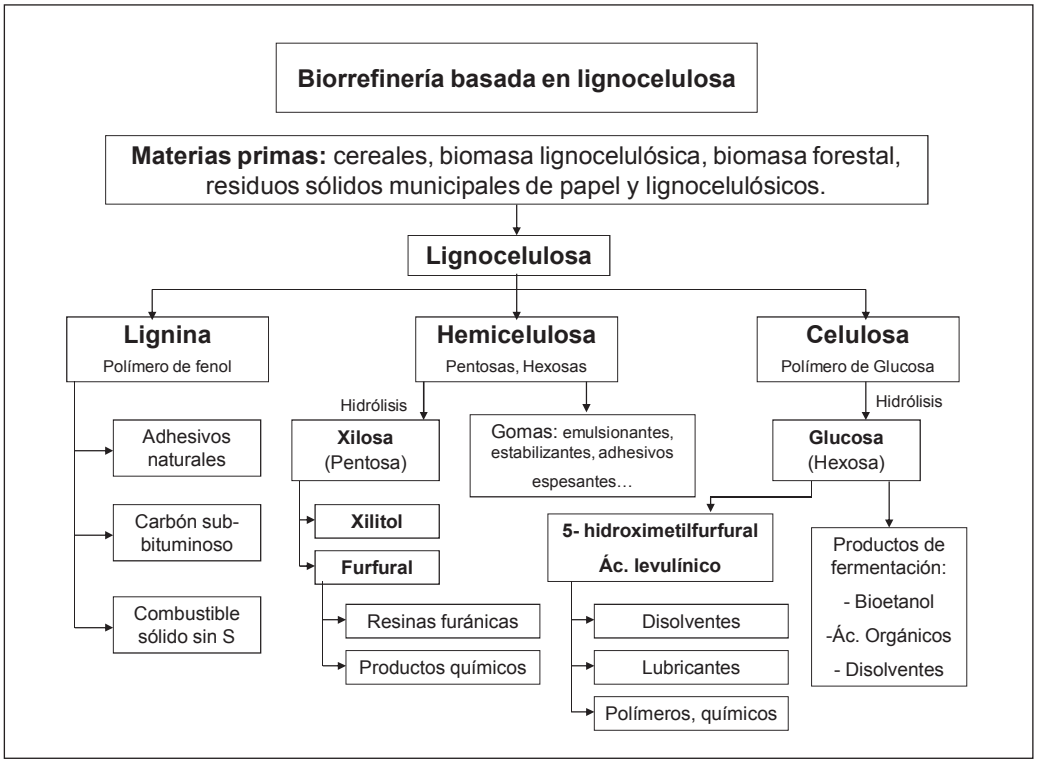

Figura 1.2. Productos de una biorrefinería basada en las transformaciones químicas de la lignocelulosa, adaptado de Kamm et al. [2]

Centrémonos en la xilosa. La xilosa es la pentosa más representativa de la hemicelulosa contenida en la lignocelulosa y es la más barata y fácilmente accesible desde la lignocelulosa. Como se observa en la Figura 1.3, los

principales derivados de la xilosa son el xilitol y el furfural. El xilitol se obtiene por hidrogenación catalítica a alta presión de la xilosa empleando catalizadores de Ni soportados o Ni Raney. Por su parte, el furfural se produce a partir de la xilosa, tal y como se ha descrito anteriormente.

Por otro lado, los dos productos más importantes que se pueden obtener por transformaciones químicas (no bioquímicas) de la celulosa son el 5-hidroximetilfurfural (HMF) y el ácido levulínico, ambos disponibles vía la deshidratación de hexosas catalizada por ácido. El 5-hidroximetilfurfural es un derivado de un azúcar versátil que puede ser considerado como una plataforma química desde la que se pueden obtener otros productos químicos de interés, los cuales pueden emplearse como disolventes, lubricantes y polímeros [10-12].

Resumiendo, el furfural y el hidroximetilfurfural (HMF) constituyen los productos más interesantes que pueden obtenerse en un biorrefinería a partir de transformaciones químicas de la lignocelulosa. Son dos compuestos que figuran en la lista revisada del "top 10+4" de productos prometedores obtenidos a partir de carbohidratos [13].

1.3. Furfuraloquímica

El furfural (2-furaldehído, $C_5H_4O_2$) es un compuesto químico que es material de partida para la síntesis industrial de diversos productos químicos, generalmente a través de la formación de alcohol furfurílico. A temperatura ambiente, el furfural es un líquido con un punto de ebullición de 161.7 ºC que es miscible con muchos disolventes exceptuando los compuestos alifáticos saturados. Recién destilado, es un líquido incoloro, estable a temperatura ambiente y bajo condiciones anaeróbicas. Es además un extractante selectivo en el refinado de aceites lubricantes, combustibles diesel y aceites vegetales.

Existen muchos otros usos del furfural, como fungicida, nematocida, adhesivo, condimento y precursor de muchos productos químicos [2]. También se usa mucho en la producción de resinas para moldes de fundición, ya que estas resinas poseen buenas propiedades de resistencia a la corrosión, térmica y de fortaleza física, entre otras [13].

Su producción fue descubierta por Döbereiner en 1821 pero solamente comenzó a ser por primera vez producto de un proceso de producción industrial después de casi un sigo cuando en 1922 Quaker Oats inició su producción industrial en USA (Cedar Rapids, Iowa) a partir de los residuos agrícolas de cáscaras de avena [13, 14].

La química del furfural se encuentra bien desarrollada y resulta ser un precursor muy versátil desde el que se pueden obtener una gran variedad variedad de productos químicos mediante reacciones químicas simples (hay descritos en bibliografía más de 50). Estos compuestos son a su vez materiales de partida para la síntesis de innumerables tipos de productos tales como disolventes, plásticos (en particular poliamidas), resinas y aditivos de combustibles con un amplio potencial en el mercado. En la Figura 1.3 se muestra un árbol familiar resumido de algunos de los productos químicos/bioquímicos técnicamente viables derivados del furfural. Algunos son productos comerciales actualmente (remarcados en rojo), como el alcohol furfurílico y el ácido furoico y otros como, por ejemplo, el furano y el tetrahidrofurano se obtuvieron desde el furfural hasta que se desarrollaron los correspondientes productos basados en fuentes fósiles [2]. Los niveles de producción actual son del orden de 300 KTons al año, siendo China el país con mayor capacidad de producción a nivel mundial (70% de la producción de furfural en el mercado). Además, cabe destacar que entre el 60-65% del furfural

sintetizado en la industria se emplea para la producción de alcohol furfurílico, el cual se emplea para la producción de resinas de fundición.

Tal como se observa en la Figura 1.3, el alcohol furfurílico y su derivado tetrahidrogenado se obtienen por hidrogenación del furfural. La furfurilamina se consigue por aminación reductiva y el ácido furoico por oxidación. Otros derivados, como las furfurildencetonas, se producen por condensación aldólica. Por último, el furfural es la llave para la producción comercial de furano por descarboxilación catalítica y tetrahidrofurano por la hidrogenación del anterior. Esto compite con la producción petroquímica a partir de la deshidratación del 1,4-butanediol, siendo una alternativa basada en la biomasa [2].

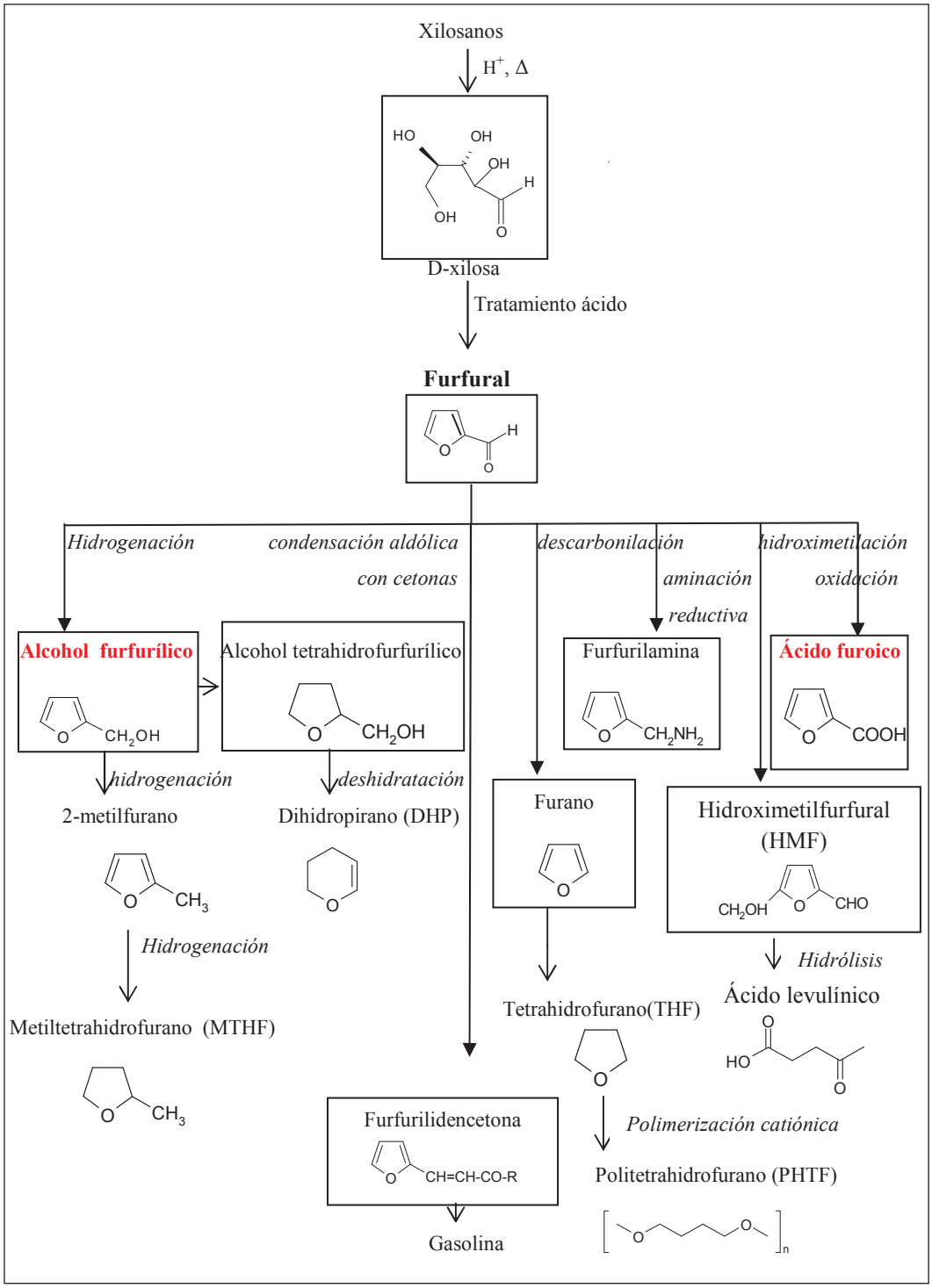

Figura 1.3. Productos químicos derivados del furfural

1.4. Selección de las reacciones estudiadas en la tesis doctoral

1.4.1 Deshidratación de xilosa a furfural

La producción de furfural se realiza hoy día directamente desde la biomasa lignocelulósica, principalmente a partir de residuos no comestibles de cosechas y de la madera. No necesita de pretratamientos previos. Los procesos de obtención implican la exposición de residuos agrícolas o forestales (cuya hemicelulosa posee un contenido en polisacáridos de xilosa, xilosanos, cercanos al 30%) a un medio acuoso ácido y temperaturas y presiones relativamente elevadas (en el rango de150 a 170ºC y hasta 10 bares de presión). Industrialmente, las materias primas más empleadas en la síntesis de furfural son: (los números dados entre paréntesis indican las producciones potenciales de furfural en cada caso) mazorca de maíz (23%), copos de avena (22%), salvado de algodón (19%), residuos de caña (17%) y copos de arroz (22%).

En esta reacción, los pentosanos (xilosanos o xilanos) presentes en la biomasa se hidrolizan a pentosa (xilosa) en una primera reacción de hidrólisis ácida y posteriormente sufren un proceso de ciclodeshidratación inducida por ácido de xilosa a furfural, según se muestra en el Esquema 1.1. Inicialmente se obtienen disoluciones acuosas de furfural que seguidamente hay que destilar y purificar para obtener furfural con una pureza superior al 98%.

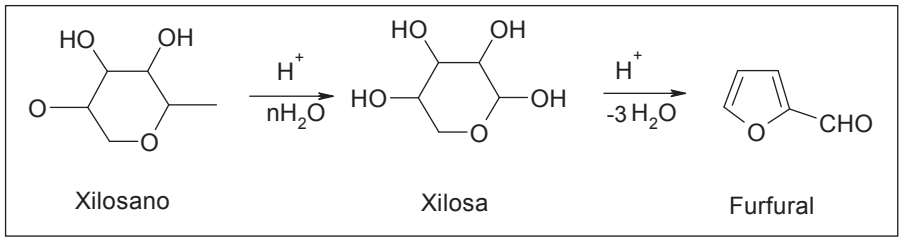

Esquema 1.1. Mecanismo de reacción simplificado de la degradación acídica de xilosano a furfural, adaptado de Dias et. al. [15]

El segundo paso de deshidratación es comparativamente más lento que la hidrólisis del xilosano. Estas reacciones secuenciales son catalizadas por ácidos por lo que es necesaria la presencia de un catalizador ácido para convertir la xilosa a furfural. No obstante, el furfural también puede formarse sin adición de catalizador mediante un mecanismo de reacción autocatalítico, ya que la descomposición térmica de la xilosa resulta en la formación de ácidos orgánicos que pueden actuar como catalizadores homogéneos en la producción de furfural [16]. Así, dependiendo de la temperatura y del tiempo de reacción, la conversión de xilosa podría alcanzar valores de hasta el 84% a 140ºC después de 24h de reacción, pero, sin embargo, las selectividades seguirían siendo bajas [15-17].

El proceso más antiguo de obtención de furfural es el proceso discontinuo de QUAKER OATS. Este proceso se concibió en 1921 y consiste en mezclar el material de partida con ácido sulfúrico en un reactor que se cierra y se calienta a presión hasta 150ºC durante 5 horas [13]. Posteriormente, el producto se recupera via stripping con vapor con el consiguiente consumo de energía, en el rango de 25-35 toneladas por tonelada de furfural producido. Además de este proceso, existen otros que generan furfural como subproducto, como los licores negros producidos en las industrias papeleras y los residuos de obtención de etanol lignocelulósico.

China (el mayor exportador a nivel mundial), adoptó este conocimiento para desarrollar su propio proceso (West pro-modified HuaxiaTechnology), mediante alimentación de mazorcas de maíz con 3-4% en peso de ácido sulfúrico. Además de estos procesos, existen otros tales como el proceso *Agrifurane, EscherWyss,Rosenlew*, *Supratherm, Stake y Suprayield*, cuyas características principales aparecen detalladas en la Tabla 1.1. Finalmente, existen otros procesos patentados, muchos con plantas de demostración: el proceso Verdernikovs, CIMV, Lignol y MTC [18].

Tabla 1.1. Resumen de los proceso industriales de obtención de furfural

	Proceso	Materia prima	Condiciones	Comentarios
1	QuakerOats*	Cáscaras de avena	426K, 5h, H_2SO_4 6wt%	50% de rendimiento teórico
2	Proceso usado en China	Restos de mazorcas de maíz	Flujo de vapor de agua 7 bar, 5h, H_2SO_4 3-4 wt%, 433K.	50% de rendimiento teórico
3	Agrifurane	Fango formado por biomasa y residuo acuoso ácido	Reactores en serie, el primero operando a 433K. H_2SO_4 1 wt%. El vapor pasa al siguiente reactor (450K).	Permite recircular el catalizador. Equipamiento costoso.
4	EscherWyss*	Alta sensibilidad al contenido de humedad	Reactor de lecho fluidizado, 443K. Hidrólisis catalítica con sulfúrico, acético y fórmico.	Bajo rendimiento por la falta de control del tiempo de residencia. Problemas de corrosión.

Tabla 1.1. Resumen de los proceso industriales de obtención de furfural (continuación)

5	Rosenlew	Bagazo	Reactor de lecho fijo con stripping con vapor. Vapor sobrecalentado a 10 bar, tiempo de residencia 120 min, 453K Reacción autocatalizada.	60% de rendimiento teórico empleando una relación vapor:furfural de 30:1.
6	Supratherm	Bagazo	473-513K por inyección de vapor de agua. Vapor rico en furfural y residuo.	Se reduce el tiempo de residencia en el reactor y se incrementa notablemente el rendimiento debido a los menores tiempos de residencia y efecto entropía.
7	Stake	Madera, bagazo	Hidrólisis a 503K seguida de una explosión de vapor de la biomasa. Reacción autocatalizada.	Rendimiento a furfural 66%
8	Suprayield	Bagazo	Temperaturas de 513K.Separación in situ de furfural por descompresión"flash". H_2SO_4 como catalizador.	Hasta 100% de recuperación del furfural por mantener la solución en ebullición. Rendimiento a furfural del 80% mediante el empleo de ácido ortofosfórico como catalizador en plantas a escala piloto.

Tabla 1.1. Resumen de los proceso industriales de obtención de furfural (continuación)

9	Verdernikovs	Residuos de celulosa	Catalizador ácido y sales añadidas.	Rendimiento a furfural 75%.
10	CIMV	Bálago, madera, bagazo	Procesado con disolventes orgánicos	Proceso reciente. Produce pulpa de papel, lignina y furfural.
11	Lignol	Licor obtenido del proceso organosolv (apartado 1.2.3)	-	Coproducción de furfural, lignina, ácido acético y etanol.
12	MTC (Multi Turbine Column)	Bálago	Se burbujea el vapor de agua a contracorriente con la alimentación. El furfural formado pasa a la fase vapor por stripping.	Rendimiento furfural 86%.

*Procesos obsoletos/Plantas cerradas

En la mayoría de los procesos industriales de obtención de furfural, tales como el empleado por Quaker Oats, se emplea normalmente el ácido sulfúrico concentrado como catalizador, aunque el ácido clorhídrico también ha sido empleado en diferentes rangos de concentraciones. El problema es que ácido sulfúrico es extremadamente corrosivo, altamente tóxico y difícil de manipular y sufre de los serios inconvenientes encontrados en los procesos catalíticos homogéneos, tales como dificultad en la separación y reciclado del ácido mineral y contaminación del producto, lo cual crea a su vez un problema de

eliminación de residuos. Esto lleva a que, actualmente, la producción comercial de furfural presente de importantes desafíos tecnológicos y problemas de tratamiento de residuos.

1.4.1.1 Mecanismos de formación de furfural

- *Mecanismo de formación de la xilosa desde xilanos:*

Los xilanos están compuestos predominantemente por xilosas en su forma cíclica unidos por enlaces glicosídicos. Zeitsch [13] sugirió un mecanismo de la hidrólisis ácida de los pentosanos (xilanos) con ácido sulfúrico diluido para dar lugar a pentosas (o xilosa) que puede ser descrito en los siguientes pasos:

1. Protonación del oxígeno del enlace glicosídico.
2. Rotura del enlace C-O generando, por un lado, un ión carbonio y, por otro lado, un grupo hidroxilo.
3. Reacción del carbocatión con el agua.
4. Formación del ión metoxi ($CO^{+}H_2$) y finalmente la liberación de un protón.

Esta secuencia de reacción se repite hasta que todos los enlaces glicosídicos desaparecen para liberar las moléculas de pentosa o xilosa, tal como se muestra en el Esquema 1.2.

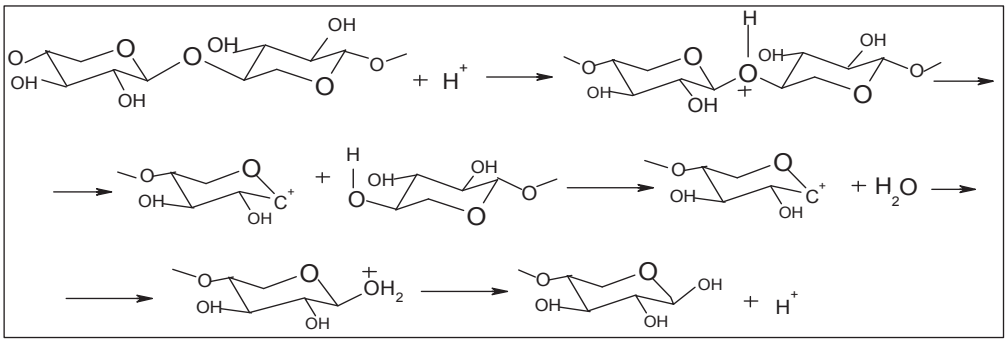

Esquema 1.2. Mecanismo de hidrólisis de xilosano a xilosa, adaptado de Zeitsch [13]

- *Mecanismo de ciclodeshidratación*

La discusión respecto a los aspectos mecanísticos de la formación de furfural podría parecer de puro interés académico. Sin embargo, un conocimiento profundo de tal mecanismo es también crucial para planear una estrategia catalítica apropiada en la industria del furfural. En cuanto al mecanismo mediante el cual transcurre la deshidratación, es bastante complejo y existe cierta controversia en torno al mismo. En la literatura se han propuesto más de un mecanismo basados en diferentes técnicas y bajo diferentes condiciones de reacción [14]. En el esquema 1.3 se engloban de manera grupal todos los mecanismos que han sido propuestos hasta el momento para la formación de furfural (siendo indicados los diferentes intermedios y compuestos finales mediante números y letras).

De acuerdo con la bibliografía, parece razonable aceptar que la reacción comienza desde la forma acíclica de las pentosas (xilosa en este caso), vía o bien la formación del intermedio 1,2-enediol (compuesto 2) y posterior deshidratación a furfural (compuesto F) [19, 20] o directamente vía la

formación de un 2,3- (α,β-)aldehído no saturado (compuesto 4) desde la xilosa (ver Esquema 1.3) [21, 22].

Según evidencia experimental, parece ser que el pH del medio juega un papel importante a la hora de decidir la ruta seguida por el mecanismo de reacción. Feather and Ahmad *et al*. [19, 20, 23] reportaron que en condiciones ácidas más bajas (pH>1), se favorece la enolización de la forma acíclica de la pentosa (xilosa) dando lugar al intermedio 1,2-enediol y subsecuente isomerización a cetopentosa (xilulosa) (compuesto 3, ver Esquema 1.3). Por tanto, bajo tales condiciones, se podrían detectar cetosas [23] y los intermedios enol tales como los compuestos 2 y 4 generalmente tautomerizarían dando lugar a los compuestos 3 y 5, respectivamente, más rápido de lo que éstos son deshidratados [19]. Esto provoca que haya más probabilidad de que se produzcan reacciones laterales no deseadas (vía 3e) que retardarían la formación de furfural. Se ha demostrado también que la enolización de la xilulosa –compuesto 3- al compuesto 3e es irreversible, llevando aparentemente a reacciones laterales [19]. No obstante, bajo tales condiciones de acidez no puede descartarse que pueda tener también lugar también un posible mecanismo de formación de furfural vía la formación directa de un 2,3-(α,β-)aldehído no saturado mediante β-eliminación de la xilosa acíclica. Este otro mecanismo supondría un camino directo para la obtención del compuesto 4 y reduciría por tanto las posibilidades de reacciones laterales de la via 3e.

Por otra parte, en condiciones de pH menores (especialmente pH<1), se ha reportado en bibliografía que tiene lugar la isomerización directa de xilosa a xilulosa, probablemente vía la formación del intermedio 1,2-enediol muy inestable que rápidamente tautomeriza a la cetopentosa, siendo ésta posteriormente deshidratada a furfural [24].

Sin embargo, aunque han sido mucho los autores que han apoyado este mecanismo desde la xilosa acíclica [19-22, 24], recientemente otros autores [25, 26] demostraron mediante cálculos mecánico-cuánticos que esta secuencia era poco probable y concluyeron que era más probable que el mecanismo de deshidratación de xilosa a furfural transcurriera partiendo de la forma cíclica de la xilosa (D-xilopiranosa), que es más abundante y mediante intermedios de reaccción también cíclicos. Según este mecanismo, el H^+ actúa sobre el oxígeno 2 (O-2) del anillo de la piranosa llevando a la formación de un intermedio 2,5-anhidroxilosa furanosa que posteriormente es deshidratado a furfural.

Por tanto, a modo de resumen, no hay aún un acuerdo común acerca del cuál es el verdadero intermedio clave de la reacción, pudiendo ser éste un cetopentosa (xilulosa), un intermedio 1,2-enediol o un aldehído 2,3- insaturado. De todas las evidencias reportadas hasta ahora, parece razonable aceptar el mecanismo propuesto por Feather y Ahmad *et al.*[19, 20] cuando los azúcares reaccionan en condiciones acídicas, aunque una isomerización directa aldosa-cetosa o una β-eliminación no pueden ser descartadas. Es difícil por tanto seleccionar un mecanismo que prevalezca frente a los otros ya que los mecanismos parecen coexistir, ganando importancia unos sobre otros de acuerdo a las diferentes condiciones de reacción y a la naturaleza del sistema disolvente/catalizador.

De la observación de todos estos mecanismos de reacción, han surgido posteriormente una serie de estrategias catalíticas. Dado que tanto la enolización de la aldosa o la isomerización directa a cetopentosa son reacciones normalmente favorecidas por condiciones básicas, la deshidratación a furfural combinada con estos dos pasos previos estaría favorecida tanto por condiciones ácidas como básicas. Por tanto, se ha estudiado en bibliografía la posibilidad de

emplear una combinación de catalizadores heterogéneos ácidos y básicos con objeto de promover la isomerización de las aldosas y posterior deshidratación a furfural, obteniéndose resultados prometedores en términos de selectividad a furfural y conversión de xilosa comparados a los resultados obtenidos cuando únicamente la catálisis homogénea o heterogénea ácida era empleada [27].

Por otra parte, también se ha reportado en bibliografía el efecto de la presencia de sales haluro y de iones de metal bi- y trivalentes en la conversión de xilosa a furfural (ver Esquema 1.3). Respecto a las sales de haluro (X^-), se ha descubierto que tienen un doble efecto positivo en la producción de furfural: por una parte producen el denominado efecto "salting-out" en los sistemas bifásicos [28, 29] y, por otro lado, aumentan directamente la velocidad de formación de furfural y su selectividad [30, 31]. Ejemplo de ello es el caso de los iones Cl^- para los que se ha demostrado que, en disoluciones acuosas ácidas, promueven la formación del intermedio 1,2 enediol que rápidamente deshidrata a furfural, incrementando así su rendimiento y selectividad [30]. En otros estudios posteriores [32], sin embargo, también se ha demostrado que su contribución a la enolización por abstracción del hidrógeno en posición α podría promover la β-eliminación hacia el compuesto intermedio 4 (ver esquema 1.3). También se han estudiado otros tipos de haluros y se ha demostrado que, en general, su efecto positivo en la formación de furfural es directamente proporcional a su carácter nucleofílico [32]. En cuanto a los cationes de metal, Gravitis *et al*. [33] también reportaron que dichos metales catalizan la reacción de carbohidratos derivados de la biomasa proporcionalmente a su potencial de ionización, mencionando un incremento en la efectividad de la reacción para los cations K^+, Na^+, Ca^{2+}, Mg^{2+} y Fe^{3+}. En este caso, existe evidencia experimental de que el mecanismo de reacción iría por la

vía de β-eliminación hacia la formación de un compuesto intermedio no saturado (4) que posteriormente deshidrata a furfural.

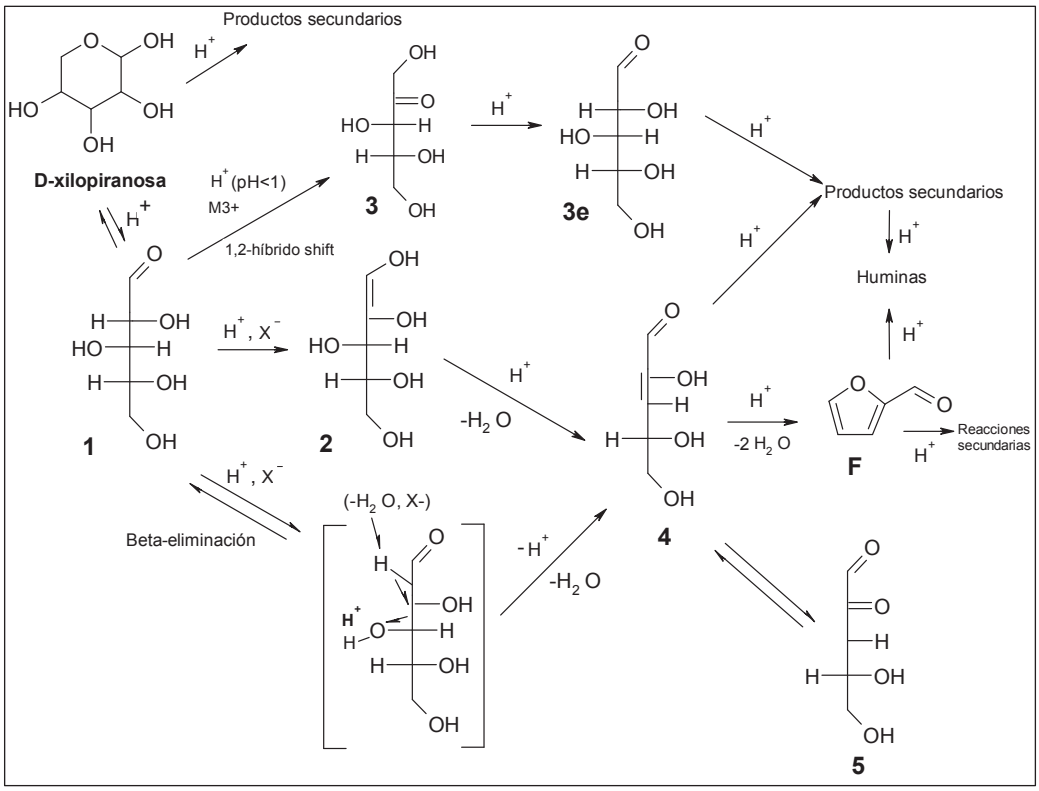

Esquema 1.3. Mecanismo plausible de deshidratación de xilosa a furfural en medio ácido. X^- indica los iones haluro y M^{3+} los cationes metálicos, respectivamente, adaptado de Danon et al. [14]

En cuanto al mecanismo en presencia de catalizadores heterogéneos ácidos, no existen aún datos en la bibliografía. Sin embargo, se ha estudiado la influencia de los tipos de centros ácidos presentes en el catalizador. Han sido varios los trabajos publicados recientemente que estudian el efecto de los centros ácidos de Lewis y de Brönsted y todo ellos están de acuerdo en que

tanto la naturaleza del centro ácido como su fortaleza determina la actividad de deshidratación de xilosa y el rendimiento a furfural. Así, por ejemplo, Weingarten *et al.* [34] demostraron que tanto los centros ácidos tipo Brönsted como Lewis catalizan tanto la reacción de deshidratación de xilosa a furfural como también las reacciones de resinificación del furfural consigo mismo para formar huminas, siendo los sitios ácidos de Lewis más activos (mayores conversiones) los que presentaban menores selectividades a furfural. Estos autores sostienen que los carbohidratos se adsorben y se activan relativamente más fácil en los sitios ácidos de Lewis que en los de Brönsted, de ahí que la conversión aumente con la concentración de centros ácidos de Lewis [35] pero también que las reacciones de condensación (reacciones no selectivas) tienen lugar preferiblemente sobre los sitios ácidos de Lewis. Por esta razón este tipo de catalizadores presentan una mayor conversión de xilosa, pero una menor selectividad a furfural.

En cuanto al mecanismo por el que transcurre la reacción en presencia de estos centros, Doiseau *et al.* han publicado recientemente que la reacción de deshidratación de xilosa a furfural puede ocurrir a través de dos rutas diferentes [36]: o directamente por deshidratación de xilosa a furfural en un único paso, lo cual demanda mayor energía (Ruta 1) o en dos pasos consecutivos: primero isomerización de xilosa a xilulosa y posteriormente deshidratación de ésta última a furfural, tal como como se muestra en el Esquema 1.4. Según estos autores, los sitios ácidos de Brönsted pueden catalizar directamente la deshidratación de xilosa a furfural mientras que los centros ácidos de Lewis catalizan la isomerización xilosa-xilulosa y hacen que la sucesiva deshidratación de xilulosa a furfural catalizada por centros Brönsted ocurra más rápido a temperaturas más bajas.

Por tanto, puede existir un cierto efecto sinérgico entre ambos tipos de centros ácidos de manera que una combinación adecuada de centros ácidos tipo Lewis y Brönsted permitiría mejorar el rendimiento a furfural de este proceso catalítico [27, 37-39]. Sin embargo, tanto la concentración relativa de ambos tipos de centros ácidos como la temperatura determinan la ruta seguida en la reacción de deshidratación de xilosa y por lo tanto su eficiencia.

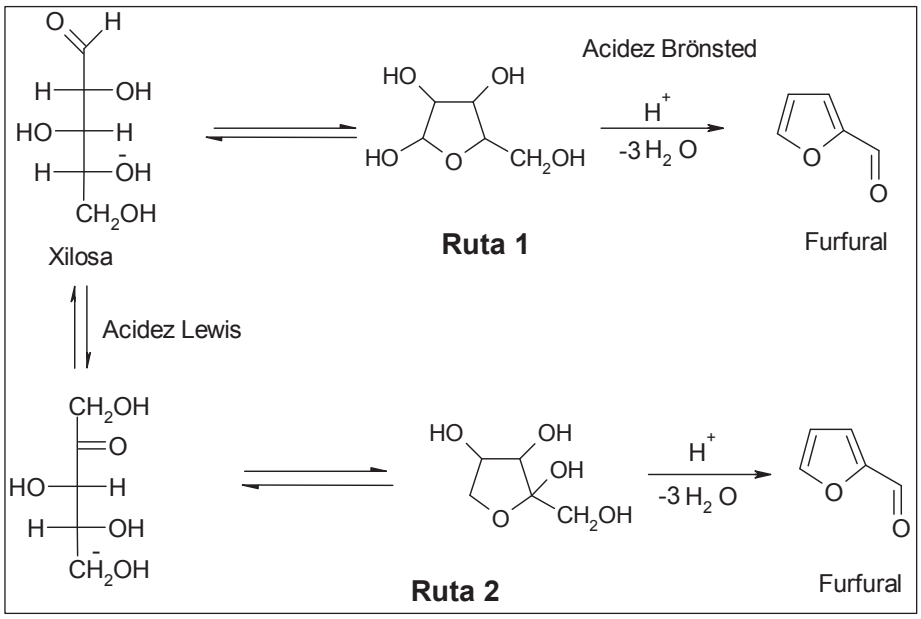

Esquema 1.4. Influencia del tipo de centros ácidos en la deshidratación de xilosa a furfural, adaptado de Aude-Claire Doiseau et al. [36]

1.4.1.2 Reacciones secundarias o laterales en la obtención de furfural

Durante la reacción de deshidratación de xilosa a furfural, además de la reacción principal, tienen lugar otras reacciones secundarias o laterales que son las responsables de las pérdidas en el rendimiento a furfural. Estas reacciones son las de condensación entre el furfural e intermedios de reacción para dar hemiacetales y acetales [13, 40], la de fragmentación de la xilosa (acíclica) para dar otros compuestos tales como acetaldehído, formaldehido, gliceraldehído, piruvaldehído, glicoaldehído, acetol y ácido láctico [16] y las de resinificación del furfural consigo mismo formando oligómeros o polímeros (Esquema 1.5). La disminución del rendimiento a furfural como consecuencia de las reacciones de condensación suele ser mucho mayor que el asociado a las reacciones de resinificación. Estas dos reacciones se evitan en gran medida cuando se incrementa la temperatura, debido al denominado "efecto entropía" que nos dice que la formación de moléculas más grandes se inhibe cuando la temperatura aumenta ya que el aumento de temperatura favorece la desintegración de las mismas [13].Cuando estas reacciones tienen lugar se generan además moléculas de mayor tamaño que son precursoras de la formación de coque sobre la superficie del catalizador. La presencia deproductos sólidos, denominados generalmente *huminas,* es una señal inequívoca de la existencia de reacciones secundarias.

La química de formación de huminas no es aún muy conocida. Algunos autores afirman que estos sólidos están formados principalmente por oligómeros de furfural [41-43], Sin embargo, algunos trabajos publicados con hidroximetilfurfural (HMF) recientemente [44, 45] han demostrado que también podrían formarse huminas por polimerización de azúcares con los productos furánicos y se ha propuesto un mecanismo para su formación como

el que se muestra en el Esquema 1.6 [45]. Por otra parte, se ha observado que cuando la temperatura de reacción es alta se forman menos sólidos. Por tanto, las condiciones de reacción deberían optimizarse para alcanzar el máximo rendimiento a furfural con mínima producción de sólidos.

También se pueden formar otros productos secundarios de interés: el diacetil (~1%) y la 2,3-pentanodiona (~0.1%) que se emplean como aditivos de margarina y en helados y pastelería, respectivamente. Otros como el ácido acético y el ácido fórmico pueden recuperarse como subproductos o eliminarse de las aguas residuales por fermentación a metano (y CO_2).

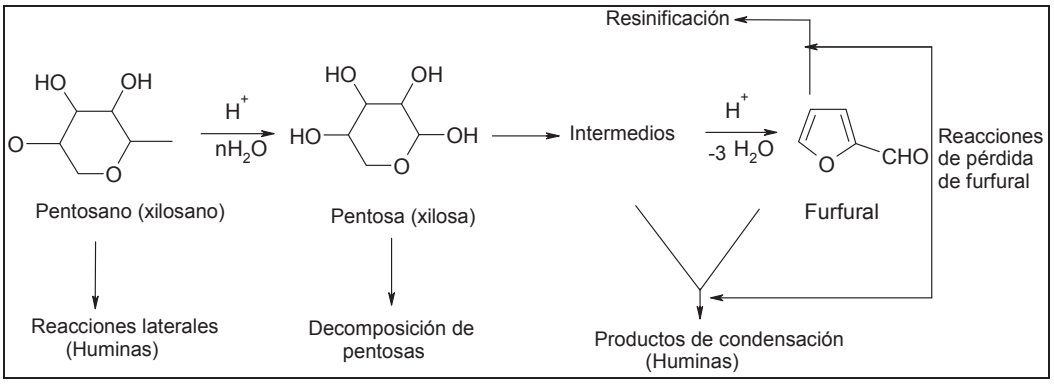

Esquema 1.5. Posibles reacciones secundarias o laterales en el proceso de conversión de xilosa a furfural

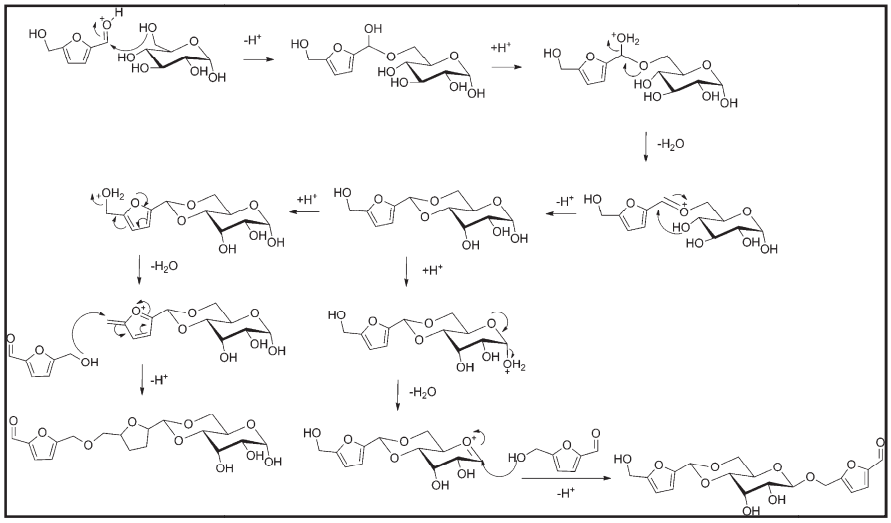

Esquema 1.6. Posible mecanismo de reacción para la formación de huminas, adaptado de Dee et al. [45]

A nivel industrial, como ya se ha visto, existen nuevos procesos para evitar estas reacciones secundarias. Ninguno de ellos se ha llevado a cabo más allá de a escala de planta piloto. Estos procesos son el "*proceso SUPRATHERM*", el "*proceso STAKE*" y el "*proceso SUPRAYIELD*" previamente mencionados y que, a continuación, pasaremos a describir con mayor detalle [13].

Tanto el proceso *SUPRATHERM* como el proceso *STAKE* emplean temperaturas elevadas comprendidas entre 200 y 240ºC mediante inyección de una corriente de vapor a alta presión. De esta manera, se reducen enormemente las pérdidas de furfural por resinificación y condensación ya que a elevadas temperaturas la velocidad de formación de furfural es mayor con respecto a la de las reacciones de resinificación y condensación por el efecto entrópico mencionado anteriormente.

En contraste, el proceso *SUPRAYIELD* apunta a conseguir el 100% de la producción de furfural tal y como se consigue en el proceso analítico de determinación de pentosas. Con este proceso analítico que se describirá a continuación se consigue transformar las pentosas con un rendimiento del 100%. El proceso básicamente consiste en mantener un medio de reacción en un estado continuo de ebullición de manera que el furfural generado en la fase líquida es, al instante, transferido a la fase vapor. Esto no puede lograrse por inyección de vapor ya que, a cualquier presión, el vapor que condensa es termodinámicamente incapaz de llevar una solución acuosa de pentosa a ebullición, debido a la elevación del punto de ebullición provocada por la pentosa. Por tanto, el calentamiento y la extracción con vapor lleva a un medio de reacción sin ebullición que deja a cualquier furfural generado disuelto temporalmente en la fase líquida donde puede sufrir reacciones de pérdida de furfural consigo mismo o con otros intermedios de reacción. En el proceso Suprayield la ebullición del medio de reacción se lleva a cabo de un modo diferente que consiste en trabajar a presión reducida para que la fase líquida esté continuamente hirviendo a las temperaturas de reacción.

Aparte de estos procesos, otra posibilidad para mejorar el rendimiento a furfural que se ha propuesto en la bibliografía es el empleo de otros disolventes orgánicos o mezclas acuosas con disolventes orgánicos y agua que podrían minimizar dichas reacciones secundarias de pérdida de furfural. Se utilizan disolventes que tengan una mayor afinidad por el furfural que por el agua, de manera que cuando se forma el furfural en el medio acuoso, que es donde está el catalizador, se transfiere mayoritariamente a la fase orgánica donde no puede transformarse por no haber catalizador.

De esta forma, se han utilizado mezclas de agua y disolventes orgánicos como tolueno, dimetilsulfóxido (DMSO) [15, 46], isobutilmetilcetona (IBMK),

diclorometano o disolventes considerados como sostenibles desde el punto de vista medioambiental tales como el ciclopentilmetiléter (CPME) [15, 47-54].

El problema de utilizar un co-disolvente es que requiere una etapa adicional para la separación del furfural del disolvente por destilación, con su correspondiente consumo energético. Por este motivo, se han desarrollado otras alternativas como la extracción de furfural mediante el empleo de líquidos iónicos [24, 55, 56], mediante el uso de CO_2 supercrítico [57] o el *stripping* con N_2 [58, 59].

Recientemente también se ha estudiado la adición de sales inorgánicas al medio de reacción para aumentar la formación de furfural. Marcotullio *et al.* probaron el HCl como catalizador junto con la adición de sales como NaCl y $FeCl_3$ al medio de reacción, observando que la selectividad a furfural se incrementaba hasta un 90% a 200ºC debido a que, según estos autores, los iones Cl^- promovían la formación del intermedio 1,2-enediol desde la forma acíclica de la xilosa [30, 32]. También se ha observado un aumento similar en los sistemas catalizados por H_2SO_4 en agua/tolueno [31]. Gravitis *et al.* [33] han propuesto que la velocidad de la reacción de deshidratación de carbohidratos es proporcional al potencial de ionización de los cationes metálicos. El efecto que ejerce la presencia de la sal no está aún claro, aunque algunos trabajos apuntan a un efecto salino de mejora del coeficiente de reparto del furfural en presencia de un co-disolvente orgánico.

1.4.1.3 Catalizadores sólidos empleados

Tal y como hemos visto anteriormente, todos los procesos tradicionales de producción de furfural están basados en catálisis ácida homogénea empleando como catalizador generalmente el ácido sulfúrico. Sin embargo, se sabe bien que estos catalizadores ácidos homogéneos son corrosivos y presentan riesgos medioambientales muy severos. Por tanto, la búsqueda de catalizadores heterogéneos resulta de vital importancia por ser más seguros y medioambientalmente más sostenibles de acuerdo con los principios de la química verde. De hecho, el número de patentes que emplean la catálisis heterogénea en la deshidratación de los monosacáridos ha crecido vertiginosamente durante los últimos años lo que ha hecho que la búsqueda de catalizadores heterogéneos adecuados para estos procesos sea un aspecto de especial relevancia [60].

Tal como se ha mencionado, la deshidratación de monosacáridos es catalizada por ácidos y en bibliografía se han estudiado una enorme variedad de catalizadores heterogéneos [60, 61]. Éstos incluyen, por una parte, **catalizadores ácidos microporosos**, de entre los cuales los dos más comúnmente estudiados han sido las zeolitas (aluminosilicatos) [15, 34, 48, 55, 62-71] y los silicoaluminofosfatos tipo zeolitas (SAPOs) [47]. Por otro lado, entre los **materiales mesoporosos**, las silicas mesoporosas [63, 64, 72-75] y las zirconias persulfatadas y sulfatadas (MSZ) también han sido testadas en la reacción de deshidratación de xilosa [17, 76]. Entre los catalizadores ácidos funcionalizados con grupos sulfónicos, Lam *at al*. recientemente publicaron el uso de catalizadores de Nafion reutilizables para producir furfurfal desde xilosa en DMSO [46]. Por su parte, los **óxidos metálicos** representan otro grupo importante de catalizadores ácidos, ampliamente probados en esta reacción [11, 34, 38, 47, 51, 59, 65, 77-82]. Otros catalizadores empleados incluyen,

heteropoliácidos [52] resinas de intercambio iónico [27, 38, 58, 65, 83, 84], nanotubos [50] y fosfatos sólidos metálicos, tales como las especies solubles de pirofosfatos de vanadilo reportados recientemente por Sádaba et at. [34, 39, 53]. Además, se han estudiado en bibliografía una enorme variedad de catalizadores basados en niobio tales como niobosilicatos microporosos (AM-11) y mesoporosos (MCM-41) [51] y niobatos y titanoniobatos [50].

Finalmente, algunos estudios bibliográficos han reportado el empleo de **materiales no porosos heterogéneos**. Entre ellos, el $CrCl_3$, un ácido de Lewis, ha sido empleado como catalizador en combinación con el HCl como catalizador ácido de Brönsted en la reacción de deshidratación de xilosa a furfural [37].

Considerando el empleo de soportes, hay que tener en cuenta que ni los soportes de alúmina ni de sílica presentan actividad en la deshidratación de monosacáridos. Por otra parte, los materiales básicos no son activos en la reacción de deshidratación tampoco pero, sin embargo, pueden catalizar la isomerización de monosacáridos. En la Tabla 1.2 se recogen de manera resumida una recopilación de algunos de los catalizadores sólidos ácidos empleados en la deshidratación de xilosa a furfural así como las condiciones de reacción empleadas y los rendimientos a furfural obtenidos.

Tabla 1.2. Resumen de los rendimientos a furfural obtenidos con diferentes catalizadores sólidos ácidos en la reacción de deshidratación de xilosa, adaptada de Agirrezabal et al. [61]

Materia prima	Tª (ºC)	Disolvente	Catalizador	Rendimiento furfural (%)	Ref.
Xilosa	170	Agua/Tolueno	H-Faujasita Si/Al=15	42	[48]
Xilosa	260	Agua/Tolueno	H_3PO_4-Mordenita 13	98	[85]
Xilosa	140	Agua/Tolueno	H-Beta	25	[70]
Xilosa	140	DMSO	H-mordenita	24	
Xilosa	110	Agua	Sn-Beta + HCl	14	[71]
		Agua	Sn-Beta + Amberlita 70	10	
Xilosa	200	Agua	H-ZSM-5	46	[62]
Xilosa	170	Agua/Tolueno	H-Nu Si/Al=29 deslaminada	47	[69]
Xilosa	170	Agua/Tolueno	Silicoaluminofosfato 11b	65	[47]
Hemicelulosa (madera de coníferas)	170	Agua	HSUY, Si/Al=15	12	[86]
Xilosa/arabinosa	100	DMF	Nafion SAC-13	10	[27]
Xilosa	140	Agua/Tolueno	MCM-41 –SO_3H	76	[15]
Xilosa	160	Agua/Tolueno	Silicato de Nb H-AM11	46	[51]
Xilosa	160	Agua/Tolueno	Ácido 12-tungtofosfórico	44	[74]
		Agua/Tolueno	PW-MCM-41	51	
Xilosa	160	Agua/Tolueno	ZrO_2 MCM-41 sulfatada	50	[17]
Xilosa	190	Agua	MSHS-SO_3H	43	[72]
Xilosa	170	NaCl+agua/1-butanol	MCM-41 (comercial)	48	[55]
Xilosa	160	Agua/Tolueno	SBA-15-SO_3H (co-condensación)	68	[63]
Xilosa	160	Agua/Tolueno	SO_4^{2-}/ZrO_2-Al_2O_3/SBA15	53	[87]

Tabla 1.2. Resumen de los rendimientos a furfural obtenidos con diferentes catalizadores sólidos ácidos en la reacción de deshidratación de xilosa (Continuación) [61]

Xilosa	170	Agua/Tolueno	SBA-propilsulfónico	82	[64]
Xilosa	160	Agua/Tolueno	SBA-arensulfónico	86	[75]
Xilosa	170	Agua/Tolueno	Beta sobre sílica TUD	74	[68]
Xilosa	170	Agua/Tolueno	Al sobre TUD	60	[88]
Xilosa	150	DMSO	Nafion 117	60	[46]
Xilosa	160	Agua/Tolueno	Exf.HTiNbO$_5$-MgO	55	[50]
Xilosa	100	Agua/Tolueno	SO_4^{2-}/SnO_2	27	[89]
Xilosa	170	Agua/n-butanol	SO_4^{2-}/ZrO_2-TiO_2	48	[90]
Xilosa	160	Agua/Tolueno	MgF2-71wt%	74	-
Xilosa	160	Agua/Tolueno	MgF2-71wt% perfluorosulfónico	78	[91]
Xilosa	125	Vapor de destilación	H2SO4 + TiO2	53	[92]
Xilosa	250	Agua	SO42-/ZrO2-773	29	[93]
		Agua		8	
Xilosa	300	Agua	ZrO_2-TiO_2	10	[94] 100
Xilosa	170	Agua/Tolueno	Zr-W-Al mesoporoso	50	[81]
Xilosa	180	Agua-Sc-CO_2	TiO_2 sulfatado	60	[57]
Xilosa	175	Agua	Nb_2O_5/Cabosil	78	[38]
Xilosa	170	Agua/Tolueno	Óxido de TiO_2-grafeno	68	[95]

1.4.1.4 Catalizadores utilizados en esta tesis

1.4.1.4.1 Nanocomposites SiO2-APES

Tal como hemos visto en el apartado anterior, se requieren catalizadores ácidos para llevar a cabo la reacción de deshidratación de xilosa a furfural. El poliestireno es un excelente material de partida para la síntesis de catalizadores con fuertes centros ácidos. En este apartado explicaremos por qué. En primer lugar porque este compuesto puede ser sulfonado mediante diferentes métodos y agentes de sulfonación dando como resultado un polímero en el cual una importante fracción de unidades monoméricas (si no todas) se encuentran sulfonadas en la posición para del anillo aromático. Los productos finales resultantes pueden estar o bien en su forma protonada, ácido poliestirensulfónico (APES) (Esquema 1.7) o intercambiado por un catión metálico (forma sulfonada metálica) [96]. Por lo tanto, si el APES fuera un catalizador activo y reutilizable, una de las principales ventajas con implicaciones medioambientales es que se podrían revalorizar residuos plásticos de naturaleza poliestirénica [97-100].

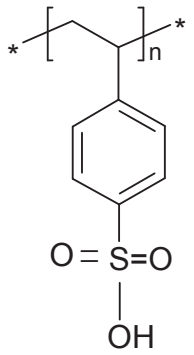

Esquema 1.7. Estructura del ácido poliestirensulfónico (APES)

Recientemente en el grupo de investigación en el que he realizado mi tesis doctoral se ha demostrado que se puede emplear este polímero soluble en diversas reacciones que requieren de centros ácidos y que tienen lugar en medio acuoso o en disolventes relativamente muy polares [101]. El buen comportamiento de este catalizador puede explicarse por el hecho de que, debido a su elevado grado de sulfonación, este polímero es soluble en disolventes polares, lo que resulta muy ventajoso con respecto a los catalizadores sólidos ya que se evitan problemas de transferencia de materia e impedimentos estéricos y además se facilita la reacción puesto que el catalizador y los reactivos permanecen en la misma fase. Sin embargo, el problema ocurre a la hora de reutilizar este catalizador, ya que se requiere de la ultrafiltración para poder separar el catalizador del medio de reacción [102]. Este proceso es, en principio, más complicado y costoso energéticamente que cualquier técnica de separación convencional (filtrado o centrifugación) por lo que se ha propuesto "heterogeneizar" este polielectrolito, es decir, anclar el polímero sobre un sólido de manera que el nanocomposite sólido así formado pueda separarse más fácilmente del medio de reacción mediante filtración convencional o centrifugación [103].

Los materiales composites orgánicos/inorgánicos son conocidos desde hace mucho tiempo. Cuando las fases inorgánicas en estos materiales son del orden de nanoescala, estos materiales se denominan comúnmente nanocomposites. En bibliografía se han descrito numerosos sólidos inorgánicos para soportar diferentes tipos de materiales orgánicos poliméricos. Entre ellos, se encuentran los nanotubos, silicatos laminados (e.g., montmorillonita, saponite), nanopartículas de metales (e.g., Au, Ag), óxidos de metal (e.g., TiO_2, SiO_2, Al_2O_3), semiconductores (e.g., PbS, CdS), entre otros [104]. De todos ellos, la sílice SiO_2 es el más importante y el más empleado normalmente ya

que es un óxido cuya preparación y caracterización están bien descritas y además es inerte. De hecho, entre los numerosos nanocomposites orgánicos/inorgánicos estudiados, los composites polímero/sílica son los más frecuentes en bibliografía.

Existen diferentes metodologías para preparar estos nanocomposites. Así, el componente orgánico puede ser introducido en la matriz inorgánica como: (i) un precursor, el cual a su vez puede ser un monómero o un oligómero; (ii) un polímero lineal ya formado (fundido, en solución o en forma de emulsión) y (iii) una red polimérica enlazada, ya sea bien físicamente (polímero lineal semicristalino) o químicamente (elastómeros). Por su parte, el componente inorgánico puede ser introducido como: (i) un precursor (e.g. tetraetilortosilicato,TEOS) ó (ii) nanopartículas ya formadas. En consecuencia se puede decir, de modo general, que existen 5 métodos distintos de preparación de los nanocomposites polímero/sílica, de acuerdo a los materiales de partida que se empleen y las técnicas usadas: mezcla física ("*blending*"), procesos sol-gel, polimerización in situ, formación de nancomposites coloidales y métodos de autoensamblaje [104, 105]. El método de "*blending*" consiste simplemente en mezclar físicamente las nanopartículas de sílica en el polímero. De entre todos los métodos descritos en bibliografía sólo aquellos que producen una interacción fuerte polímero-sílica, bien sea mediante enlaces covalentes o interacciones electrostáticas, son de interés para la aplicación en reacciones catalíticas ya que si se quiere evitar la lixiviación del polímero se necesita un anclaje o fijación más fuerte entre polímero y la sílica. Por lo tanto, la metodología de mezcla física no es de relevancia práctica para nuestro propósito ya que las interacciones son de tipo físico y muy débiles. El proceso sol-gel se lleva a cabo en presencia de un polímero orgánico ya formado y un precursor inorgánico o simultáneamente por polimerización conjunta de los

monómeros respectivos. La polimerización in-situ consiste en polimerizar el monómero sobre la superficie de un sólido inorgánico previamente formado. Los nanocomposites coloidales representan una nueva categoría de nanocomposites con propiedades remarcables debido a la combinación y estructuración de sus componentes orgánicos e inorgánicos dentro de las nanopartículas y son materiales que pueden dividirse en sistemas con corazón de polímero y armazón inorgánico o vicerversa (lo que se conoce como sistemas "core-shell"). Finalmente, los métodos de autoensamblaje dan lugar a nanocomposites compuestos de componentes orgánicos e inorgánicos a nivel de nanoescala que son espontáneamente organizados mediante interacciones no covalentes [104, 105].

Todas estas metodologías han recibido especial atención en los últimos años y se han empleado en una enorme variedad de aplicaciones. Sin embargo, para el propósito de esta Tesis doctoral que es poder anclar macromoléculas de APES ya formadas como forma de revalorización de los residuos poliestirénicos, la metodología de polimerización in-situ no es válida ya que el polímero se forma a partir de sus monómeros. En el grupo en el que he realizado la tesis se ha utilizado una variante del proceso descrito en bibliografía para la síntesis de nanocomposites APES/sílica en el que el polímero es anclado a la sílica por medio de interacciones iónicas [106]. Previamente se había demostrado que esta metodología de preparación era interesante ya que, aunque durante el primer ciclo de reacción el nanocomposite perdía parte del polímero utilizado inicialmente en la síntesis, una parte permanecía y el nanocomposite podía reutilizarse durnate varios ciclos [54].Los nanocomposites SiO_2-APES sintetizados en este trabajo se han preparado siguiendo esta metodología que aparecerá descrita con más detalle en el apartado de resultados correspondiente de esta Tesis doctoral (Capítulo 2 y 3).

1.4.1.4.2 El óxido de niobio como catalizador

El estado de oxidación más común es +5, y por lo tanto es habitual encontrarlocomo *óxido de niobio*(V). El pentóxido de niobio (Nb_2O_5) es un sólido blanco,estable al aire e insoluble; únicamente el HF o mezclas de HF y HNO_3 puedendisolverlo. Su estructura es extremadamente complicada y presentapolimorfismo.

El Nb_2O_5 está formado por octaedros NbO_6 conectados por aristas yvértices. De forma ocasional, también se encuentran estructuras NbO_7 y NbO_8en fases de óxidos de niobio. De igual forma, el ácido nióbico ($Nb_2O_5 \cdot xH_2O$),que es un óxido polimérico insoluble que precipita con una cantidad indeterminada de agua, presenta propiedades similares al Nb_2O_5 amorfo,donde existen octaedros NbO_6 ligeramente distorsionados, NbO_7 y NbO_8; además, posee una pequeña cantidad de octaedros NbO_6 altamentedistorsionados. El catión Nb(V) es voluminoso y tiene dificultades para ubicarse en un hueco tetraédrico formado por aniones óxido, por lo que muy pocos compuestos presentan una estructura NbO_4 con coordinación tetraédrica (solamente compuestos tales como YNbO4, YbNbO4, LaNbO4, andSmNbO4) [107, 108]. Además, los octaedros altamente distorsionados NbO_6 poseen enlaces Nb=O que se asocian con centros ácidos de Lewis. Por el contrario, los octaedros NbO_6 ligeramente distorsionados, así como los grupos NbO_7 y NbO_8,únicamente tienen enlaces Nb-O que pueden generar centros ácidos de tipo Brönsted [109]. El ácido nióbico tiene una acidez fuerte ($H_o \leq -5.6$) y presenta centros ácidos de ambos tipos, Lewis y Brönsted. En caso de ser soportado, permanece enlazado al soporte incluso en presencia de agua por lo que actúa como un catalizador efectivo en aquellas reacciones en las que el agua participa como reactivo o producto.

Por tanto, debido al elevado carácter ácido de los materiales basados en Nb_2O_5 y a su estabilidad y tolerancia al agua, cada vez es más frecuente su empleo en catálisis, donde puede actuar como promotor, fase activa o soporte, ya sea en catálisis ácida o redox. Así, se han empleado catalizadores basados en niobio para catalizar otras reacciones, como deshidrataciones de alcoholes [110, 111], reacciones de deshidrogenación [111, 112], oxidación [113], alquilación [110, 114],esterificación [115, 116], isomerización [117], hidrogenolisis [118, 119], hidrogenación [120, 121], hidrodesulfuración [122, 123] e hidrólisis y deshidratación de azúcares [59, 79, 80, 124], entre otras.

En concreto, los catalizadores que contienen niobio han demostrado ser muy activos en la deshidratación de diferentes monosacáridos [59, 78-80]debido a sus excelentes propiedades ácidas que se mantienen incluso en medio acuoso [125] y a su estabilidad hidrotermal [126]. Una tarea importante en el desarrollo de catalizadores basados en óxido de niobio es aumentar su superficie para mejorar sus propiedades texturales, y que ello influya de forma directa en su comportamiento catalítico. Con este fin, el óxido de niobio se ha soportado sobre otros óxidos de elevada superficie, de forma que estando soportado exponga una mayor superficie activa a los reactivos que en su estado másico, siendo la sílica y la alúmina los soportes más estudiados [127, 128].Así, se ha estudiado el efecto que tienen el soporte empleado, el precursor deniobio utilizado y los métodos de preparación. Estos estudios han demostrado que la elección del soporte es un parámetro crucial, ya que afecta a la reactividad de las especies de óxido de niobio presentes sobre la superficie del catalizador y, por tanto, a su comportamiento catalítico. Se ha demostrado además que los centros ácidos tipo Lewis se encuentran presentes en todos los sistemas basados en óxido de niobio soportado, mientras que los centros Brönsted parecen limitarse a los materiales Nb_2O_5/Al_2O_3 y Nb_2O_5/SiO_2 [109]. Concretamente, la

introducción de Nb(V) en una matriz de sílica, donde los cationes de Si están tetracoordinados, puede hacer que la acidez resultante predominante en el óxido mixto Nb_2O_5/SiO_2sea de tipo Lewis o Brönsted dependiendo de la coordinación tetraédrica (NbO_4) u octaédrica (NbO_6), respectivamente, del niobio en el material, la cual a su vez depende de la relación de niobia a sílica en la composición de partida de la muestra [79].

Por otra parte, entre los sólidos ácidos empleados como soportes, los óxidos mixtos silíceos, tales como silica-alúmina ósílica-zirconia, entre otros, han atraído especial interés en catálisis debido a su fácil preparación, a su posibilidad de modificar sus propiedades superficiales mediante un control de la composición y a sus buenas propiedades ácidas en diversas reacciones de interés. En general, se considera que estos óxidos poseen tanto centros ácidos tipo Brönsted como centros ácidos de Lewis, siendo siempre mayoritario la presencia de grupos silanoles ácidos en su superficie (centros Brönsted) y en menor proporción las especies ácidas de Lewis asociadas a las especies de metal deficientes electrónicamente [129]. Además, según la hipótesis propuesta por *Tanabe et at*. [110, 130] para la generación de acidez en un óxido mixto de sílica-zirconia, dónde la sílica es siempre el componente mayoritario, se pueden genrar nuevos sitios ácidos de Brönsted (Figura 1.4).

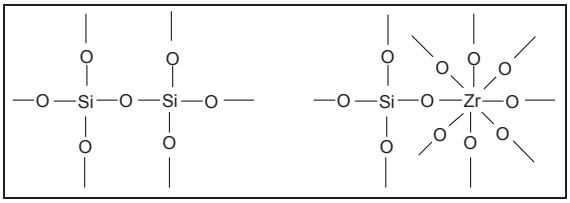

Figura 1.4. Estructuras modelo para la generación de acidez en el óxido mixto de Sílica-Zirconia, adaptado de Tanabe at al. [130]

Sin embargo, se ha demostrado en bibliografía que cuando se mezclan juntos diferentes óxidos, la naturaleza ácida de los óxidos resultantes puede verse modificada hacia una acidez predominante de tipo Brönsted o de tipo Lewis con modificación de su fortaleza ácida al mismo tiempo. Así, *Gervasini et at.* demostraron recientemente que en el caso del óxido de hierro soportado sobre un soporte de sílica-zirconia, el óxido de Fe (III) altamente disperso sobre el soporte proporcionaba predominantemente acidez Lewis en los materiales sintetizados [129].

En resumen, podemos concluir que los materiales basados en óxido de niobio resultan muy interesantes para su aplicación en catálisis, debido a la posibilidad de modular sus propiedades texturales y ácidas, como lo corrobora el interés creciente para su empleo en diferentes procesos catalíticos. Por esta razón, se ha elegido esta fase activa para el desarrollo del presente trabajo de Tesis Doctoral, donde el óxido de niobio soportado sobre un soporte comercial de SiO_2-ZrO_2 se ha empleado como catalizador sólido ácido en la reacción de deshidratación de xilosa a furfural (para más detalle ver Capítulo 4 de resultados).

1.4.2 Reacción de esterificación de ácido oleico con metanol

La búsqueda de combustibles alternativos para motores diésel ha incrementado especialmente su interés en los últimos años debido a la disminución de las reservas de petróleo y a las severas consecuencias medioambientales causadas por los gases que se derivan del uso de combustibles de motor de origen fósil. Con este fin,se han propuesto diferentes procedimientos para la producción de biocombustibles derivados de aceites, destacando la *reacción de transesterificación* para la obtención de *biodiésel*

porque se requieren condiciones de trabajo suaves y por la calidad del combustible obtenido [131].

El biodiésel es una mezcla de ésteres alquílicos de ácidos grasos (normalmente ésteres metílicos) que puede emplearse como combustible alternativo o como un aditivo al diésel convencional derivado del petróleo [132, 133]. En la reacción de transesterificación, que es el procedimiento más empleado para la síntesis de biodiésel, los triglicéridos de un aceite vegetal o una grasa animal reaccionan con un alcohol de cadena corta (normalmente metanol aunque también se ha propuesto la utilización de etanol) en presencia de un catalizador (generalmente básico) para dar lugar a la formación de una mezcla de los denominados FAME (del inglés, *FattyAcidMethylEsthers* en el caso de que se use metanol) (biodiésel) y glicerina como subproducto de la reacción (Esquema 1.8). En la industria los catalizadores más empleados son el NaOH y KOH (catalizadores homogéneos) ya que son baratos y de mayor disponibilidad.

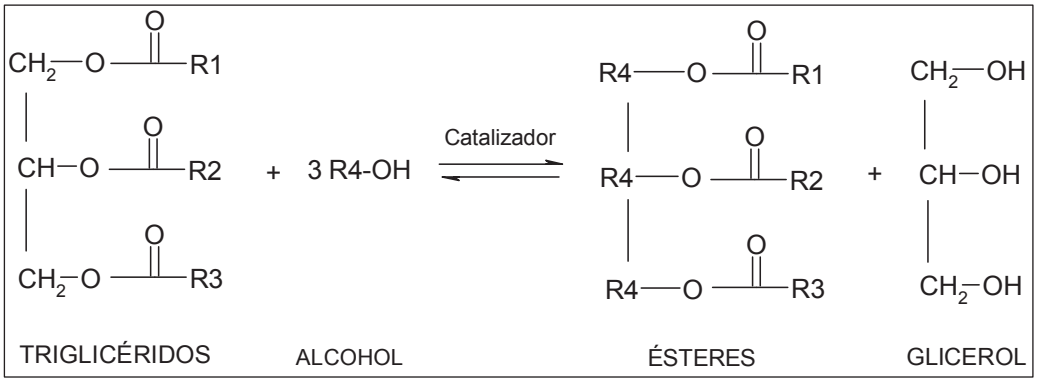

Esquema 1.8. Reacción de transesterificación para la obtención de biodiésel

Sin embargo, existen muchos aceites, especialmente los aceites de baja calidad como aceites usados o grasas animales, que presentan un alto índice de

acidez, es decir, altos niveles de agua y de ácidos grasos libres (FFA, del inglés, *Free FattyAcids*) [134, 135], de manera que estos ácidos grasos libres pueden reaccionar con los catalizadores alcalinos para formar jabones que emulsionan el aceite y complican el proceso de separación de los ésteres alquílicos [136, 137]. Por tanto, se requiere una etapa previa de pretratamiento para convertir los ácidos grasos libres a ésteres alquílicos de ácidos grasos, denominada reacción de esterificación [138]. La esterificación es el proceso mediante el cual un ácido graso reacciona con una molécula de alcohol en presencia de un catalizador ácido para formar un éster y agua (Esquema 1.9). Se ha publicado en bibliografía el empleo de numerosos catalizadores sólidos ácidos con objeto de evitar los problemas bien conocidos asociados a la catálisis homogénea que emplea ácidos minerales o inorgánicos líquidos. Conviene resaltar que, de todos los ácidos grasos, el ácido oleico es el preferido para evaluar la efectividad de los catalizadores sólidos ácidos en la reacción de esterificación ya que es el ácido graso más común encontrado en el aceite vegetal y además se encuentra presente extensamente en las materias primas de biodiésel de más bajo coste. Entre algunos de los ejemplos de catalizadores sólidos ácidos que se han empleado en la esterificación del ácido oleico se encuentran los siguientes: zirconias sulfatadas [139], óxidos de estaño sulfatados [140], óxidos de estaño con wolframio [136], ácido nióbico sulfatado [141], alúmina sulfatada [142], silicasmesoporosas modificadas [143], sólidos ácidos basados en carbón [144], zeolitas modificadas [145], resinas [146], heteropoliácidos [147], organoarcillas [148] y caolín [149].

Esquema 1.9. Reacción de esterificación para la obtención de biodiésel

En el capítulo 3 de esta Tesis Doctoral se presentarán los resultados obtenidos empleando los nanocomposites de SiO_2-APES en la reacción de esterificación de ácido oleico con metanol. La naturaleza ácida de estos catalizadores y el empleo de un disolvente menos polar que el agua (metanol), que implica menos problema de lixiviación del polímero, justifican esta exploración.

1.5. Bibliografía

[1] Ministerio de Industria, Turismo y Comercio. Instituto para la diversificación y Ahorro de la Energía (IDAE), (2011).
[2] B.G. Kamm, P.R., Kamm, M., Biorefineries (2006).
[3] F. Cherubini, Energy Conversion and Management, 51 (2010) 1412-1421.
[4] M.A.d.S. Bernades, (2011).
[5] S. Fernando, S. Adhikari, C. Chandrapal, N. Murali, Energy and Fuels, 20 (2006) 1727-1737.
[6] G.W. Huber, S. Iborra, A. Corma, Chemical Reviews, 106 (2006) 4044-4098.
[7] V. Menon, M. Rao, Progress in Energy and Combustion Science, 38 (2012) 522.
[8] D.M. Alonso, J.Q. Bond, J.A. Dumesic, Green Chemistry, 12 (2010) 1493-1513.
[9] A.S. Mamman, J.M. Lee, Y.C. Kim, I.T. Hwang, N.J. Park, Y.K. Hwang, J.S. Chang, J.S. Hwang, Biofuels, Bioproducts and Biorefining, 2 (2008) 438-454.
[10] D.M. Alonso, S.G. Wettstein, M.A. Mellmer, E.I. Gurbuz, J.A. Dumesic, Energy and Environmental Science, 6 (2012) 76-80.
[11] D.M. Alonso, S.G. Wettstein, J.A. Dumesic, Chemical Society Reviews, 41 (2012) 8075-8098.
[12] D.M. Alonso, S.G. Wettstein, J.A. Dumesic, Green Chemistry, 15 (2013) 584-595.
[13] K.J. Zeitsch, *Sugar Series 13*, Elsevier Science, 1ª Edición (2000).
[14] B. Danon, G. Marcotullio, W. De Jong, Green Chemistry, 16 (2014) 39-54.
[15] A.S. Dias, M. Pillinger, A.A. Valente, Journal of Catalysis, 229 (2005) 414-423.
[16] M.J. Antal Jr, T. Leesomboon, W.S. Mok, G.N. Richards, Carbohydrate Research, 217 (1991) 71-85.
[17] A.S. Dias, S. Lima, M. Pillinger, A.A. Valente, Catalysis Letters, 114 (2007) 151-160.
[18] W. De Jong, G. Marcotullio, International Journal of Chemical Reactor Engineering, 8 (2010) 1542-6580.
[19] T. Ahmad, L. Kenne, K. Olsson, O. Theander, Carbohydrate Research, 276 (1995) 309-320.

[20] M.S. Feather, D.W. Harris, S.B. Nichols, Journal of Organic Chemistry, 37 (1972) 1606-1608.
[21] C.D. Hurd, L.L. Isenhour, Journal of the American Chemical Society, 54 (1932) 317-330.
[22] W.A. Bonner, M.R. Roth, Journal of the American Chemical Society, 81 (1959) 5454-5456.
[23] D.W. Harris, M.S. Feather, Carbohydrate Research, 30 (1973) 359-365.
[24] J.B. Binder, J.J. Blank, A.V. Cefali, R.T. Raines, ChemSusChem, 3 (2010) 1268-1272.
[25] X. Qian, M.R. Nimlos, M. Davis, D.K. Johnson, M.E. Himmel, Carbohydrate Research, 340 (2005) 2319-2327.
[26] M.R. Nimlos, X. Qian, M. Davis, M.E. Himmel, D.K. Johnson, Journal of Physical Chemistry A, 110 (2006) 11824-11838.
[27] A. Takagaki, M. Ohara, S. Nishimura, K. Ebitani, Chemistry Letters, 39 (2010) 838-840.
[28] R. Xing, W. Qi, G.W. Huber, Energy and Environmental Science, 4 (2011) 2193-2205.
[29] E.I. Gürbüz, S.G. Wettstein, J.A. Dumesic, ChemSusChem, 5 (2012) 383-387.
[30] G. Marcotullio, W. De Jong, Green Chemistry, 12 (2010) 1739-1746.
[31] C. Rong, X. Ding, Y. Zhu, Y. Li, L. Wang, Y. Qu, X. Ma, Z. Wang, Carbohydrate Research, 350 (2012) 77-80.
[32] G. Marcotullio, W. De Jong, Carbohydrate Research, 346 (2011) 1291-1293.
[33] J. Gravitis, N. Vedernikov, J. Zandersons, ACS Symposium Series United Nations University Institute of Advanced Studies, 9 (2001) 110-122.
[34] R. Weingarten, J. Cho, G.A. Tompsett, W.C. Conner Jr, G.W. Huber, Journal of Catalysis, 279 (2011) 174-182 .
[35] V.V. Ordomsky, J. Van Der Schaaf, J.C. Schouten, T.A. Nijhuis, ChemSusChem, 5 (2012) 1812-1819.
[36] A.C. Doiseau, F. Rataboul, L. Burel, N. Essayem, Catalysis Today, 226 (2014) 176-184.
[37] V. Choudhary, S.I. Sandler, D.G. Vlachos, ACS Catalysis, 2 (2012) 2022-2028.
[38] I. Agirrezabal-Telleria, C. García-Sancho, P. Maireles-Torres, P.L. Arias, Cuihua Xuebao/Chinese Journal of Catalysis, 34 (2013) 1402-1406.
[39] B. Pholjaroen, N. Li, Z. Wang, A. Wang, T. Zhang, Journal of Energy Chemistry, 22 (2013) 826-832.
[40] H.S. A.P. Dunlop, Quaker Oats Co. US 2838 523 (1958).

[41] I. Van Zandvoort, Y. Wang, C.B. Rasrendra, E.R.H. Van Eck, P.C.A. Bruijnincx, H.J. Heeres, B.M. Weckhuysen, ChemSusChem, 6 (2013) 1745-1758.
[42] S.K.R. Patil, J. Heltzel, C.R.F. Lund, Energy and Fuels, 26 (2012) 5281-5293.
[43] S.K.R. Patil, C.R.F. Lund, Energy and Fuels, 25 (2011) 4745-4755.
[44] J. Herzfeld, D. Rand, Y. Matsuki, E. Daviso, M. Mak-Jurkauskas, I. Mamajanov, Journal of Physical Chemistry B, 115 (2011) 5741-5745.
[45] S.J. Dee, A.T. Bell, ChemSusChem, 4 (2011) 1166-1173.
[46] E. Lam, E. Majid, A.C.W. Leung, J.H. Chong, K.A. Mahmoud, J.H.T. Luong, ChemSusChem, 4 (2011) 535-541.
[47] S. Lima, A. Fernandes, M.M. Antunes, M. Pillinger, F. Ribeiro, A.A. Valente, Catalysis Letters, 135 (2010) 41-47.
[48] C. Moreau, R. Durand, D. Peyron, J. Duhamet, P. Rivalier, Industrial Crops and Products, 7 (1998) 95-99.
[49] M.J. Campos Molina, R. Mariscal, M. Ojeda and M. López Granados, Bioresource Technology, 126 (2012) 321-327.
[50] A.S. Dias, S. Lima, D. Carriazo, V. Rives, M. Pillinger, A.A. Valente, Journal of Catalysis, 244 (2006) 230-237.
[51] A.S. Dias, S. Lima, P. Brandao, M. Pillinger, J. Rocha, A.A. Valente, Catalysis Letters, 108 (2006) 179-186.
[52] A.S. Dias, M. Pillinger, A.A. Valente, Applied Catalysis A: General, 285 (2005) 126-131.
[53] I. Sádaba, S. Lima, A.A. Valente, M. López Granados, Carbohydrate Research, 346 (2011) 2785-2791.
[54] I. Sádaba, M. Ojeda, R. Mariscal, M.L. Granados, Applied Catalysis B: Environmental, 150-151 (2014) 421-431.
[55] J. Zhang, J. Zhuang, L. Lin, S. Liu, Z. Zhang, Biomass and Bioenergy, 39 (2012) 73-77.
[56] C. Sievers, I. Musin, T. Marzialetti, M.B.V. Olarte, P.K. Agrawal, C.W. Jones, ChemSusChem, 2 (2009) 665-671.
[57] Y.C. Kim, H.S. Lee, Journal of Industrial and Engineering Chemistry, 7 (2001) 424-429.
[58] I. Agirrezabal-Telleria, A. Larreategui, J. Requies, M.B. Güemez, P.L. Arias, Bioresource Technology, 102 (2011) 7478-7485.
[59] C. García-Sancho, I. Agirrezabal-Telleria, M.B. Güemez, P. Maireles-Torres, Applied Catalysis B: Environmental, 152-153 (2014) 1-10.
[60] R. Karinen, K. Vilonen, M. Niemela, ChemSusChem, 4 (2011) 1002-1016.

[61] I. Agirrezabal-Telleria, I. Gandarias, P.L. Arias, Catalysis Today, 234 (2013) 42-58.
[62] R. O'Neil, M.N. Ahmad, L. Vanoye, F. Aiouache, Industrial and Engineering Chemistry Research, 48 (2009) 4300-4306.
[63] X. Shi, Y. Wu, H. Yi, G. Rui, P. Li, M. Yang, G. Wang, Energies, 4 (2011) 669-684.
[64] I. Agirrezabal-Telleria, J. Requies, M.B. Guémez, P.L. Arias, Applied Catalysis B: Environmental, 145 (2012) 34-42.
[65] E.I. Gürbüz, J.M.R. Gallo, D.M. Alonso, S.G. Wettstein, W.Y. Lim, J.A. Dumesic, Angewandte Chemie - International Edition, 52 (2013) 1270-1274.
[66] L.R. Ferreira, S. Lima, P. Neves, M.M. Antunes, S.M. Rocha, M. Pillinger, I. Portugal, A.A. Valente, Chemical Engineering Journal, 215-216 (2013) 772-783.
[67] M.M. Antunes, S. Lima, A. Fernandes, M. Pillinger, M.F. Ribeiro, A.A. Valente, Applied Catalysis A: General, 417-418 (2012) 243-252.
[68] S. Lima, M.M. Antunes, A. Fernandes, M. Pillinger, M.F. Ribeiro, A.A. Valente, Applied Catalysis A: General, 388 (2010) 141-148.
[69] S. Lima, M. Pillinger, A.A. Valente, Catalysis Communications, 9 (2008) 2144-2148.
[70] S.B. Kim, S.J. You, Y.T. Kim, S. Lee, H. Lee, K. Park, E.D. Park, Korean Journal of Chemical Engineering, 28 (2011) 710-716.
[71] V. Choudhary, A.B. Pinar, S.I. Sandler, D.G. Vlachos, R.F. Lobo, ACS Catalysis, 1 (2011) 1724-1728.
[72] G.H. Jeong, E.G. Kim, S.B. Kim, E.D. Park, S.W. Kim, Microporous and Mesoporous Materials, 144 (2011) 134-139.
[73] X. Wang, S. Cheng and J.C.C. Chan, Journal of Physical Chemistry C, 111 (2007) 2156-2164.
[74] A.S. Dias, M. Pillinger, A.A. Valente, Microporous and Mesoporous Materials, 94 (2006) 214-225.
[75] I. Agirrezabal-Telleria, J. Requies, M.B. Güemez, P.L. Arias, Applied Catalysis B: Environmental, 145 (2014) 34-42.
[76] K. Watanabe, N. Yamagiwa, Y. Torisawa, Organic Process Research and Development, 11 (2007) 251-258.
[77] I. Sádaba, M. Ojeda, R. Mariscal, R. Richards, M.L. Granados, Catalysis Today, 167 (2010) 77-83.
[78] P. Carniti, A. Gervasini, S. Biella, A. Auroux, Catalysis Today, 118 (2006) 373-378.
[79] P. Carniti, A. Gervasini, M. Marzo, Catalysis Today, 152 (2010) 42-47.

[80] C. García-Sancho, J.M. Rubio-Caballero, J.M. Mérida-Robles, R. Moreno-Tost, J. Santamaría-González, P. Maireles-Torres, Catalysis Today, 234 (2014) 119-124.
[81] M.M. Antunes, S. Lima, A. Fernandes, J. Candeias, M. Pillinger, S.M. Rocha, M.F. Ribeiro, A.A. Valente, Catalysis Today, 195 (2012) 127-135.
[82] I. Agirrezabal-Telleria, Y. Guo, F. Hemmann, P.L. Arias, E. Kemnitz, Catalysis Science and Technology, 4 (2014) 1357-1368.
[83] J. Tuteja, S. Nishimura, K. Ebitani, Bulletin of the Chemical Society of Japan, 85 (2012) 275-281.
[84] I. Agirrezabal-Telleria, J. Requies, M.B. Güemez, P.L. Arias, Green Chemistry, 14 (2012) 3132-3140.
[85] J. Lessard, J.F. Morin, J.F. Wehrung, D. Magnin, E. Chornet, Topics in Catalysis, 53 (2010) 1231-1234.
[86] P.L. Dhepe and R. Sahu, Green Chemistry, 12 (2010) 2153-2156.
[87] X. Shi, Y. Wu, P. Li, H. Yi, M. Yang, G. Wang, Carbohydrate Research, 346 (2011) 480-487.
[88] S. Lima, M.M. Antunes, A. Fernandes, M. Pillinger, M.F. Ribeiro, A.A. Valente, Molecules, 15 (2010) 3863-3877.
[89] T. Suzuki, T. Yokoi, R. Otomo, J.N. Kondo, T. Tatsumi, Applied Catalysis A: General, 408 (2011) 117-124.
[90] J. Zhang, J. Li, L. Lin, BioResources, 9 (2012) 4194-4204.
[91] I. Agirrezabal-Telleria, F. Hemmann, C. Jäger, P.L. Arias, E. Kemnitz, Journal of Catalysis, 305 (2013) 81-91.
[92] H.D. Mansilla, J. Baeza, S. Urzúa, G. Maturana, J. Villaseñor, N. Durán, Bioresource Technology, 66 (1998) 189-193.
[93] A. Chareonlimkun, V. Champreda, A. Shotipruk, N. Laosiripojana, Fuel, 89 (2010) 2873-2880.
[94] A. Chareonlimkun, V. Champreda, A. Shotipruk, N. Laosiripojana, Bioresource Technology, 101 (2010) 4179-4186.
[95] P.A. Russo, S. Lima, V. Rebuttini, M. Pillinger, M.G. Willinger, N. Pinna, A.A. Valente, RSC Advances, 3 (2013) 2595-2603.
[96] F. Kucera and J. Jancár, Polymer Engineering, Science, 38 (1998) 783-792.
[97] W.W. Sulkowski, A. Wolinska, B. Szoltysik, W.M. Bajdur, A. Sulkowska, Polymer Degradation and Stability, 90 (2005) 272-280.
[98] Y. Inagaki, M. Kuromiya, T. Noguchi, H. Watanabe, Langmuir, 15 (1999) 4171-4175.
[99] I. Bekri-Abbes, S. Bayoudh, M. Baklouti, Journal of Polymers and the Environment, 14 (2006) 249-256.

[100] R.M.N. De Assunca˜o, B. Royer, J.S. Oliveira, G.R. Filho, L.A. De Castro Motta, Journal of Applied Polymer Science, 96 (2005) 1534-1538.
[101] M.L. Granados, A.C. Alba-Rubio, I. Sádaba, R. Mariscal, I. Mateos-Aparicio, A. Heras, Green Chemistry, 13 (2011) 3203-3212.
[102] T.J. Dickerson, N.N. Reed, K.D. Janda, Chemical Reviews, 102 (2002) 3325-3344.
[103] J.H. Clark, Pure and Applied Chemistry, 73 (2001) 103-111.
[104] H. Zou, S. Wu, J. Shen, Chemical Reviews, 108 (2008) 3893-3957.
[105] G. Kickelbick, Progress in Polymer Science (Oxford), 28 (2003) 83-114.
[106] R. Tamaki, Y. Chujo, Chemistry of Materials, 11 (1999) 1719-1726.
[107] I. Nowak, M. Ziolek, Chemical Reviews, 99 (1999) 3603-3624.
[108] J.M. Jehng, I.E. Wachs, Chemistry of Materials, 3 (1991) 100-107.
[109] J.M. Jehng, I.E. Wachs, Catalysis Today, 8 (1990) 37-55.
[110] K. Tanabe, S. Okazaki, Applied Catalysis A, General, 133 (1995) 191-218.
[111] C. Guo, Z. Qian, Catalysis Today, 16 (1993) 379-385.
[112] K. Kunimori, H. Oyanagi, H. Shindo, Catalysis Letters, 21 (1993) 283-290.
[113] J.M. Jehng, A.M. Turek, I.E. Wachs, Applied Catalysis A, General, 83 (1992) 179-200.
[114] M. Morais, E.F. Torres, L.M.P.M. Carmo, N.M.R. Pastura, W.A. Gonzalez, A.C.B. Dos Santos, E.R. Lachter, Catalysis Today, 28 (1996) 17-21.
[115] V.S. Braga, I.C.L. Barros, F.A.C. Garcia, S.C.L. Dias, J.A. Dias, Catalysis Today, 133-135 (2008) 106-112.
[116] T. Iizuka, S. Fujie, T. Ushikubo, Z.h. Chen, K. Tanabe, Applied Catalysis, 28 (1986) 1-5.
[117] S. Hasegawa, H. Aritani, M. Kudo, Catalysis Today, 16 (1993) 371-377.
[118] P.A. Burke, E.I. Ko, Journal of Catalysis, 116 (1989) 230-239.
[119] R. Rodrigues, N. Isoda, M. Gonçalves,, F.C.A. Figueiredo, D. Mandelli, W.A. Carvalho, Chemical Engineering Journal, 198-199 (2012) 457-467.
[120] E.I. Ko, J.M. Hupp, N.J. Wagner, Journal of Catalysis, 86 (1984) 315-327.
[121] T. Iizuka, Y. Tanaka, K. Tanabe, Journal of Molecular Catalysis, 17 (1982) 381-389.
[122] C. Geantet, J. Afonso, M. Breysse, N. Allali, M. Danot, Catalysis Today, 28 (1996) 23-30.
[123] N. Allali, E. Prouzet, A. Michalowicz, V. Gaborit, A. Nadiri, M. Danot, Applied Catalysis A: General, 159 (1997) 333-354.
[124] C. Carlini, M. Giuttari, A.M.R. Galletti, G. Sbrana, T. Armaroli, G. Busca, Applied Catalysis A: General, 183 (1999) 295-302.

[125] T. Okuhara, Chemical Reviews, 102 (2002) 3641-3666.
[126] K. Nakajima, Y. Baba, R. Noma, M. Kitano, J. N. Kondo, S. Hayashi, M. Hara, Journal of the American Chemical Society, 133 (2011) 4224-4227.
[127] F.M.T. Mendes, C.A. Perez, R.R. Soares, F.B. Noronha, M. Schmal, Catalysis Today, 78 (2003) 449-458.
[128] V.S. Braga, J.A. Dias, S.C.L. Dias, J.L. De Macedo, Chemistry of Materials, 17 (2005) 690-695.
[129] A. Gervasini, C. Messi, D. Flahaut, C. Guimon, Applied Catalysis A: General, 367 (2009) 113-121.
[130] K. Tanabe, Catalysis Today, 78 (2003) 65-77.
[131] E.M. Shahid, Y. Jamal, Renewable and Sustainable Energy Reviews, 15 (2011) 4732-4745.
[132] T. Suganya, S. Renganathan, Bioresource Technology, 107 (2012) 319-326.
[133] K. Ramachandran, T. Suganya, N. Nagendra Gandhi, S. Renganathan, Renewable and Sustainable Energy Reviews, 22 (2013) 410-418.
[134] J.H. Van Gerpen, B. He, RSC Energy and Environment Series, 2010 (2010) 382-415.
[135] A. Talebian-Kiakalaieh, N.A.S. Amin, H. Mazaheri, Applied Energy, 104 (2013) 683-710.
[136] A. Sarkar, S.K. Ghosh, P. Pramanik, Journal of Molecular Catalysis A: Chemical, 327 (2010) 73-79.
[137] D.Y.C. Leung, X. Wu, M.K.H. Leung, Applied Energy, 87 (2010) 1083-1095.
[138] G. Santori, G. Di Nicola, M. Moglie, F. Polonara, Applied Energy, 92 (2012) 109-132.
[139] C.A.R. Melo Junior, C.E.R. Albuquerque, J.S.A. Carneiro, C. Dariva, M. Fortuny, A.F. Santos, S.M.S. Egues, A.L.D. Ramos, Industrial and Engineering Chemistry Research, 49 (2010) 12135-12139.
[140] J.I. Moreno, R. Jaimes, R. Gómez and M.E. Niño-Gómez, Catalysis Today, 172 (2011) 34-40.
[141] M.K. Pietre, L.C.P. Almeida, R. Landers, R.C.G. Vinhas, F.J. Luna, Reaction Kinetics, Mechanisms and Catalysis, 99 (2010) 269-280.
[142] M. Álvarez, M.J. Ortiz, J.L. Ropero, M.E. Niño, R. Rayon, F. Tzompantzi and R. Gómez, Chemical Engineering Communications, 196 (2009) 1152-1162.
[143] A. Martín, G. Morales, F. Martínez, R. Van Grieken, L. Cao, M. Kruk, Journal of Materials Chemistry, 20 (2010) 8026-8035.
[144] J.C. Juan, J. Zhang, Y. Jiang, W. Cao, M.A. Yarmo, Catalysis Letters, 117 (2007) 153-158.

[145] K.H. Chung, D.R. Chang, B.G. Park, Bioresource Technology, 99 (2008) 7438-7443.
[146] S.M. Son, H. Kimura, K. Kusakabe, Bioresource Technology, 102 (2011) 2130-2132.
[147] C.F. Oliveira, L.M. Dezaneti, F.A.C. Garcia, J.L. de Macedo, J.A. Dias, S.C.L. Dias, K.S.P. Alvim, Applied Catalysis A: General, 372 (2010) 153-161.
[148] M. Ghiaci, B. Aghabarari, A. Gil, Fuel, 90 (2011) 3382-3389.
[149] L.A.S. Nascimento, L.M.Z. Tito, R.S. Angélica, C.E.F. da Costa, J.R. Zamian, G.N. da Rocha Filho, Applied Catalysis B: Environmental, 101 (2011) 495-503.

2. OBJETIVOS

El principal **Objetivo** de la presente Tesis doctoral es desarrollar nuevos procesos catalíticos basados en catalizadores sólidos para obtener furfural desde los azúcares C5 hemicelulósicos (principalmente, xilosa) .La búsqueda de catalizadores heterogéneos resulta de vital importancia por ser más seguros y medioambientalmente más sostenibles de acuerdo con los principios de la química verde. Puesto que la reacción de deshidratación de xilosa a furfural requiere la presencia de catalizadores ácidos, esta Tesis doctoral implica el estudio de catalizadores ácidos heterogéneos.

De acuerdo con este objetivo general, esta tesis se ha dividido en dos objetivos parciales (Esquema 2.1). Un primer objetivo parcial se ha dirigido a la búsqueda de un disolvente orgánico medioambientalmente sostenible que mejore el rendimiento a furfural. Un segundo objetivo se ha dirigido a la búsqueda y el estudio de catalizadores ácidos heterogéneos utilizando el disolvente propuesto en el objetivo parcial anterior.

Para alcanzar este segundo objetivo parcial, la investigación se ha dirigido al estudio de dos tipos de catalizadores. Una parte importante del esfuerzo investigador de esta tesis se ha dirigido a encontrar las condiciones de síntesis apropiadas para que los nanocomposites SiO_2-APES alcancen la mayor carga de polímero ácido APES y que sean estables en el medio de reacción.

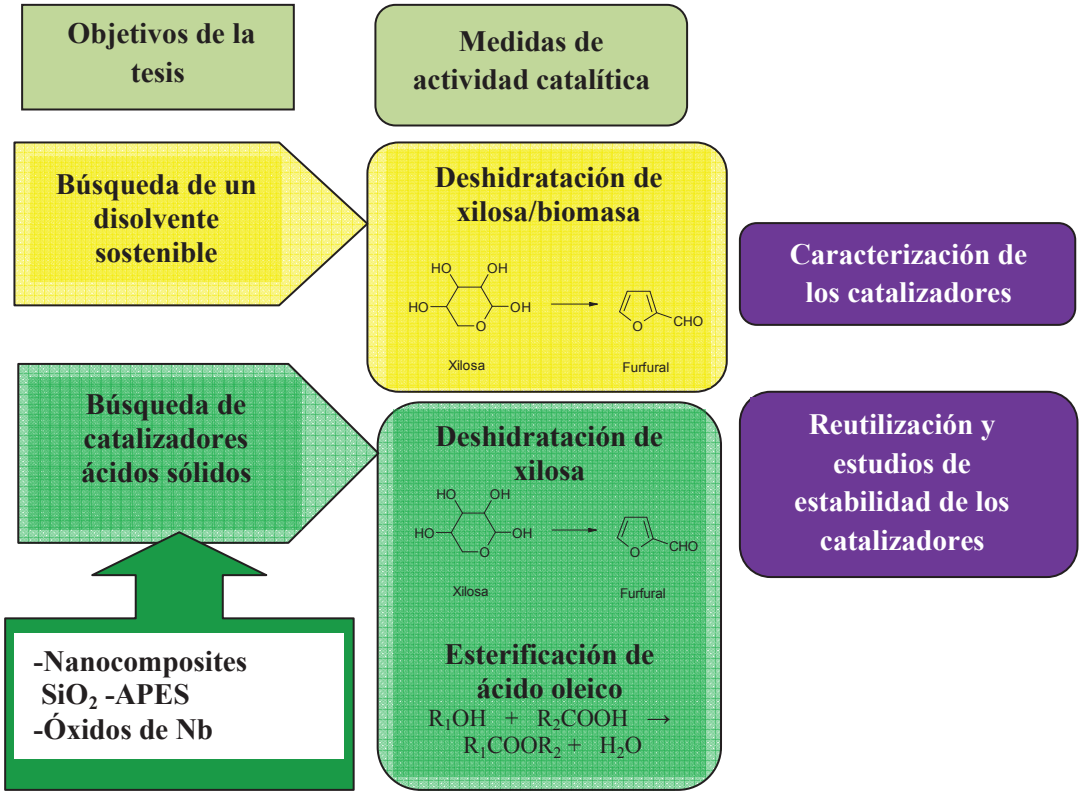

Esquema 2.1. Esquema de los objetivos de esta tesis doctoral

En el capítulo 6, que concierne a este objetivo parcial, también se explorará otra reacción de gran interés en biorrefinería: la esterificación de ácido oleico para la producción de biodiésel. Esta reacción requiere, al igual que la reacción de xilosa a furfural, la presencia de catalizadores ácidos. La razón de esta exploración es encontrar otras aplicaciones catalíticas a los nanocomposites SiO_2-APES en reacciones que tengan lugar en condiciones menos exigentes hidrotermalmente y con un menor impacto en la lixiviación.

La reacción de esterificación tiene lugar en un medio no acuoso (metanol/aceite) y a temperaturas más moderadas.

Por último, el otro tipo de catalizadores que se ha estudiado para este segundo objetivo parcial están basados en óxido de Nb. La investigación se ha dirigido al estudio del comportamiento catalítico en la reacción de deshidratación de xilosa a furfural tanto de óxido de niobio másico como de catalizadores de niobio soportados. Paralelamente, esta investigación se ha orientado a la búsqueda exhaustiva de adecuados sistemas de reacción monofásicos y/o bifásicos que minimicen la desactivación del catalizador por deposición de huminas e incrementen así su estabilidad y durabilidad.

3. METODOLOGÍA EXPERIMENTAL

ÍNDICE

El objetivo de este capítulo es proporcionar los detalles técnicos necesarios y suficientes para que los resultados puedan ser reproducidos. El capítulo se estructura en tres apartados. Primeramente, se presenta una relación de los catalizadores empleados en cada uno de los diferentes apartados de esta memoria. Su preparación, en cambio, se explicará con más detalle en el capítulo de resultados correspondiente. A continuación, una descripción detallada de los métodos de reacción empleados durante el desarrollo de esta tesis doctoral. Finalmente, se resumen brevemente las técnicas de caracterización empleadas, mencionando el propósito de su empleo así como un breve comentario sobre el fundamento teórico de la técnica, dando una descripción detallada del procedimiento y de las condiciones experimentales seguidas para obtener los resultados.

3.1. Preparación de catalizadores

Debido a la diversidad de catalizadores y métodos de preparación empleados, se ha preferido trasladar a cada capítulo de resultados la descripción detallada del tipo de catalizador empleado así como su nomenclatura y procedimiento de síntesis para facilitar así la comprensión. No obstante, a modo de resumen, la Tabla 3.1 recoge los datos de cada tipo de catalizador empleado, así como el capítulo en el que se emplea.

Tabla 3.1. Resumen de catalizadores empleados

Objetivo	Reacción	Capítulo	Catalizador	Pág.
Búsqueda de un disolvente sostenible	Deshidratación de xilosa/biomasa	4	H_2SO_4	123
Búsqueda de catalizadores ácidos sólidos	-Deshidratación de xilosa y esterificación de ácido oleico	5,6	APES/Si-APTES	149,213
	-Deshidratación de xilosa	7	NBO Nb/Si-Zr sol-gel Nb/Si-Zr impregnación húmeda	249

3.2. Reactivos comerciales de partida

En este apartado se presentan los distintos reactivos de partida (sólidos, líquidos y gaseosos).

En cuanto a los **reactivos sólidos** adquiridos de casas comerciales, se indica la misma y su grado de pureza:

- D-(+)-xilosa (Sigma Aldrich, BioXtra, ≥99%)
- D-(+)-glucosa (Sigma-Aldrich, 99.5%)
- L-(+)-arabinosa (Sigma-Aldrich, ≥99%)
- D-(+)-galactosa (Sigma-Aldrich, ≥99%)
- D-(+)-manosa (for microbiology, Sigma-Aldrich)
- D- (+)-celobiosa (for microbiology, Sigma-Aldrich)

- Xilitol (Sigma-Aldrich, ≥99%)
- NaCl (Panreac, 98%)
- KOH (Panreac, 90%)
- KBr (SpectroGD Powder, Sigma-Aldrich)
- $CaCO_3$ (Sigma-Aldrich, A.C.S Reagent)
- *Amberlita 70* (Amberlyst)
- *Biomasa del cardo"Cynara Cardunculus"*
- Etóxido de niobio (V) (NBE, Sigma-Aldrich, 99,95%)
- Óxido de niobio hidratado (NBO, Companhia Brasileira de Metalurgia e Mineraçao, CBMM)
- Silica-zirconia en polvo (5% en peso de ZrO_2, Grace Company)

Los **reactivos líquidos** empleados para el desarrollo de esta Tesis doctoral han sido:

- 2-furaldehído-furfural- (reagent grade, Sigma- Aldrich, 99%)
- Ciclopentil metil éter (anhidro, Sigma-Aldrich, ≥99.9%)
- Ácido octanoico (Sigma-Aldrich, 98%)
- 5-hidroximetilfurfural (Sigma-Aldrich, 99%)
- Ácido levulínico (Sigma-Aldrich, 98%)
- H_2SO_4 (Panreac, 96%)
- HCl (Sigma-Aldrich, 37%)
- Tetraetilortosilicato (TEOS, Sigma-Aldrich, ≥99%)
- 3- aminopropiltrietoxisilano (APTES, Sigma-Aldrich, ≥98%)
- Disolución acuosa de ácido poliestirensulfónico (APES, 18% en peso en agua, MW= 75000, 5.4 mmoles·H^+·g^{-1}, Sigma-Aldrich)

- Aceite de girasol grado alimenticio
- Metanol (anhidro, Panreac, 99.5%)
- Ácido oleico (Sigma-Aldrich, 90%)
- Acetonitrilo (Sigma-Aldrich, ≥99.9%)
- Tetrahidrofurano (THF, HPLC Grade, Scharlau)
- Palmitato de etilo (Fluka, ≥95%)
- 2-propanol –isopropanol- (Sigma-Aldrich, ≥99,5%)
- γ-valerolactona (Sigma-Aldrich, 99%)
- 1-propanol (Sigma Aldrich, ≥99.5%)
- Ciclohexano (VWR, HiPerSolv CHROMANORM® para HPLC, >99%)
- 2-feniletilamina (PEA, Fluka, >99%)
- Disolución de hidróxido amónico (Fluka, purum, ~28% en peso en agua)
- Complejo de oxalato de niobio amonio (ANBO, CBMM)
- Agua purificada Elix

Finalmente los **gases** utilizados, han sido suministrados por Air Liquid, y tienen la pureza (% en volumen) que se muestra a continuación:

- O2 (N-40), 99,99 %
- N2 (N-45), 99,995 %
- He (N-50), 99,999 %
- Ar (N-50), 99,999 %.

3.3. Medidas de actividad catalítica

En este apartado se detallan las condiciones experimentales desarrolladas para llevar a cabo las reacciones propuestas en los objetivos del presente trabajo. Concretamente, se han incluido la descripción de los equipos experimentales, las condiciones de operación y separación y el correspondiente sistema analítico de los productos tras reacción empleado para llevar a cabo las medidas de actividad catalítica, así como las condiciones de activación de los catalizadores en el caso oportuno.

3.3.1 Reacción de deshidratación de xilosa mediante el empleo de ácido sulfúrico como catalizador

3.3.1.1 Reactor de mezcla perfecta de vidrio

Las medidas de actividad catalítica de la reacción de deshidratación de xilosa fueron obtenidas en dos laboratorios diferentes y con sistemas catalíticos distintos. Por tanto, a continuación se detalla la descripción experimental de las medidas realizadas en el Instituto de Catálisis y Petroleoquímica del CSIC. Más adelante, se explicarán los equipos y condiciones de reacción empleadas para las medidas de realizadas en el Departamento de Química de la Universidad Degli Studi de Milán.

La reacción de deshidratación de xilosa se llevó a cabo en un reactor de mezcla perfecta de vidrio con paredes gruesas capaces de soportar presiones de hasta 10 bares. Este reactor (*Ace Pressure Tube*) suministrado por Sigma-Aldrich (Figura 3.1) tiene un volumen de 15 mL y dispone de un tapón de PTFE con una junta de FETFE. El reactor se cargó con una disolución acuosa

(5 g) de D-(+)-xilosa al 10% en peso y H_2SO_4 al 1% en peso, ambos respecto de la fase acuosa total. En aquellos experimentos llevados a cabos en mezclas bifásicas de agua-ciclopentil metil éter (CPME), las proporciones másicas CPME:fase acuosa se variaron manteniendo constante la masa de disolución total (5g). En aquellos experimentos llevados a cabo además en presencia de NaCl, el NaCl se añadió a la disolución acuosa que contiene el 10% en peso de xilosa y el 1% en peso de H_2SO_4 como catalizador (ambos cálculos referidos a la solución acuosa libre de sal). Previamente a su carga, el reactor se purgó con un flujo de N_2 durante 10 minutos para desplazar el aire presente en el reactor. Este reactor se introduce en un baño de aceite a la temperatura de reacción seleccionada y se agita con un agitador magnético a 700 rpm.

Debido a la imposibilidad de tomar muestra en el transcurso de la reacción, se ha seguido la cinética de la reacción mediante el empleo de un reactor distinto para cada tiempo de reacción ensayado. Una vez transcurrido el tiempo necesario, la reacción se paró sumergiendo el reactor en agua fría para enfriarlo. En el caso de reacciones llevadas a cabo en presencia de CPME, las fases acuosas y orgánicas se separaron dejando el reactor en reposo por decantación.

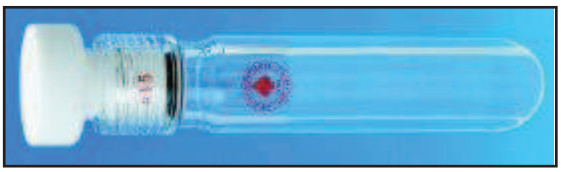

Figura 3.1. Reactor de mezcla perfecta Ace Pressure Tube

3.3.1.2 Análisis de los productos de reacción

El procedimiento experimental para llevar a cabo las medidas de actividad catalítica y el análisis para la cuantificación los productos de reacción se muestra en la Figura 3.2. Una vez transcurrida la reacción, se añadieron 200 mg de D-(+)- glucosa y 40 mg de ácido octanoico, como estándares internos de la fase acuosa y orgánica, respectivamente y se agitó para asegurar su completa disolución. Previo al análisis de cada fase, la disolución se filtró a vacío mediante un sistema Vac Elut de Varian con una columna filtrante de PVDF de 450 nm para eliminar posibles subproductos sólidos de la reacción. Seguidamente, alícuotas de ca. 2 mL se tomaron de cada fase y se filtraron denuevo a través de un filtro de poliétersulfona de Millipore de 0.22 μm y se analizaron finalmente en un cromatógrafo de líquidos de alta presión (HPLC) Agilent 1200 series equipado con un detector de índice de refracción. La xilosa y el furfural en la fase acuosa se separaron en una columna de intercambio de iones Rezex Bio-Rad Aminex HPX-87H 300 x 7,8 mm (Phenomenex), empleando como eluyente una disolución 0,005 M de H_2SO_4 a 328 K con un flujo de 0,4 mL·min-1. La fase orgánica se separó en una columna de fase reversa XDB C18 4,6 x 150 mm (Agilent Zorbax Eclipse) con una disolución 80% en volumen de metanol en agua como fase móvil a 0,5 mL·min-1 y 313 K. La cuantificación se realizó usando un detector de índice de refracción (RID).

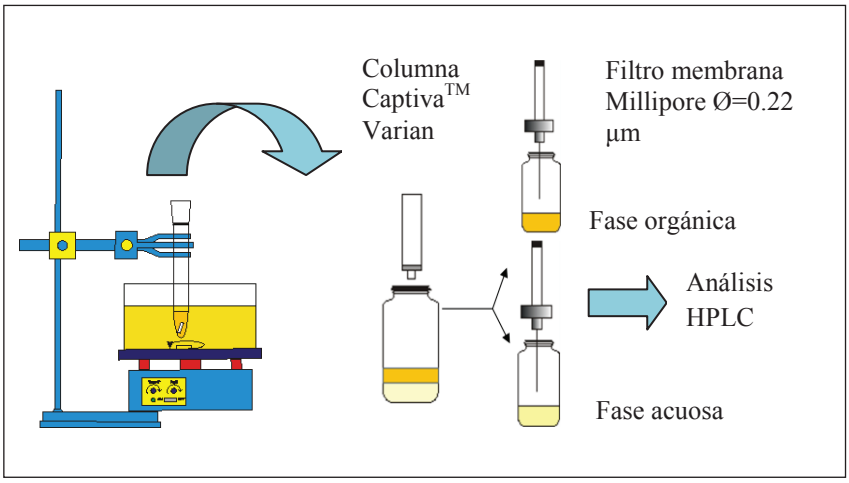

Figura 3.2. Representación esquemática del procedimiento de análisis de las medidas de actividad catalítica

Los valores de conversión de xilosa y de rendimiento y selectividad a furfural se calcularon en base a la concentración inicial de monosacárido y se calcularon utilizando las ecuaciones 3.1, 3.2 y 3.3.

Conversión de xilosa (mol %) = $\frac{m^0_{xilosa} - m_{xilosa}}{m^0_{xilosa}}$ x 100 ***Ecuación 3.1***

Rendimiento (furfural) (mol %) = $\frac{m_{furfural}}{m^0_{xilosa}}$ x 100 ***Ecuación 3.2***

Selectividad (furfural) (mol %) = $\frac{m_{furfural}}{m^0_{xilosa} - m_{xilosa}}$ x 100 ***Ecuación 3.3***

donde:

m^o_{xilosa} = número de moles de xilosa presente inicialmente

m_{xilosa} = moles de xilosa después de reacción.

$m_{furfural}$ = moles de furfural después de reacción (suma de los moles de furfural presente en la fase orgánica y acuosa, respectivamente).

3.3.2 Reacción de hidrólisis y deshidratación de la biomasa del cardo mediante el empleo de ácido sulfúrico como catalizador

3.3.2.1 Acondicionamiento y caracterización de la biomasa del cardo

Tal como se ha comentado en los objetivos de este trabajo, la biomasa lignocelulósica que se empleó como materia prima de partida en este apartado fue la biomasa del cardo ("Cynara cardunculus"). Esta biomasa fue suministrada por la Universidad Complutense de Madrid y, previamente a su recepción, fue molturada y tamizada hasta un tamaño máximo de 1mm. En primer lugar, se determinó el contenido en agua de la biomasa de partida. Para ello, ca. 300 mg de biomasa húmeda se introdujeron en un matraz y se calentaron a 373K durante toda la noche. Así, el contenido en agua de la biomasa (8.70% en peso) se determinó por diferencia de pesada entre los pesos de biomasa húmeda y seca. El matraz que contiene la biomasa seca se tapa rápidamente para evitar su rehidratación.

También se llevó a cabo un análisis de los contenidos en carbohidratos de la biomasa del cardo con objeto de poder determinar los rendimientos a los diferentes productos. Este análisis se realizó en tres muestras de biomasa del cardo siguiente el procedimiento analítico descrito por el Laboratorio Nacional de Energía Renovable (NREL) para la "*Determinación de Lignina y Carbohidratos Estructurales en muestras de biomasa sólidas"* [1]. Este procedimiento emplea un proceso de hidrólisis en dos pasos para fraccionar la biomasa en formas que son más fácilmente cuantificables. Durante la hidrólisis,

los carbohidratos constituyentes de la biomasa se hidrolizan en sus correspondientes formas monoméricas que son ya solubles en el líquido de hidrólisis y se pueden medir por cromatografía de líquidos de alta resolución (HPLC). El procedimiento es el siguiente: en primer lugar, se pesa ca. 300 mg de biomasa del cardo en un reactor de vidrio de ca. 90 mL con tapón roscado de teflón y paredes gruesas (*Ace Pressure Tube*), previamente pesado y tarado. A continuación, se añaden ca. 3mL de una disolución de H_2SO_4 al 72% en peso y se agita muy bien durante 1 minuto con la ayuda de una varilla de vidrio con objeto de homogeneizar bien la mezcla. Posteriormente, el reactor se introduce en un baño con agua a 30ºC durante 60 minutos, agitando cada 5-10 minutos sin retirar el reactor del baño. Durante este período de tiempo tiene lugar la hidrólisis de los carbohidratos contenidos en la biomasa. Una vez completado el período de hidrólisis, se retira el reactor del baño y se diluye la mezcla ácida hasta una concentración del 4% añadiendo ca. 84 mL de agua desionizada mediante el empleo de una bureta. Seguidamente, se agita la mezcla con objeto de eliminar la separación de fases entre las dos concentraciones de ácido.

Paralelamente, se prepararon un set de patrones de azúcares (SRS) que serán sometidos también a condiciones ácidas con objeto de determinar las pérdidas debido a la destrucción de azúcares durante la hidrólisis con ácido diluido. Estos patrones deberían incluir todos los monosacáridos (glucosa, xilosa, galactosa, arabinosa y manosa) en concentraciones próximas a las de la muestra problema. Una vez pesadas las correspondientes cantidades de cada monosacárido, se añadieron 348 µL de H_2SO_4 al 72% y 10 mL de agua desionizada y esta mezcla se transfirió a un reactor de vidrio similar al empleado para la muestra de biomasa real. Ambos reactores de vidrio con muestras SRS y biomasa, respectivamente, se colocaron en un baño a 121ºC

durante 1 hora y, una vez transcurrida la reacción, se añadió el estándar interno (xilitol, ca. 100 mg) a cada reactor para su análisis posterior. Para ello, se tomaron alícuotas (ca. 10 mL) de ambos reactores y se neutralizaron con $CaCO_3$ hasta pH 5-6. Finalmente, los líquidos sobrenadantes se analizaron por cromatografía de líquidos para determinar su contenido en azúcares.

3.3.2.2 Análisis del contenido en carbohidratos de la biomasa del cardo

Como se ha comentado en el apartado anterior, antes de evaluar la actividad catalítica de la biomasa del cardo en presencia de ácido sulfúrico como catalizador, es necesario determinar su contenido en carbohidratos. Para el cálculo del contenido en carbohidratos se consideró la cantidad de agua presente en la biomasa húmeda.

El análisis de las muestras se llevó a cabo en un cromatógrafo de líquidos de alta resolución (HPLC) (Agilent 1200 Series), equipado con un detector de índice de refracción (RI) y una columna Aminex HPX-87P (300 X7.80 mm) (Phenomenex, USA) a 328K. Como fase móvil se emplea agua desionizada a una velocidad de flujo de 0.6 $ml \cdot min^{-1}$. Antes de efectuar dicho análisis, se tomó una alícuota de muestra de ca.10 mL y se filtró a través de un filtro de jeringa de nylon de 0.22 μm de diámetro de poro con objeto de eliminar la mayor parte de los productos sólidos. El análisis de cada muestra se llevó a cabo por duplicado y los porcentajes en masa de cada carbohidrato en la biomasa seca y húmeda, respectivamente, se determinaron a partir de las curvas de calibración obtenidas con las muestras de referencia.

3.3.2.3 Reactor de mezcla perfecta de vidrio

Las medidas de actividad catalítica de la reacción de hidrólisis y deshidratación de la biomasa del cardo se llevaron a cabo en el mismo sistema de reacción y bajo el mismo protocolo que el descrito en el apartado 3.3.1.1. En el reactor de vidrio se añadieron una disolución acuosa de biomasa al 4% en peso y una concentración determinada de H_2SO_4 como catalizador, ambos referidos a la fase acuosa.

3.3.2.4 Análisis de los productos de reacción

El análisis de los productos de reacción en este caso se hizo según el siguiente procedimiento. Una vez terminada la reacción, el reactor se saca del baño de aceite para su enfriamiento. En este caso, se determinó el contenido de los diferentes monosacáridos y el contenido en furfural, 5-hidroximetilfurfural (HMF) y ácido levulínico como productos de reacción. Una vez que se encuentra a temperatura ambiente, se añaden 50 mg de xilitol y 10 mg de ácido octanoico como estándares internos de las fases acuosa y orgánica, respectivamente y se agita durante varios minutos antes de dejarlas decantar. Una vez separadas las fases, se toman alícuotas de ambas fases y se filtran siguiente el mismo procedimiento explicado en la sección anterior.

El análisis de las fases acuosas de reacción se llevó a cabo en el mismo cromatógrafo de líquidos (HPLC) Agilent 1200 series empleado para los experimentos de deshidratación de xilosa. Para el análisis del contenido en azúcares en fase acuosa se empleó una columna de intercambio de iones Rezex Bio-Rad Aminex HPX-87P 300 x 7,8 mm y para el análisis de productos de reacción (furfural, HMF y ácido levulínico) en fase acuosa, una columna

también de intercambio de iones Rezex Bio-Rad Aminex HPX-87H 300 x 7,8 mm (ambas de Phenomenex). En el primer caso, agua desionizada se empleó como eluyente con un flujo de 0.6 ml·min^{-1} y a una temperatura de 328K, mientras que en el segundo caso una disolución 0.005M de H2SO4 a 328K con un flujo de 0.4 ml·min^{-1} fue elegido. En el caso de reacciones bifásicas agua-CPME, el análisis de los productos de reacción en la fase orgánica se llevó a cabo en un cromatógrafo de gases (GC) (Varian CP3800), mediante una columna capilar ZB-WAXplus (30m x 0.32 mm x 0.50 μm) con fase estacionaria de polietilenglicol conectada a un detector de ionización de llama (FID). De esta disolución, se inyecta 1 μL en el cromatógrafo. La temperatura del inyector es de 543K, la del detector de 553K y la del horno del cromatógrafo de 493K. Como gas portador se emplea una He.

La cantidad de carbohidratos y de productos de deshidratación presente en las mezclas de reacción se calcularon a partir de las correspondientes curvas de calibración corregidas con los estándares internos y los rendimientos a productos (Y_i) se calcularon empleando la ecuación 3.4.

$$Y_i \text{ (mol \%)} = \frac{m_{\exp(i)}}{m_{máxima\ (i)}}\ x100 \quad \textbf{\textit{Ecuación 3.4}}$$

donde:

m_{exp} (i) = masa de producto i presenta en la mezcla de reacción.

$m_{máxima}$ (i)= máxima cantidad de producto i que puede obtenerse desde la biomasa del cardo (calculados en base a los contenidos en carbohidratos presentes en la biomasa determinados según se ha explicado en la sección 3.3.2.1).

3.3.3. Reacción de deshidratación de xilosa mediante el empleo de nanocomposites APES- Si-APTES como catalizadores

3.3.3.1 Reactor de mezcla perfecta de vidrio

Las medidas de actividad catalítica se llevaron a cabo en el reactor discontinuo de vidrio descrito en el apartado 3.3.1.1, es decir, un reactor de vidrio de ca. 15 mL con tapón roscado de teflón (Ace Pressure Tube). Todos estas reacciones se realizaron en sistema bifásico agua:CPME. Previo a la reacción, se pasó un flujo de N_2 durante 10 minutos para desplazar el aire presente en el reactor. En una reacción típica, se añadieron al reactor 1.5 g de agua desionizada, 3.5 g de CPME (2.33 g CPME/g disolución acuosa), 150 mg de xilosa (10% en peso respecto al agua) y 75 mg de catalizador molido y tamizado a un tamaño inferior a 106 μm (radio másico catalizador:xilosa =0.5).Tras este proceso, el reactor se sumergió en un baño de aceite a 453K con agitación magnética a 1500 rpm, dando comienzo la reacción. Una vez transcurrido el tiempo deseado, la reacción se paró sumergiendo el reactor en agua fría.

En el capítulo 2, para realizar las medidas de reutilización se empleó de nuevo el mismo sistema de reacción como el descrito en el apartado 3.3.1.1 ya que este reactor puede ser acomodado fácilmente en el interior de una centrífuga, facilitando de este modo la separación del catalizador de la mezcla de reacción y por lo tanto su reutilización. En este caso se emplearon las mismas proporciones de todos los reactantes en un volumen total de 5 mL y se siguió el mismo método de análisis anteriormente explicado. La diferencia es que, una vez finalizada la reacción y analizada las fases, se somete a

centrifugación con objeto de recuperar el catalizador. El catalizador recuperado se sometió a sucesivas etapas de lavado-centrifugación en agua y CPME con el fin de eliminar la xilosa y restos de otros compuestos orgánicos que pueden haber quedados débilmente adheridos en la superficie del catalizador y pudieran interfieran en la estimación de las propiedades catalíticas de los ciclos sucesivos. Finalmente, el agua y el disolvente se separaban del catalizador por centrifugación y posterior secado a 348K bajo flujo de N_2.

3.3.3.2 Análisis de los productos de reacción

El análisis de los productos de reacción se hizo según el procedimiento descrito en el apartado 3.3.1.2.

3.3.4. Reacción de esterificación de ácido oleico con metanol mediante el empleo de nanocomposites APES-Si-APTES como catalizadores

3.3.4.1 Reactor de mezcla perfecta de vidrio

Las reacciones se llevaron a cabo en el reactor de vidrio descrito en el apartado 3.3.1.1, agitado magnéticamente a 1000 rpm y colocado en un baño de aceite precalentado a una temperatura de 333K. En un experimento típico, se añadieron al reactor 0.872 g de metanol, 2 g de aceite de girasol (relación molar metanol: aceite de 12), 0.1 g de ácido oleico (relación molar ácido oleico: aceite de 0.05) y 40 mg de catalizador previamente molturado y molido (relación molar catalizador: ácido oleico =0.4). Como se explicó anteriormente, la

reacción comienza en el momento en que se introduce el reactor en el baño con aceite y termina sumergiendo el reactor en agua fría.

3.3.4.2 Análisis de los productos de reacción

Una vez finalizada la reacción, se añadieron 0.1 g de etil palmitato disuelto en tetrahidrofurano (THF) como estándar interno y, después de agitar bien la disolución para disolver adecuadamente el estándar, la mezcla de reacción se centrifugó. Posteriormente, una alícuota de ca. 2 mL se tomó de la mezcla y se filtró a través de un filtro de poliértersulfona de 0.22 μm con objeto de eliminar restos de catalizador y otros productos sólidos que puedan formarse durante el transcurso de la reacción.

Los productos de reacción se analizaron empleando un cromatógrafo de líquidos (HPLC) Agilent 1200 series equipado con un detector de índice de refracción (RI) y una columna XDB- C18 (5μm, 4.6 x 150 mm) a una temperatura de 308 K. Como fase móvil se empleó una disolución al 5% en volumen de THF en acetonitrilo con un flujo de 0.6 $ml \cdot min^{-1}$.

3.3.5. Reacción de deshidratación de xilosa mediante el empleo de catalizadores basados en niobio

En el caso de la reacción de deshidratación de xilosa empleando catalizadores basados en niobio se emplearon dos sistemas catalíticos. Las medidas a bajas temperaturas se realizaron en un reactor de vidrio de 15 mL de capacidad (Ace Pressure Tube), descrito anteriormente. En el caso de los estudios de reutilización o de experimentos a temperaturas mayores se empleó un reactor de acero inoxidable a presión. La razón de esta elección en el caso de

las reutilizaciones es que este sistema permite la extracción del líquido reteniendo el catalizador en su interior con ayuda de un filtro. Por su parte, los experimentos de estabilidad en continuo a baja temperatura y para largos tiempos en corriente se llevaron a cabo empleando un reactor de lecho fijo en continuo.

3.3.5.1 Reactor de mezcla perfecta de vidrio

Las reacciones se llevaron a cabo en el reactor de vidrio descrito en el apartado 3.3.1.1. En un experimento típico, 4.5 % en peso de xilosa, 3% en peso de catalizador (relación másica xilosa: catalizador 0.67), ambos respecto a la fase acuosa total (5g), se añadieron al reactor. Una vez cargado el reactor, se sumergió en un baño de aceite a la temperatura deseada con agitación de 1500 rpm. La temperatura de reacción seleccionada fue de 403 K. En el caso de reacciones en mezclas bifásicas agua: CPME, 1.5 g de agua y 3.5 g de CPME (relación másica CPME: agua =2.33) se emplearon. En el caso de las reacciones llevadas a cabo en sistemas monofásicos agua/ γ-valerolactona y agua/isopropanol, una relación másica 1:9 y volumétrica del 20% de isopropanol en agua fueron empleadas, respectivamente.

El análisis de los productos de reacción se hizo según el procedimiento descrito en el apartado 3.3.1.2.

3.3.5.2 *Reactor de mezcla perfecta a presión*

El equipo de reacción empleado en los estudios de reutilización de los catalizadores fue un reactor de acero de Autoclave Engineers de 100 mL, equipado con un agitador mecánico MagneDrive (Figura 3.3).

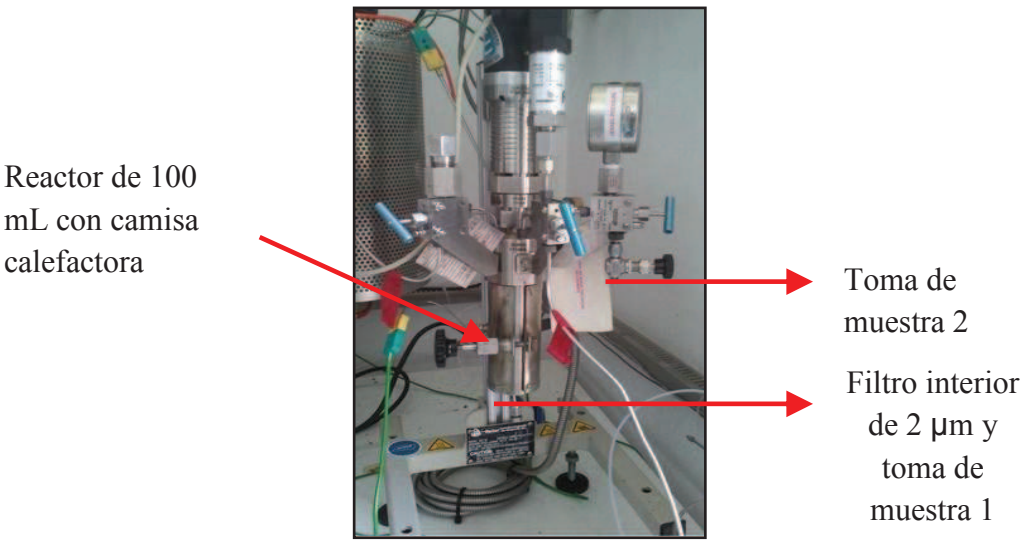

Figura 3.3. Reactor Autoclave Engineers

La elección de este reactor se basa en el hecho de que, además de que tiene mayor capacidad que el de vidrio (descrito en el *apartado 3.3.5.1*.) por lo que permite incorporar mayor cantidad de catalizador y aguanta presiones más elevadas, dispone de un filtro de acero inoxidable de 2 µm en el fondo del reactor a la salida del mismo que permite la toma de muestras sin pérdidas de catalizador, siendo de este modo fácilmente reutilizado sin pérdidas (toma de muestra 1 en *Figura 3.3*). El control de temperatura se realizó con una camisa calefactora controlada termostáticamente. Además, el reactor se fabricó también con la posibilidad de incorporar un tubo buzo de acero inoxidable en el interior

del reactor para la toma de muestra por la parte superior en caso de que el filtro inferior se taponara por deposición del catalizador (toma de muestra 2 en *Figura 3.3*). Este tubo buzo permite también la incorporación de un filtro de acero inoxidable de 2 μm con objeto de poder tomar muestra por la parte superior y evitar así pérdidas de catalizador durante los ciclos de reutilización.

En una reacción típica, se añadieron al reactor 500 mg de catalizador (5% en peso respecto la fase acuosa) y 1.5 g de D-(+)-xilosa (10% en peso respecto la fase acuosa) y se disolvieron en 50 g de mezcla agua-CPME en proporciones 1:2.33 en masa (15 g de disolución acuosa total y 35 g de CPME). Una vez cargado el reactor y previamente a dar comienzo al programa de temperatura, éste se purgó tres veces haciéndole pasar una corriente de N_2 con objeto de desplazar el aire del interior del reactor. Posteriormente, el reactor se presurizó hasta una presión interior de 5 bar y, en este momento, se lanzó el programa de temperatura con objeto de alcanzar la temperatura de reacción deseada. Estos experimentos de reutilización se llevaron a cabo a un temperatura de 453K y bajo agitación de 1000 rpm. El control de este equipo se puede hacer tanto de forma manual mediante controladores situados junto al reactor como por control remoto utilizando el software ADKIR instalado en un ordenador. Este software permite controlar totalmente el equipo a distancia y de manera programada, pudiendo realizar diferentes sesiones secuenciadas, modificando cualquier parámetro del equipo en cualquiera de ellas, tales como rampa de temperatura, temperatura del reactor etc.... En la *Figura 3.4* se muestra el esquema de una sesión de este programa.

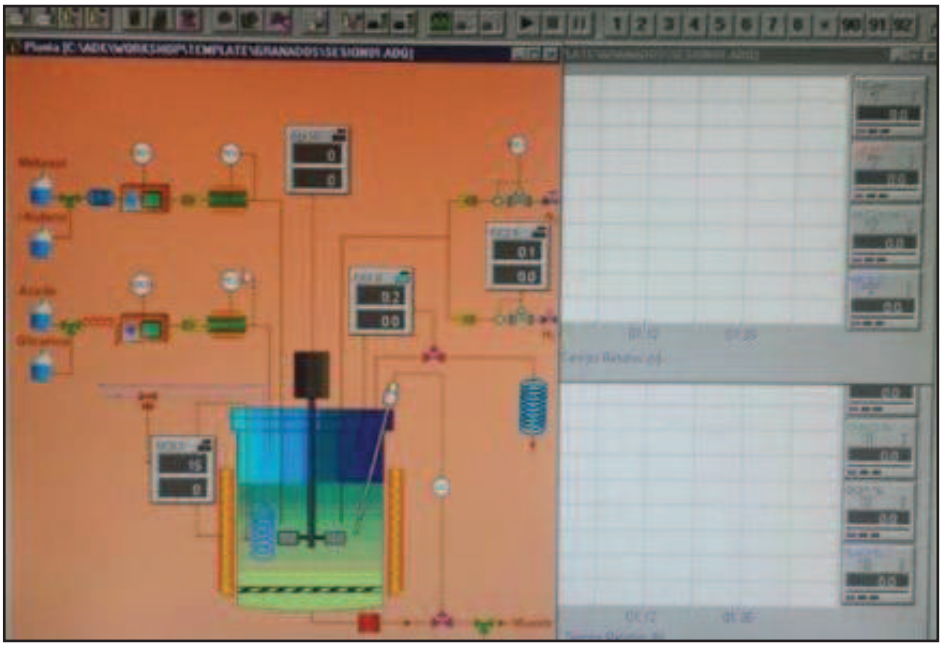

Figura 3.4. Esquema del programa de control remoto, software ADKIR, del equipo de reacción Autoclave Engineers

Una vez alcanzada la temperatura deseada, se inicia la agitación dando comienzo la reacción. Transcurrido el tiempo, la agitación se paró mediante parado de la agitación y el reactor se dejó enfriar hasta temperatura ambiente. Una vez frío, a través de las válvulas situadas o bien en la parte inferior del reactor o en la parte superior, se sacó el líquido de reacción para su análisis posterior, manteniendo el catalizador dentro del reactor para consecutivos ciclos.

El análisis de los productos de reacción se llevó a cabo de manera similar a como se ha explicado en la sección 3.3.1.2 pero a escala mayor. Una vez sacado todo el líquido del reactor, se añadieron 500 mg de D-(+)- glucosa y 500 mg de ácido octanoico como estándares internos para la fase acuosa y

orgánica, respectivamente. El análisis de las alícuotas de ambas fases se efectuó siguiendo el mismo procedimiento descrito en la sección 3.3.1.2.

3.3.5.1 Reactor de lecho fijo en continuo

Los experimentos de estabilidad en continuo para largos tiempos en corriente (hasta 100 h) se llevaron a cabo tanto en agua como en sistema monofásico agua/isopropanol. Estos experimentos se efectuaron en una línea de reacción en continuo como el que aparece en la Figura 3.5. Se trata de un sistema de reacción equipado con un reactor tubular de lecho fijo (1), una bomba (HPLC, Waters 501) (2) que permite el bombeo continuo de la disolución contenida en un matraz (3) por el lecho catalítico. Tanto el reactor como el precalentador (4) estaban introducidos en un horno con circulación de aire caliente forzada (5) que permitía mantener la temperatura constante durante la reacción en 403K. Además, la presión en el reactor se regulaba con una válvula micrométrica situada a la salida de la línea de reacción (6), manteniéndose entre 10 y 20 bar con objeto de evitar la evaporación del disolvente y la formación de burbujas dentro del lecho catalítico.

El reactor de lecho fijo se cargó con 1g de catalizador, previamente tamizado a un tamaño entre 25 y 45 mesh (700-350 μm) y colocado entre dos lechos de arena de 0.5 g cada uno (tamizado también con un tamiz de entre 45 y 60 mesh (350-250 μm)). Una solución acuosa de xilosa de concentración 0.3M se alimentaba continuamente al reactor de lecho fijo desde un matraz que lo contenía. La velocidad de flujo se mantuvo constante a 0.1 $ml \cdot min^{-1}$ obteniéndose así un tiempo de contacto de 10 $min \cdot g \cdot ml^{-1}$. Se eligió el flujo más bajo con objeto de tener el máximo tiempo de contacto posible. Una vez

iniciada la reacción, se dejaron pasar ca. 100 mL de disolución (~16h) antes de la primera toma de muestra con objeto de asegurar que se han alcanzado las condiciones de estado estacionario.

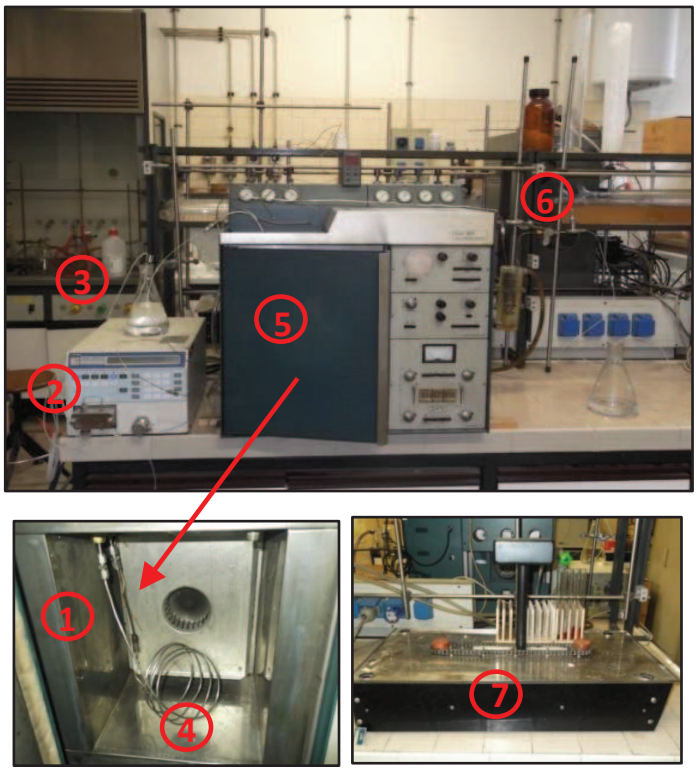

Figura 3.5. Sistema de reacción en continuo

Una vez alcanzadas las condiciones de estado estacionario, se tomaron diferentes muestras a diferentes intervalos de tiempo con objeto de medir la estabilidad del catalizador para largos tiempos en corriente. Estas muestras se iban recogiendo en un colector programado (7) y, una vez recogidas, se seleccionaron una serie de ellas para su análisis. El análisis de los productos de reacción se efectuó mediante cromatografía de líquidos de alta resolución

(HPLC) empleando un cromatógrafo compuesto de un inyector manual (Waters U6K), una bomba (wáter 510), un calentador (Water CHM) para la columna (Sugar Pack I) que opera a 90ºC y un detector de índice de refracción (Waters 410) para el análisis de los productos. Como fase móvil se empleó una disolución acuosa 10^{-4} M de Ca-EDTA.

3.4. Técnicas de caracterización de los catalizadores

En este apartado se describen las diferentes técnicas de caracterización que se han utilizado para obtener información acerca de las propiedades de los catalizadores sólidos preparados. El objetivo del análisis consiste en completar la información sobre los sólidos, con objeto de explicar su comportamiento catalítico y poder establecer relaciones estructura-actividad. En primer lugar se explica la importancia de la técnica aplicada y la información que nos proporciona, para a continuación hacer una breve descripción del fundamento teórico y del equipo empleado y el procedimiento experimental seguido para la obtención de los datos, incluyendo el pre-tratamiento realizado si es el caso. En la Tabla 3.2 se recoge un resumen de las técnicas utilizadas y la información proporcionada por cada una de ellas. Se ha preferido mantener la nomenclatura correspondiente a las siglas inglesas, puesto que son más conocidas.

Tabla 3.2. Resumen de las técnicas de caracterización empleadas.

Técnica de caracterización	Tipo de caracterización	Información proporcionada
Análisis químico elemental (microanálisis)	Análisis químico	Composición
Fluorescencia de Rayos X por Reflexión Total (TXRF)		Composición
Isotermas de adsorción de N_2	Textural	Área superficial, diámetro y volumen de poro
Difracción de rayos X (XRD)	Estructural	Fases cristalinas
Análisis termogravimétrico (TGA)		Cambio de peso
Resonancia Magnética Nuclear (NMR)		Estructura molecular
Espectroscopia fotoelectrónica de rayos X (XPS)	Superficial	Análisis cuali y semicuantitativo de los átomos superficiales
Espectroscopia Infrarroja por reflectancia difusa (DRIFT)		Detección de presencia de especies catalíticas
Adsorción-desorción volumétrica líquido-sólido		Acidez gracias a la adsorción de moléculas sonda

3.4.1 Análisis químico elemental

3.4.1.1 Análisis elemental (microanálisis) C, H, N, S

Los compuestos orgánicos se caracterizan por estar compuestos de carbono e hidrógeno, por lo que es extremadamente importante la determinación precisa de estos elementos. Además, si el objeto de estudio son los catalizadores basados en sílice y ácido poliestirensulfónico (APES), esta técnica resulta de gran ayuda para conocer el contenido en S de los mismos, ya que esto puede darnos idea de la cantidad de grupos sulfónicos presentes en el compuesto.

El principal método para la determinación de carbono, hidrógeno, nitrógeno y azufre, es la técnica de microcombustión [2]. Los analizadores elementales automatizados realizan la operación de manera programada para un carrusel de muestras y el seguimiento de la composición se hace con medidas *on-line* de los gases de combustión.

El microanálisis se basa en la oxidación total de la muestra (previamente desgasificada) mediante una combustión instantánea y completa con flujo de oxígeno puro a 1173K que transforma la muestra en productos de combustión (CO_2, H_2O, N_2 y SO_2), lo cuales, mediante un gas portador (Helio), son arrastrados hasta unos sensores individuales y selectivos para CO_2, H_2O y SO_2 por celdas de infrarrojos que aseguran una medición libre de interferencias y rápida, al realizarse al mismo tiempo que se está produciendo la combustión. Estos gases, posteriormente, son eliminados para poder medir el nitrógeno por termoconductividad diferencial. Sus principales aplicaciones son la determinación porcentual de carbono, hidrógeno, nitrógeno y azufre de gran variedad de compuestos tanto orgánicos, inorgánicos, farmacéuticos, plásticos,

productos agrícolas, suelos, etc. independientemente de su estado de agregación (sólidas, líquidas o viscosas). Mediante esta determinación se contribuye a la confirmación de la estructura de un compuesto, además de ser un criterio de pureza.

Para realizar los análisis se empleó un Analizador Elemental LECO CHNS-932 (Figura 3.6).

Figura 3.6. Analizador elemental *LECO CHNS-932.*

3.4.1.2 Fluorescencia de Rayos X por Reflexión Total (TXRF)

La técnica de Fluorescencia de Rayos X por reflexión Total (TXRF) se empleó para analizar la composición de los catalizadores basados en sílice y ácido poliestirensulfónico (capítulo 2 y 3), ya que el silicio no se detecta mediante la técnica anterior de microanálisis.

Se basa, en líneas generales, en el estudio de las emisiones de fluorescencia de rayos X generados después de la excitación de una muestra

mediante una fuente de rayos X. Los átomos presentes en la muestra analizada son excitados de modo que los electrones de las capas internas son arrancados o promocionados a niveles de energía superiores. Los electrones de otras capas minimizan su energía ocupando los huecos electrónicos que quedan libres, de modo que la energía asociada a dichas transiciones se re-emiten en forma de fotones. A estas emisiones se las conoce como emisiones de fluorescencia o radiación secundaria y presentan unas energías características del átomo que las genera y una intensidad que depende directamente de la concentración de dicho átomo en la muestra. El resultado es un espectro de dispersión de energía, donde aparecen simultáneamente todas las líneas asociadas a los elementos químicos presentes. Analizando la posición de los máximos de intensidad, se identifican los elementos presentes (Análisis Cualitativo), integrando cada uno de los perfiles elementales se obtienen sus proporciones másicas y añadiendo un elemento patrón de concentración conocida se obtiene la cuantificación de dichos elementos (Análisis Cuantitativo). Esta técnica es capaz de analizar cualitativa y cuantitativamente 75 elementos comprendidos entre el Si (Z=14) y el U (Z=92) tanto a nivel de mayoritarios (wt.%) como de elementos traza (ppb) dentro de un rango dinámico de 105.

Los análisis se llevaron a cabo en un espectrómetro Atomika 8030C FEI (Cameca, Alemania) equipado con un tubo de rayos X dual Mo/W operando a 3 kW y un monocromador multicapa. El detector de Si(Li) empleado posee un área activa de 80 mm^2 y una resolución de 150 eV a 5.9 keV (Mn Kα). Para el estudio cuantitativo se emplearon las líneas espectrales Kα del Si y S.

3.4.2 Caracterización textural: Isotermas de Adsorción de N_2

Esta técnica se empleó en la caracterización de los diferentes catalizadores preparados en el presente trabajo, aportando información sobre el área específica y tamaño de poro de los mismos. También sirvió para comprobar si el catalizador basado en sílice funcionalizada con grupos organosulfónicos perdía actividad en la reutilización por la modificación de su estructura porosa.

El procedimiento más extendido para analizar la estructura micro y mesoporosa de un catalizador sólido se basa en la determinación de las isotermas de adsorción-desorción de nitrógeno a su temperatura de ebullición (77 K) [2]. Se representa el volumen de nitrógeno adsorbido por gramo de catalizador frente a la presión de equilibrio, normalmente expresada como presión relativa (P/P_o), donde P_o es la presión de saturación del N_2 a 77 K. El análisis de la morfología de las ramas de adsorción-desorción de la isoterma da información acerca de la textura porosa, mientras que la superficie específica se determina por el método conocido como BET (Brunauer, Emmett y Teller) [3].

Las isotermas de adsorción se realizaron en un equipo TRISTAR 3000 de Micromeritics (Figura 3.7). Las muestras se desgasificaron previamente a 393 K durante 12 h en un sistema de vacío para la eliminación de contaminantes gaseosos y/o líquidos físicamente adsorbidos en poros y superficie externa. Para la adquisición y el análisis de los datos se emplearon las aplicaciones ASAP 2010 y Tristar 3000 respectivamente.

Figura 3.7. Micromeritics TRISTAR 3000.

3.4.3 Caracterización estructural

3.4.3.1 Difracción de rayos X (XRD)

El análisis por difracción de rayos X se aplicó a los catalizadores de niobio tanto másico como soportados ya calcinados, para determinar sus fases cristalinas presentes así como para dar una idea de la distribución de la fase de niobio activa en el soporte.

La técnica de difracción de rayos X está basada en el efecto de difracción de los rayos incidentes que poseen las sustancias cristalinas. Los átomos actúan como redes de difracción tridimensionales de rayos incidentes monocromáticos cuando la longitud de onda es del orden de la distancia entre átomos. En estas condiciones cada sustancia produce un difractograma único que puede ser empleado para su identificación. El fundamento teórico de la técnica se basa en la Ley de Bragg ($n\lambda=2\cdot d\cdot \text{sen}\theta$) [4]. El equipo empleado en los análisis es un difractómetro de Rayos X Policristal X´Pert Pro PANalytical, con una rendija automática y un filtro de níquel. La fuente de rayos X es de Cu-Kα

(λCu-Kα_1=0,15406 nm y λCu-Kα_2=0,154443 nm), con una relación Kα_1/Kα_2 de 0,5. Los difractogramas se registraron en la modalidad de pasos en un intervalo de ángulos de Bragg (2θ) entre 15º y 80º, paso de 0,02º y tiempo de acumulación de 1 segundo. Posteriormente, los difractogramas fueron analizados empleando el programa X'Pert HighScore Plus.

3.4.3.2 Análisis termogravimétrico (TGA)

Los análisis termogravimétricos permiten seguir la pérdida de peso que experimentan las muestras en función de la temperatura [2]. Esta técnica permite hacer un estudio de la estabilidad térmica de los catalizadores, por lo que sirve de ayuda en la selección de la temperatura de activación óptima, a la que se pierde el agua fisisorbida y otros compuestos orgánicos que puedan existir, sin que lo haga la fracción activa. Por tanto, estos análisis se realizaron en todos los catalizadores preparados, tanto en los basados en silicio APES como en los basados en niobio.

El procedimiento de análisis consiste en colocar la muestra en un platillo de una microbalanza que se introduce a su vez en un horno de alta precisión. El estudio se lleva a cabo en una atmósfera dinámica o estática de un gas determinado. Mientras se aumenta la temperatura, se registra la variación del peso en función de la temperatura o del tiempo teniendo en cuenta la velocidad de calentamiento del horno. Los análisis termogravimétricos se realizaron en un equipo Mettler Toledo TGA/SDTA 851e (Figura 3.8). La cantidad de muestra empleada fue de 30-50 mg en polvo. Las muestras se calentaron desde temperatura ambiente hasta 1073 K (rampa de calentamiento de 5 K· min-1) en atmósfera de aire sintético.

Figura 3.8. Mettler Toledo TGA/SDTA 851e.

3.4.3.3 Resonancia magnética nuclear (NMR)

Esta técnica tiene la ventaja de posibilitar el estudio de la estructura molecular de un catalizador polimérico.

El fenómeno de la resonancia magnética nuclear se basa en la interacción de los momentos magnéticos de los núcleos con campos magnéticos [2]. La interacción de los momentos con los campos creados por otros átomos, produce una modificación de los niveles de energía, la cual produce variaciones en la posición y forma de las líneas que componen el espectro. Esto hace posible identificar el entorno ocupado por los átomos en el interior del sólido. En particular, el efecto de apantallamiento producido por los electrones que rodean a cada núcleo, produce una variación de la frecuencia de resonancia que es característica del átomo en ese entorno. Esta variación es conocida como

desplazamiento químico y viene expresada en partes por millón respecto a la posición de la línea de un compuesto tomado como referencia.

En esta Tesis Doctoral se recogen los espectros NMR de ^{29}Si y ^{13}C de los catalizadores de APES/Si-APTES. Los espectros se registraron en un espectrómetro Bruker Avance 400-WB (Figura 3.9) operando a 500 MHz. Las muestras en polvo finamente molidas y secadas durante varios días a 373K en un horno, se transfirieron rápidamente a rores de ZrO_2 (4 mm) y fueron cerradas con tapones kel-F para prevenir la rehidratación del polímero. Las frecuencias de referencia empleadas para los núcleos de ^{29}Si y ^{13}C fueron 79.49 y 100.32 MHz, respectivamente. Los espectros ^{13}C NMR se adquirieron con una anchura espectral de 35 KHz mediante 1024 barridos y se registró con un tiempo de adquisición de 3,5 ms y un tiempo de relajación de 4 s. Los espectros ^{29}Si NMR se adquirieron como resultado de 1000 acumulaciones después de irradiación directa con una amplitud espectral de 15 KHz, un tiempo de relajación de 60 s y pulsos de π/4 a 50 KHz. La señal a -91.2 ppm fue usada como referencia secundaria relativa a la referencia primaria.

Figura 3.9. Espectrómetro Bruker Avance 400-WB

3.4.4 Caracterización superficial

3.4.4.1 Espectroscopia fotoelectrónica de rayos X (XPS)

Mediante esta técnica se analizaron los catalizadores sólidos de poliestireno litiados y silanizados (bloque de resultados 5) ya que nos ayuda a saber si hemos incorporado azufre y silicio en la estructura del catalizador y, sobre todo, el entorno químico de los mismos.

La espectroscopia fotoelectrónica de rayos X se basa en el efecto fotoelectrónico, que consiste en la emisión de electrones procedentes de los niveles internos de los átomos que se produce cuando una muestra se irradia con un haz de rayos X monoenergético de alta energía ($h \cdot \nu$). Cuando la energía del fotón excede la energía de ligadura del electrón excitado, este se emitirá con una cierta energía cinética, que debe cumplir la ecuación del efecto fotoelectrónico.

$$E_c = h \cdot \nu - E_b - \Phi$$

Donde E_c es la energía cinética del electrón emitido, $h \cdot \nu$ la energía de excitación, E_b la energía de ligadura del electrón excitado y Φ la función de trabajo del espectrómetro.

En un espectro XPS se representa la intensidad de flujo de electrones emitidos por la muestra en función de su energía cinética o, más frecuentemente, frente a la energía de ligadura de los mismos. Cada elemento se identifica por una energía de ligadura, aunque la información más importante se basa en que se puede obtener información sobre el entorno químico del átomo (estado de oxidación y coordinación) a partir de pequeñas variaciones de la misma. También pueden llevarse a cabo medidas cuantitativas ya que la

intensidad de una línea fotoelectrónica es proporcional al número de átomos de ese elemento presentes en la muestra. Esta técnica es **superficial**, ya que solamente los fotoelectrones procedentes de las capas más externas tienen oportunidad de escapar del material y llegar al detector [2].

Un problema específico del análisis de catalizadores no metálicos es el efecto de carga positiva de la muestra como resultado de la emisión continua de electrones y el desplazamiento a energías de ligadura mayores. Este efecto puede resolverse con el uso de un patrón interno si se supone que este desplazamiento es homogéneo en toda la muestra. Así, es habitual tomar como energía de ligadura de referencia la de los electrones 1s del carbono (284,6 eV) que se encuentran presentes en todas las muestras como consecuencia de la contaminación de hidrocarburos ambientales adsorbidos.

Los espectros fotoelectrónicos de rayos X se realizaron en un espectrómetro VG ESCALAB 200R (Fisons). Está equipado con un analizador semiesférico y cinco detectores tipo channeltron. Dispone de una fuente de emisión de rayos X de doble ánodo, Mg-Kα (hν =1253,6 eV) y Al-Kα (hν =1486,6 eV) que opera a 12kV y 10 mA. La presión de trabajo en la cámara es inferior a 5·10-8 mbar. Para evitar el contacto con la atmósfera, los sólidos se calcinaron en flujo de aire y argón tras lo cual fueron sumergidos en isooctano evitando cualquier contacto con el aire ambiente. El isooctano protege el catalizador de la hidratación y de la carbonatación debido al H_2O y CO_2 atmosféricos. Para hacer los análisis se tomó una muestra de la mezcla catalizador- isooctano y rápidamente se transfirió a un portamuestras de acero inoxidable que posee un hueco en forma de cilindro (8 mm de diámetro y 1 mm de altura). Mediante un disco de teflón la muestra se somete a presión a fin de proporcionar una superficie plana y homogénea. Además, esto evita el arrastre

de material en la etapa de desgasificación. Posteriormente el portamuestras se introdujo en la cámara de pretratamientos, donde se realizó la desgasificación previa de la muestra, eliminándose el isoocatano que empapaba los poros de la misma. Una vez alcanzado un alto vacío en la cámara de pretratamiento se transfirió la muestra a la cámara de análisis.

Las intensidades de los picos se evaluaron mediante el cálculo de la integral de cada pico después de suavizar y ajustar la curva experimental resultante a una combinación lineal de curvas lorentzianas y gaussianas de proporción variable. Los valores del factor de sensibilidad atómica se tomaron de Wagner *et ál.*[5].

3.4.4.2 Espectroscopia infrarroja por reflectancia difusa (DRIFT)

La técnica DRIFT se empleó para detectar la presencia de grupos sulfónicos y distinguir entre grupos aminos protonados y no protonados en los capítulos de esta tesis doctoral dedicados al estudio de los catalizadores de sílica- APES en diferentes reacciones (capítulos 2 y 3). La aparición de estos grupos daban cuenta de la presencia de interacciones electrostáticas entre el polímero y los grupos aminopropil presentes en la matriz de sílica.

El principio teórico de la técnica de espectroscopia infrarroja (IR) es la interacción de la muestra con radiación infrarroja incidente, que origina una transición entre niveles vibracionales de las moléculas de la muestra. Así, el espectro infrarrojo consiste en una representación gráfica de la intensidad de la radiación infrarroja medida en el detector en función de la longitud de onda, o más comúnmente, el número de onda ($\nu = c / \lambda = c \cdot \omega$, siendo ν la frecuencia, c

la velocidad de la luz, λ la longitud de onda y ω el número de onda). Se utiliza el método con transformada de Fourier que minimiza el tiempo de adquisición, a la vez que el interferómetro disminuye la relación señal/ruido.

El método de reflectancia difusa (Diffuse Reflectance IR Fourier Transform Spectroscopy DRIFTS) se basa en la medida de la radiación dispersada en todas las direcciones por las partículas de polvo orientadas al azar. Esta radiación se dirige al detector mediante un espejo elipsoidal [2]. La principal ventaja de esta técnica reside en la simplificación en la preparación de las muestras y la posibilidad de realizar tratamientos en flujo. El espectro producido por la reflectancia difusa no muestra una correlación directa entre la intensidad de las bandas y la concentración, ya que lo primero depende del camino óptico recorrido por la radiación. Por lo tanto, para experimentos cuantitativos se emplea la función de Kubelka-Munk:

$$f(\mathrm{R}_\infty) = \frac{(1-R_\infty)^2}{2R_\infty} = \frac{k}{s}$$

Donde $f(R\infty)$ es el espectro corregido y $R\infty$ es la relación entre el espectro de la muestra y la del compuesto de referencia (KBr, en nuestro caso). k es el coeficiente de absorción molar de la muestra y s es el coeficiente de dispersión.

Los espectros DRIFTS fueron obtenidos con un espectrómetro FTIR Nicolet 5700 equipado con una cámara de reflectancia difusa *in situ* y un detector de alta sensibilidad MCT-A (Figura 3.10). Todos los espectros fueron registrados con una resolución de 4 cm-1 con una acumulación de 128 barridos y presentados en unidades de Kubelka- Munk. Las muestras finamente divididas fueron colocadas en el portamuestras y pretratadas en corriente de Ar

(50 mL·min-1) a 373 K durante 60 minutos para eliminar el agua fisisorbida y otras moléculas de bajo punto de ebullición antes de coleccionar el espectro de la muestra a temperatura ambiente.

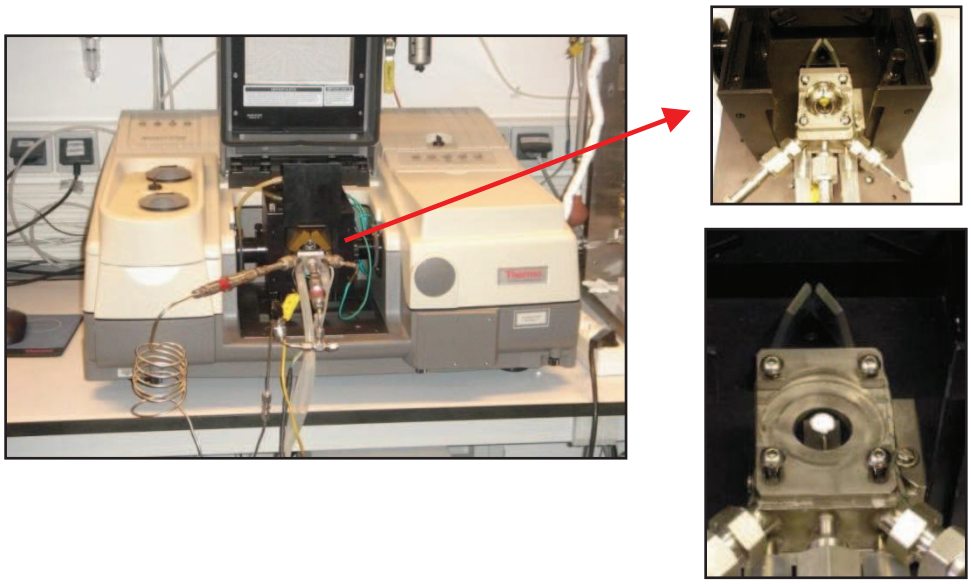

Figura 3.10. Espectrómetro FTIR NICOLET 5700 y detalle de la celda DRIFT.

3.4.4.3 Adsorción- desorción volumétrica líquido- sólido

Se trata de un método para la determinación de la acidez tanto efectiva (en un medio apolar y aprótico) como intrínseca, es decir, la acidez superficial que desarrolla el catalizador en un medio de reacción que posee una cierta polaridad y proticidad [6, 7]. Como se comentó anteriormente, en la caracterización de catalizadores basados en niobio resulta de gran importancia conocer la acidez efectiva "real" que presenta el catalizador en contacto con un determinado medio de reacción ya que esto podría ayudarnos a establecer

relaciones entre acidez superficial y actividad para reacciones llevadas a cabo en fase líquida y, así, explicar el mejor o peor comportamiento de un catalizador determinado en un disolvente dado.

Las medidas de acidez en fase líquida se llevaron a cabo a 303K en una línea en recirculación (Figura 3.11) que comprende un detector UV monocromático (Waters, 2487, λ= 254 nm) y una bomba de HPLC (Waters 515) que impulsa la solución a través de la muestra situada en una columna termostatizada. Dentro de la columna, la muestra (típicamente 0.1-0.3 g de muestra molida y tamizada a 45÷60 mesh) se coloca en un reactor de acero inoxidable (4 mm de diámetro interno y 8 cm de longitud) entre dos lechos de arena y, previamente a llevar a cabo las medidas de acidez, la muestra es activada a 350ºC durante 4 h en flujo de aire (8 $mL \cdot min^{-1}$) y, posteriormente, rellenada con el líquido que recircula. Para llevar a cabo las medidas de acidez, en el reservoir de que consta el sistema se van inyectando sucesivas dosis de diferentes concentraciones conocidas feniletilamina (molécula sonda) en ciclohexano (disolvente apolar y aprótico) o en los disolventes en los cuales se desea medir la acidez en una línea en la cual el disolvente continuamente va recirculando. Así, para cada inyección, la solución de feniletilamina (PEA) recircula hasta que se alcanza el equilibrio de adsorción, revelado por el alcance de una estabilidad en la señal del detector. De esta forma, conociendo la concentración de feniletilamina inyectada y la concentración en el equilibrio se puede conocer la cantidad de PEA adsorbida y, asumiendo una estequiometria 1:1 de adsorción de PEA en el sitio ácido, se puede determinar el número de sitios ácidos por unidad de masa de muestra a cada concentración de equilibrio, obteniéndose así las isotermas de adsorción donde se representa la

concentración de PEA adsorbido ($mmol \cdot g^{-1}$) frente a la concentración de PEA inyectado ($mol \cdot l^{-1}$).

Una vez recogida la primera isoterma de adsorción de PEA de la muestra fresca, se hace pasar disolvente puro durante 30 minutos a través de la muestra ya saturada y se recoge una nueva isoterma de adsorción. Por comparación de ambas isotermas, se determina el número total de sitios ácidos más fuertes.

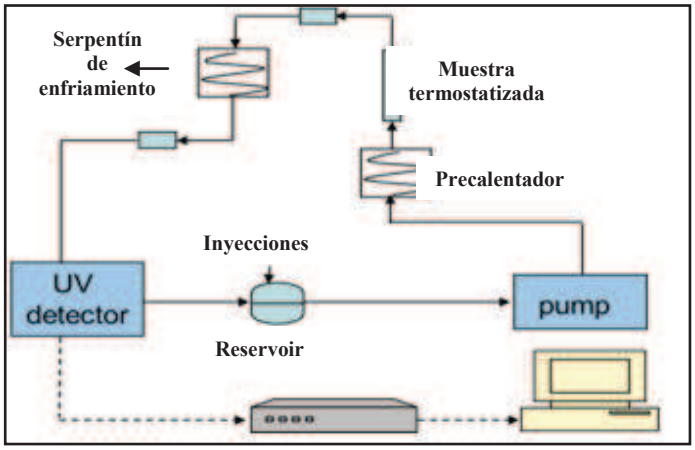

Figura 3.11. Esquema del sistema empleado para la determinación de la acidez en fase líquida

3.5. Bibliografía

[1] B.H. A. Sluiter, R. Ruiz, C. Scarlata, J. Sluiter, D. Templeton, D. Crocker, *National Renewable Energy Laboratory*, (2008).
[2] M. Faraldos, C. Goberna, *Técnica de análisis y caracterización de materiales*, CSIC, Madrid (2002).
[3] S. Brunanuer, P.H. Emmett, E. Teller, Journal of the American Chemical Society, 60 (1938) 309-319.
[4] R. Jenkins, R.L. Synder, *Introduction to X- Ray powder difractometry* (1995).
[5] C.D. Wagner, L.E. Davis, M.V. Zeller, J.A. Taylor, R.H. Raymond, L.H. Gale, 3 (1981) 211-225.
[6] P. Carniti, A. Gervasini, S. Biella, A. Auroux, Catalysis Today, 118 (2006) 373-378.
[7] P. Carniti, A. Gervasini, S. Biella and A. Auroux, Chemistry of Materials, 17 (2005) 6128-6136.

4. CYCLOPENTYL METHYL ETHER: A GREEN CO-SOLVENT FOR THE SELECTIVE DEHYDRATION OF LIGNOCELLULOSIC PENTOSES TO FURFURAL [a]

[a]**M.J. Campos Molina,** R. Mariscal, M. Ojeda, M. López Granados. Cyclopentyl methyl ether: A green co-solvent for the selective dehydration of lignocellulosic pentoses to furfural.

Bioresource Technology 126 (2012) 321–327

Outline

1. Introduction

Furfural constitutes a platform compound that can be converted into a wide range of industrially important chemicals. It is a versatile precursor to obtain a wide variety of chemical products through relatively simple reactions (more than 50 have been described in the literature) [1-3]. Nowadays, furfural is industrially produced from pentoses (xylose and arabinose) contained in lignocellulosic biomass by a cyclodehydration reaction catalyzed by acids [4, 5]. D-xylose is the more abundant pentose in most of lignocellulosic feedstocks [6]. The industrial process makes use of aqueous solutions of mineral acids as catalysts, typically H_2SO_4. The overall reaction involves the hydrolysis of pentosan into pentoses (mostly xylose) and the successive (much slower) dehydration of the latter to form furfural [7, 8].

During the xylose cyclodehydration reaction other non selective processes can take place, thus lowering the potential yield to the desired product (furfural). These side reactions include the condensation of furfural with intermediates of the pentose-to-furfural conversion (to give acetals and hemiacetals, and with derived oligomers (humins)), resinification reactions of furfural with itself producing oligomers and polymers [5, 9], and finally, fragmentation or decomposition reactions of xylose to other compounds such as glyceraldehydes, pyruvaldehydes, glycoaldehydes, acetol and lactic acid [4].

When these loss reactions take place significantly, the pentose molecules are not selectively converted to furfural and the final furfural yield is smaller compared to the theoretical one [5]. Different technological approaches have been proposed to cope with the furfural loss reactions such as SUPRATHERM and SUPRAYIELD processes [5]. Besides, very recently,

stripping with N2 under semi-batch conditions has been reported at lab-scale experiments, resulting in very high furfural yields (close to 100%) [10].

Furfural formation is performed normally in H_2O because it is the most common, greener and unexpensive solvent. Alternative solvents have been also investigated, as dimethyl sulfoxide (DMSO, results in S contamination) [7, 11], ionic liquids (very expensive and toxics) [12, 13] and supercritial CO_2 (very expensive technology) [14]. Some polymer adsorbents have been also proposed to be able to recover furfural from aqueous solutions [15].

Other interesting alternatives to prevent loss reactions of furfural are biphasic systems using H_2O and an organic solvent, as for instance, toluene, n-butanol, methyl isobutyl ketone (MIBK), and dichloromethane, which have been shown to improve furfural yields [7, 16-23]. The strategy is to make use of the partition coefficient of furfural between H_2O and the solvent, which reflects the higher affinity of furfural to the organic phase where, once it is transferred, cannot react because of the absence of catalyst (typically H_2SO_4) in this latter phase. The utilization of cyclopentyl methyl ether (CPME) as organic solvent in the selective dehydration of xylose to furfural is presented in this chapter. This solvent is a more environmentally friendly option than the solvents mentioned above, and it has been also tested as a good solvent in different organic reactions [24]. Besides, it presents other favorable properties, including low boiling point (379 K), low formation of peroxides, relative stability under acidic and basic conditions, low solubility in water coupled with a narrow range of explosion limits that render CPME an alternative to other ethereal solvents such as tetrahydrofurane (THF), 2-methyl tetrahydrofurane (2-MeTHF), dioxane or 1,2-dimethoxyethane (DME) [24] and to the other solvents mentioned above.

All these characteristics highlight CPME as a promising solvent for catalytic production of furfural from lignocellulose.

In this chapter, we report on the suitability of CPME as a solvent to improve the furfural yield from xylose and lignocellulosic biomass solutions. Particularly, the study has been conducted with lignocellulose from Cynara cardunculus (commonly known as cardoon). To the best of our knowledge, C. cardunculus lignocelluloses has never been reported as a feedstock for furfural production, unlike other feedstocks such us corncobs [25], oat hulls, bagasse [26], birch or beech wood [27], rice hulls [28], olive stones [29], etc. Cardoon is a dicotyledonous perennial herb [30] with a potential as lignocellulosic feedstock for biofuels and bio-based derived chemicals in Mediterranean climate regions [30, 31] owing to its relative high biomass productivities and adaptability to the hot and dry climate conditions of these areas. The specific conclusions drawn from this study can be extended to other lignocellulosic feedstocks.

2. Methods

2.1. Materials

D(+)-Xylose (≥99%), D(+)-glucose (99.5%), L(+)-(arabinose) (≥99%), D(+)-galactose (≥99%), D(+)-mannose for microbiology, D(+)-cellobiose for microbiology, xylitol (≥99%), 2-furaldehyde reagent grade (99%), anhydrous cyclopentyl methyl ether (CPME) (≥99.9%), octanoic acid (98%), 5-hydroxymethylfurfural (99%) and levulinic acid (98%) were purchased from Sigma–Aldrich. H_2SO_4 (96%) and pure NaCl were purchased from Panreac

Química S.A. All materials were used without further purification. Milli-Q H_2O was used for preparation of all aqueous solutions.

2.2. Catalytic dehydration of pure xylose

As a general procedure, the dehydration of xylose was performed in a 15 mL Ace sealed pressure glass reactor charged with an aqueous solution (5 g) of xylose (10 wt.%) and H_2SO_4 (1 wt.%). In those experiments including the addition of an organic solvent, the CPME/aqueous phase mass ratio was varied while maintaining constant the total weight (5 g), that is, a given fraction of the aqueous solution containing xylose and H_2SO_4 was withdrawn and the amount of CPME was incorporated. In those experiments conducted with NaCl addition, NaCl was added to the aqueous solution containing 10 wt.% xylose and 1 wt.% H_2SO_4 (referred to the NaCl free aqueous solution).

The reaction mixture was magnetically stirred (700 rpm) and placed in a preheated oil bath at a given temperature. The reaction was stopped by removing the reactor from the oil bath and rapidly cooled down by immersion in H_2O at room temperature. In the case of reactions conducted with CPME, aqueous and organic phases were separated by decantation. Then, internal standards (200 mg of D (+)-glucose for aqueous phase and 40 mg of octanoic acid for organic phase) were added to the quenched reaction mixtures and stirred to ensure their complete dissolution. Aliquots were taken (ca. 2 mL) from each phase and prior to analysis they were first filtered by a Varian CaptivaTM column (0.45 μm of pore diameter) to eliminate most of solids, and then filtered again through a syringe filter (polyethersulfone Millipore filter, 0.22 μm). Aqueous aliquots were analyzed with a HPLC chromatograph

Agilent 1200 series equipped with a refraction index (RI) detector and a Bio-Rad Aminex HPX-87H column (300 x 7.8 mm). A 0.005 M H_2SO_4 mobile phase was employed as eluent at 328 K and 0.4 mL/min flow rate. In the case of the organic aliquots, analyses were also conducted by HPLC using a XDB C-18 reverse phase column (Agilent). An 8:2 v/v CH_3OH:H_2O mobile phase was utilized at 313 K and 0.5 mL/min flow rate.

Xylose conversion, furfural yield and furfural selectivity values were based on the initial concentration of monosaccharide and calculated as:

$$\text{Xylose conversion (mol\%)} = \frac{m^o_{xyl} - m_{xyl}}{m^o_{xyl}} x100 \quad \textbf{\textit{Equation 4.1}}$$

$$\text{Furfural yield (mol\%)} = \frac{m_{fur}}{m^o_{xyl}} x100 \quad \textbf{\textit{Equation 4.2}}$$

$$\text{Furfural selectivity (mol\%)} = \frac{m_{fur}}{m^o_{xyl} - m_{xyl}} x100 \quad \textbf{\textit{Equation 4.3}}$$

where m^o_{xyl} refers to the number of xylose moles present initially, and m_{xyl} and m_{fur} refers respectively to the moles of xylose and furfural in the reaction mixture after a specific time. It is important to bear in mind that when an organic solvent is added, furfural appears in both the aqueous and organic phases, although mainly in the organic phase. Therefore, m_{fur} is the sum of the furfural moles present in both phases.

2.3. Cardoon biomass conditioning, characterization and catalytic dehydration of carbohydrates

C. cardunculus biomass was ground and sieved to a maximum size of 1 mm. To determine the water content, 300 mg of wet biomass was introduced in a flask and heated at 373 K overnight. Water content (8.70 wt.%) was determined by difference between the wet and dry weights. To prevent any rehydration, the flask containing the dry sample was capped.

The analysis of the carbohydrates content in C. cardunculus biomass is required to determine the yields to the different products. The analysis was conducted in three samples of cardoon biomass following the analytical procedure of the National Renewable Energy Laboratory ‘‘Determination of Structural Carbohydrates and Lignin in Biomass’’. For calculation of carbohydrates content, the amount of H_2O in wet biomass was considered. A HPLC Agilent 1200 series chromatograph equipped with a RI detector and an Aminex HPX-87P column (Phenomenex, USA) was used for the quantitative analysis of carbohydrates. Deionized H_2O was used as the mobile phase at a flow rate of 0.6 mL/min. Each biomass sample was analyzed by duplicate experiments for glucose, xylose, galactose, arabinose and mannose. The mass percentage of each carbohydrate in dry biomass was determined from calibration curves obtained with reference samples and corrected with an internal standard (xylitol). The average values of polysaccharides are glucan (37%), xylan (15%), galactan (4%), arabinan (1%) and mannane (1%), and they are similar to those reported elsewhere [32]. Lignin, ashes, proteins, and other minor components are also present in the biomass [32].

As a general procedure, the dehydration experiments of cardoon biomass were performed in a sealed pressure glass reactor (see Section 2.2) charged with a 4 wt.% biomass aqueous solution and with a given concentration of H_2SO_4 as catalyst, both referred to aqueous phase. The experiments were carried out at a given temperature and under magnetic stirring (700 rpm). Experiments with CPME and/or NaCl addition were also conducted as in previous tests with xylose.

The reaction was stopped after a specific time by removing the reactor from the oil bath and subsequent immersion in H_2O at room temperature. In the case of experiments with CPME, two phases were separated by decantation. In the reaction mixture obtained after reaction, the content in the different monosaccharides, furfural, 5-hydroxymethylfurfural (HMF) and levulinic acid were determined. The latter two products arise from the dehydration of hexoses present both in the hemicellulose and cellulose. Our main interest is on furfural production, but the HMF and levulinic acid yields are also provided. All reaction samples were mixed with an internal standard (50 mg xylitol for aqueous phase; 10 mg octanoic acid for organic phase) and aliquots from both phases were taken and filtered as explained in the previous section. The aqueous samples were analyzed with a HPLC Agilent 1200 series chromatograph equipped with a RI detector. Two columns were used for analysis of aqueous phase: Bio-Rad Aminex HPX-87P (300 mm x 7.8 mm pre-packed column) for analysis of sugars content and Bio-Rad Aminex HPX-87H (300 x 7.8 mm pre-packed column) for analysis of content of furfural, HMF and levulinic acid in aqueous phase. Milli-Q H_2O was employed as eluent (328 K, 0.6 mL/min) for carbohydrates analysis, while a 0.005 M H2SO4 mobile phase (328 K, 0.4 mL/min) was used for the analysis of furfural, HMF and levulinic

acid. In the case of reactions with CPME, the concentration of products (furfural, HMF and levulinic acid) in the organic phase was determined with a gas chromatograph (Varian CP-3800) equipped with a ZBWAXplus column (30 m x 0.32 mm x 0.25 lm) and a flame ionization detector (FID).

The amount of carbohydrates and dehydration products present in the reaction mixtures were calculated from calibration curves corrected with internal standards, and product yields (Y_i) were calculated as follows:

$$Y_i(\%) = \frac{m_{exp}(i)}{m_{máx}(i)} x100$$

where m_{exp} (i) refers to the mass of the product i present in the reaction mixture and $m_{máx}$ (i) refers to the maximum amount of product i that can be obtained from cardoon biomass. The latter amounts were calculated based on the content reported above and taking into account that furfural arises from pentoses (C5 carbohydrates) and HMF and levulinic acid from hexoses (C6 carbohydrates) and that those contents are referred to dry mass whereas the biomass used in the catalytic experiments was wet and contains 8.7 wt.% H_2O.

3. Results and discussion

3.1. Dehydration of xylose to furfural

Before conducting the experiments with cardoon biomass, a preliminary investigation was carried out with aqueous solutions of xylose. The effect of the addition of CPME on xylose transformation was first investigated. The study was also extended to the addition of NaCl to the reaction mixture, because it

has been previously shown that the addition of different salts (KCl, NaCl, $CaCl_2$, $MgCl_2$ or $FeCl_3$) to the reaction mixture exhibits a positive effect on the xylose conversion to furfural [23, 33-35]. The reasons for this behavior it is not clear yet. *Marcotullio et al*. suggested that Cl^- favors the selective path to furfural through the formation of the 1,2 enediol intermediate [33, 34]. Among the different metal halides that have demonstrated this effect, NaCl has been selected in this thesis because of its accessibility and low price.

3.1.1. Effect of the incorporation of CPME on furfural yield.

As indicated earlier, it is well known that the presence of an organic solvent increases the selectivity to furfural due to the extraction of furfural by the organic solvent, thus preventing undesired furfural secondary reactions occurring in the aqueous phase. Hence, the effect of the addition of different amounts of CPME to the aqueous xylose solution was first studied. These experiments were conducted at 433 K for 120 min by varying the amount of CPME added to the reaction mixture (5 g of total solution) and keeping constant the other reactions conditions (1 wt.% H_2SO_4 and 10 wt.% xylose in the aqueous phase). The results are summarized in Figure 4.1. The addition of CPME results in a slight increase of the xylose conversion from 48% without CPME up to 61% for a CPME/aqueous phase mass ratio = 0.67 (2 g CPME). For larger CPME concentrations, xylose conversion remains rather constant. The furfural yield and consequently the furfural selectivity improve in a continuous manner. An optimization work would be required for selecting the optimum CPME amount to achieve the maximum furfural yield and

productivity, but for the general purpose of this thesis, a CPME/aqueous phase mass ratio = 2.33 was selected for further experiments. This amount of CPME was selected because although larger CPME concentration would result in higher furfural yields, the amount of aqueous solution, and therefore of xylose, would be in practice very small.

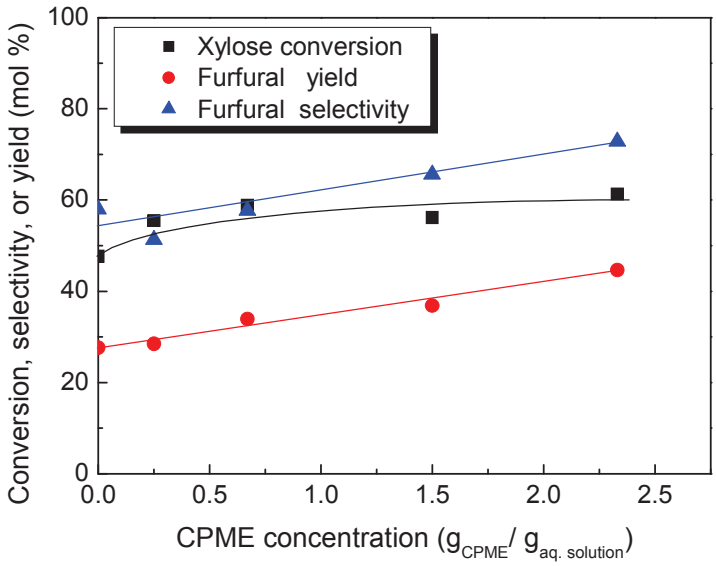

Figure 4.1. Effect of the addition of different amounts of CPME on xylose conversion (■), furfural yield (●), and furfural selectivity (▲). Reaction conditions: 1 wt.% H_2SO_4 and 10 wt.% xylose in aqueous phase, 433 K, 120 min.

Figure 4.2 shows the temperature effect (423–453 K) on xylose dehydration to furfural (60 min reaction) without CPME and with a CPME/aqueous phase mass ratio equals to 2.33 (3.5 g CPME). Figure 4.2 clearly shows that xylose conversion and furfural yield are larger in the

presence of CPME in the temperature range here studied. Thus, at 453 K, furfural yield reaches a value close to 60% at ~85% xylose conversion, whereas for the CPME free system, these values are 40 and 75%, respectively.

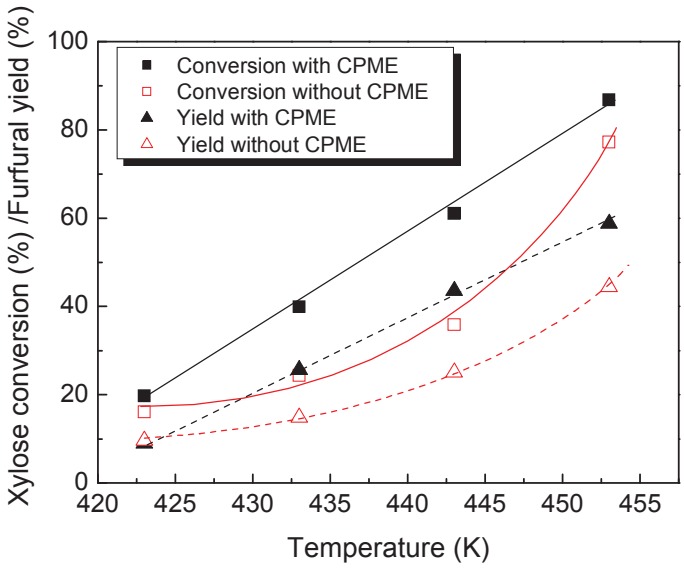

Figure 4.2. Temperature effects on xylose conversion without (□) and with (■) CPME addition and on furfural yield without (Δ) and with (▲) CPME. Reaction conditions: 1wt.% H_2SO_4, 10 wt.% xylose, CPME/aqueous phase mass ratio = 2.33, 60 min reaction.

3.1.2. Effect of the simultaneous presence of CPME and NaCl on furfural yield

Since it has been demonstrated that NaCl addition results in a substantial improvement of the furfural formation rate, it was decided to explore the simultaneous addition of CPME and NaCl to the reaction mixture and find out

whether CPME maintains its positive effect in the presence of NaCl. First, the dependence of xylose conversion and furfural yield on the NaCl concentration was investigated. The amount of NaCl added to aqueous solution was changed while keeping constant the rest of reaction conditions (1 wt.% H_2SO_4 and 10 wt.% xylose referred to aqueous solution, 5 g total aqueous solution, 433 K, 20 min). For these experiments, the addition of NaCl is expressed as weight of NaCl added per weight of aqueous solution containing xylose and H_2SO_4 (free of NaCl). Figure 4.3 clearly shows that the addition of NaCl up to a value of 0.3–0.4 g NaCl/g aqueous solution increases both xylose conversion and furfural yield. Further additions of NaCl do not result in faster reaction rates.

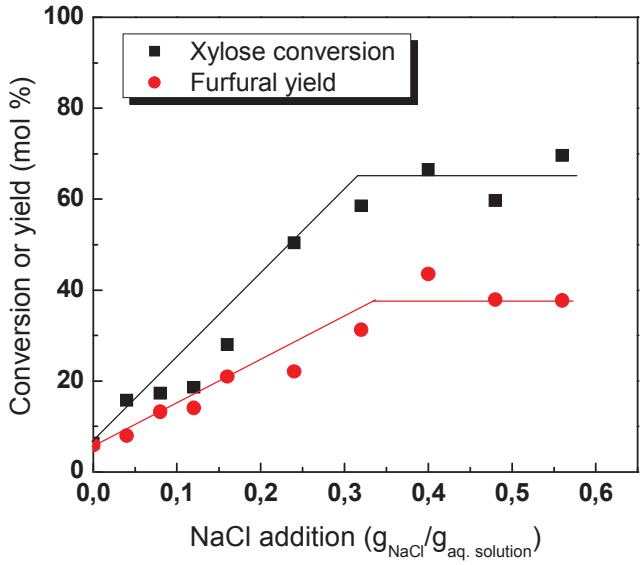

Figure 4.3. Effect of NaCl concentration on xylose conversion (■) and furfural yield (●). Reaction conditions: 1 wt.% H_2SO_4 and 10 wt.% xylose, 433 K, 20 min.

The next step was to study the effect of CPME addition to an aqueous solution containing 0.33 g NaCl per gram of aqueous solution. The rest of the reaction conditions (1 wt.% H_2SO_4 and 10 wt.% xylose referred to NaCl free aqueous solution, 5 g total reaction mixture, 433 K, and 20 min reaction time) were maintained. Figure 4.4 clearly evidences that the addition of CPME does not result in an increase of the reaction rate of xylose transformation (actually there is a slight decrease in xylose conversion from ca. 80% to 75% when CPME is added at a CPME/aqueous phase mass ratio of 4). In contrast, the yield to furfural continuously increases upon CPME incorporation (and consequently so does the furfural selectivity), counteracting the lower conversion values. As observed, the selectivity increases continuously, reaching near 90% for the higher CPME concentration (4 g CPME/g aq. solution). It must be also stressed that the selectivity to furfural reaches a value above 80% for a CPME/aqueous phase mass ratio equal to 2.33.

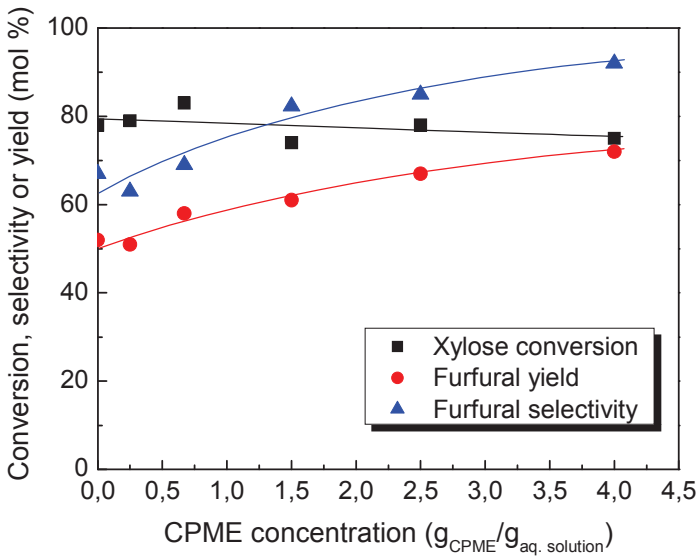

Figure 4.4. Effect of CPME/ addition on xylose conversion (■) furfural yield (●) and selectivity to furfural (▲) in the presence of NaCl. Reaction conditions: 0.33 $g_{NaCl}/g_{aq.\ solution}$, 1wt.% H_2SO_4 and 10 wt.% xylose referred to the aqueous phase, 5 grams of total solution, 433 K, 20 min.

Table 4.1 summarizes the effect of CPME and NaCl addition on the intrinsic furfural formation rate or turnover frequency (TOF, expressed as $mol_F \cdot mol_{H+}^{-1} \cdot s^{-1}$) at 433 K. This figure clearly demonstrates that the simultaneous presence of CPME and NaCl in the reaction mixture results in a remarkable improvement of the furfural formation rate with respect to the individual addition of CPME or NaCl.

Catalytic tests co-adding toluene and NaCl under the reactions conditions indicated in Table 4.1 were also conducted with the intention of

comparing the behavior of CPME with toluene (results not shown here). Toluene has been selected because is a widely used co-solvent for xylose cyclodehydration to furfural [4]. It was found that CPME compares well with toluene since similar furfural formation rates are obtained for both solvents. It was also found that, as for toluene, approximately 93% of the furfural is concentrated in the CPME.

Table 4.1. Comparison of the intrinsic furfural formation rates (expressed as TOF) determined at different reaction conditions: 1 wt.% H_2SO_4 and 10 wt.% xylose in the aqueous phase, 433 K, 20 min, CPME/aqueous phase mass ratio= 2.33, NaCl/aqueous phase mass ratio = 0.33.

Furfural formation rate · 10^3 ($mol_F \cdot mol_{H+}^{-1} \cdot s^{-1}$)	Without NaCl	With NaCl
Without CPME	1.5	2.8
With CPME	2.0	3.6

3.2. Furfural from Cynara cardunculus biomass

As demonstrated in Section 3.1, the simultaneous presence of CPME and NaCl in the reaction mixture results in a remarkable improvement of the furfural yield and selectivity. These results encouraged us to investigate the effect of CPME and NaCl with real biomass. In a first set of experiments, the effect of CPME addition to reaction mixture on the furfural production from cardoon biomass was explored, and in further experiments, the effect of co-adding NaCl and CPME was investigated.

3.2.1 Effect of CPME addition on furfural yield

Cardoon biomass hydrolysis and subsequent dehydration of hemicellulosic pentoses to furfural were conducted in the absence and in the presence of CPME. First, a series of kinetic experiments were conducted at 443 K and 4 wt.% biomass with respect to water phase (Figure 4.5a). In a second series, CPME was incorporated to the reaction mixture at CPME/aqueous phase mass ratio = 2.33 (Figure 4.5b), similarly to those previous experiments with xylose solutions. In addition to xylose (C5 monosaccharide), cardoon biomass also contains significant amounts of C6 monosaccharides (hexoses) in hemicellulose and cellulose components. Consequently, HMF and levulinic acid may be also produced as a result of dehydration reactions of these hexoses. It is must be borne in mind that the reported yield values to different products refers here to the maximum theoretical amount that can be produced from cardoon biomass according to its composition (Table 4.1). Thus, yield to furfural refers to the maximum amount that can be produced from pentoses contained in cardoon biomass. The glucose and their derived products, levulinic acid and HMF, very likely arise mainly from the hemicellulose as theirs yields are rather low throughout all the reaction times investigated. For longer reaction time, the hemicellulose has been extensively hydrolyzed.

A comparison between the results displayed in Figure 4.5a and b indicate that CPME does not exhibit any remarkable effect on the rates of C5 and C6 carbohydrates released from hemicellulose, as well as on the rates of HMF and levulinic acid formation. However, there is a clear positive effect on the furfural yield, especially at longer reaction times, where measured yield to furfural is close to the maximum achievable amount. These results clearly evidence that when CPME is present, furfural is rapidly transferred to the

organic phase, preventing the non-selective furfural degradation reactions (formation of humins and furfural polymerization) and leading to furfural yield close to the maximum that can be theoretically achievable. In contrast, in the absence of CPME, those non selective reactions of furfural are not inhibited, resulting in furfural yields lower than 60%.

3.2.2 Effect of the simultaneous presence of CPME and NaCl on furfural yield

In this series of experiments, the effects of the simultaneous presence of NaCl and CPME on the formation of furfural from C5 sugars present in cardoon lignocellulose are investigated. Figure 4.6a and b compare respectively cardoon biomass hydrolysis and subsequent carbohydrates dehydration without and with CPME addition and using NaCl-containing biomass solutions (NaCl/aqueous phase mass ratio = 0.4).

First, the results obtained when NaCl is incorporated to a CPME free reaction mixture (Figure 4.6a) are evaluated. A comparison with the data presented in Figure 4.5a (NaCl free) shows that NaCl addition has a remarkable effect on the release of C5 carbohydrates from hemicellulose and consequently, on the reaction rate of furfural formation. A significantly shorter reaction time (30 vs. 240 min.) is now required to achieve a maximum in the furfural yield that can be reached in the absence of CPME (close to 60%). Longer reaction times result in the degradation of furfural and in the decline on the furfural yield. Another remarkable result is that NaCl also favors the cellulose depolymerization to glucose and its transformation to levulinic acid (such products were barely observed in Figure 4.5a).

The effect of simultaneous addition of CPME and NaCl on the furfural formation is shown in Figure 4.6b. It can be noticed that the CPME presence exhibit two very positive effects: (i) the furfural yields are close to 100%, and (ii) longer reaction times do not result in the degradation of furfural. Indeed, even after 240 min of reaction, furfural yield is still close to 100%, what indicates that CPME addition not only favors high furfural selectivity, but also prevents furfural degradation by keeping it in the CPME phase. It is also important to stress that at short reaction times (no longer than 30 min.), it is possible to selectively transform the hemicellulosic C5 carbohydrates to furfural, whereas the cellulose-derived glucose is neither released nor dehydrated to levulinic acid or HMF.

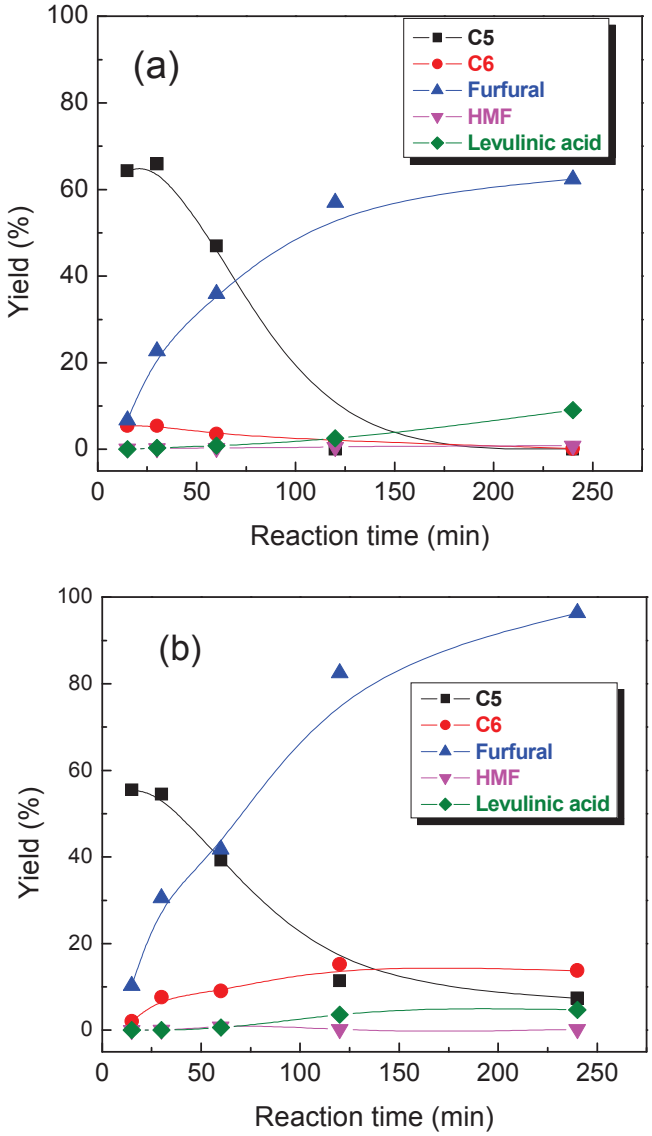

Figure 4.5. Yield to soluble hexoses (C6), pentoses (C5), furfural, HMF and levulinic acid as a function of reaction in the absence of CPME (a) and in the presence of CPME (b, CPME/aqueous phase ratio = 2.33). Reactions conditions: 4 wt.% biomass and 1 wt.% H_2SO_4 with respect to the aqueous phase, 5 g total reaction mixture, 443 K.

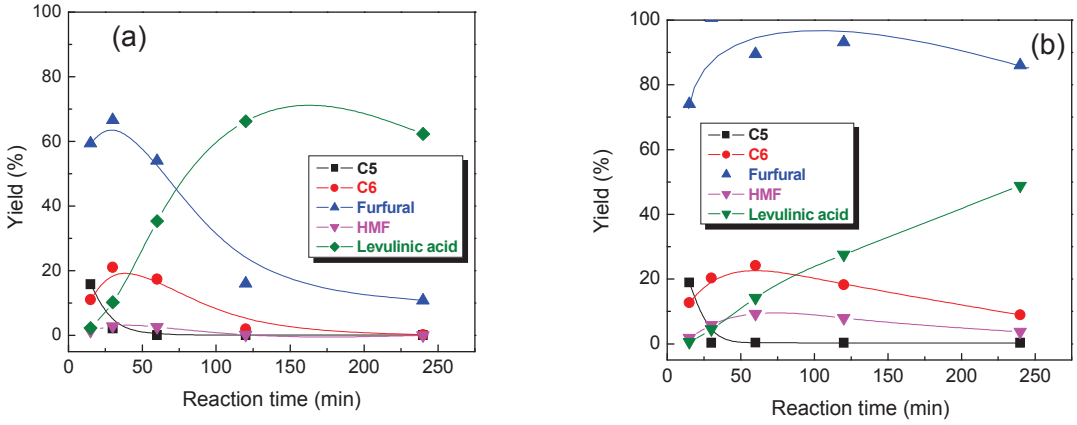

Figure 4.6. Yield to soluble hexoses (C6), pentoses (C5), furfural, HMF and levulinic acid as a function of reaction time from NaCl-containing cardoon biomass solutions in the absence of CPME (a) and in the presence of CPME (b, CPME/aqueous phase ratio = 2.33). Reactions conditions: 4 wt.% biomass and 1 wt.% H_2SO_4 with respect to the aqueous phase, NaCl/aqueous phase mass ratio = 0.4, 5 g total reaction mixture, 443 K.

4. Conclusions

The biphasic system H_2O/CPME using H_2SO_4 as catalyst allows the selective conversion of lignocellulosic pentoses into furfural, improving the overall furfural yield up to values near 100%. If the CPME effect is combined with NaCl addition, the reaction rate of furfural formation from hemicellulosic pentoses is notably accelerated and much shorter reaction times are required to produce furfural at such high yields. The NaCl results also in a remarkable acceleration of cellulose hydrolysis to glucose and its subsequent dehydration products. Reaction time can be adjusted to achieve the selective transformation of pentoses while preventing the transformation of cellulosic glucose.

5. Bibliography

[1] B.G. Kamm, P.R.; Kamm, M., Biorefineries (2006).
[2] I. Sádaba, S. Lima, A.A. Valente, M. López Granados, Carbohydrate Research, 346 (2011) 2785-2791.
[3] N. Alonso-Fagúndez, M.L. Granados, R. Mariscal, M. Ojeda, ChemSusChem, 5 (2012) 1984-1990.
[4] R. Karinen, K. Vilonen, M. Niemela, ChemSusChem, 4 (2011) 1002-1016.
[5] K.J. Zeitsch, The Chemistry and Technology of Furfural and Its Many By-products,Sugar Series,vol. 13, Elsevier, The Netherlands,2000.
[6] A.S. Mamman, J.M. Lee, Y.C. Kim, I.T. Hwang, N.J. Park, Y.K. Hwang, J.S. Chang, J.S. Hwang, Biofuels, Bioproducts and Biorefining, 2 (2008) 438-454.
[7] A.S. Dias, M. Pillinger, A.A. Valente, Journal of Catalysis, 229 (2005) 414-423.
[8] X. Shi, Y. Wu, H. Yi, G. Rui, P. Li, M. Yang, G. Wang, Energies, 4 (2011) 669-684.
[9] S.J. Dee, A.T. Bell, ChemSusChem, 4 (2011) 1166-1173.
[10] I. Agirrezabal-Telleria, A. Larreategui, J. Requies, M.B. Güemez, P.L. Arias, Bioresource Technology, 102 (2011) 7478-7485.
[11] E. Lam, E. Majid, A.C.W. Leung, J.H. Chong, K.A. Mahmoud, J.H.T. Luong, ChemSusChem, 4 (2011) 535- 541.
[12] J.B. Binder, J.J. Blank, A.V. Cefali, R.T. Raines, ChemSusChem, 3 (2010) 1268-1272.
[13] C. Sievers, I. Musin, T. Marzialetti, M.B.V. Olarte, P.K. Agrawal, C.W. Jones, ChemSusChem, 2 (2009) 665-671.
[14] Y.C. Kim, H.S. Lee, Journal of Industrial and Engineering Chemistry, 7 (2001) 424-429.
[15] K. Jerˇábek, L. Hanková, Z. Prokop, Reactive Polymers, 23 (1994) 107-112.
[16] J. Zhang, J. Zhuang, L. Lin, S. Liu, Z. Zhang, Biomass and Bioenergy, (2012).
[17] J.N. Chheda, Y. Román-Leshkov, J.A. Dumesic, Green Chemistry, 9 (2007) 342-350.
[18] H. Amiri, K. Karimi, S. Roodpeyma, Carbohydrate Research, 345 (2010) 2133-2138.

[19] R. Weingarten, J. Cho, W.C. Conner Jr, G.W. Huber, Green Chemistry, 12 (2010) 1423-1429.
[20] S. Lima, A. Fernandes, M.M. Antunes, M. Pillinger, F. Ribeiro, A.A. Valente, Catalysis Letters, 135 (2010) 41-47.
[21] C. Moreau, R. Durand, D. Peyron, J. Duhamet, P. Rivalier, Industrial Crops and Products, 7 (1998) 95-99.
[22] M.L. Granados, A.C. Alba-Rubio, I. Sádaba, R. Mariscal, I. Mateos-Aparicio, A. Heras, Green Chemistry, 13 (2011) 3203-3212.
[23] T.S. Hansen, J. Mielby, A. Riisager, Green Chemistry, 13 (2010) 109-114.
[24] K. Watanabe, N. Yamagiwa, Y. Torisawa, Organic Process Research and Development, 11 (2007) 251-258.
[25] W. Dedsuksophon, K. Faungnawakij, V. Champreda, N. Laosiripojana, Bioresource Technology, 102 (2010) 2040-2046.
[26] A. Singh, K. Das, D.K. Sharma, Industrial and Engineering Chemistry Product Research and Development, 23 (1984) 257-262.
[27] X. Lu, K. Yamauchi, N. Phaiboonsilpa, S. Saka, Journal of Wood Science, 55 (2009) 367-375.
[28] H.D. Mansilla, J. Baeza, S. Urzúa, G. Maturana, J. Villaseñor, N. Durán, Bioresource Technology, 66 (1998) 189-193.
[29] D. Montané, J. Salvadó, C. Torras, X. Farriol, Biomass and Bioenergy, 22 (2002) 295-304.
[30] J. Fernandez, M.D. Curt, P.L. Aguado, Industrial Crops and Products, 24 (2006) 222-229.
[31] J. Gominho, A. Lourenco, P. Palma, M.E. Lourenco, M.D. Curt, J. Fernández, H. Pereira, Industrial Crops and Products, 33 (2010) 1-6.
[32] M. Ballesteros, M. José Negro, P. Manzanares, I. Ballesteros, F. Sáez , J.M. Oliva, Applied Biochemistry and Biotechnology, 137-140 (2007) 239-252.
[33] G. Marcotullio, W. De Jong, Green Chemistry, 12 (2010) 1739-1746.
[34] G. Marcotullio, W. De Jong, Carbohydrate Research, 346 (2011) 1291-1293.
[35] L. Liu, J. Sun, M. Li, S. Wang, H. Pei, J. Zhang, Bioresource Technology, 100 (2009) 5853-5858.

5. SYNTHESIS OF SILICA XEROGEL-POLY (STYRENESULPHONIC ACID) NANOCOMPOSITES AS ACID CATALYSTS: EFFECT OF TEMPERATURE AND POLYMER CONCENTRATION ON THEIR TEXTURAL AND CHEMICAL PROPERTIES [a]

[a]**M.J. Campos Molina,** R. Mariscal, M. López Granados. Silica-poly(styrenesulphonic acid) nanocomposites as acid catalysts: effects of temperature and polymer concentration on their textural and chemical properties.

Enviado a Journal of Sol-Gel Science and Technology

Outline

1. Introduction

Polystyrene (PS) is an excellent starting point for the synthesis of acid catalysts. PS can be sulphonated using different methods and different sulphonated agents, affording the acid polymer poly-(styrene sulphonic acid) (PSSA). An interesting consequence of this methodology is that PSSA polymer can be prepared from waste polystyrene [1-4],which enables the revalorisation of waste polystyrene as acid catalysts: Waste To Catalyst (WTC) concept [5]. This will have a positive impact on the price and the environmental friendliness of the catalyst. We previously reported the use of this soluble polymer in reactions that require acid sites like xylose to furfural reaction [6]. We studied this reaction for two reasons; first because furfural, a chemical derived from sugars, has been identified as a relevant chemical platform for the future deployment of biorefineries [7]. A number of biofuels and chemicals can be derived from this bio-based chemical [8-13]. Furfural is obtained through the dehydration of C5 sugars present in lignocelluloses (like xylose) in the presence of acid catalysts. Mineral acids such as HCl and H_2SO_4 exhibit the highest activity for the latter reactions [12, 14]. Using robust solid catalysts that can be separated from the reaction prevents the environmental and economic drawbacks associated with the use of mineral acids [7, 15-17]. Second reason is because this reaction is conducted in the presence of water. PSSA is dissolved in water and then the acid sites are more accessible to reactant molecules and the diffusion of reactants to active sites (or products from) was facilitated. No sulphur leaching was observed and the polymer could be reused for several runs without observable deactivation.

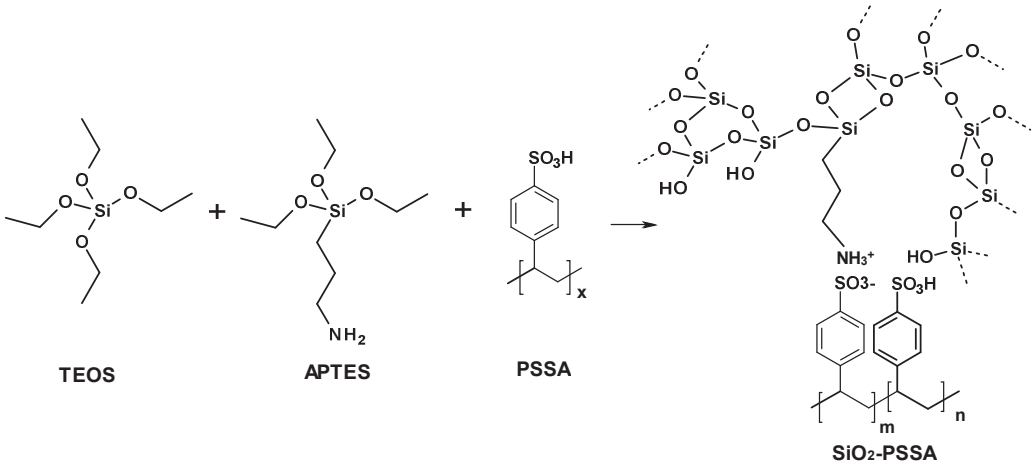

Scheme 5.1. Schematic illustration of the preparation of SiO_2-PSSA nanocomposites.

The reuse of this soluble polymer relies on the ability to separate it from the reaction mixture by ultrafiltration [18], a more complex procedure than conventional filtration or centrifugation. To overcome this disadvantage, anchoring of the soluble polymer on an inorganic solid matrix forming silica-polymer nanocomposites [19] can allow the solid catalyst so formed to be separated by centrifugation or conventional filtration. In a previous work, a SiO_2xerogel-PSSA organic-inorganic hybrid nanocomposite was prepared through a sol-gel process [20]. The sulphonic sites of the polymer catalysed the hydrolysis and condensation reactions of the organosilane precursors to form the SiO_2 matrix. One of the Si organosilane precursors possessed aminopropyl functionality (see Scheme 5.1),which provided the formed SiO_2 particles with aminopropyl groups, which served as anchoring sites for PSSA molecules via acid-base reactions between the sulphonic acid groups and the amino groups of

the SiO_2 particles. These electrostatic interactions stabilised the polymer within the SiO_2 matrix and allowed the catalyst to be reused [20].

The feasibility of the preparation of this inorganic-organic nanocomposite and its utilization for xylose to furfural reaction has already been demonstrated [20, 21] but an exhaustive study is required to explore the effects of different synthesis parameters on the most relevant physical-chemical properties of these SiO_2xerogel-PSSAnanocompositecatalysts.In this work the investigation of the effect of temperature of the sol-gel processing and of the initial polymer concentration used in the synthesis medium is reported for the first time (S/N at. ratio, i.e. PSSA/APTES mol ratio); the TEOS/APTES mol ratio was held constant throughout the study (Si/N close to 11). Our purpose was to reveal how relevant these two properties are for significant textural and chemical properties of the nanocomposites and for the effective retention of the polymer by the silica xerogel matrix.

In addition to activity and selectivity, an essential property of the solid catalysts is hydrothermal stability. Catalyst must withstand the severe conditions under which reaction proceeds: aqueous solutions at temperatures between 423-473 K. Phenomena such as leaching of active sites, sintering, hydration and poisoning and/or fouling frequently occur under these conditions and result in the deactivation of the catalyst. Attention will also be paid to the hydrothermal stability of these SiO_2xerogel-PSSA nanocomposite catalysts.

2. Experimental

2.1. Synthesis of catalysts

The nanocomposites were prepared using the sol-gel route via the co-condensation of tetraethyl orthosilicate (TEOS, Sigma-Aldrich, ≥99%) and

(3- aminopropyl) triethoxysilane (APTES, Sigma-Aldrich, ≥98%) in the presence of an aqueous solution of PSSA (Sigma-Aldrich, 18 wt.% solution in water, MW = 75000, 5.4 mmoles·H^+·g^{-1}) according to a previously reported methodology [19]. The required amounts of the aqueous PSSA solution, TEOS and APTES were added to a round-bottom glass flask (for synthesis at T < 373 K) or to a stainless steel reactor lined with Teflon (for synthesis at T ≥373 K). The reactor was closed and maintained at a given reaction temperature overnight (in the case of the glass flask, stirring was provided). For a first series of samples, the amounts of TEOS, APTES and PSSA used in the synthesis were maintained constant while the synthesis temperature was varied (298, 348, 373, 423 and 473 K) (Si-PSSA-T series). A second series of solids were prepared by changing the initial S/N at. ratio, that is, the initial concentration of PSSA but by keeping the Si/N atomic ratio and the synthesis temperature close to 11 and 348 K, respectively (Si- PSSA-S/N series). In this latter series the initial concentration of PSSA was selected as to have an initial S/N at. ratio of 2.2, 4.4, 8.8 and 24. Details of the preparation are provided in the Supplementary Information at the end of this chapter. The obtained solid was centrifuged and subjected to successive cycles of washing with water at room temperature until a close to neutral pH was achieved. The washing steps were conducted to remove most of the weakly retained polymer molecules. Finally, the solid was dried at 393 K overnight. Tables 5.1 and 5.2 summarize the different types of prepared catalysts, their nomenclature and some chemical properties of interest of the obtained solids. In all cases, the initial Si/N atomic ratio (the relative concentration of amino groups) was close to 11.

An aminopropyl-functionalized SiO_2 free of PSSA was also prepared following the same method shown above but with sulphuric acid as the acid catalyst. The required amount of sulphuric acid (1.5 mL of 96 wt. % sulphuric acid, equivalent to 27 mmol) to incorporate an equivalent amount of protons (or S) as that used for the SiO_2-PSSA nanocomposite with S/N = 2.2 and Si/N= 11 was used.

Other chemicals used in the experiments were D-(+)-xylose (≥99%), 2-furaldehyde (reagent grade, 99%), cyclopentyl methyl ether (CPME) (≥99%) and octanoic acid (98%), which were all supplied by Sigma-Aldrich. All of the materials were used without further purification, and Milli-Q H_2O was used for the preparation of all aqueous solutions.

2.2. Characterization of the catalysts

The elemental analysis of the solids (C, H, N and S concentrations) was performed using a LECO CHNS-32 analyzer. In a typical procedure, 1 mg of solid was placed in an Ag crucible and combusted at 1333 K under a pure O_2 atmosphere. The CO_2, H_2O and SO_2 gases were quantified using Fourier transform infrared (FT-IR) spectroscopy, and N_2 was determined by differential thermal conductivity.

The actual Si content in the samples was determined by total reflection X-ray fluorescence (TXRF) using an Atomika 8030C TXRF spectrometer (Cameca, Germany) equipped with a 3 kW Mo/W dual-target X-ray tube and a W/C double multilayer monochromator. A Si(Li) detector with an active area of 80 mm^2 and a resolution of 150 eV at 5.9 keV (Mn Kα) was used for the detection and measurement of the produced X-rays.

TXRF analysis was also used to determine the concentration of S (in mg/L) in the aqueous phase after the reaction.

The concentration of acid sites in the different samples was determined by acid– base titration. A known amount of previously dried catalyst (100 mg) was placed in contact with *ca*. 25 mL of an aqueous solution that contained 1 g of NaCl and stirred at 323 K overnight. The objective was to exchange protons between the sulphonic groups and sodium ions. Then, the solution was filtered using a Varian Captiva^{TM} column with a pore diameter of 0.45 μm (the retained solid was repeatedly washed with water), and the resulting filtrate solution was titrated with a 0.005 M KOH solution (previously standardized with dry potassium acid phthalate). A few drops of an ethanolic solution of phenolphthalein were used to determine the end point.

Thermogravimetric (TGA) analyses of the different solids were conducted using a Mettler Toledo TGA/SDTA 851e instrument by heating the samples in synthetic air from room temperature to 1073 K at a heating rate of 5 K·min^{-1}.

Nitrogen adsorption– desorption isotherms were recorded at liquid nitrogen temperature (77 K) using a Micromeritics ASAP 2420 apparatus. The samples were degassed at 393 K for 12 h prior to determining the adsorption isotherms. The surface areas were calculated using the Brunauer– Emmett– Teller (BET) equation, and the mean pore diameters were obtained by applying the Barrett–Joyner–Halenda (BJH) method to the adsorption branch.

Diffuse reflectance infrared Fourier transform (DRIFT) spectra were recorded with a Nicolet 5700 spectrophotometer equipped with an *in situ* chamber, a Praying Mantis diffuse reflectance accessory and a high– sensitivity Hg-Cd–Te detector. The spectra were obtained at a resolution of 4

cm^{-1} with a total of 128 scans. In a typical measurement, finely ground samples (ca. 50 mg) were placed in the cup of the *in situ* DRIFT chamber. The sample was preheated under an Ar flow (ca. 50 $mL \cdot min^{-1}$) at 373K for 60 min before recording the infrared spectra at room temperature.

^{13}C and ^{29}Si solid-state NMR spectra of the samples were recorded using a Bruker AV-400-WB spectrometer equipped with a triple-channel probe. Powder samples were finely ground and dried for several days at 373 K in an oven and then rapidly transferred to ZrO_2 rotors (4 mm) and capped with Kel-F caps to prevent hydration of the polymer. Frequencies of 100.32 and 79.49 MHz were used for ^{13}C and ^{29}Si nuclei, respectively. The samples were spun at 10 kHz. The CP-MAS ^{1}H-^{13}C spectra were recorded using a spectral width of 35 KHz, an excitation pulse for ^{1}H of 3.4 μs, a contact time of 3.5 ms and a relaxation time of 4 s, with ^{1}H tppm-15 decoupling at 80 KHz. The number of scans was 1024 for the ^{13}C spectra. The ^{13}C chemical shift was referenced to the adamantane CH_2 signal (29.5 ppm) as a secondary reference relative to TMS as the primary reference. The ^{29}Si MAS-NMR spectra are the result of 1000 accumulations after direct irradiation at a spectral width of 15 kHz, a relaxation delay of 60 s and pulses of $\pi/4$ at 50 kHz. The kaolin signal (-91.2 ppm) was used as a secondary reference relative to TMS as the primary reference.

2.3. Catalytic activity tests

All catalysts were tested in batch experiments for the dehydration of xylose to furfural in a biphasic system. These catalytic experiments were performed in a 15 mL Ace sealed glass pressure reactor, which was flushed

with nitrogen before use, magnetically stirred (1500 rpm) and placed in a preheated oil bath at the selected temperature. In practice, 1.5 g of water, 3.5 g of CPME as an organic solvent (2.33 g CPME/g aqueous solution), 150 mg of xylose (10 wt. % with respect to water) and 75 mg of finely ground catalyst previously sieved to a size of < 106 μm (5 wt. % with respect to water, catalyst/xylose wt. ratio = 0.5) were poured into the reactor. The green solvent CPME has been reported to be an excellent solvent for improving the furfural yield [22]. The reaction was initiated when the charged reactor was immersed in the oil bath, and it was stopped by removing the reactor from the oil bath and rapidly cooling by immersion in water at room temperature. Then, an internal standard for the organic phase (40 mg of octanoic acid) was added to the quenched reaction mixture, and after gentle agitation for several minutes, the mixture was centrifuged to separate both phases. A 2 mL aliquot was collected from the organic layer. After the organic phase was aliquoted, an internal standard for the aqueous phase (200 mg of D (+)-glucose) was added to the remaining reaction mixture and, after agitation for several minutes and centrifugation, an aliquot (*ca.* 2 mL) was collected from the aqueous layer for analysis. Prior to analysis, both the organic and aqueous aliquots were filtered through a 0.22 μm polyethersulphone Millipore filter to remove the remaining catalyst and the solid humins formed during the reaction. The aqueous aliquots were analysed using HPLC with an Agilent 1200 series chromatograph equipped with a refractive index (RI) detector and a Bio-Rad Aminex HPX-87H column (300x7.8 mm) for the analysis of xylose and furfural in the aqueous phase. A 0.005 M H_2SO_4 mobile phase was employed as the eluent with a flow rate of 0.4 mL/min at 328 K. For the organic aliquots, the analysis of furfural in this phase was conducted using a

gas chromatograph (CG) (Varian CP-3800) equipped with a ZBWAX plus column (30 mx0.32 mmx0.25μm) and a flame ionization detector (FID).

3. Results and discussion

3.1. Characterization of the catalysts

Table 5.1 summarises the actual concentrations of the most relevant atoms in the fresh nanocomposites of the Si-PSSA-T series. The results for the hydrothermally treated samples (HT) will be discussed later. This table also includes the nominal values for the concentration of these atoms deduced from the actual amounts of TEOS, APTES and PSSA employed during the synthesis. The S concentration (mmol $S \cdot g_{cat}^{-1}$) is related to the actual polymer loading. It can be observed that the synthesis temperature strongly affects the actual polymer loading, being maximum for $T \leq 348$ K. Regarding the N content (mmol $N \cdot g_{cat}^{-1}$) and the Si/N ratio values, which are related to the actual loading of amino groups, they are close to those theoretically expected for the Si-PSSA-298 and Si-PSSA-348 samples. The factual incorporation of a greater amount of aminopropyl groups in the xerogel favours the retention of the polymer, and thus, the Si-PSSA-298 and Si-PSSA-348 nanocomposites exhibit the largest S loading.

Notably, the Si/N content passed through a maximum for Si-PSSA-373: there are fewer amino groups in this sample and consequently less sulphonic groups (polymer loading). For the nanocomposites prepared at higher temperatures (423 and 473 K), the N loading increased again (Si/N ratio decreased), however, the S loading (polymer retention) did not recover to the

levels reached in the nanocomposites prepared at 298 and 348 K. Higher synthesis temperature resulted in poorer retention of the polymer.

Table 5.1. Experimental concentrations of relevant atoms in the nanocomposites prepared under different temperatures of synthesis (Si-PSSA-T series).

Catalyst	mmol S· g_{cat}^{-1} (1.98) [a]	mmol N· g_{cat}^{-1} (0.9) [a]	at. Si/N (11.1) [a]	at. S/N (2.2) [a]	mmol H^+· g_{cat}^{-1}	
					Fresh	HT [b]
Si-473	0.53	1.14	17.1	0.47	0.06	0.04
Si-PSSA-298	1.56	0.98	11.6	1.58	0.45 (0.58) [c]	0.24
Si-PSSA-348	1.26	0.86	11.8	1.46	0.27 (0.40) [c]	0.18
Si-PSSA-373	0.69	0.56	21.3	1.25	0.14 (0.13) [c]	0.03
Si-PSSA-423	0.47	0.74	19.9	0.64	0.04	0.02
Si-PSSA-473	0.73	0.92	17.2	0.80	0.06	0.02

[a] Values in brackets correspond to theoretical values determined from the nominal concentration incorporated in the preparation mixture

[b] HT stands for hydrothermally treated nanocomposite

[c] Values in brackets were obtained from the difference between mmolS·$g_{cat}^{-1}$and mmol N·g_{cat}^{-1}

Another relevant chemical parameter is the concentration of actual available acid sites (mmolH^+·g_{cat}^{-1}), which was determined by acid– base titration. The actual values were smaller than the S content because a portion of the sulphonic groups were neutralized by aminopropyl groups and in addition because not all of the sulphonic groups can be titrated (most likely because some of the polymer is trapped within the SiO_2 particles or in

inaccessible pores). The bracketed values in this column were calculated as the difference between the actual S and N loadings: for Si–PSSA–298, Si–PSSA–348 and Si–PSSA–373, this difference value is positive and close to the actual concentration of acid sites. For the remainder of the nanocomposites, the polymer retention was very poor and the N loading was larger than the S loading (actual S/N at.ratio <1), and consequently, the amount of free acid sites was very low. In other words, there were more aminopropyl groups than sulphonic sites, and therefore, the sulphonic sites of the polymer were neutralized to a large extent. Note that the blank Si–473 sample, which was prepared without PSSA but with sulphuric acid, also retained S, mostly through interactions of sulphuric sites with the amino groups. However, the number of free acid sites was also very low because the S loading was smaller than the amino group loading. Notably, the actual S/N ratio for Si–473 was close to 0.5, which indicates that the two protons of one sulphuric acid molecule were neutralized by two amino groups.

In principle and based on the concentration of acid sites, it could be concluded that the Si–PSSA–298 and Si–PSSA–348 catalysts are nanocomposites with largest acid sites loading. However, we must also consider the textural properties and hydrothermal stability because these properties also critically define the overall activity of the catalysts.

Table 5.2 summarises the concentrations of the most relevant atoms in the nanocomposites of the Si–PSSA–S/N series. Regarding the actual S content in the fresh samples, it is clear that this magnitude increased as the initial concentration of polymer increased. For the Si–PSSA–2.2 sample, the actual S loading (mmol $S \cdot g_{cat}^{-1}$) was not considerably different from the nominal value

(1.26 vs. 1.98). Remarkably, for the remainder of the samples, the increase in the actual S loading was not enhanced proportionally to the nominal value. For example, the nominal value used in the synthesis went from 1.98 mmol S· g_{cat}^{-1} for the Si–PSSA–2.2 catalyst to 4.68 for the Si– PSSA–24 catalyst (2.36 times greater); however, the actual increase was only 1.5– fold (from 1.26 to 1.88). This is also evident in the S/N at. ratio: the nominal initial value used in the synthesis increased from 2.2 to 24 (almost 11 times greater), whereas the actual value increased from 1.46 to 2.27 (1.5 times).

The amount of acid sites available in the catalyst (mmol $H^{+}\cdot g_{cat}^{-1}$) follows the same trend as the S loading. Again the loading of acid sites was smaller than the loading of S (a portion of the sulphonic groups were neutralised by the amino groups). The S and consequently the acid site loadings are comparable to those of other sulphonated silicas reported elsewhere (1.1–1.2 [23, 24], 0.32-0.67 [25] and 0.44–1.69 mmoles $H^{+}\cdot g_{cat}^{-1}$ [26] for sulphonic–SBA–15 systems; 0.1-0.4 mmoles $H^{+}\cdot g_{cat}^{-1}$ for sulphonic–MCM–41systems [27]; and 0.18-0.20 mmoles $H^{+}\cdot g_{cat}^{-1}$ for SBA–15 grafted poly–(styrene sulphonic acid) prepared by surface– initiated atom–transfer radical polymerisation methodologies [28]).

The N content (mmol N· g_{cat}^{-1}) was quite similar for all of the catalysts (between 0.86-0.83). The actual N loading was larger than the nominal value, which is more evident for the Si–PSSA–8.8 and Si–PSSA–24 samples: not all the intended polymer was ultimately retained, and comparatively, there was more N than initially expected. However, the Si/N atomic ratio was almost constant for all of the catalysts and close to the nominal value, indicating that almost all of the intended aminopropyl groups were incorporated in the SiO_2 matrix.

Table 5.2. Experimental concentrations of relevant atoms in the nanocomposites prepared at 348 K with different initial polymer concentrations (Si- PSSA- S/N series).

Catalyst	mmol S· g_{cat}^{-1}	mmol N· g_{cat}^{-1}	at. Si/N (11.1)[b]	at. S/N	mmol H^+ ·g_{cat}^{-1}	
					Fresh	HT[b]
Si-PSSA-2.2 (also named as Si-PSSA-348)	1.26 (1.98)[a]	0.86 (0.90)[a]	11.8	1.46 (2.2)[a]	0.27 (0.4)[c]	0.18
Si-PSSA-4.4	1.60 (2.90)	0.86 (0.66)	12.8	1.86 (4.4)	0.68 (0.74)	0.24
Si-PSSA-8.8	1.81 (3.78)	0.83 (0.43)	12.9	2.18 (8.8)	0.82 (0.98)	0.32
Si-PSSA-24	1.88 (4.68)	0.83 (0.19)	11.8	2.27 (24)	0.94 (1.05)	0.43

[a]Values in brackets correspond to theoretical values determined from the nominal concentration incorporated in the preparation mixture

[b]HT stands for hydrothermally treated nanocomposite

[c] Values between brackets were obtained by difference between mmolS·g_{cat}^{-1} and mmol N·g_{cat}^{-1}

To summarise all the chemical data, it is clear that adding more polymer to the synthesis mixture results in a greater S loading and greater acid site loading. However, Si-PSSA-4.4 represents a trade-off between the amount of polymer added to the synthesis mixture and the actual final S loading. A 2-fold or 5-fold increase of the initial concentration of polymer (Si-PSSA-8.8 and Si-PSSA-24, respectively) resulted in only a 13 % and a 17 % increase in the S loading.

Figure 5.1 presents the nitrogen adsorption-desorption isotherms for the fresh catalysts of Si–PSSA–T series, as well as that for the blank SiO_2 prepared without PSSA (Si-473) (the isotherms for the hydrothermally treated catalysts are also included in this figure, but they will be discussed later). Table 5S1 in Supplementary Information presents the main textural parameters determined from the isotherms, a more extended discussion is also provided therein concerning the isotherms displayed in Figure 5.1.

The synthesis temperature clearly affects the textural properties of the fresh catalysts (see Figure 5.1A). The catalysts synthesized at lower temperatures (298 and 348 K) exhibit isotherms characteristic of non–porous materials, and their BET surface areas are negligible, very likely due to the presence of polymer covering and/or filling the pores [20]. The surface of the solid is then defined by the solid polymer, which is not a porous material; therefore, its N_2 retention is negligible. As the synthesis temperature increased beyond 348 K, the catalysts exhibited measurable N_2 adsorption. Thus, the isotherm for the catalyst synthesised at 373 K is assigned to type I, which essentially corresponds to microporous solids that contain a relatively small amount of mesopores (see Table 5S1 in Suppementary information section at the end of this chapter). The shape of the hysteresis loops corresponds to type H4. The activated adsorption (gentle slope) observed for relative pressures greater than 0.1 suggests that the presence of polymer molecules within the micropores prevents the rapid filling of the pores. Higher pressures are required to push the N_2 into the micropores.

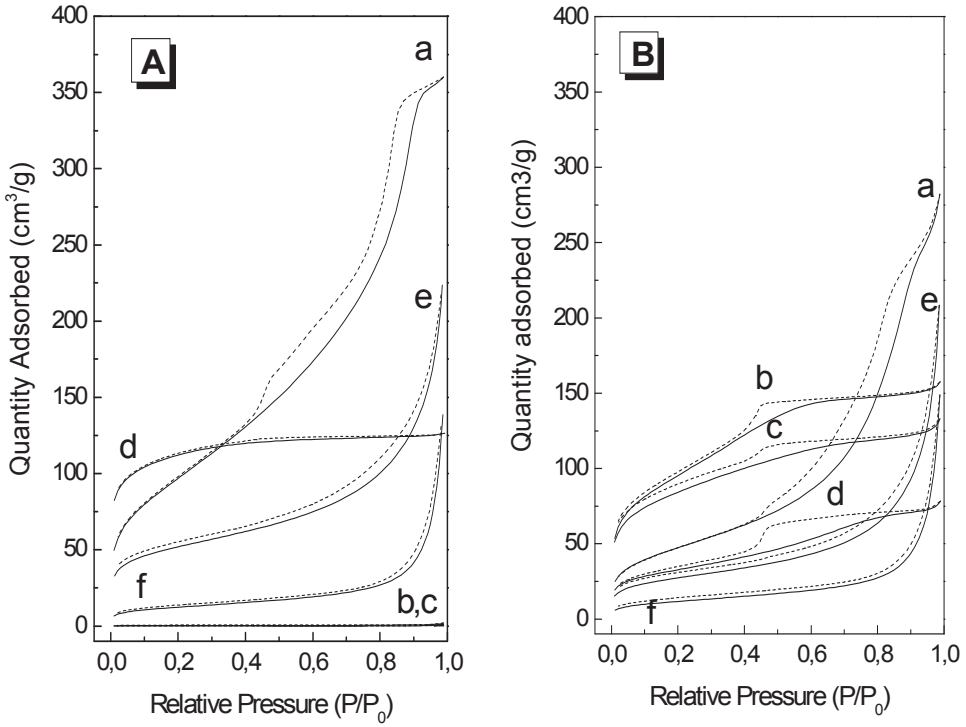

Figure 5.1. N_2 adsorption (solid lines) and desorption (dashed lines) isotherms of Si-PSSA-T series and of the blank sample without PSSA (Si-473): A) fresh catalysts; B) catalysts after hydrothermal treatment in CPME/water at 453 K: a) Si-473; b) Si-PSSA-298; c) Si-PSSA-348; d) Si-PSSA-373; e) Si-PSSA-423; and f) Si-PSSA-473.

When the synthesis temperature increased to 423 K, the shape of the isotherm changed to that of a mesoporous material (type IV isotherm). The specific surface area decreased and the solid also presents micropores (equivalent to 0.6 times of mesopores, see Table 5S1 in Supplementary information section). The pore size distribution determined using the BJH method indicated a wide distribution of mesopores with an average pore size

greater than 100 nm. The higher temperature used for the synthesis with respect to the previous sample resulted in coarsening and sintering of the SiO_2 particles, thereby creating interparticle mesopores at the expense of micropores.

The Si–PSSA–473 catalyst exhibited a type IV isotherm, which is characteristic of mesoporous solids (average mesopore diameter determined using the BJH method is greater than 100 nm) with little contribution of micropores. This catalyst also presented a smaller BET surface area.

Finally, the blank Si–473 sample, which was also prepared at this temperature but by using H_2SO_4, exhibited an isotherm characteristic of only a mesoporous solid and a much larger specific surface area. It is clear that the presence of polymer filling the pores in the nanocomposite strongly modifies the texture of the solid. Notably, the desorption branch for sample Si–473 closed at a P/P_0 of *ca.* 0.4 due to the sudden evaporation of N_2 from the pores (tensile strength effect). However, this effect was not observed in any of the Si–PSSA nanocomposites: the loop did not close below this P/P_0, regardless of synthesis temperature. This is very evident in the Si–PSSA–423 sample. In these cases, a process known as low-pressure hysteresis occurred. This phenomenon is associated with the swelling of an inelastic and non-rigid porous structure during the adsorption cycle, associated with the lack of rigidity caused by the presence of the polymer inside the pores in our study. The low-pressure hysteresis could also be due to irreversible adsorption because the pore size is approximately the width of the adsorbate molecule (N_2). Nonetheless, this option can be excluded because the cycle closed abruptly in the blank Si–473 sample and it did not in the nanocomposites,

indicating that the presence of the polymer within the pores must be responsible for the low-pressure hysteresis phenomenon.

The textural properties of the catalysts of the Si-PSSA-S/N series presented isotherms with the same characteristics as that of the Si-PSSA-348 (also named Si-PSSA-2.2) catalyst (figures not shown for the sake of brevity), corresponding to non- porous materials. These catalysts presented null values for the BET surface area. The filling of the pores by polymer molecules explains the lack of adsorptive properties.

Thermogravimetric analysis of the organic-inorganic polymer nanocomposites (see Figures 5S1 and 5S2 in the Supplementary Information section) revealed that in all cases, the materials are thermally stable up to 600 K, and no deterioration or combustion of the polymer was observed below this temperature, which is a considerably higher temperature than that used in the xylose dehydration reaction (443-473 K).

In summary, the isotherm studies indicate that the synthesis temperature defines the textural properties. At synthesis temperatures lower than 373 K, it appears likely that the solids are essentially microporous, although the large polymer retention results in extended blocking of the pores by the polymer and the surface is not available for N_2 adsorption. This behaviour is independent of the S/N at. ratio used in the synthesis. At 373 K, the solid is essentially microporous, there is less polymer loading within the silica pore network and the adsorption of N_2 on the silica surface is thus possible. At synthesis temperatures greater than 373, the retention of the polymer is even lower but is still visible in the isotherm features (low-pressure hysteresis). The sintering and coarsening of silica particles at these synthesis temperatures result in solids with lower specific areas and larger fractions of mesopores.

Figure 5.2 presents the DRIFT spectra of two representative samples (Si-473 and Si- PSSA-348) in the 4000-1100 cm^{-1} region. Spectra were recorded after the samples were heated at 423 K under an Ar flow. Table 5.3 summarises the main bands appearing in the Figure 5.2 along with the assignments. The assignments of the bands are based on references [20, 29-32]. A more detailed discussion concerning this assignment is presented in the Supplementary Information section. Several aspects must be stressed: first aspect refers to the presence of bands from PSSA in the Si-PSSA-2.2 spectrum at 3060 and 2930, 1598, 1495, 1470 1450, 1412 and 1355 cm^{-1}. Another evidence of the presence of polymer is that the silanol vibrations at 3729 and 3658 cm^{-1} detected in Si- 473 sample are absent in Si- PSSA- 348 spectrum which indicates that these vibrations are being perturbed by the presence of the polymer. The protonation of the Si-OH groups by the sulphonic moieties of the polymer ($R\text{-}SO_3^-$ -$^+$H-HO-Si) is responsible for this perturbation. Another interesting aspect concerns the position of the vibrations of amino groups at 3267 and 3160 cm^{-1} (ν_{as} and ν_s) and at 1620 and 1512 cm^{-1} (δ_{as} and δs) indicating that amino groups are protonated; amine groups hydrogen bonded to silanol groups appear at different wavenumbers [20, 31]. The possibility that the protonation of amine groups had been accomplished by the acidic silanol groups can be excluded (see discussion in Supplementary Information). Note that most of the amine groups are protonated because bands from free or H-bonded amines are not observed; therefore, amine groups are highly involved in the stabilisation of the polymer through electrostatic interactions. In summary, the DRIFT data showed that both the polymer and amino-functionalized silica interact through electrostatic interactions driven by acid-base reactions between sulphonic and amino groups (see Scheme 5.1).

These interactions result in the stabilisation of the polymer in the silica matrix [20]. The polymer can also be retained by interactions between sulphonic and silanol groups, but this interaction is weaker [20]. The DRIFT spectrum of the Si–PSSA–4.4 sample was similar to that of Si–PSSA–348 (also named Si–PSSA–2.2, see Figure 5S3 in the Supplementary Information section). The bands assigned to sulphonated polymer were more intense, and the position of the bands corresponding to the amino groups also implied that the amino groups were protonated and therefore participating in electrostatic interactions with sulphonic groups.

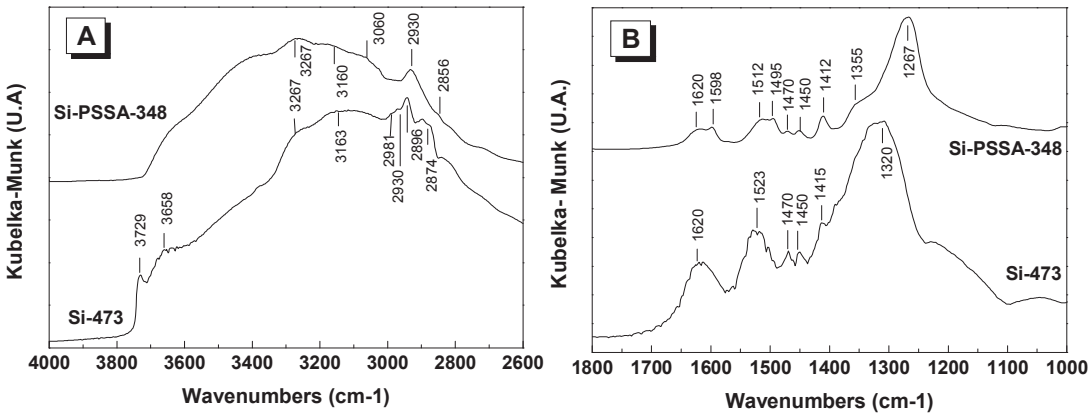

Figure 5.2. DRIFT spectra of some representative catalysts after heating at 423K under an Ar flow: a) between 4000-2600 cm-1; b) between 1800-1000 cm^{-1}

Table 5.3. Assignments of DRIFT bands

Si-473	Si-PSSA-348	Assignment
3729		ϒO-H) in isolated silanol [29, 30]
3658		ϒO-H) in H-bonded vicinal silanol and/or ϒO-H) in silanol H-bonded to water
3267	3267	ν_{as}(N-H) in R-NH_3^+ [20, 31]
3163	3160	ν_s(N-H) in R-NH_3^+ [20, 31]
	3060	ν(C-H) in aromatic ring [20]
2981		ν_{as}(C-H) in CH_3 (ethoxy group) [31]
2930	2930	ν_{as}(C-H) in CH_2 (ethoxy group or propylamine or polymer backbone) [20, 31]
2896		ν_s(C-H) in CH_3(ethoxy group) or in CH_2 (propylamine) [31]
2874		ν_s(C-H) in CH_2 (propylamine)[31]
1620	1620	δ_{as}(N-H) in R-NH_3^+ [20, 31]
	1598	ν(C-C) in aromatic ring [20]
1523	1512	δ_s(N-H) in R-NH_3^+ [20, 31]
	1495	ν(C-C) in aromatic ring [20]
1470	1470	ν(C-H) in CH_2 (propylamine and polymer backbone)[31].
	1450	δ (C-H) in CH_2 (propylamine and polymer backbone) and ν(C-C) in aromatic ring
1415	1412	w(C-H) and/or t(C-H) in CH_2 (propylamine and polymer backbone) [31]
	1355	ν_{as} O=S=O in SO_3H [32]
1320	1267	ν_{as} (Si-O-Si) in SiO_2 [20]

C-H deformation bands in CH_2: δ scissoring; w wagging; t twisting

Figure 5.3 presents the ^{13}C and ^{29}Si MAS NMR spectra of different catalysts after being stored in an oven at 373 K for several days. The spectra of Si-473, Si-PSSA-348, Si-PSSA-373 and Si-PSSA-473 will be discussed below, and that of Si-PSSA-348-HT (hydrothermally treated) will be discussed later.

The ^{29}Si spectra provide insight into the degree of condensation of the silica networks in the different catalysts. The two broad overlapping resonances at –109 and –102 ppm are assigned to the Q^4 and Q^3 siloxane species of the silica framework, respectively ([Q^n= $Si(OSi)_n(OR)_{4-n}$], where n= 4 or 3 and R = alkoxy or H) [33-36]. The Q^4 signal represents the Si atoms in fully condensed $Si(O-Si)_4$ tetrahedra. This signal predominates in the nanocomposite prepared at 473 K (as well as in the blank silica that was also prepared at 473 K), indicating an extensively condensed silica framework. The less intense Q^3 resonance signal primarily originates from $(SiO)_3Si-OH$ units. The amount of unhydrolised ethoxy residues is quite low (according to the DRIFT results and to the ^{13}C MAS-NMR results, as will be explained below). In contrast, for the samples prepared at lower T (348 and 373 K), the Q^3 signal is as intense as the Q^4 signal, and a weak Q^2 (n=2) signal at –93 ppm (originating from $(SiO)_2Si-(OH)_2$-like species) is also visible. The fact that the amount of Q^{2-3} species is larger indicates that the silica framework is less condensed, as expected considering the lower synthesis temperature and aging.

The detection of the resonance at –66 ppm (weak although observable) in all of the samples indicates the presence of aminopropyl-functionalised Si atoms [34, 37]. This signal corresponds to alkylsiloxane T^3 units ($R'Si(OSi)_3$), where R´ corresponds to aminopropyl groups. The presence of T^2 species $R'(SiO)_2(OH)$ cannot be excluded because the signal is quite broad and exhibits an incipient shoulder at lower shifts. The intensity of this signal is smaller in the Si-PSSA-373 sample, which is consistent with the lower N loading observed for this sample during the elemental chemical analysis.

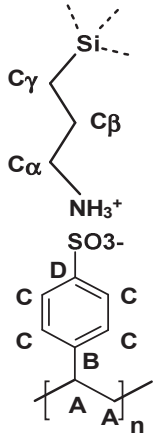

Scheme 5.2: Assignments of ^{13}C MAS-NMR signals

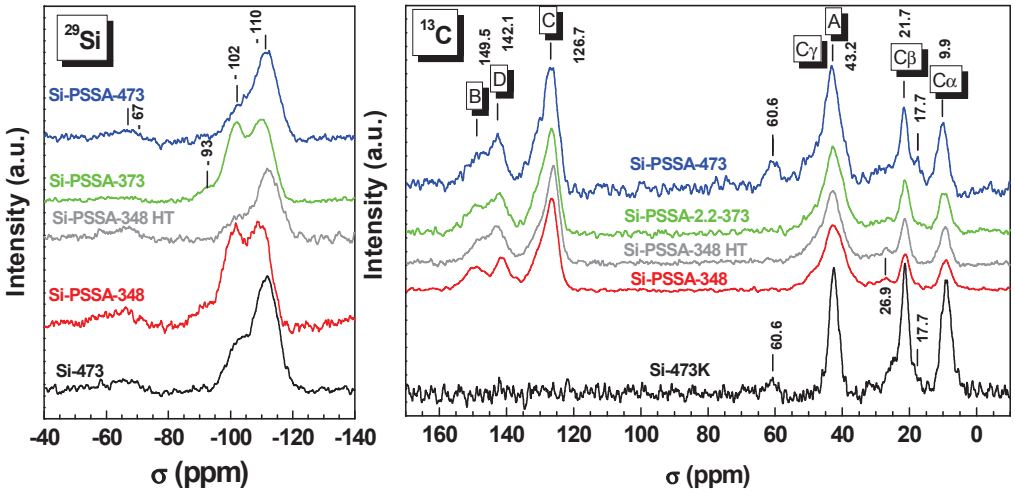

Figure 5.3.^{29}Si MAS-NMR and ^{13}C CP-MAS-NMR spectra of some of the catalysts

In the ^{13}C spectra, four signals from the polymer are clearly identified in all the Si–PSSA catalysts: 43.2, 142.1, 149.5 and 126.7 ppm (see Scheme 5.2 for assignments) [6, 20]. Two additional peaks can also be observed, arising from the C atoms of the aminopropyl groups at 9.8 and 21.7 ppm ($C\alpha$ and $C\beta$, respectively). The signal from $C\gamma$ should appear at approximately 45–50 ppm, but it is overshadowed by the peak at 43.2 ppm from the polymer. In fact, in the Si-473 catalyst, the three bands corresponding to carbons the aminopropyl group have the same intensity, but in the polymer–containing samples, the signal at 43.2 is more intense because it is superimposed with that of the polymer. Two weak peaks are observed at approximately 61 and 18 ppm in the samples prepared at 473 K; these peaks may arise from ethanol groups occluded in the SiO_2 matrix (they cannot arise from ethoxy groups, $-SiOCH_2CH_3$, that were hydrolysed during the preparation of the catalyst because Q^2 signals were not detected in this sample) [38]. The feature at *ca*. 27 ppm is assigned to a side band of the main signal at 126 ppm.

The $C\alpha$ and $C\beta$ resonances of the aminopropyl group are sensitive to protonation. The positions of these peaks correspond to protonated amine groups ($R–NH_3^+$) [38-40] because it is well established that these signals are shifted by *ca*. 2 and 5 ppm, respectively, to lower shieldings in unprotonated amines. As explained in the DRIFT discussion, the protonation results from the interaction with sulphonic groups (protonation from acidic silanols was excluded). For the Si-473 catalyst, the protonation of amino groups results from the excess sulphuric acid employed during the synthesis. Therefore, the NMR results agree with the conclusions derived from the DRIFT analysis: the polymer is retained by the silica through the formation of electrostatic

interactions driven by the acid-base reactions between the sulphonic and amino groups.

Moreover, the NMR results indicate that synthesis at lower temperatures results in structures with a smaller degree of condensation of the SiO_4 tetrahedra and therefore in a less compact network.

Catalytic properties in the dehydration of xylose to furfural

All of these hybrid materials were tested in the cyclodehydration reaction of xylose to furfural because this reaction requires acid sites. This reaction is relevant within the context of biorefineries and the valorisation of biomass. Moreover, this reaction is conducted in aqueous medium and at relatively high temperatures (423–473 K) and is therefore an excellent reaction for assessing the hydrothermal stabilities of this type of nanocomposite. The measurements were conducted in a biphasic medium composed of water and cyclopentyl methyl ether (CPME). It has previously been demonstrated that this green solvent improves the furfural yield by avoiding side loss reactions [22]. Figure 5.4 compares the catalytic performance of the Si–PSSA–T series. The results clearly demonstrate that the catalysts play a role in the production of furfural because the xylose conversions and furfural yields are larger than those obtained when no catalyst is present (autocatalytic reaction). The furfural yield is smaller than conversion due to the side reactions giving rise to humins, oligomers and other degradation products [7, 14, 22, 41]. The PSSA-SiO_2 catalysts synthesized at $T \leq 373$ K exhibited the best catalytic properties, with xylose conversions and furfural yields all greater than 50 and 35 %, respectively. As a first approximation, it can be stated that the

catalysts that possess larger amounts of free acid sites exhibit better activity. Surprisingly, the catalyst prepared by adding sulphuric acid rather than PSSA (Si-473) exhibited the largest reaction rates for both xylose conversion and furfural production. However, the stabilities of the different catalysts must also be investigated due to the importance of finding a stable catalyst under the investigated reaction conditions.

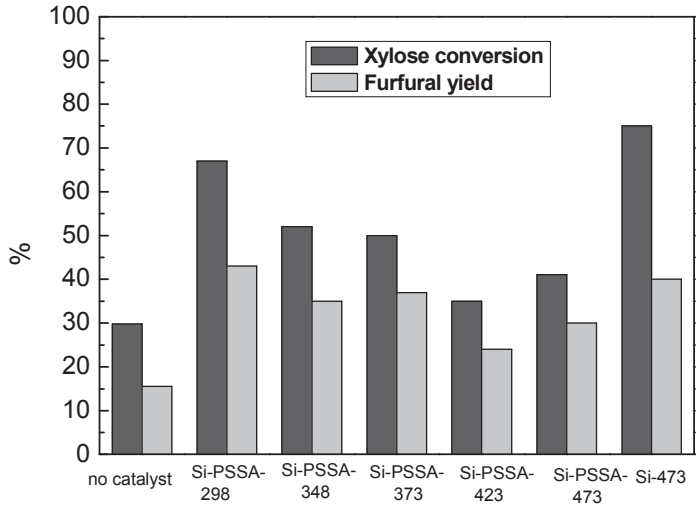

Figure 5.4. Xylose conversion and furfural yield for the autocatalytic reaction and for the catalysts prepared at different temperatures. Reaction conditions: 10wt. % xylose and 5 wt% catalyst in the aqueous phase, CPME/ aqueous phase mass ratio= 2.33; 5 g of total solution, 453K, 120min)

Figure 5.5 presents the xylose conversions and furfural yields at 453 K for the catalysts of the Si-PSSA-S/N series as a function of reaction time. This figure also includes the results from a blank experiment (no

catalyst). It must be remembered that Si-PSSA-2.2 is equivalent to previous Si-PSSA-348 sample. A substantial enhancement of the catalytic properties can be observed when comparing the Si-PSSA-4.4 and Si-PSSA-2.2 catalysts. Thus, at 180 min, the furfural conversion increased from *ca.* 60 % to *ca.* 90%, respectively, and the furfural yield increased from 35 % to *ca.* 60 %. In principle, these results are in agreement with the largest S and acid site loadings found in the Si- PSSA-4.4 catalyst. The catalytic behaviours of the other two catalysts with larger nominal S/N ratios (8.8 and 24) were only slightly better than that of the Si-PSSA-4.4 catalyst, which is in agreement with their modest increase in polymer loading.

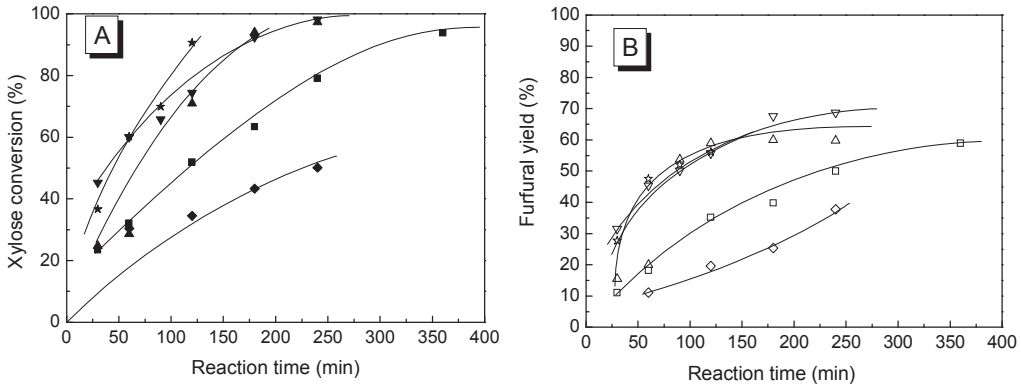

Figure 5.5. Comparison of xylose conversion (A) and furfural yield (B) for the different catalysts prepared with different initial polymer concentrations. (■,□) Si-PSSA-2.2; (▲,△) Si-PSSA-4.4; (▼,▽) Si-PSSA-8.8; (★,☆) Si-PSSA-24; and (◆,◇) withoutcatalyst. Reaction conditions: 10 wt. % xylose and 5 wt. % catalyst in the aqueous phase, CPME/aqueous phase mass ratio = 2.33; 5 g total solution, temperature of reaction 453 K.

The recycling experiments were conducted at 453 K with 120 min of reaction time. The catalytic runs were conducted intending at not achieving a very large conversion with the intention of facilitating the detection of a decrease in catalytic activity. Once the reaction ended, the liquid mixture was cooled, and then the analysis was conducted as explained in Section 2.3 of this chapter. After analysis, the catalyst was washed first with water and finally with CPME to remove the xylose and organics weakly retained by the solid, which can interfere in the estimation of the catalytic properties in successive runs. The water and CPME were removed by centrifugation followed by evaporation at 348 K under a N_2 flow.

Regarding the first series of nanocomposites (Si–PSSA–T) the results demonstrated that (see Figure 5S4 in Supplementary Information for further details and deeper discussion) all of the nanocomposites underwent an intense deactivation during the first run. The catalytic properties of the second run were significantly lower than those observed for the first run. For subsequent runs deactivation seems to be stopped although the residual activity was quite close to that of blank experiments (no catalyst).The PSSA-free Si-473 catalyst, which notably exhibited a very high initial activity, experienced a severe deactivation in the first run and a constant decline in successive runs; its final conversion and yield values are not considerably different from the thermal conversion without catalyst. The high activity of this catalyst in the first run is associated to the leaching of the very active sulphuric acid molecules. Improvements in the synthesis of the SiO2-PSSA nanocomposites are needed to obtain better catalytic properties that can be differentiated from the performance of the autocatalytic conversion (no catalyst) and of the Si-473 catalyst.

Recycling experiments were also conducted for the Si-PSSA-4.4 and Si-PSSA-24 nanocomposites and results represented in Figure 5.6, that also includes for comparison purposes the reusability properties of Amberlyst 70, a resin with sulphonic acid groups (acid site loading = 2.55 mmol $H^+ \cdot g_{cat}^{-1}$). The xylose conversion and furfural yield for the autocatalytic reaction (blank experiment without catalyst) are also represented in the graphs. The Si-PSSA-4.4 catalyst is visibly deactivated during the first run. However, in successive runs, the deactivation was considerably less intense, and in fact, the conversion and yield values for the 2nd and subsequent runs appear to stabilize at approximately 50 and 35 %, respectively, within experimental error. These values are greater than those of Si-PSSA-2.2 (approximately 35 % and 25 %, respectively), which are presented in Figure 5S4 (in that figure, this catalyst was named Si-PSSA-348). Moreover, these values are better than those obtained without catalysts (30 and 15 %, respectively). Si-PSSA-24 sample, the catalyst with the largest initial acid loading, is also visibly deactivated during the first run and the deactivation progressed continuously during the consecutive runs to reach conversion and yield values similar to those of Si-PSSA-4.4 in the 4th and 5th runs.

We further compare our results with those of a commercial sulphonic acid resin, Amberlyst-70. As shown in Figure 5.6, the catalytic activity of fresh sample was larger than those of the nanocomposites, which is consistent with the largest loading of acid sites. However, Amberlyst 70 exhibited also a clear and progressive deactivation with consecutive catalytic runs, very likely related to the leaching of sulphonic groups and with deposits of organic molecules over the surface. This behavior is opposite to that of the nanocomposites, which appear to reach a quite stable behaviour after deactivation during the initial

cycles. Therefore although Si-PSSA-24 and Amberlyst-70 catalysts are very active in the first run, they do not present superior performance upon reutilization than Si-PSSA-4.4 nanocomposite.

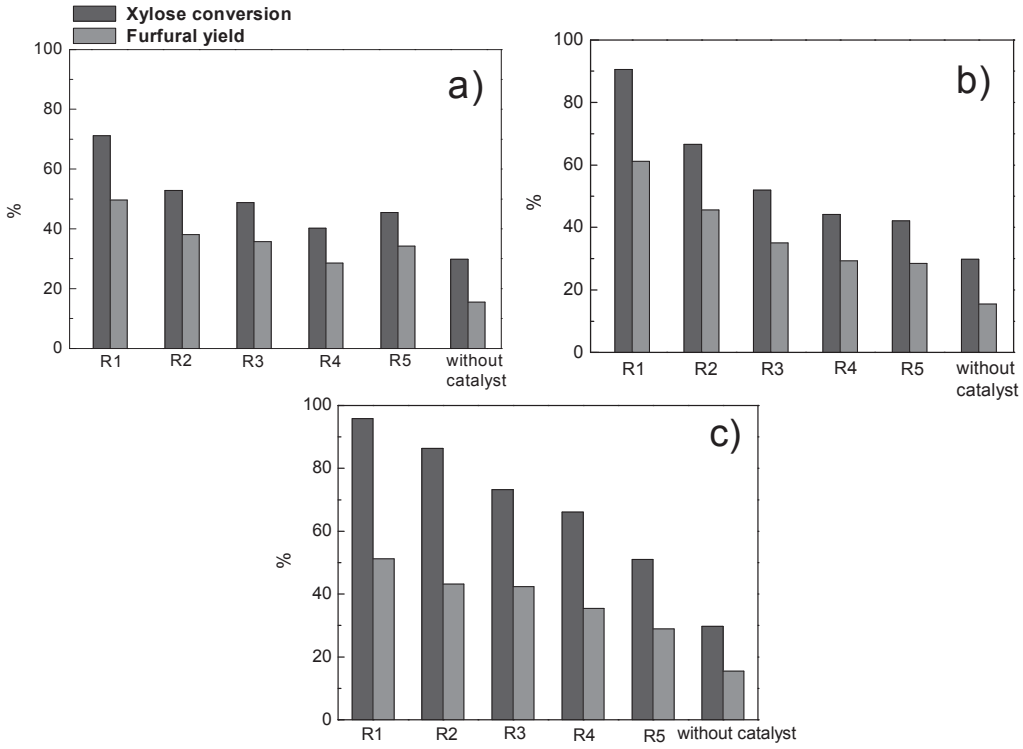

Figure 5.6. Recycling of the catalysts synthesised at 348 K with different polymer loadings: a) Si-PSSA-4.4; b) Si-PSSA-24 and c) Amberlyst 70. Reaction conditions: 10 wt. % xylose and 5 wt. % catalyst in the aqueous phase, CPME/aqueous phase mass ratio = 2.33; 5 g total solution, temperature of reaction 453 K, time of reaction 120 min.

Characterisation of hydrothermally treated nanocomposites.

The amount of S lost during the recycling tests was determined by TXRF analyses of the aqueous phase obtained after the successive runs. CPME phase was not analysed because when a SiO_2-PSSA nanocomposite is stirred in CPME/water mixtures, it is preferentially suspended in aqueous droplets or surrounded by the aqueous phase. Catalyst surface (hydrophilic) has no affinity for CPME, a very apolar solvent. Moreover, the leached polymer is not soluble in CPME. It is clear that the leaching of the sulphonic polymer occurs (see Figure 5S5 and discussion therein for further information and discussion), the most substantial loss of sulphur (and consequently, of polymer), essentially during the first run. The leaching was considerably less important in further runs (only in certain cases, the loss of sulphur was also significant for the second run). The total amount of S lost in the different samples ranged from 20-30% of the initial content. Previous results have shown that the contribution of leached species to the overall activity is important in the first run; while in further runs the contribution becomes negligible [20]. This is in agreement with the decrease of the leaching of acid sites depicted in Figure 5S5.

The changes in the chemical and textural properties experienced by the catalysts after being subjected to the reaction conditions were also investigated different techniques. To prevent interferences from humins, resins and other hydrocarbons being deposited over the catalyst surface during reaction (see Figure 5S6 in the SI section for evidence of these deposits), the nanocomposites were subjected to the reaction conditions but without the incorporation of xylose.

The acid sites loading of the nanocomposites of the Si-PSSA-T series after hydrothermal treatment are summarised in Table 5.1. That of the nanocomposites prepared at higher temperatures (373, 423 and 473 K) were almost negligible (0.02-0.03 mmol $H^+ \cdot g_{cat}^{-1}$). However Si-PSSA-298 and Si-PSSA-348 nanocomposites still present a significant fraction of the retained molecules that withstood the hydrothermal conditions and actually their acid site loadings after the hydrothermal treatement (0.24 and 0.18 mmol $H^+ \cdot g_{cat}^{-1}$) were even larger than those of the fresh nanocomposites prepared at $T \geq 373$ K. Very likely the PSSA molecules that are retained are those with a large number of electrostatic interactions with amino groups whereas those leached away present less number of electrostatic interactions and are less firmly retained by the solid. These more firmly retained PSSA with the greatest number of acid-base interactions between sulphonic and amino groups has a limited number of active free acid sites left for reaction. Finally, hydrothermally treated Si-473 solid also presents a negligible acid site loading, demonstrating that sulphuric acid was also leached.

Table 5.2 also includes the acid loadings of the Si-PSSA-S/N series after hydrothermal treatment. The titration revealed that the acid loading substantially decreased after hydrothermal treatment: from 0.27 to 0.18, from 0.74 to 0.24, from 0.82 to 0.32 and from 0.94 to 0.43 mmol $H^+ \cdot g^{-1}$ for the nanocomposites with nominal S/N =2.2, 4.4, 8.8 and 24, respectively. This decrease in the acid site loading is in agreement with the deactivation of the catalyst observed in Figure 5.6 during reuse.

Si-PSSA-24 sample still exhibits after the hydrothermal treatment a concentration of free acid sites larger than Si-PSSA-4.4. However its catalytic performance after several reuses was quite similar to that of Si-PSSA-4-4. This

suggests that the acid loading is not the only property that defines the catalytic activity; the textural properties must be also considered (as it will be shown below, the Si-PSSA-4.4 nanocomposite after thermal treatment exhibits a substantially larger amount of mesopores and therefore a texture with a large fraction of more accessible pores). Besides the deposition of organic products may also participate in the deactivation, via fouling or poisoning of the catalyst.

The isotherms of the Si-PSSA-T nanocomposites series after hydrothermal treatment are shown in Figure 5.1B, (their primary textural properties are reported in Table 5S1, see Supplementary Section for further details and discussion). As shown in Figure 5.1B, the isotherms of the Si-PSSA-298 and Si-PSSA-348 change from that representative of non-porous materials to a type I isotherm (H2-like hysteresis loops) characteristic of solids that are essentially microporous. All of these changes in the textural properties are compatible with the leaching of part of the polymer, which leaves the pores accessible for filling with N_2. The polymer molecules still remain within the micropores since desorption branch did not close at P/P_0=0.4. The hydrothermal treatment also results in densification of the xerogel structure and sintering of the silica particles, creating interparticle mesopores. The changes in the Si-PSSA-373 solid are also compatible with a densification process (there is decrease in the N_2 retention by micropores and the presence of mesopores was also evident in the H2-type hysteresis loop). The isotherm for Si-PSSA-423 after the hydrothermal treatment is quite similar to that obtained for the fresh sample, however the textural parameters deduced from this isotherm indicate that the solid experienced a loss in specific surface (from 187.1 to 97.8 m^2/g) from both micropores and mesopores. However, the isotherm of Si-PSSA-473

after hydrothermal treatment and the textural parameters deduced from it are essentially the same as those obtained for the fresh sample. We have to consider that the solid was synthesized a 473 K, which is 20 K greater than the temperature of the hydrothermal treatment. Remarkably, the Si-473 xerogel prepared without polymer and at 473 K exhibited a significant decrease in specific surface area. These data further highlight the role of the polymer in stabilizing the pore networks in Si-PSSA nanocomposites.

Regarding the Si-PSSA-S/N series, these nanocomposites also exhibited a considerable change in textural properties after the hydrothermal treatment. Results can be consulted in Figure 5S7 and Table 5S3 in Supplementary Information: they changed from non-porous materials to porous materials with a quite high specific surface area. The solids became essentially microporous, although mesopores were also present (pore width diameters of approximately 3-4 nm were estimated using the BJH method in the adsorption branch). Leaching of the polymer and condensation of the silica network explain the appearance of micro- and mesopores. Note that the hydrothermally treated Si-PSSA-4.4 nanocomposites presented the largest BET surface and the largest amount of mesopores. Notwithstanding that the acid sites loading of this catalyst is smaller than that of Si- PSSSA-8.8 and 24 after the hydrothermal treatment, its better textural properties may be in the origin of its better reutilization properties.

Figure 5.3 also presents the ^{29}Si MAS-NMR and ^{13}C CP-MAS-NMR spectra of the Si-PSSA-348 solid after the hydrothermal treatment. The ^{13}C spectrum is very similar to that of the fresh sample: the presence of polymer and of protonated amine is evidenced by the signals at 43.2, 126.7, 142.1 and 149.5 ppm and by the signals at 9.9 and 21.7, respectively. In contrast, changes

are evident in the ^{29}Si spectrum of the hydrothermally: the signals at -109 and -102 ppm assigned to the Q^4 and Q^3 siloxane species now predominate, and the Q^2 signal at -93 ppm (originating from $(SiO)_2Si-(OH)_2$-like species) faded away. In fact, the spectrum of this sample closely resembles those of nanocomposites prepared at higher temperatures, which are also presented in Figure 5.3. Therefore, the silica framework of the hydrothermally treated Si-PSSA-348 solid is now more condensed as a consequence of the densification process that occurred during treatment, which is in agreement with the N2 isotherm results.

4. Conclusions

In summary, SiO_2 xerogel-PSSA nanocomposites can be prepared using sol-gel procedures with TEOS and APTES precursors. The ionic interactions between amino groups (incorporated in the silica) and the sulphonic groups of the polymer are responsible for the retention of the polymer. The optimum synthesis temperature is 348 K; in practice, higher temperatures result in lower polymer loadings in the prepared nanocomposites. Lower synthesis temperatures result in larger polymer retention, but other properties, such as the hydrothermal stability of the polymer molecules and the textural properties, must also be considered. The nanocomposite prepared at 348 K combined a good initial polymer loading and better hydrothermal stability. An optimum S/N at.ratio for the synthesis was not found since the actual polymer loading increases when the initial concentration of the polymer increases. However, an initial S/N ratio between 4 and 8 is recommended; a larger initial ratio does not result in a substantial increase in the actual polymer loading, nor does it improve the reusability properties of the nanocomposites. When the

SiO_2xerogel-PSSA nanocomposites were used as catalysts for the reaction investigated (xylose to furfural reaction), they deactivate regardless of the synthesis temperature and the S/N at. ratio used in the synthesis. Leaching of the polymer is the primary cause of deactivation, but the deposition of organic molecules over the surface of the nanocomposites cannot be excluded as source of deactivation because they can result in fouling and/or poisoning of the active sites.

The hydrothermal stability of these nanocomposites was affected by polymer leaching during the first reutilisation cycles. Lixiviation becomes considerably less intense in successive runs. Apparently, the weakly retained polymer molecules are initially removed, and only the more firmly retained PSSA molecules remain. Most likely, these more firmly retained PSSA molecules are those with the greatest number of acid-base interactions between sulphonic and amino groups, and therefore, a limited number of active free acid sites are left for reaction. Further research is required to assess the catalytic behaviour of these SiO_2xerogel-PSSA nanocomposites in other reactions driven by acid sites and to improve the hydrothermal stability of the SiO_2xerogel-PSSA nanocomposites against the leaching of polymer.

5. Supplementary information

- **Preparation of the Si-PSSA-T series**

For the first series of samples (Si-PSSA-T series), the synthesis temperature was varied (298, 348, 373, 423 and 473 K) while the amounts of TEOS, APTES and PSSA used in the synthesis were maintained constant. In practice, *ca.* 5 g of PSSA (corresponding to 27.8 g of PSSA aqueous solution), *ca.* 25.7 g of TEOS and *ca.* 2.7 g of APTES (corresponding to S/N and Si/N atomic ratios of 2.2 and close to 11, respectively) were added to the synthesis reactor. These S/N and Si/N ratios were the same as those used in previous exploratory work [20]. The catalysts are referred to as Si-PSSA-T (where T is temperature of synthesis in K), where Si indicates the presence of silica in the catalysts, followed by PSSA in the cases where polymer was present during the synthesis. For this series, because the nominal S/N and Si/N ratios both remained unchanged during the synthesis, no other identifiers are required in the sample labels, except that of the temperature.

- **Preparation of the Si-PSSA-S/N series**

A second series of solids were prepared by changing the initial concentration of PSSA but by keeping constant the Si/N atomic ratio and the synthesis temperature close to 11 and 348 K, respectively. The concentration of PSSA was selected as to have an initial S/N at. ratios of 2.2, 4.4, 8.8 and 24. In practice, the required amounts of the aqueous PSSA solution (to have *ca*. 10, 20 and 54 grams of PSSA), TEOS (25.2 g) and APTES (2.7 g) were introduced in the round-bottom glass flask used for the synthesis. Then the same protocol

explained above was followed. The samples were denoted as Si-PSSA-S/N, where S/N refers to the S/N at. ratio. Note that Si-PSSA-348, which was investigated in the previous section and prepared at 348 K with an initial S/N atomic ratio = 2.2, is now labelled Si-PSSA-2.2.

- **N_2 adsorption isotherms**

Table 5S1 presents the main textural parameters determined from the isotherms. The adsorption branch of the isotherm was used to estimate the pore size diameter. Some of these materials presented a considerable fraction of micropores; therefore, estimating the specific surface areas of these materials using the BET method is not realistic. The BET surface area of the micropores reflects the retention capacity of micropores, whereas the BET surface area of mesopores estimates its monolayer capacity. The methodology proposed by Rouquerol et al. was employed to accurately determine the BET retention capacity of microporous-mesoporous materials, and the t-plot method was used to distinguish between the micropores and the external surface due to the mesopores [20].

Table 5S1. Textural properties of nanocomposites prepared using different synthesis temperatures (initial Si/N close to 11 and S/N= 2.2, respectively) and after hydrothermal treatment with water/CPME at 453 K.

Catalyst	BET (m^2/g)	Micropores (m^2/g)	Mesopores (m^2/g)	Micro/ mesopores	Pore sizediam. (nm)
Si-473					
fresh	355.0	0	355.0	0	17.5
HT[a]	171.4	0	171.4	(-)	12.5
Si-PSSA-298					
fresh	<1	<1	<1	-	nd
HT	339.8	327.4	12.5	26.2	3.0[b]
Si-PSSA-348					
fresh	<1	<1	-	-	nd
HT	301.7	278.2	23.5	11.83	2.6[b]
Si-PSSA-373					
fresh	415.3	411.3	3.9	105.46	< 1
HT	116.1	96.9	19.2	5.05	5.0[b]
Si-PSSA-423					
fresh	187.1	70.3	116.8	0.60	100
HT	97.8	16.7	81.1	0.21	> 100
Si-PSSA-473					
fresh	44.2	9.7	34.5	0.28	100
HT	41.9	3.3	38.6	0.08	> 100

[a] HT stands for hydrothermally treated nanocomposite

[b] Mean pore diameter of mesopores (pore size of micropores could not be determined because they were smaller than 1 nm)

The catalysts synthesised at lower temperatures (298 and 348 K) exhibit isotherms characteristic of non-porous materials, and their BET surface areas are negligible due to the presence of polymer covering and/or filling the pores [20]. As the synthesis temperature increased beyond 348 K, the catalysts exhibited measurable N_2 adsorption. The isotherm for the catalyst synthesised at 373 K is assigned to type I, which essentially corresponds to microporous solids that contain a relatively small amount of mesopores. The shape of the hysteresis loops corresponds to type H4. Table 5S1 indicates that this solid is essentially microporous because more than 98% of the BET retention capacity corresponds to the filling of micropores. The pore size distribution calculated by applying the BJH algorithm to the adsorption branch did not present any maximum in the range of investigated pressures (pore diameter larger than 1 nm), indicating that the average size of the pores is less than 1 nm. In contrast, the activated adsorption (gentle slope) observed for relative pressures greater than 0.1 suggests that the presence of polymer molecules within the micropores prevents the rapid filling of the pores. Higher pressures are required to push the N_2 into the micropores.

When the synthesis temperature increased from 373 to 423 K, the isotherm apparently corresponds to a mesoporous material (type IV isotherm) but, as shown in Table 5S1, micropores are also present because their retention capacity is equivalent to 60 % of that of the mesopores. The Si-PSSA-473 catalyst exhibited a type IV isotherm, which is characteristic of mesoporous solids (average mesopore diameter determined using the BJH method is greater than 100 nm); the contribution of micropores was smaller than in the previous case. This catalyst also presented a smaller BET surface area. Finally, the blank Si-473 sample, which was also prepared at this temperature but by using

H_2SO_4, exhibited an isotherm characteristic of only a mesoporous solid and a much larger specific surface area. It is clear that the presence of polymer filling the pores in the nanocomposite strongly modifies the texture of the solid.

- **Thermogravimetric analysis of fresh catalysts**

Thermogravimetric analyses were made for all the freshly prepared nanocomposites. As seen from the Figure 5S1, all the catalysts where polymer is present exhibited a three-stage thermal degradation profile. For all the samples, a weight loss below 127ºC is observed, which is due to the removal of the adsorbed water on either the hygroscopic polymer or on silica network. The second weight loss between 600 and 800 K corresponds to the removal of the sulfonic acid groups and the last feature at temperatures over 800 K is due to the combustion of the polymer main chain [6, 42]. Remarkably, the weight loss associated to sulphonic groups is quite in harmony with the sulphur loading determined by elemental chemical analysis. These weight loss processes associated with the presence of the polymer in the solid structure are superimposed over the removal of hydroxyl groups from the silica and combustion of aminopropyl groups. A contribution from the combustion of ethoxy groups from unhydrolyzed TEOS and APTES occluded in the three-tridimensional structure of the silica cannot be discarded. As it is shown, these later combustion processes appeared in the blank Si-473 prepared without PSSA in which the weight loss stage corresponding to the polymer chain must be absent.

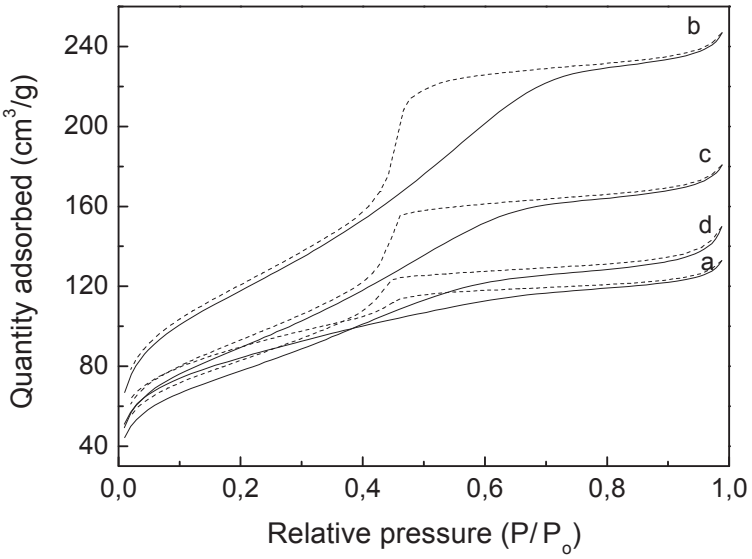

Figure 5S1.Thermogravimetric analysis of catalysts prepared at different synthesis temperatures

Figure 5S2 shows the TG analysis of the samples prepared at 348 K but by increasing the initial polymer loading. According to this figure, all of the catalyst present the same weight loss processes as the catalysts prepared under different synthesis temperature. It is observed again three weight loss processes: one below 127 ºC corresponding to the water adsorbed; the second in the range between 600-800K that corresponds to the combustion the sulfonic acid groups and the last one at temperatures over 800 K which is due to the combustion of the polymer backbone [42], superimposed over the removal of hydroxyl groups from silica and combustion of aminopropyl groups from APTES. All of them lose the same amount of physisorbed water but, as it would be expected, the loss of polymer increases as the polymer loading in the catalysts is higher.

Again, in all of the cases, the materials are again thermally stable up to 600K, which is a temperature much higher than that frequently used in xylose dehydration (443-473K).

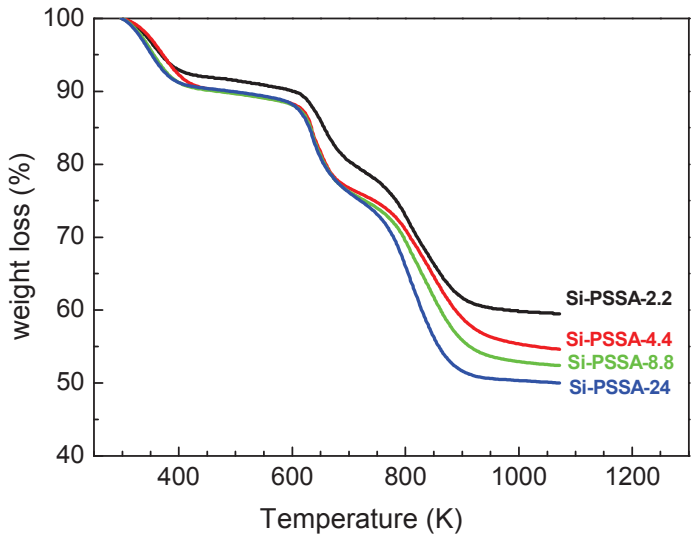

Figure 5S2. TGA of catalysts synthesized at 348K and with different polymer charge (in air)

- **DRIFT spectra of fresh catalysts**

Table 5S2 summarises the assignment of the bands observed in the DRIFT spectra of Si-PSSA-2-1 and Si-473 (Figure 5.2 of this chapter).

Table 5S2. Assignments of DRIFT bands

Si-473	Si-PSSA-2.2	Assignment
3729		ϒO-H) in isolated silanol [29, 30]
3658		ϒO-H) in H-bonded vicinal silanol and/or ϒO-H) in silanol H-bonded to water [29, 30]
3267	3267	ν_{as}(N-H) in R-NH_3^+ [20, 31]
3163	3160	ν_s(N-H) in R-NH_3^+ [20, 31]
	3060	ν(C-H) in aromatic ring [20]
2981		ν_{as}(C-H) in CH_3 (ethoxy group) [31]
2930	2930	ν_{as}(C-H) in CH_2 (ethoxy group or propylamine or polymer backbone) [20, 31]
2896		ν_s(C-H) in CH_3(ethoxy group) or in CH_2 (propylamine) [31]
2874		ν_s(C-H) in CH_2 (propylamine) [31]
1620	1620	δ_{as}(N-H) in R-NH_3^+ [20, 31]
	1598	ν(C-C) in aromatic ring [20]
1523	1512	$\delta_{.s}$(N-H) in R-NH_3^+ [20, 31]
	1495	ν(C-C) in aromatic ring [20]
1470	1470	ν(C-H) in CH_2 (propylamine and polymer backbone)[31]
	1450	δ (C-H) in CH_2 (propylamine and polymer backbone) and ν(C-C) in aromatic ring [20, 31]
1415	1412	w(C-H) and/or t(C-H) in CH_2 (propylamine and polymer backbone) [31]
	1355	ν_{as} O=S=O in SO_3H [32]
1320	1267	ν_{as} (Si-O-Si) in SiO_2 [20]

C-H deformation bands in CH_2: δ scissoring; w wagging; t twisting

The Si-473 catalyst exhibits typical bands from O-H groups (3729 and 3658 cm^{-1}) at the surface of SiO_2 (isolated OH silanol and silanols H-bonded to either other surface OH groups or to surface H_2O molecules). The two weaker bands at *ca.* 3267 and 3163 cm^{-1} arise from (N-H) stretching vibrations in

protonated amine groups (the bands attributed to bending of the amine groups are located at 1620 and 1523 cm^{-1}). The sulphuric acid used in the synthesis is retained by interactions with the amine groups, and the latter become protonated. C-H stretching vibration bands from propylamine groups at 2981, 2930, 2896 and 2874 cm^{-1} and bands from ethoxy groups originating apparently from the incomplete hydrolysis of TEOS and APTES are also visible. The C-H bending bands of these alkyl groups are located at 1470, 1450 and 1415 cm^{-1}. The very intense band at 1320 cm^{-1} is assigned to the Si-O-Si lattice vibration of the silica network.

The DRIFT spectrum of the Si-PSSA-348 catalyst exhibits distinct features compared to that of Si-473 resulting from the presence of the polymer. The region for the (C-H) stretching vibration is now dominated by bands at 3060 and 2930 cm^{-1} associated with the polymer backbone. Propylamine groups also present ν(C-H) bands that must be superimposed with those of the polymer, thereby explaining the lack of resolution in this region of the spectrum. Bands from ethoxy groups are absent, indicating that the hydrolysis of TEOS is now complete. The presence of sulphonic groups is also evidenced by the asymmetric stretching vibration of the (O=S=O) bond in sulphonic groups at 1355 cm^{-1}. The symmetric stretching vibration that must be located at *ca.* 1125 cm^{-1} cannot be observed because it is overshadowed by the considerably more intense band at 1267 cm^{-1} arising from Si-O-Si lattice vibration of the silica network.

Interestingly, the pattern of silanol vibrations also differs from that of Si-473, which indicates that these vibrations are being perturbed by the presence of the polymer. The protonation of the Si-OH groups by the sulphonic moieties of the polymer ($R\text{-}SO_3^-\text{–}^+H\text{–}HO\text{-}Si$) is responsible for this

perturbation. Two new deformation (C-H) vibrations from the polymer are now visible at 1598 and 1495 cm^{-1}. The polymer also exhibits two additional C-H deformation bands at 1470 and 1412 cm^{-1}, which coincide with those of propylamine groups. With respect to the N-H DRIFT features of $R\text{-}NH_3^+$ groups, bands at 3267 and 3160 cm^{-1} (N-H stretching) and at 1620 and 1512 cm^{-1} (N-H bending) are also visible. The presence of sulphonic groups explains the protonation. The presence of amine groups hydrogen bonded to silanol groups are not considered because they should appear at different wavenumbers [20, 31].

The possibility that the protonation of amine groups had been accomplished by the acidic silanol groups can be excluded. The protonation of amine groups by silanol groups is mediated by the presence of water molecules at the surface of functionalised silica, but this protonation is reversed by the removal of water by either outgassing or by heating above 373 K [38, 39]. The removal of water would then result in a shift of the amine bands to wavenumbers of H-bonded amine vibrations that are located at higher wavenumbers. This shift does not occur in our case: the positions of the amine bands in the sample reported here do not change while heating under a N_2 flow. Therefore, the positions of the amine bands in the DRIFT spectrum demonstrate that for the sample described in Figure 5.2, the protonation of amine groups is driven by sulphonic groups. Note that most of the amine groups are protonated because bands from free or H-bonded amines are not observed; therefore, amine groups are highly involved in the stabilisation of the polymer through electrostatic interactions.

Figure 5S3 compares the DRIFT spectrum of Si-PSSA-4.4 catalyst with that of Si-PSSA-2.2 (or as it is also named, Si-PSSA-348) after heating the

sample at 423 K under Ar flow. The spectrum of Si-473 sample, prepared without polymer but with H_2SO_4, is also included also for comparison purposes. The main bands are also summarized in Table 5S2. The spectra of the Si-APES-4.4 sample shows the same bands observed for the Si-APES-2.2 solid, but the polymer bands are more intense as the polymer loading is now larger. The band at 2930 arising from vibrations of C-H in polymer backbone become noticeable but, however, the band at 3060 cm^{-1} arising from vibrations of C-H bonds in aromatic ring is not that much larger. The bands at 3267 and 3160 cm^{-1} corresponding to, respectively, symmetric and asymmetric stretching vibration of protonated amine group ($R\text{-}NH_3^+$) and the band at 1620 and 1512 cm^{-1}, assigned to asymmetric and symmetric (N-H) bending vibrations in these groups, also appeared in this case but with larger intensity than in Si-APES-2.2 catalyst due to the presence of a larger polymer loading (free and H-bonded amines present the bands at substantially lower wavenumbers) [31].

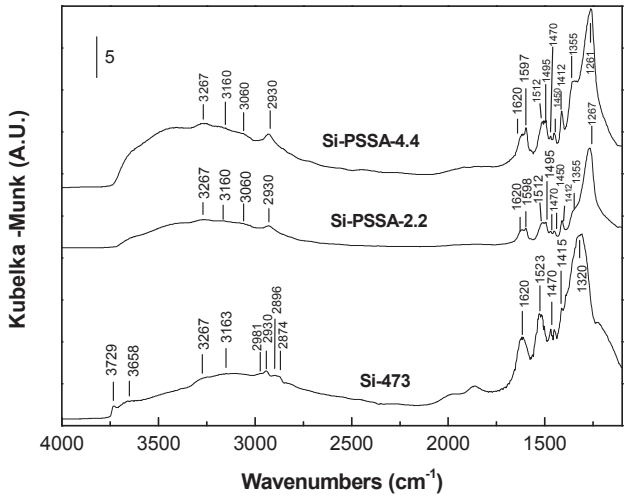

Figure 5S3. DRIFT spectra of the most representative catalysts after heating at 423K under Ar flow

- **Reutilisation of nanocomposites in the reaction of xylose dehydration to furfural**

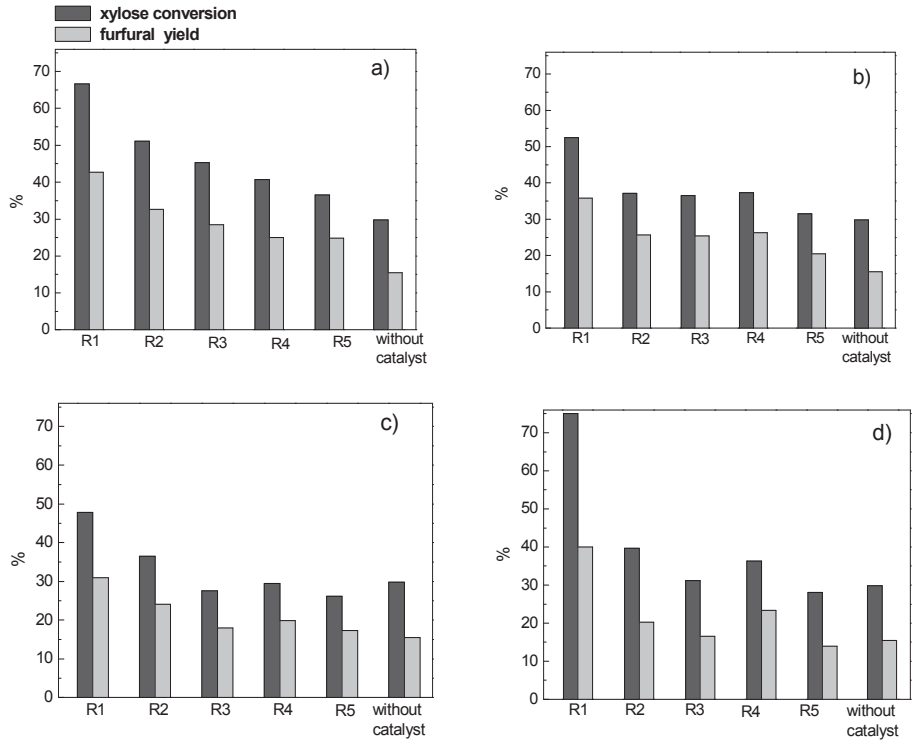

Figure 5S4. Recycling of the catalysts synthesised at different temperatures: a) Si-PSSA-298, b) Si-PSSA-348, c) Si-PSSA-473 and d) Si-473. Reaction conditions: 10 wt. % xylose and 5 wt. % catalyst in the aqueous phase, CPME/aqueous phase mass ratio= 2.33; 5 g total solution, 453 K, 120 min.

Figure 5S4 shows the xylose conversions and furfural yields for consecutive runs. The xylose conversion and furfural yield for the autocatalytic reaction (without catalyst) are also included in the graph. All of the catalysts

underwent deactivation. Si-PSSA-298, the catalyst with the largest amount of acid sites and with the best performance during the first run, exhibited continuous deactivation in the subsequent runs. After five runs, this catalyst presented conversion and yield values slightly greater than those obtained in the autocatalytic experiment (40 % and 25 %, respectively), but it appears that further runs would result in a closer approximation to the autocatalytic data. Si-PSSA-348 exhibited deactivation during the first run, but after this run, it appeared to reach a more stable state with the conversion consistently scattered around 35 % and the yield maintained at approximately 25 %. These values are only slightly greater than the autocatalytic values (30 and 15 %, respectively). The activity of Si-PSSA-473 decreased after the first run, and the remaining activity was similar to that achieved without the use of a catalyst. The other two catalysts synthesised at 373 and 423 K also exhibited also significant deactivation after 5 runs (results not shown for the sake of brevity).

- **Chemical analysis of the reaction mixture after successive cycles: S leaching**

The amount of S lost during the recycling tests was analysed by TXRF analyses of the aqueous phase obtained after the successive runs were conducted. It is assumed that the leached polymer is not soluble in CPME. In practice, organic and aqueous phases from the reaction mixture were separated by centrifugation, and an aliquot of the aqueous phase was collected for analysis and filtered through a 0.45 μm filter. Figure 5S5 presents the amount of S present in the solution expressed as the loss of S relative to that initially present in the fresh catalyst. The results indicate that the most substantial loss of

sulphur (and consequently, of polymer) occurred during the first run. After the first run, the leaching was considerably less intense. In certain cases, the loss of sulphur was also significant for the second run. The Si-PSSA-298 sample exhibited a more persistent loss (still shows a significant loss during the fourth run), which is in agreement with the sustained loss of activity detected for this sample during the reutilisation tests.

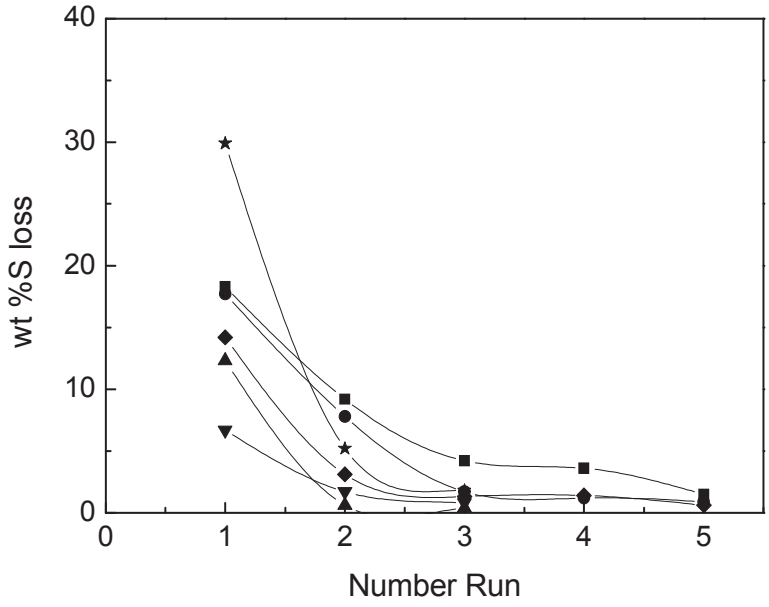

Figure 5S5. Loss of sulphur expressed as wt. % of S initially present in the first run: (■) Si-APES-2.2-298; (●) Si-PSSA-348; (▲) Si-PSSA-373; (▼) Si-PSSA-423; (◆)Si-PSSA-473; and (★) Si-473. Reaction conditions: 10 wt. % xylose and 5 wt. % catalyst in the aqueous phase, CPME/ aqueous phase mass ratio= 2.33; 5 g total solution, 453 K, 120 min.

- **Thermogravimetric analysis of used catalysts**

After using in the reaction, all the used catalysts were characterized through different analysis techniques with the purpose to link structure with activity and stability of all the tested catalysts. First, thermogravimetric analysis of two used catalysts after all the recycling runs were conducted from room temperature to 1073 K under air atmosphere and the results are shown in Figure 5S6. As it is shown, both reused catalysts only present two stages thermal degradation profile: a first weight loss below 127 ºC corresponding to the removal of the water adsorbed at the catalysts and a second larger weight loss between 500 and 900K overlapped to the weight loss of the polymer. The difference in this region of the thermogravimetric analysis between fresh and used catalyst corresponds to the removal of organic deposits accumulated on the catalyst surface during the reaction. This hypothesis was also corroborated by the increasing of the carbon content in the used catalysts obtained by elemental analysis (results not shown). Besides, the catalysts changed the color from white (the color of the fresh catalyst) to brown at the end of the reaction, even after being washing with water and CPME as a solvent. That indicates that an important part of the accumulated organic matter is not dissolved in CPME.

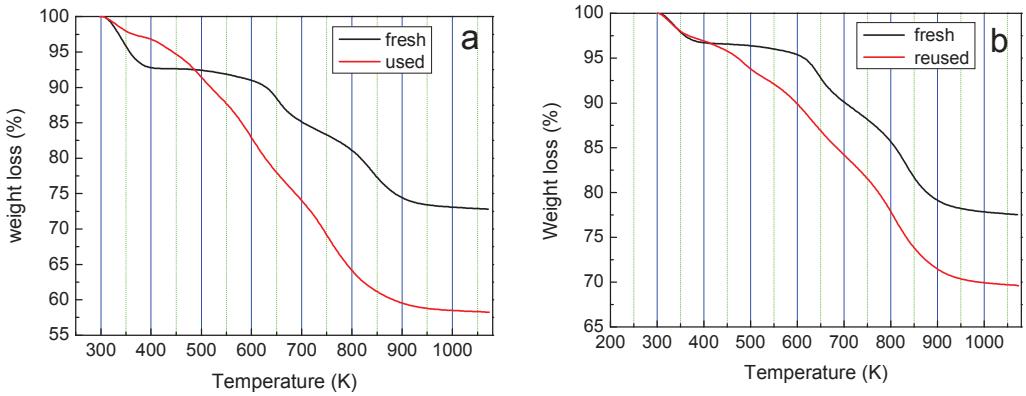

Figure 5S6. TGA of used catalysts (in air) after recycling runs: a)Si-PSSA-2.2-373 and b)Si-PSSA-2.2-423

- **Hydrothermal treatment of nanocomposites in H_2O/CPME mixturesat 453K: isotherms and textural properties**

The changes in the acid loading and in the textural properties of the catalysts after being subjected to the reaction conditions were investigated by titration and by N_2 physisorption. To prevent interferences from humins, resins and other hydrocarbons being deposited over the catalyst surface (see Figure 4S4 section for evidence of these deposits), the nanocomposites were subjected to the reaction conditions in H_2O/CPME mixtures but without the incorporation of xylose. In practice, 200 mg of each catalyst, 1.5 g of water and 3.5 g of CPME (CPME/ aqueous phase mass ratio= 2.33) were poured into the same glass reactor in which the catalytic reactions were conducted and stirred at 463 K overnight. This treatment time represents more than five reuse cycles; thus, it is a very reasonable approximation of the leaching and of the textural changes

that can occur during reuse of the catalysts. Subsequently, the reaction mixture was cooled and centrifuged to separate the liquid from the solid catalyst. The solid was then washed again to remove all of the polymer molecules that leached but that may be weakly retained. After the liquid was centrifuged, the treated solid was dried at 120ºC overnight, and its acid site loading was determined as explained above.

The isotherms of the hydrothermally treated nanocomposites are shown in Figure 5.1B, (their primary textural properties are reported in Table 5S1, see Supplementary Section for further details and discussion). As shown in Figure 5.1B, the isotherms of the catalysts synthesised at temperatures $T \leq 348$ K change from that representative of non-porous materials to a type I isotherm characteristic of solids that are essentially microporous. The hysteresis loops corresponded to type H2, and the desorption branch did not close at $P/P_0 = 0.4$. As explained above, this result indicates the presence of polymer within the micropores. All of these changes in the textural properties of Si-PSSA-298 and Si-PSSA-348 are compatible with the leaching of part of the polymer, which leaves the pores accessible for filling with N_2. Note that some mesopores are present and that the hydrothermal treatment may result in densification of the xerogel structure and sintering of the silica particles, thereby creating interparticle mesopores. The pore size distribution estimated by applying the BJH method to the adsorption branch provided a mean pore diameter of *ca*. 3 nm for the mesopores in the Si-PSSA-298 and Si-PSSA-348 nanocomposites. The Si-PSSA-373 solid also exhibited a change in the shape of the isotherm, but the nature of the change was different: it changed from a type I isotherm with almost no hysteresis loop to an isotherm in which the presence of mesopores

was evident in the H2-type hysteresis loop. The loop closed again at $P/P_0 < 0.4$, indicating the presence of polymer within the micropores. This change was also accompanied by a decrease in the specific area, apparently because of the sintering and densification of the silica xerogel network. In fact, the N_2 retention by micropores significantly decreased (from 415.3 to 116.1 m^2/g), whereas that by mesopores increased (from 3.9 to 19.2 m^2/g). Therefore, this solid underwent a change during the hydrothermal treatment from being an essentially microporous solid to an essentially mesoporous solid, whereas in the first two cases, the solids became essentially microporous. It appears that the presence of a larger loading of polymer in fresh Si-PSSA-298 and Si-PSSA-348 before treatment is responsible for the stabilisation of the microporosity in these solids.

The isotherm for Si-PSSA-423 after the hydrothermal treatment quite similar to that obtained for the fresh sample: type IV with a H4-like hysteresis loop. However, the textural parameters deduced from this isotherm indicate that the solid experienced a loss in specific surface area (from 187.1 to 97.8 m^2/g) from both micropores and mesopores. The isotherm of Si-PSSA-473 after hydrothermal treatment and the textural parameters deduced from it are essentially the same as those obtained for the fresh sample. We have to consider that the solid was synthesised a 473 K, which is 20 K greater than the temperature of the hydrothermal treatment. Remarkably, the Si-473 xerogel prepared without polymer and at 473 K exhibited a significant decrease in specific surface area. These data further highlight the role of the polymer in stabilising the pore networks in Si-PSSA nanocomposites.

Table 5S3. Textural properties of nanocomposites prepared at 348 K with different initial polymer concentration (initial nominal Si/N =11) and after hydrothermal treatment with water/CPME at 453K .

Catalyst	BET (m^2/g)	Micropores (m^2/g)	Mesopores (m^2/g)	Micro/ Mesopores Ext.[a]	Averagesize diameter (nm)
Si-PSSA-2.2	301.7	278.2	23.5	11.8	2.6
Si-PSSA-4.4	418.3	385.6	32.7	11.8	4.3
Si-PSSA-8.8	318.6	291.9	26.8	10.9	4.0
Si-PSSA-24	275.9	248.7	27.3	9.1	3.1

[a] Calculated as the ratio between the area of the micropores and the area of mesopores (Rouquerol method).

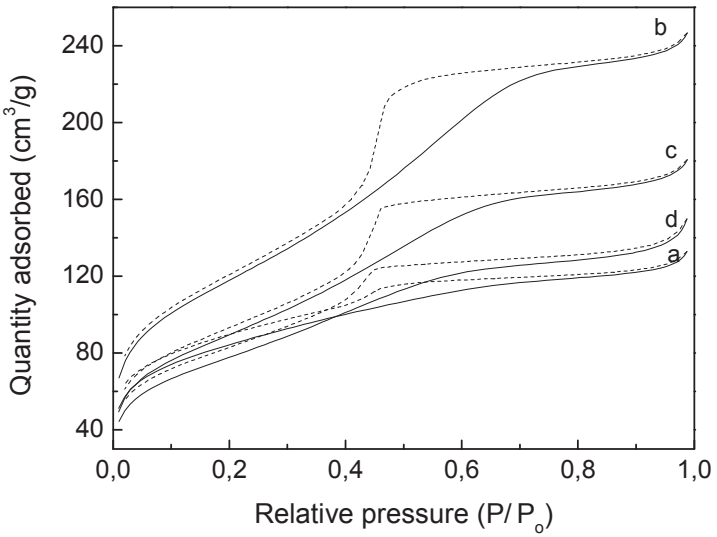

Figure 5S7. N_2 adsorption (solid lines) and desorption (dashed lines) isotherms of catalysts with different polymer charge after hydrothermal treatment in CPME/water at 453K: a) Si-PSSA-2.2; b) Si-PSSA-4.4; c) Si-PSSA-8.8; d.Si-PSSA-24.

6. Bibliography

[1] W.W. Sulkowski, A. Wolinska, B. Szoltysik, W.M. Bajdur, A. Sulkowska, Polymer Degradation and Stability, 90 (2005) 272-280.
[2] Y. Inagaki, M. Kuromiya, T. Noguchi, H. Watanabe, Langmuir, 15 (1999) 4171-4175.
[3] I. Bekri-Abbes, S. Bayoudh, M. Baklouti, Journal of Polymers and the Environment, 14 (2006) 249-256.
[4] R.M.N. De Assuncao, B. Royer, J.S. Oliveira, G.R. Filho, L.A. De Castro Motta, Journal of Applied Polymer Science, 96 (2005) 1534-1538.
[5] N. Alonso-Fagúndez, V. Laserna, A.C. Alba-Rubio, M. Mengibar, A. Heras, R. Mariscal, M.L. Granados, Catalysis Today, 234 (2014) 285-294.
[6] M.L. Granados, A.C. Alba-Rubio, I. Sádaba, R. Mariscal, I. Mateos-Aparicio, A. Heras, Green Chemistry, 13 (2011) 3203-3212.
[7] R. Karinen, K. Vilonen, M. Niemela, ChemSusChem, 4 (2011) 1002-1016.
[8] S.G. Wettstein, D. Martin Alonso, E.I. Gürbüz, J.A. Dumesic, Current Opinion in Chemical Engineering, 1 (2012) 218-224.
[9] J.P. Lange, E. Van Der Heide, J. Van Buijtenen, R. Price, ChemSusChem, 5 (2012) 150-166.
[10] A. Corma Canos, S. Iborra, A. Velty, Chemical Reviews, 107 (2007) 2411-2502.
[11] B.V. Timokhin, Russian Chemical Reviews, 68 (1999) 73-84.
[12] D.W. Rackemann, W.O. Doherty, Biofuels, Bioproducts and Biorefining, 5 (2011) 198-214.
[13] J.J. Bozell, L. Moens, D.C. Elliott, Y. Wang, G.G. Neuenscwander, S.W. Fitzpatrick, R.J. Bilski, J.L. Jarnefeld, Resources, Conservation and Recycling, 28 (2000) 227-239.
[14] K.J. Zeitsch, The Chemistry and Technology of Furfural and Its Many By-products, *Sugar Series, vol. 13*, Elsevier Science, The Netherlands (2000).
[15] P.A. Russo, S. Lima, V. Rebuttini, M. Pillinger, M.G. Willinger, N. Pinna, A.A. Valente, RSC Advances, 3 (2013) 2595-2603.
[16] L.R. Ferreira, S. Lima, P. Neves, M.M. Antunes, S.M. Rocha, M. Pillinger, I. Portugal, A.A. Valente, Chemical Engineering Journal, 215-216 (2013) 772-783.
[17] S. Lima, P. Neves, M.M. Antunes, M. Pillinger, N. Ignatyev, A.A. Valente, Applied Catalysis A: General, 363 (2009) 93-99.

[18] T.J. Dickerson, N.N. Reed, K.D. Janda, Chemical Reviews, 102 (2002) 3325-3344.
[19] S. Pandey, S.B. Mishra, Journal of Sol-Gel Science and Technology, 59 (2011) 73-94.
[20] I. Sádaba, M. Ojeda, R. Mariscal, M.L. Granados, Applied Catalysis B: Environmental, 150-151 (2014) 421-431.
[21] R. Tamaki, Y. Chujo, Chemistry of Materials, 11 (1999) 1719-1726.
[22] M.J. Campos Molina, R. Mariscal, M. Ojeda, M. López Granados, Bioresource Technology, 126 (2012) 321-327.
[23] J.A. Melero, L.F. Bautista, G. Morales, J. Iglesias, R. Sánchez-Vázquez, Chemical Engineering Journal, 161 (2010) 323-331.
[24] .A. Melero, L.F. Bautista, J. Iglesias, G. Morales, R. Sánchez-Vázquez, I. Suárez-Marcos, Topics in Catalysis, 53 (2010) 795-804.
[25] C. Pirez, J.M. Caderon, J.P. Dacquin, A.F. Lee, K. Wilson, ACS Catalysis, 2 (2012) 1607-1614.
[26] I I. Agirrezabal-Telleria, J. Requies, M.B. Guémez, P.L. Arias, Applied Catalysis B: Environmental, 115-116 (2012) 169-178.
[27] A.S. Dias, M. Pillinger, A.A. Valente, Journal of Catalysis, 229 (2005) 414-423.
[28] A. Martín, G. Morales, F. Martínez, R. Van Grieken, L. Cao, M. Kruk, Journal of Materials Chemistry, 20 (2010) 8026-8035.
[29] G. Orcel, J. Phalippou, L.L. Hench, Journal of Non-Crystalline Solids, 88 (1986) 114-130.
[30] P. Innocenzi, Journal of Non-Crystalline Solids, 316 (2003) 309-319.
[31] H. Okabayashi, I. Shimizu, E. Nishio, C.J. O'Connor, Colloid and Polymer Science, 275 (1997) 744-753.
[32] X.D. Fan, C. Geraldine Bazuin, Macromolecules, 28 (1995) 8209-8215.
[33] X. Shi, Y. Wu, H. Yi, G. Rui, P. Li, M. Yang, G. Wang, Energies, 4 (2011) 669-684.
[34] X. Wang, S. Cheng, J.C.C. Chan, Journal of Physical Chemistry C, 111 (2007) 2156-2164.
[35] J.D. Wright, N.A.J.M. Sommerdijk, CRC Press (2000).
[36] C.J. Brinker, D.M. Smith, R. Deshpande, P.M. Davis, S. Hietala, G.C. Frye, C.S. Ashley, R.A. Assink, Catalysis Today, 14 (1992) 155-163.
[37] S. Chen, S. Hayakawa, Y. Shirosaki, E. Fujii, K. Kawabata, K. Tsuru, A. Osaka, Journal of the American Ceramic Society, 92 (2009) 2074-2082.
[38] G. Stephen Caravajal, D.E. Leyden, G.R. Quinting, G.E. Maciel, Analytical Chemistry, 60 (1988) 1776- 1786.

[39] C.H. Chiang, N.I. Liu, J.L. Koenig, Journal of Colloid And Interface Science, 86 (1982) 26-34.
[40] J.E. Sarneski, H.L. Surprenant, F.K. Molen, C.N. Reilley, Analytical Chemistry, 47 (1975) 2116-2124.

[41] S.J. Dee, A.T. Bell, ChemSusChem, 4 (2011) 1166-1173.
[42] Z. Bai, S.J. Rodrigues and T.D. Dang, Journal of Membrane Science, 383 (2011) 189-196.

6. SYNTHESIS OF SILICA XEROGEL-POLY (STYRENESULPHONIC ACID) NANOCOMPOSITES AS ACID CATALYSTS: EFFECTS OF SOLVENT, AGING PROTOCOL AND APTES CONCENTRATION USED FOR THE SYNTHESIS ON THEIR TEXTURAL AND CHEMICAL PROPERTIES[a]

[a]**M.J. Campos Molina,** R. Mariscal, M. López Granados. Silica-poly(styrenesulphonic acid) nanocomposites as promising acid catalysts.

Enviado a Polymer Composites

Outline

1. Introduction

Soluble polymers have found applications as catalysts in a very wide number of reactions [1]. Of special interest are those directed at transforming biomass to valuable chemicals and biofuels [2-4] as this strategy will have a definitive impact in the substitution of an economy based in oil by another based on renewable resources. Thus polymers like sulfonated hyperbranched poly(aryleneoxindole)s [5] and poly(styrene sulphonic acid) (hereinafter referred as PSSA) [6] have been tested in reactions for valorization of biomass to valuable products, like cellulose conversion to levulinic acid, biodiesel synthesis, xylose to furfural transformation and oxidation with hydrogen peroxide of furfural to maleic and succinic acid. The former polymers presented acid sites required to catalyse those reactions and moreover were soluble in the reaction medium (water or methanol). Consequently they presented the advantages of homogenous catalysts because the access of reactants to the active sites (and the way out of products) are easier than in solid catalysts. In addition they can be reutilized by separation of the reaction mixture by ultrafiltration membranes. Other technologies can also been used to recover the polymer as dialysis or precipitation/recrystallization but all are perceived as cumbersome, not simple and cost effective for practical applications. Heterogenisation of the soluble polymers oninorganic solid supports can be an attractive solution. The so formed polymer composite (nanocomposites when the size of the particles of inorganic solid is in the range of nm) combines the advantages of soluble polymers (polymer will still be solvated by the liquid) and of the inorganic solids (ease of separation by more ordinary procedures like centrifugation or conventional filtration). Within this context, the synthesis of

SiO_2-PSSA nanocomposites has been achieved by polymerization of monomers like styrene or styrene sulphonic acid on the surface of the SiO_2 [7, 8]. However we have followed a different approach and explored the preparation of these polymer-silica nanocomposites by anchoring the pre-formed sulphonated polymer on amino functionalized SiO_2xerogel. Tetraethyl orthosilicate (TEOS) and 3-aminopropyl (triethoxysilane) (APTES) were used as source of SiO_2. A sol-gel method was used to obtain a silica xerogel through hydrolysis-condensation of the organosilanes (see scheme 6.1). PSSA provides itself the acid pH required to form the SiO_2 gel and APTES provides the amino groups. The acid-base reaction between the sulphonic acid and the amino groups of the aminofunctionalised silica forms ionic interactions responsible of the retention of the polymer by the silica [9, 10]. In our case an almost fully sulphonated PSSA was used (*y*, the fraction of non sulphonated rings,is smaller than 0.05; consequently *x*, is the fraction of sulphonated rings, is > 0.95). An at. N/S ratio (APTES/PSSA mol ratio) much smaller than 1 was selected for the synthesis. Therefore *m* (the fraction of sulphonic groups supposedly anchored on amino groups) is much smaller than *n* (the fraction non anchored on amino groups; m + n = x) and therefore free acid sites are available.

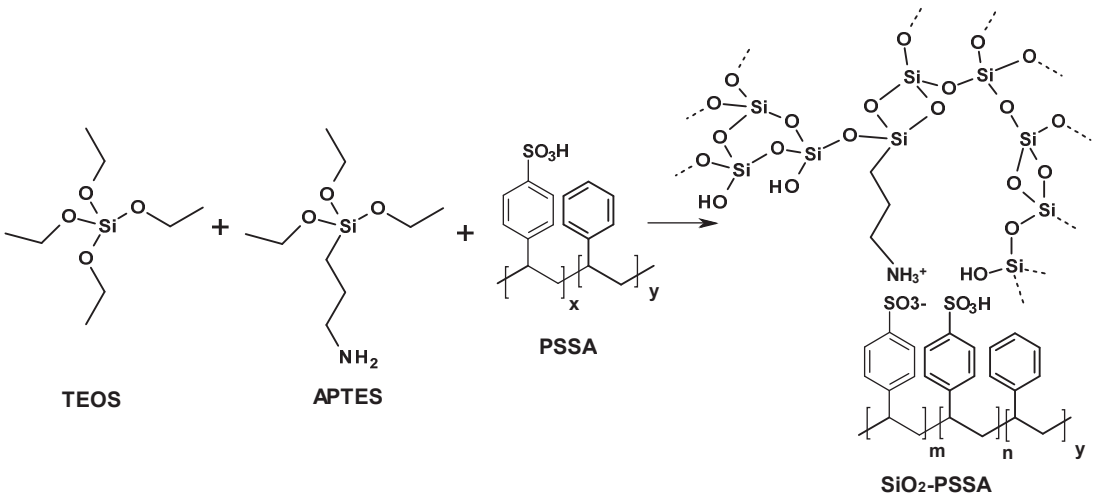

Scheme 6.1. Schematic representation of the preparation of the SiO_2-PSSA nanocomposites by the sol-gel methodology used in this study

As indicated above, the approach described in Scheme 6.1 makes use of already prepared PSSA. Interestingly PSSA can be obtained from polystyrene (PS) by sulphonation and, actually, we have also demonstrated that in practice PS waste can be sulphonated to form PSSA and be used as catalyst (Waste-To-Catalyst concept, WTC) [11]. Consequently there is no need of using fresh monomers to prepare this type of acid catalysts but to recycle PS waste.

In an attempt of finding the best preparation conditions in terms of polymer loading (acid sites loading) and hydrothermal stability, we have previously explored the effect of two variables of synthesis: temperature of synthesis and the S/N at. ratio initially used for the preparation (PSSA/APTES ratio). The rest of variable of synthesis were kept constant. We have found that

an at. S/N ratio between 4.4-8.8 and a temperature of synthesis = 348 K resulted in nanocomposites with the largest acid sites loading and with the best hydrothermal properties in terms of stability of the catalyst [12]. However when the nanocomposites were used in the xylose to furfural reaction, the catalysts deactivated upon reutilization, mainly because of an intense polymer leaching.

Consequently improvement of the hydrothermal stability is still needed. And moreover it is also interesting to explore other possible catalytic applications of these nanocomposites. In the investigation presented here, we report the effect of other variables of synthesis on the chemical and catalytic behavior of SiO_2-PSSA nanocomposite. These variables were the utilization of methanol as solvent to prepare the nanocomposite (instead of water), the time of aging of the gel, the slow evaporation of the water before the drying of the gel and the N/Si at. ratio used during the synthesis. Besides the xylose to furfural reaction, we have extended the study of the catalytic activity to the esterification of fatty acids with methanol to render fatty acid methyl esters (FAME). Both reactions are of interest in the valorization of biomass to renewable chemicals and to biofuels [6, 10, 11, 13]. Furfural has been considered a valuable bio-derived chemical platform, entry point of a number of other commodities and biofuels [14]. The esterification of fatty acid to FAMEs is a key reaction for the valorization of low quality oils to biodiesel [15]. In addition to these practical reasons, these two reactions represent two extreme cases when exploring the hydrothermal stability of the SiO_2-PSSA nanocomposites: aqueous phase at moderately high reaction temperatures, on one side, and organic medium (methanol and oil) at low reaction temperature, on the other side. Therefore with these two reactions we are delimiting the type

of reaction this type catalyst can be applied for. We have paid specific attention to the reusability of the nanocomposites and, specifically, to the stability against leaching.

2. Experimental

2.1. Preparation of catalysts

The nanocomposites were prepared by sol-gel methodology by co-condensation of tetraethyl orthosilicate (TEOS, Sigma-Aldrich, ≥ 99%) and (3-aminopropyl) triethoxysilane (APTES, Sigma-Aldrich, ≥98%) in the presence of PSSA (MW = 75000, 5.4 mmoles·H^{+}·g^{-1}) according to a methodology described elsewhere [10]. PSSA was supplied by Sigma-Aldrich as a 18 wt.% aqueous solution. The required amounts of the aqueous PSSA solution, TEOS and APTES were introduced in a round glass flask vessel and the mixture stirred vigorously. The reactor was immersed into an oil bath at 348 K and kept at this temperature overnight. The solid so formed after aging was filtrated with filter paper of 8 μm. To fully remove the weakly retained polymer, the solid was subjected to successive washes with water at room temperature until neutral pH. Finally, the solid was dried at 393 K overnight.

In a first series of samples the initial amount of APTES and TEOS were varied as to have an atomic N/Si ratio of 0.05, 0.09 and 0.20 respectively, maintaining constant the PSSA/APTES mol ratio (S/N = 4.4). In practice ca. 5 g of APTES, ca. 18.3 g of PSSA solution and ca. 89.4, 47.1 and 18.8 g of TEOS, respectively, were incorporated to the synthesis reactor. The nanocomposites of

this series were named as *Si-(N/Si)-PSSA-4.4* where N/Si is refered to the ratio used in the synthesis whereas 4.4 is the initial at. S/N ratio. We kept the ratio S/N =4.4 in the labeling to distinguish them from the other nanocomposites investigated in this chapter.

The effect of the utilization of methanol instead of water as the medium for the synthesis was also explored. APTES and TEOS are not soluble in water and therefore when using water two phases exist initially: the organic layer with APTES and TEOS and the aqueous solution of PSSA. On the contrary APTES, TEOS and PSSA are soluble in methanol and a single phase is available from the very beginning. 5 g of dried PSSA solid, ca. 9.18 g of water (the amount required to fully hydrolyze TEOS and APTES), ca. 25.7 g of TEOS and ca. 2.7 g of APTES were incorporated to the synthesis flask that was earlier filled with ca. 100 ml of methanol, enough to solubilize all reactants. The gel formed was aged overnight at 348 K. Then the solid was filtered, washed and dried as indicated above.

A modification Si-0.09-PSSA-4.4 sample was prepared by extending the aging period with respect to that used so far: instead of aging at 348 K overnight, gel was aged in contact with the mother liquor for 1 week. In practice, ca.10 g of PSSA, TEOS (25.7 g) and APTES (2.7 g) were introduced in the reactor and left aging for one week at 348K. Then the solid was filtrated, washed and dried as indicated above.

A last sample was prepared by subjecting the gel aged overnight at 348 K to a second aging period at 333 K, but allowing both the water and ethanol from the hydrolysis of the organosilanes to slowly evaporate. The resulting solid was dried as usual at 393 K overnight. In this case a sample corresponding to an atomic S/N ratio and N/Si ratio of 24 and 0.09, respectively was

synthesized. An initial amount of polymer much larger than previously used was used aiming at preparing a nanocomposite with a larger loading of polymer. This catalyst is referred as *Si-0.09-PSSA-24-ev* where 0.09 and 24 refers, respectively, to the N/Si and S/N initially used during the synthesis and *ev* ending refers to the fact that solvent has been removed before drying. For comparison purposes a blank sample was prepared without the slow evaporation, following the same N/Si and S/N ratios: once the gel was formed and aged overnight at 348 K it was filtered, washed and dried at 373 K as usual. It was named *Si-0.09-PSSA-24*.

Other chemicals used in the experiments were D(+)-xylose (≥99%), 2-furaldehyde reagent grade (99%), cyclopenthyl methyl ether (CPME) (≥99%), octanoic acid (98%), oleic acid (90%) and acetonitrile (≥99.9%) all supplied by Sigma-Aldrich. Methanol (99.5%) from Panreac, tetrahydrofuran (THF, HPLC grade) from Scharlau, ethyl palmitate (≥95%) from Fluka and commercial sunflower oil were also used. All materials were used without further purification and mili-Q H_2O was used for preparation of all aqueous solutions.

2.2. Characterisation of nanocomposites

The elemental analysis of the solids (C, H, N and O concentration) was performed on a LECO CHNS-32 analyzer. Typically, 1 mg of solid was placed in an Ag crucible and combusted at 1333 K under a pure O_2 atmosphere. The CO_2, H_2O and SO_2 gases were quantified by Fourier transform infrared (FT-IR) spectroscopy while N_2 was determined by differential thermal conductivity.

The actual Si content of the samples was determined by total reflection X-ray fluorescence (TXRF) using an Atomika 8030C TXRF spectrometer

(Cameca Germany) equipped with a 3 kW Mo/W dual target X-ray tube and a W/C double monochromator multilayer. A Si (Li) detector with an active area of 80 mm^2 and a resolution of 150 eV at 5.9 keV (Mn Kα) was used for detection and measurement of the produced X-rays.

The amount of acid sites of the different polymer hybrids were determined by acid-base titration. In practice a known amount of catalyst (100 mg), previously dried, was put in contact with ca. 25 mL of an aqueous solution containing 1 g of NaCl and stirred at 323 K overnight. The aim was to produce the exchange between protons from sulphonic groups and sodium ions. After that, the solution was filtered and the retained solid was repeatedly washed with water) and the resulting filtrate solution titrated with a 0.005 M KOH solution (previously standardized with dry potassium acid phfhalate). A few drops of an ethanolic solution of phenolphthalein were used to determine the end point.

The ^{13}C and ^{29}Si solid state NMR spectra of the samples were recorded in an AV-400-WB Bruker spectrometer equipped with a tripe channel probe. Powder samples were finely grounded and dried for several days at 373 K in an oven and then rapidly transferred to ZrO_2 rotors (4 mm) and capped with Kel-F caps to prevent the hydration of the polymer. Frequencies used were 100.32 and 79.49 MHz for ^{13}C and ^{29}Si nuclei, respectively. Samples were spun at 10 kHz. The CP-MAS ^{1}H-^{13}C spectra were recorded by using a spectral width of 35 KHz, excitation pulse for ^{1}H of 3,4μs, contact time of 3,5ms and a relaxation time of 4 s, with ^{1}H tppm15 decoupling at 80 KHz. The number of scans was 1024 for ^{13}C spectra. ^{13}C chemical shift is referenced to the adamantane CH_2 signal (29.5 ppm) as secondary reference relative to the TMS as a primary reference. ^{29}Si MAS-NMR spectra are the result of 1000 accumulations after direct irradiation at a spectral width of 15 KHz, a relaxation delay of 60 s and

pulses of $\pi/4$ at 50 KHz. Kaolin signal (-91.2 ppm) was used like secondary reference relative to a TMS as primary reference.

2.3. Catalytic activity of nanocomposites

The catalytic experiments of xylose dehydration were performed in a 15 mL Ace sealed pressure glass reactor flushed with nitrogen before use, magnetically stirred (1000 rpm) and placed in a preheated oil bath at a selected temperature. In practice,1.35 g of water, 3.5 g of CPME as organic solvent (2.33 g CPME/g aqueous solution), 150 mg of xylose (10 wt. % with respect to water) and 75 mg of finely grounded catalyst previously sieved to a size < 106 μm (5 wt. % with respect to water, catalyst/xylose wt. ratio = 0.5) were poured into the reactor. CPME solvent has been reported as an excellent solvent to improve furfural yield [13]. The reaction is stopped by removing the reactor from the oil bath and rapidly cooled down by immersion in water at room temperature. Then, internal standard for organic phase (40 mg of octanoic acid) was added to the quenched reaction mixture and after gently agitation for several minutes, mixture was centrifuged to separate both phases. A 2 mL aliquot was taken from the organic layer. Once the organic phase has been aliquoted, internal standard for aqueous phase (200 mg of D (+)-glucose) was added to the left reaction mixture and, after agitation for several minutes and centrifugation, an aliquot (ca. 2 mL) was taken from the aqueous layer for analysis. Both organic and aqueous aliquots were filtered through a filter 0.22 filter μm to remove the left catalyst and the solid humins formed during the reaction. Aqueous aliquots were analyzed with a HPLC Agilent 1200 series chromatograph equipped with a refraction index (RI) detector and a Bio-Rad

Aminex HPX-87H column (300x7.8 mm) for analysis of xylose and furfural in aqueous phase. A 0.005 M H_2SO_4 mobile phase was employed as eluent with 0.4 mL/min flow rate and at 328 K. In the case of organic aliquots, analysis of furfural in this phase was conducted by gas chromatography (CG) (Varian CP-3800) equipped with a ZBWAX plus column (30mx0.32mmx0.25um) and a flame ionization detector (FID).

The catalytic experiments of esterification of oleic acid were performed in the same Ace sealed pressure glass reactor magnetically stirred (1000 rpm) and placed in a preheated oil bath at a selected temperature (333 K). For a typical experiment 0.872 g of methanol, 2 g of sunflower oil (methanol/oil mol ratio = 12), 0.1 g of oleic acid (FFA/oil wt. ratio =0.05) and 40 mg of finely grounded catalyst (3.3 wt% respect to the total solution, catalyst/FFA wt. ratio= 0.4) were poured into the reactor. Then, internal standard (0.1 g of ethyl palmitate in THF) was added to the quenched reaction mixture and after gently agitation for several minutes, mixture was centrifuged. A 2 mL aliquot was taken from the solution and filtered through a 0.22 μm filter to remove the solid. Then, this aliquot was analyzed with a HPLC Agilent 1200 series chromatograph equipped with a refraction index (RI) detector and a XDB-C18 column (5μm, 4.6 x 150 mm) for analysis of all the reactants and products. A solution of 5%v/v of THF in acetonitrile mobile phase was employed as eluent with 0.6 mL/min flow rate and at 308 K.

3. Results and Discussion

3.1. Characterisation of the nanocomposites

3.1.1 Chemical and acidity analyses

The Si-(N/Si)-PSSA-4.4 series

Table 6.1 shows the experimental concentration of the relevant atoms of the nanocomposites. The concentration of S in the nanocomposites (mmol $S \cdot g_{cat}^{-1}$), and consequently the amount of polymer retained by the xerogel, increases as N/Si increases. This is reasonable because as the relative amount of APTES increases with respect to that of TEOS there will be more amino groups available for anchoring the polymer molecules. However the amount of retained polymer is in practice smaller than that theoretically expected (see the value between brackets in the mmol $S \cdot g_{cat}^{-1}$ column) indicating that part of the polymer is not retained and is leached away during synthesis. Consequently, since there is less polymer than expected, the N concentration is larger.

Table 6.1. Experimental concentration of relevant atoms in the relevant nanocomposites

Name	mmolS·g_{cat}^{-1}	mmolN·g_{cat}^{-1}	mmol H^+·g_{cat}^{-1}[b]	at. N/Si[c]	at. S/N
Si-0.05-PSSA-4.4	1.22 (2.14)[a]	0.52(0.49)[a]	0.59(0.70)[d]	0.05(0.05)[a]	2.3 (4.4)[a]
Si-0.09-PSSA-4.4	1.92 (2.90)[a]	0.73(0.66)[a]	0.99(1.19)[d]	0.09(0.09)[a]	2.6 (4.4)[a]
Si-0.20-PSSA-4.4	2.43(3.82)[a]	1.29 (0.87)[a]	0.88 (1.14)[d]	- (0.2)[a]	1.9 (4.4)[a]
Si-0.09-PSSA-24	1.88 (4.68)[a]	0.83 (0.19)[a]	0.94 (1.05)[d]	0.08(0.09)[a]	2.27(24)[a]
Si-0.09-PSSA-24-ev	4.49 (4.68)[a]	0.25 (0.19)[a]	4.03 (4.24)[d]	0.12(0.09)[a]	17.92 (24)[a]

[a]Values between brackets refers to nominal concentration incorporated to the preparation mixture

[b]Determined by titration with KOH 0,005M of the released H^+ (after exchange with Na^+)

[c]Si content determined by TXRF analysis of solid catalysts

[d]Values between brackets were obtained by difference between mmolS·$g_{cat}^{-1}$and mmol N·g_{cat}^{-1}

The experimental S concentration is larger than that of N and therefore there are more sulphonic groups than amino groups. As a consequence non neutralized sulphonic sites are available and solid present acid sites. In principle since the amount of polymer increases upon N/Si nominal ratio, there would be more acid sites. However the acid sites concentration reaches a maximum for Si-0.09-PSSA-4.4 (0.99 mmol H^+·g_{cat}^{-1}) and slightly become smaller for Si-0.2-PSSA-4.4 (0.88 mmol H^+·g_{cat}^{-1}). The reason is that the N concentration also increases within this series and for the latter sample the relative increase of N concentration (1.29 mmol N·g_{cat}^{-1}) is larger than for the S loading. In consequence, there are less free sulphonic sites (not neutralized by amino groups).

Type of solvent and time aging the gel

Changing water for methanol in the synthesis did not result in any increase of the amount of polymer retained by the silica xerogel. Same conclusion was reached when the gel was aged for one week (instead that overnight) in the mother aqueous solution. None of these modifications are useful for improving the loading of acid sites. These samples were discarded for further studies.

Effect of evaporation of the water before drying

In this case, instead of filtering the solid formed after aging overnight at 348 K, water and ethanol (the latter formed from the hydrolysis of organosilanes) were gently removed at 333 K by evaporation at mild temperature. The solid formed after evaporation was subsequently dried as usual at 393 K. The intention of the evaporation is that while drying, gel shrinks and collapses and polymer can be trapped by entangling in the network of the gel particles what may be of help to firmly retaining the polymer (besides the electrostatic interactions). Additionally, in an attempt of increasing the polymer loading in the resulting nanocomposite, very high polymer concentration is used for the synthesis (S/N = 24). The experimental concentrations of the relevant atoms for these samples are also tabulated in Table 6.1.

Blank Si-0.09-PSSA-24 nanocomposite presents S and acid sites concentration similar to Si-0.09-PSSA-4.4 one (see Table 6.1). The incorporation of more PSSA to the preparation mixture did not improve the polymer loading, indicating that a large fraction of the polymer is not retained by the functionalized silica and it is leached during the filtration step.

As expected, the nanocomposite prepared by slow evaporation presents a very large S and acid sites concentration; we have to bear that this nanocomposite was not subjected to a filtration step during preparation and therefore all polymer used for the preparation must be in the solid. The question that still remains is whether the slow evaporation can result in the stabilization of the polymer (entangled within the network of silica aging particles) and consequently in a nanocomposite with better hydrothermal stability against leaching. This question will be later answered when studying the stability and reusability of the nanocomposite in the reactions investigated in this article.

3.1.2 NMR studies

Figure 6.1 displays the ^{29}Si MAS-NMR and ^{13}C CP-MAS-NMR spectra of the most representative nanocomposites prepared. Regarding the ^{29}Si spectra the broad resonance at -101 ppm is assigned to Q^3siloxane species of the silica framework and appears in all Si-(N/Si)-PSSA-4.4 series samples ([Q^n = $Si(OSi)_n(OR)_{4-n}$] where n=3 and R = alkoxy or H)[16-19]. Q^3 resonance mostly originates from $(SiO)_3Si$-OH units (according to DRIFT studies the amount of unhydrolized ethoxy residues must be quite low [12]). The signal at -110 ppm corresponds Q^4 species (n=4, Q^4 represents Si atoms in fully condensed Si(O-Si)$_4$tetrahedra). The latter signal becomes relatively more intense for the sample with the larger N/Si (0.09 and 0.2) indicating that in these samples the silica framework is more condensed. On the other hand, a weak Q^2 (n=2) signal at -90 ppm (originating from $(SiO)_2Si$-$(OH)_2$ like species) is also incipiently visible. These latter signals were of very low intensity for the Si-0.09-PSSA-24-ev

sample, in agreement with chemical analyses that showed that this sample is very concentrated in polymer.

Besides these signals the detection in all the fresh samples of the resonance at -67 ppm (weak although observable) indicates the presence of aminopropylfuncionalized Si atoms [17, 20]. This signal corresponds to alkylsiloxaneT^3 units ($R'Si(OSi)_3$), where R´ corresponds to aminopropyl group. The presence of T^2 species $R'(SiO)_2(OH)$ cannot be discarded as the signal is T^3 signal is quite wide and presents an incipient shoulder at lower shifts assignable to T^2 signals. The intensity of this signal is smaller for Si-0.09-PSSA-4.4 and Si0-0.05-PSSA-4.4 catalysts, respectively, that is in harmony with the lower N loading observed for these samples by elemental chemical analysis. The presence of these T^i signals also demonstrates that aminopropyl groups are present in the samples, in agreement of the detection of N by chemical analysis

Regarding the ^{13}C spectra of the Si-(N/Si)-PSSA-4.4 series, these nanocomposites displayed a similar NMR profile. Four signals coming from the polymer are clearly identified: one at 42.4 ppm from not aromatic CH and CH_2 carbons, other at 140.2 ppm from the aromatic C atom bearing the sulphonic group, other at 126.7 ppm from aromatic C linked to the aliphatic chain and finally another signal at 149.5 ppm from the rest of the C aromatic atom in the aromatic ring [6]. Two additional peaks can be also observed arising from C atoms of the aminopropyl groups at 9.2 and 21.2 ppm from the carbon atoms bearing the amino group (C_α) and that at β position with respect to the latter (C_β), respectively. The signal from Cγ should be at around 45-50 ppm but is overshadowed by the peak at 42.4 ppm from the polymer. The weak feature at

ca. 27 ppm is assigned to a side band of the main signal at 126 ppm. In the case of Si-0.09-PSSA-24-ev the signals arising from the polymer become predominant whereas those from aminopropyl groups are much weaker. This corresponds to a nanocomposite with a high concentration of polymer and then relatively less silica, and therefore the intensity of the C peaks from the aminopropyl groups also are lower.

The C_α and C_β resonances of the aminopropyl group are sensitive to protonation. The positions of these peaks correspond to protonated amine groups ($R\text{-}NH_3^+$) [10, 21-23] because those of unprotonated amines are shifted by *ca*. 2 and 5 ppm, respectively, to lower shieldings in unprotonated amines. The protonation results from the interaction with sulphonic groups (protonation from acidic silanols was excluded) [10]. These protonation of the amino groups by acid-base reaction with the sulphonic groups is responsible of the anchoring of the polymer in the solid and of the retention of the polymer.

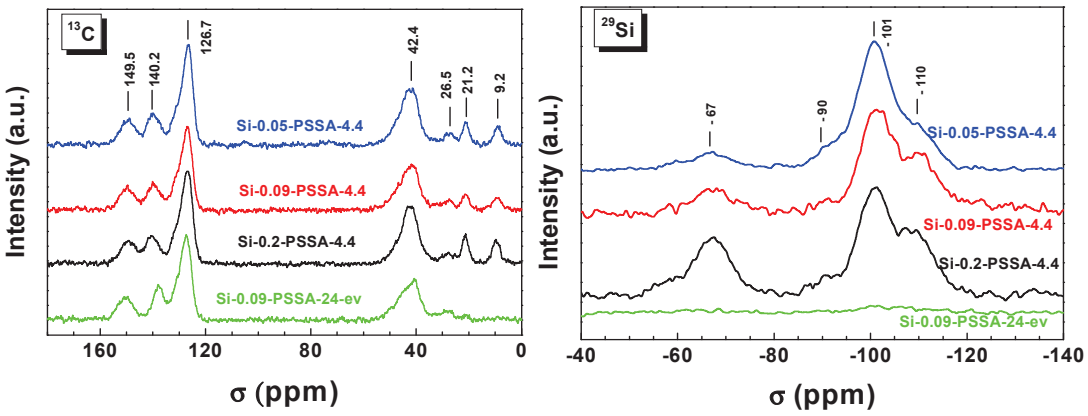

Figure 6.1.^{29}Si MAS-NMR and ^{13}C CP-MAS-NMR spectra of nanocomposites

3.2. Catalytic activity

3.2.1 Catalytic activity of nanocomposites in xylose dehydration to furfural

Figure 6.2 displays the catalytic properties of the most relevant nanocomposites studied in this chapter. The catalysts prepared by changing the solvent or by lengthening the aging period were not included as these modifications did not represent an improvement in the acid loadings. Concerning the Si-(N/Si)-PSSA-4.4 series, a rapid perusal of the results shows that the conversion and yield values rises upon the acid sites concentration: the Si-0.09-PSSA-4.4 sample, with the largest acid sites loading, present the best activity and yield to furfural. So as a first approximation, the number of acid sites (polymer loading) is a key variable defining the catalytic properties. The comparison between Si-0.09-PSSA-24 and Si-0.09-PSSA-24-ev is also in agreement with this conclusion as the latter presents the highest acid sites concentration among the nanocomposites prepared in this study and so is the catalytic performance.

However the loading of acid sites is not the only property defining the catalytic performance of the nanocomposites: Si-0.09-PSSA-4.4 and Si-0.09-PSSA-24 present similar acid sites loading and their catalytic activity are dissimilar. Texture or accessibility of the reactant molecules to the active sites must be another relevant property. It must be taken into account that polymer is anchored and entangled within a network of silica particles, so porosity and tortuosity must be also considered to define the catalytic activity. Unfortunately texture of nanocomposites cannot be studied as they presented a lack of

adsorption of N_2 because part of the polymer is also filling the pores and this substantially reduces the N_2 adsorption [10]**.**

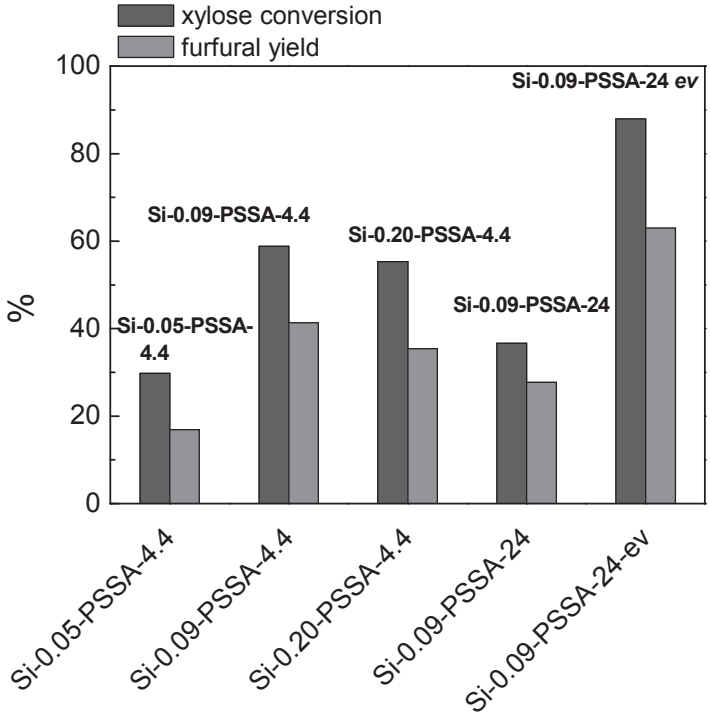

Figure 6.2. Comparison of xylose conversion and furfural yield for the different catalysts studied. Reaction conditions: 10 wt. % xylose and 5 wt. % catalyst in the aqueous phase, CPME/aqueous phase mass ratio = 2.33; 5 g total solution, temperature of reaction 453 K, time of reaction 30 min.

Figure 6.3 presents the reutilization of the two most active nanocomposites represented in Figure 6.2. For the sake of simplicity only

furfural yields are represented. A remarkable deactivation was observed for Si-0.09-PSSA-4.4 nanocomposite during the first run, a residual activity is observed for the rest of runs. On the other hand a close to complete deactivation was detected for Si-0.9-PSSA-24-ev.

A likely cause of deactivation can be the leaching of the polymer during reaction. With the intention of assessing on the leaching, the chemical analyses of the nanocomposites resulting from hydrothermally treating the fresh nanocomposites with the same reaction mixture but without xylose (only CPME and water) at 453 K overnight were carried out. In practice, 400 mg of each catalyst, 1.5 grams of water and 3.5 grams of CPME (CPME/ aqueous phase mass ratio= 2.33) were poured into the glass reactor where catalytic reactions were conducted and stirred at 180ºC overnight. This time of treatment represents more than five reutilization cycles so it is a very reasonable approximation to the changes in properties that can occur on the nanocomposites during reutilization. After that, the reaction mixture was cooled and centrifuged to separate the liquid from the solid catalyst. The solid was then washed again with water to remove all not retained polymer. Once the liquid was centrifuged, the treated solid was dried at 393 K overnight and the S and acid site loading determined as explained above. Thus Si-0.09-PSSA-4.4 presented 1.28 mmol $S \cdot g_{cat}^{-1}$ and 0.22 mmol $H^{+} \cdot g_{cat}^{-1}$ after this hydrothermally treatment, representing respectively 67 % and 22 % of the values of fresh sample (see table 1). Si-0.9-PSSA-24-ev nanocomposite after the hydrothermal treatment presented 1.77 mmol $S \cdot g_{cat}^{-1}$ and 0.69 mmol $H^{+} \cdot g_{cat}^{-1}$ representing respectively 39 % and 17 % of the values of the fresh nanocomposite. These results confirmed that the polymer loading and, what is more important, the loading of free acid sites remaining after hydrothermal treatment are very

limited and so must be the residual activity left for successive runs. Low hydrothermal stability of the nanocomposites explains the unsatisfactory reusability properties.

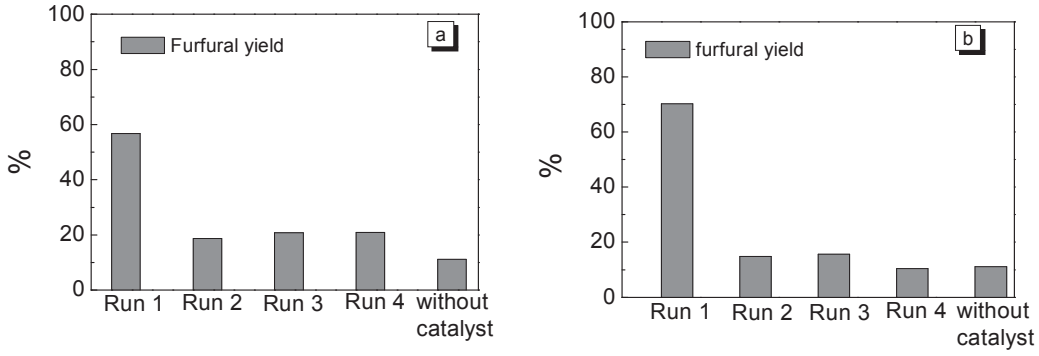

Figure 6.3. Reutilization of a) Si-0.09-PSSA-4.4 and b) Si-0.09-PSSA-24-ev catalysts Reaction conditions: 10 wt. % xylose and 5 wt. % catalyst in the aqueous phase, CPME/aqueous phase mass ratio= 2.33; 5 g total solution, 453 K, 60 min.

3.2.2. Catalytic activity in the esterification of fatty acids

This reaction is less demanding from the stability point of view than previous one as it is conducted in the presence of methanol and oil, less polar compounds, and at much lower temperature (333 K). It must be noticed that this reaction is biphasic (methanol is immiscible in oil), and the fatty acid (oleic acid) is majorly present in the oil phase.

Figure 6.4a compares the activity of Si-0.2-PSSA-4.4 nanocomposite with that of commercial sulphonic resin (Amberlyst 70). It is clearly

observed that nanocomposite compares favorably well with Amberlyst 70 especially when considering conversion of oleic acid and yield to FAME values at longer reaction time. Yield to FAME is in both cases smaller than conversion of oleic acid, very likely because part of the fatty acid is either chemisorbed or physisorbed within the pores network of the solid and accounted as converted.

Figure 6.4b compares the performance of the relevant nanocomposites studied in this article. Among the different catalyst tested, Si-0.2-PSSA-4.4 and Si-0.09-PSSA-4.4-ev displayed the best performance. As in the case of furfural reaction, the presence of free acid sites in the nanocomposite is a key property but it is not the only feature having a role. Thus Si-0.2-PSSA-4.4, Si-0.09-PSSA-4.4 and Si-0.09-PSSA-24 nanocomposites presented similar free acid sites loading and their performance is very alike. We hypothesized that textural porosity may have an important effect on the final activity because accessibility of voluminous free fatty acid to the active acid site is deeply related with the porosity of the solid.

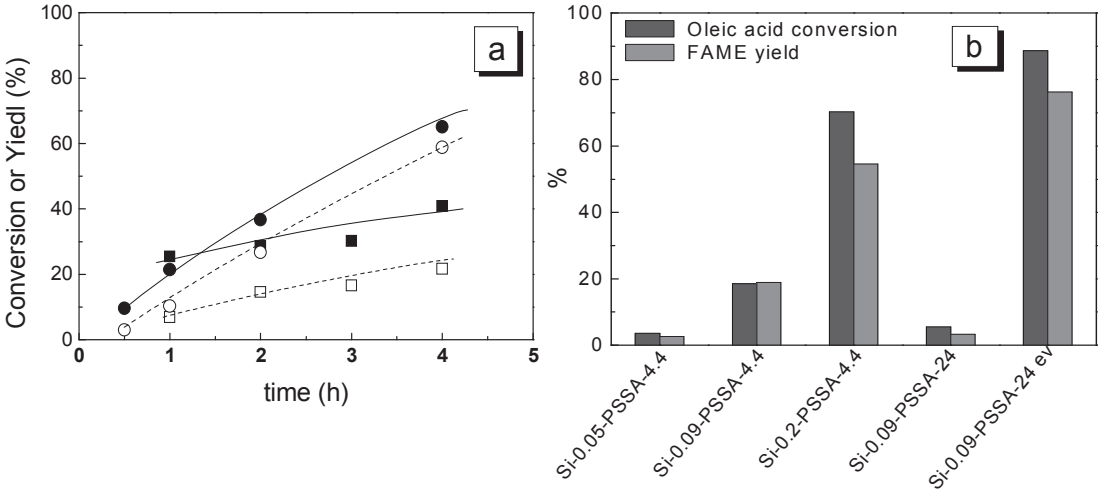

Figure 6.4. a) Oleic acid conversion (filled symbols) and FAME yield (empty symbols): (●,○): Si-0.2-PSSA-4.4 catalyst; (■,□)Amberlyst 70. Reaction conditions: 2 g of sunflower oil, methanol/oil mol ratio =12, FFA/oil wt. ratio =0.05, 3.3wt% catalyst (catalyst/FFA wt. ratio =0.4), 333 K; b)Oleic acid conversion and FAME yield for different catalysts. Reaction conditions: 2 g of sunflower oil, methanol/oil mol ratio =12, FFA/oil wt. ratio =0.05, 3.3wt% catalyst (catalyst/FFA wt. ratio =0.4), 333 K, 240 min.

Figure 6.5 compares the reusability behavior of the two most active catalysts in this reaction with those of Amberlyst 70. The improvement in the catalytic performance exhibited in the second run with respect to the first run is very likely related with the swelling by methanol experienced by the resin during the progress of the first run what may improve the accessibility of the reactant molecules to the acid sites present in the innermost region of the resin

particles [24]. Amberlyst 70 is very stable along the six runs investigated. On the other hand, both nanocomposites are initially more active than Amberlyst 70. They are quite stable for five runs although an incipient deactivation was observed in the last sixth run investigated, more intense in the Si-0-09-PSSA.4.4-ev case. In any case they presented a higher stability in this reaction than for the furfural reaction.

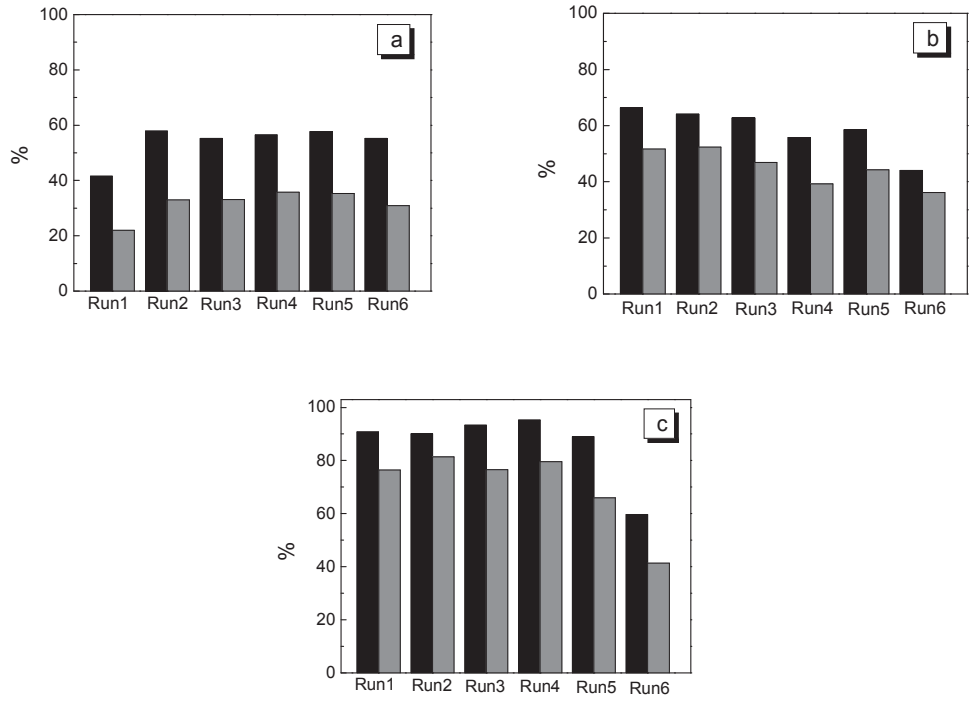

Figure 6.5. Reutilization of a) Amberlyst 70, b) Si-0.2-PSSA-4.4, c) Si-0.09-PSSA-24- ev. Black bars correspond to oleic acid conversion and grey bars to FAME yield. Reaction conditions: 4 g of sunflower oil, methanol/oil mol ratio =12, FFA/oil wt. ratio =0.05, 3.3wt% catalyst (catalyst/FFA wt. ratio =0.4), 333 K, 240 min.

To gain information about the stability of the nacocomposites in the reaction mixture, leaching experiments were conducted by subjecting the nanocomposites to six consecutive leaching treatments consisting in contacting with methanol at 333 K for 4 hours. In practice after each run, the catalyst was centrifuged and the liquid phase removed. The solid was subsequently washed and centrifuged twice more with THF to remove the remaining methanol. The solid was dried at 323 K overnight and then a sample of solid was taken for elemental analysis before the next washing steps. The results of S concentration in the solid after the consecutive runs are shown in Figure 6.6. Si-0.2-PSSA-4.4 nanocomposite presents a loss of S content of 14% with respect to its initial content. However, in the next runs no relevant loss of S is observed and the nanocomposite presented an average concentration of ca. 2.2mmol$S \cdot g^{-1}$. This residual loss of polymer is in agreement with the stability of the activity observed for this nanocomposite. On the other hand, the Si-0.09-PSSA-24-ev catalyst exhibited a remarkable loss of S loading (52% of loss respect to its initial content). The loss for subsequent cycles is irrelevant, keeping a S concentration close to 2.0 mmol$S \cdot g^{-1}$ in the next washing runs.It is worth mentioning that, in spite of the intense leaching of polymer observed during the first treatment for Si-0.09-PSSA-24-ev nanocomposite, no deactivation is observed in the catalytic activity. The lack of loss of polymer observed in successive runs is in agreement with the improved reusability properties displayed by this nanocomposite. The overall conclusion of these experiments is that in this reaction leaching of polymer only takes place during the first run, corresponding to the most weakly retained polymer molecules (the latter are important in the Si-0.09-PSSA-24-ev sample). Other causes of deactivation must be taking place. Fouling of the surface by heavier molecules, formed by

secondary reactions of fatty acids and triglycerides present in the oil, has been proposed to deactivate sulphonic silicas [25].

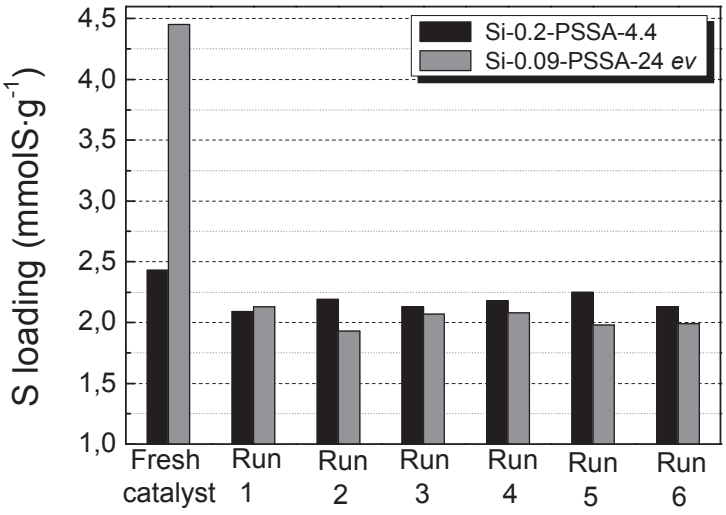

Figure 6.6. S concentration for different catalysts (mmolS·g^{-1}) after the consecutive runs of leaching. Reaction conditions: 40 mg of catalyst, 5 g of methanol, 333K, 240 min.

Another set of experiments, summarized in Figure 6.7, were conducted to estimate the contribution of the leached polymer to the overall activity. In practice the leached polymer was collected by contacting ca. 40 mg of catalyst and ca. 5 g of methanol in the glass reactor and stirred for 4 hours at 333 K. After this time, the reactor was cooled and the methanol solution was centrifuged to separate the liquid which contains the leached polymer from the catalyst. The remained solid was subsequently washed with methanol and

centrifuged three more times. The methanol solutions from the treatment and the washings steps were accumulated in another Ace reactor and evaporated at 323 K overnight to dryness. The solid residue recovered (the dried leached polymer) was used as a soluble catalyst for the esterification reaction. This treatment was repeated three times with the same catalyst to estimate the contribution in three successive runs and the results of the activity of these tree cycles of leaching are shown in Figure 7 for both Si-0.2-PSSA-4.4 and Si-0.09-PSSA-24-ev catalysts.

The results of the Figure 6.7 indicate that for both nanocomposites the contribution of leached species is very relevant for the first reaction cycle. In the case of Si-0.09-PSSA-4.4 the homogenous contribution is still important for the second run but negligible for the third run. In the case of Si-0.09-PSSA-24-ev nanohybrid the homogeneous contribution is already negligible in the second run. These results are in agreement with those in Figure 6.6 that showed that leaching was more important in the first cycles.

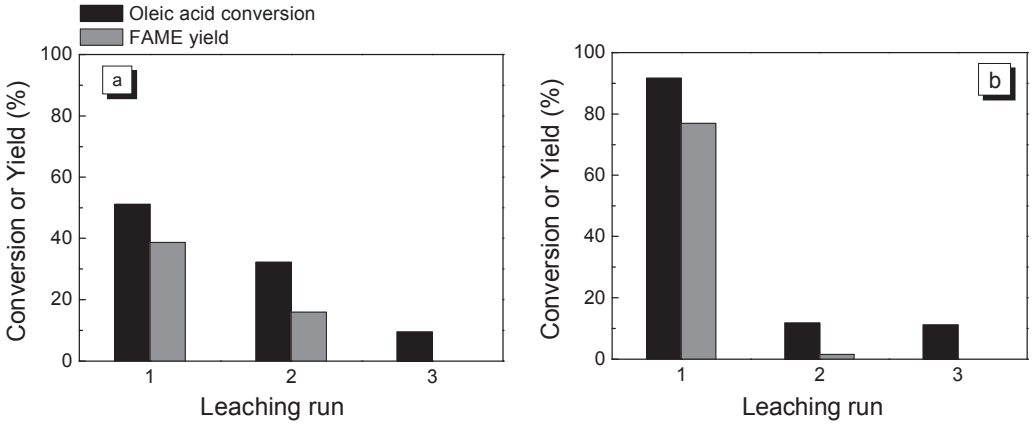

Figure 6.7. Oleic acid conversion and FAME yield of the leached species after in the consecutive leaching runs for the different catalysts: a) Si-0.2-PSSA-4.4; b) Si-0.09-PSSA-24-ev. Reaction conditions: 4 g of sunflower oil, methanol/oil mol ratio =12, FFA/oil wt. ratio =0.05, 3.3wt% catalyst (catalyst/FFA wt. ratio =0.4), 333 K, 240 min.

It is noticeable that the homogeneous contribution for the first run, for both catalysts, is quite similar to the overall activity displayed by the solid catalyst. This may erroneously suggest that for the first run all the activity is due to the leached species: the leaching of the polymer is minor in the second and successive runs and the activity of the solid in these reaction cycles is still as high as that displayed in the first cycle. Therefore this type of experiments seems to overestimate the leaching contribution. It may be possible that leaching rate is not fast and of the same order of the reaction rate. The experiments conducted in Figure 6.7 in practice measured the contribution of the species leached after 4 h of leaching treatment and does not exactly

represent the real situation during the course of the reaction. The homogeneous contribution can be low at the beginning but increasing with the reaction time along with the heterogeneous contribution.

Besides we have also to take into account that removal of weakly retained PSSA polymer allows the access of the reactants to fresh anchored sulphonic polymer that explains why in successive cycles, when there is no significant leaching, the solid is still very active. In summary, a more correct conclusion is that contribution of leaching is only important for the first runwhereas the activity measured in second and successive runs are due to the firmly retained PSSA.

4. Conclusions

Polymer-SiO_2 nanocomposites involving PSSA acid polymer can be prepared by sol-gel methodologies; an amino functionalized organosilane (APTES) is required to provide the anchoring sites for the retention of the acid polymer by the silica particles network. The acid sites loading present in the nanocomposites increases upon the N/Si ratio used for the synthesis up to an at. N/Si ratio = 0.09. Beyond this value, acid sites loading did not increase further. The utilization of methanol as solvent to conduct the synthesis instead of water did not result in an improvement of the acid sites loading, neither a long period of aging. The slow evaporation, before the drying process, of the mother liquor resulting from the sol-gel synthesis results in a very high concentration of acid polymer loading.

When this type of nanocomposites is used as catalyst for the reaction of transformation of xylose to furfural, a reaction representative of those conducted at relatively high temperatures in water medium, they significantly deactivated, mainly due to the extensive leaching of the acid polymer. The leaching is driven by the harsh conditions at which the reaction is conducted (aqueous environment at 453 K). On the contrary when used for the esterification of oleic acid with methanol to yield biodiesel, a reaction conducted in organic medium and at milder temperatures (333 K), the deactivation by leaching is significantly improved.

5. Bibliography

[1] T.J. Dickerson, N.N. Reed, K.D. Janda, Chemical Reviews, 102 (2002) 3325-3344.
[2] A. Corma Canos, S. Iborra, A. Velty, Chemical Reviews, 107 (2007) 2411-2502.
[3] D.M. Alonso, S.G. Wettstein, J.A. Dumesic, Green Chemistry, 15 (2013) 584-595.
[4] S.G. Wettstein, D. Martin Alonso, E.I. Gürbüz, J.A. Dumesic, Current Opinion in Chemical Engineering, 1 (2012) 218-224.
[5] S. Van De Vyver, J. Thomas, J. Geboers, S. Keyzer, M. Smet, W. Dehaen, P.A. Jacobs, B.F. Sels, Energy and Environmental Science, 4 (2011) 3601-3610.
[6] M.L. Granados, A.C. Alba-Rubio, I. Sádaba, R. Mariscal, I. Mateos-Aparicio, A. Heras, Green Chemistry, 13 (2011) 3203-3212.
[7] H. Zou, S. Wu, J. Shen, Chemical Reviews, 108 (2008) 3893-3957.
[8] A. Martín, G. Morales, F. Martínez, R. Van Grieken, L. Cao, M. Kruk, Journal of Materials Chemistry, 20 (2010) 8026-8035.
[9] R. Tamaki, Y. Chujo, Chemistry of Materials, 11 (1999) 1719-1726.
[10] I. Sádaba, R. Mariscal, M.L.Granados, Applied Catalysis B: Environmental, 150-151 (2014) 421-431.
[11] N. Alonso-Fagúndez, V. Laserna, A.C. Alba-Rubio, M. Mengibar, A. Heras, R. Mariscal, M.L. Granados, Catalysis Today, 234 (2014) 285-294.
[12] M.J. Campos Molina, R.Mariscal, M.L. Granados, submitted to Journal of Sol-Gel Science and Technology.
[13] M.J. Campos Molina, R. Mariscal, M. Ojeda, M. López Granados, Bioresource Technology, 126 (2012) 321-327.
[14] J.J. Bozell, G.R. Petersen, Green Chemistry, 12 (2010) 539-554.
[15] J.A. Melero, J. Iglesias, G. Morales, Green Chemistry, 11 (2009) 1285-1308.
[16] X. Shi, Y. Wu, H. Yi, G. Rui, P. Li, M. Yang, G. Wang, Energies, 4 (2011) 669-684.
[17] X. Wang, S. Cheng, J.C.C. Chan, Journal of Physical Chemistry C, 111 (2007) 2156-2164.
[18] J.D. Wright, N.A.J.M. Sommerdijk, Sol-Gel Materials Chemistry and applications, CRC Press.

[19] C.J. Brinker, D.M. Smith, R. Deshpande, P.M. Davis, S. Hietala, G.C. Frye, C.S. Ashley, R.A. Assink, Catalysis Today, 14 (1992) 155-163.
[20] S. Chen, S. Hayakawa, Y. Shirosaki, E. Fujii, K. Kawabata, K. Tsuru, A. Osaka, Journal of the American Ceramic Society, 92 (2009) 2074-2082.
[21] G. Stephen Caravajal, D.E. Leyden, G.R. Quinting, G.E. Maciel, Analytical Chemistry, 60 (1988) 1776-1786.
[22] C.H. Chiang, N.I. Liu, J.L. Koenig, Journal of Colloid And Interface Science, 86 (1982) 26-34.
[23] J.E. Sarneski, H.L. Surprenant, F.K. Molen, C.N. Reilley, Analytical Chemistry, 47 (1975) 2116-2124.
[24] D.M. Alonso, M.L. Granados, R. Mariscal, A. Douhal, Journal of Catalysis, 262 (2009) 18-26.
[25] A.C. Alba-Rubio, F. Vila, D.M. Alonso, M. Ojeda, R. Mariscal, M. LÃ³pez Granados, Applied Catalysis B: Environmental, 95 (2010) 279-287.

7. NIOBIUM BASED-CATALYSTS FOR THE DEHYDRATION OF XYLOSE TO FURFURAL[a]

[a]**M.J. Campos Molina,** P. Carniti, A. Gervasini, M. López Granados. Exploitment of niobium oxide effective acidity for xylose dehydration to furfural.

Catalysis Today

Outline

1. Introduction

Furfural is an important chemical species produced from pentosan-rich biomass, in particular by xylose dehydration. Currently, conventional processes of furfural production utilize mineral acids as catalysts but the development of more friendly acid solid catalysts with separable and reusable properties is required to prevent the environmental and economic drawbacks associated to homogeneous catalysis such as extreme corrosion, high toxicity, and excessive waste disposal.

In the past years, many solid acid catalysts have been developed and successfully applied in this reaction [1-11]. A problem arrives when water is concerned as reaction solvent because in water or in general in highly protic and polar solvents, only very few solid acids can maintain the desirable acidity due to the solvent-surface interactions by solvation and coordination abilities of such solvents. The discovery of the water-tolerant properties of several solid acids containing niobium [12] has opened the possibility to use such materials as efficient catalysts in reactions where water is concerned as reactant, product, or solvent. Thus, different acid-catalyzed reactions, such as hydrolysis, dehydration, condensation, and esterification, among others, have been performed using niobium based catalysts [9, 13, 14].

In particular, the hydrated niobium pentoxide, $Nb_2O_5 \cdot nH_2O$ (NBO), which is usually called niobic acid, is considered one of the most promising water-tolerant solid acid catalyst [15, 16]. The lively acid properties of niobic acid, which can be maintained also in water, have been exploited in several reactions of biomass transformation as dehydration of pentoses and hexoses to

obtain platform compounds such as furfural and 5-hydroxymethylfurfural (HMF), respectively [9, 17, 18].

The catalytic dehydration of pentoses and hexoses in water with niobic acid presents different disadvantages to overcome for practical application; in particular, low selectivity and yield to the main products (furfural and HMF) that are mainly associated to the formation of side-products, as humins and other insoluble polymeric condensation by-products. These insoluble by-products cause activity declining and surface deactivation, as they deposit on the catalyst surface. Neither the routes through which humins are formed nor their molecular structure have yet been unequivocally established. Infrared spectroscopic experiments suggest that humins are formed via aldol addition/condensation involving the 2,5-dioxo-6-hydroxy-hexanal (DHH) species. From DHH, humins can grow as it is highly reactive and undergoes aldol addition/condensation with available aldehydes and ketones [19-21]. Both Lewis (LAS) and Brönsted (BAS) acid sites are involved in the mechanism of humin formation, and it seems that the strong acid site density of niobic acid is responsible for the fast decrease of activity observed [14, 22]. In order to decrease the acid site density of the catalyst surfaces and to enhance the catalyst stability, supported or dispersed niobic acid on/in high surface area oxides have been already developed [11, 23, 24].Good catalyst stability during long-term activity in the fructose dehydration has been observed on niobia deposited on silica [23]; unfortunately, fructose conversion was low likely due to the chemical inertness of silica. The choice of a more adequate support for niobia could improve catalyst activity in sugar dehydration reactions.

Moreover, the choice of the reaction solvent for the acid-catalyzed conversion of carbohydrate biomass is of high importance because it is

desirable that the formed by-products are soluble, to improve the catalyst stability and durability. If water is the most frequently used solvent, due to its excellent substrate solubilization properties and to low cost, other friendly solvents are searched for improving the catalyst stability, in particular. Many different liquid solvents have been investigated as reaction medium instead of pure water, such as ionic liquid solvents [25], organic solvents [26, 27] and water/organic solvent biphasic systems [28, 29]. Different anhydrous solvents such as toluene [3], DMSO [1], methyl isobutyl ketone (MIBK) [30], or cyclopentyl methyl ether (CPME) [28] have been used as extracting solvent leading to furfural yields generally higher than the use of water. The use of solvents in homogeneous aqueous solution, such as water/1-butanol system, has been also suggested in different carbohydrate dehydration reactions in order to improve the selectivity towards the target product [2, 27, 31].

Therefore, the present study continues our investigation on hydrated niobium pentoxide and niobia-based catalysts in connection with the most exhaustive research of adequate monophase or biphase systems to minimize catalyst deactivation and increase catalyst stability and durability. Furthermore, silica-zirconia supporting niobia samples prepared by impregnation or sol-gel process, respectively, in comparison with pure NBO, are here presented for xylose dehydration studied at different temperatures (130-180°C) in batch and fixed bed continuous reactors (to approach pilot plan conditions) using various solvents, to point out catalyst performances and limitations.

2. Experimental

2.1. Materials

D-(+)-Xylose (≥99%), anhydrous cyclopentyl methyl ether (CPME) (≥ 99.9%), octanoic acid (98%),γ-valerolactone(99%), 2-propanol (≥99.5%), 1-propanol (≥99.5%), niobium(V) ethoxide ($Nb(OCH_2CH_3)_5$, 99.95%, NBE), 2-phenylethylamine (PEA), and hydrochloric acid (37%) were purchased from Sigma- Aldrich. Ammonium hydroxide (NH_4OH) solution (purum, ~28% in water) was purchased from Fluka. Both hydrated niobium oxide (NBO) in pellets (with graphite) and in powder form and ammonium niobium oxalate complex ($NH_4[NbO(C_2O_{4)2}(H_2O)]\cdot(H_2O)_m$, ANBO) were kindly furnished from Companhia Brasileira de Metalurgia e Mineraçao (CBMM, Brazil). Silica-zirconia (5 wt.% ZrO_2)was supplied from Grace Company.

All the materials were used without further purification. Milli-Q H_2O was used for preparation of all aqueous solutions.

2.2. Catalyst preparation and characterization

Silica-zirconia (SZ) has been utilized as support of the NbO_x active phase, that has been deposited at 10 wt.% of Nb by classical wetness impregnation (Nb/SZ_i) and by a *sol-gel* like method (Nb/SZ_{sg}) modifying the procedures described in Ref. 32. Ammonium niobium oxalate complex ($NH_4[NbO(C_2O_{4)2}(H_2O)]\cdot(H_2O)_m$(ANBO) and niobium (V) ethoxide ($Nb(OCH_2CH_3)_5$ (NBE) were used as Nb sources, respectively.

For Nb/SZ_i preparation, a finite amount of SZ (ca. 15 g) was first dried at 120ºC for 4 hours. The adequate amount of ANBO was dissolved in ca. 70

mL of water and it was added to SZ. The aqueous suspension of SZ in the presence of ANBO was kept overnight under vigorous stirring at room temperature. After 16 h of contact, water was mild evaporated in a rotavapor under vacuum between 40-50ºC for 5 hours and eventually the solid obtained was dried in the oven at 120ºC overnight and calcined at 550ºC for 8 hours.

For Nb/SZ_{sg} preparation, ca. 18 g of SZ was first dried at 120°C for 4 h, then an amount of ca. 80 mL of 1-propanol was added under stirring, afterwards several drops of HCl 37% were added to the suspension (pH 1-2). After ca. 2 h, NBE (5 mL dissolved in ca. 10 mL of 1-propanol) was added to the slurry keeping it under stirring for other 2 hours. Then, ammonium hydroxide (NH_4OH) solution (~20 mL) was added dropwise to obtain gelation. The unripe solid was aged at room temperature two nights, then it was dried in a rotavapor at r.t. for several hours, to eliminate the excess of propanol and dried at 120ºC overnight. Eventually, the solid was calcined at 550ºC for 8 hours.

Thermal gravimetric analyses (TGA) were performed on the dried samples in a TGA analyzer from PerkinElmer (TGA7), with a scan of 10 $ºC \cdot min^{-1}$, from 25 to 800ºC under flowing air. For better evidencing of the thermal events, differential thermogravimetric curves (DTGA) were also calculated from the parent TGA profiles.

Microstructure analysis of the samples have been determined by adsorption and desorption of nitrogen at -196°C (Sorptomatic 1900 instrument) and successive numerical interpretation of the collected isotherms by BET and BJH models for the specific surface area and pore size distribution, respectively. Prior to measurement, the sample (ca. 0.1-0.3 g) crushed and sieved as 45-60 mesh particles was introduced in the sample holder and thermally activated at 350ºC for 16 h under vacuum.

Powder X-ray diffraction (XRD) patterns were recorded in the 15–80° 2θ range in scan mode (0.02° step, 1 s) using a X'Pert Pro PANalytical diffractometer with CuK_α radiation of 0.154046 nm. Diffractograms were analyzed with the X'Pert High Score Plus software.

Scanning electron micrographs (SEM) were collected by a LEO-1430 coupled with energy-dispersive X-ray spectroscopy (EDX) working with an accelerating voltage of 20 kV.

The acid titrations with PEA have been carried out at 30°C in a recirculation chromatographic line (HPLC), comprising a pump (Waters 515) and a monochromatic UV detector (Waters, model 2487, λ = 254 nm) [23]. Successive dosed amounts of PEA solution in cyclohexane or in water were injected into the line in which cyclohexane or water continuously circulated. The attainment of the adsorption equilibrium was revealed by the attainment of stable UV-detector signal. The sample (ca. 0.1 g crushed and sieved as 80–200 mesh particles) was placed in a sample holder (stainless steel tube, 4 mm i.d. and 8 cm of length) between two sand pillows. Prior to the measurement, the sample was activated at 350°C for 4 h in flowing air (8 mL min-1) and then filled with the liquid.

After the collection of the first adsorption isotherm of PEA on the fresh sample (I run), pure solvent was allowed to flow for 30 min through the PEA-saturated sample and then a new adsorption of PEA was repeated (II run). The collected isotherms were interpreted following Langmuir equation (equation 7.1):

$$\mathbf{PEA_{ads} / PEA_{ads,max} = b_{ads}\,[PEA]_{eq} /(1+ b_{ads}\,[PEA]_{eq})} \quad \textit{Equation 7.1}$$

Where b_{ads} is the adsorption constant. From the conventional linearized equation, reporting $[PEA]_{eq}/PEA_{ads}$ *vs.* $[PEA]_{eq}$, the values of $PEA_{ads,max}$ could be obtained. Assuming a 1:1 stoichiometry for the PEA adsorption on the acid site, the value of $PEA_{ads,max}$ obtained from the I run isotherm corresponded to the number of total acidic sites, while, the value of $PEA_{ads,max}$ obtained from the II run isotherm corresponded to the number of weak acidic sites. The number of strong acid sites was obtained as the difference between the number of total and of weak sites.

2.3. Catalytic tests of xylose dehydration

2.3.1 Catalytic tests of xylose dehydration with different solvents

All catalysts were tested in the dehydration of xylose to furfural in batch conditions with the different selected reaction solvents at lower (130°C) and higher (160-180°C) temperature.

Screening tests in different solvents were performed in a magnetically stirred (1500 rpm) Ace sealed pressure glass reactor (15 mL of volume) placed in a preheated oil bath at 130°C for 6 h. Typical conditions used were: 4.5 wt.% of xylose and 3wt.% of powder catalyst (catalyst/xylose wt. ratio, 0.67). The mass ratios of the solvents used were: for the biphasic water/CPME system, 3:7, for the monophasic water/γ-valerolactone, 1:9, and water/isopropanol (20%v/v), 8:2.

Kinetic tests in water/γ-valerolactone at 160°C and in water/CPME at 180°C were carried out, with different amounts of catalyst and xylose respect to those used for the screening tests, following the reaction for 4 h.

The reaction started when the charged reactor was immersed in the oil bath (130°C) and stopped by removing the reactor from the oil bath and rapidly cooled down by immersion in water at room temperature. Then, in case of biphasic systems, internal standards for organic phase (octanoic acid) and for aqueous phase (D (+)-glucose) were added to the quenched reaction mixture and after gently agitation for several minutes, ca. 2 mL aliquot was taken from the each phase for the analysis after filtration (polyethersulfone Millipore filter 0.22 μm).

Aqueous aliquots were analyzed with a HPLC Agilent 1200 series chromatograph equipped with a refraction index (RI) detector and a Bio-Rad Aminex HPX-87H column (300x7.8 mm) for analysis of xylose and furfural in aqueous phase. A 0.005 M H_2SO_4 mobile phase was employed as eluent with 0.4 mL/min flow rate and at 55°C. In the case of organic aliquots, analysis of furfural in this phase was conducted by gas chromatography (CG) (Varian CP-3800) equipped with a ZBWAX plus column (30mx0.32mmx0.25um) and a flame ionization detector (FID).

2.3.2 Catalyst stability tests

Recycling experiments of the catalysts were performed in a 100 mL Parr stainless steel reactor mechanically stirred at high temperature (180°C) in water/CPME, 3:7 mass ratio, and 10 wt.% of xylose and 5 wt.% of catalyst. The reactor was first loaded with xylose and catalyst powder and the corresponding amount of solvent. After purging with N_2, the reactor was pressurized (500 kPa) and temperature increased to reach 180°C without stirring. Once reached the stable reaction temperature, the mixture started reacting by stirring at 1000 rpm

(zero time). The reaction was halted by stopping stirring and then the reactor was quenched to room temperature. The solution was taken out from the reactor and internal standards for aqueous and organic phase were added as above described before the analysis.

After the first reaction cycle, the catalyst inside the reactor was washed several times with the reaction solvent to eliminate the rests of xylose and organics weakly retained by the solid; the liquid was then removed from the reactor and the catalyst was left inside the reactor to dry for the next run.

Catalyst stability tests for long times on stream (up to 100 h) in water and water/isopropanol solution (20% v/v isopropanol) were carried out in a continuous reaction line equipped with a tubular catalytic reactor and a dosing pump (HPLC pump, Waters 501). The reactor and pre-heater were assembled in an oven with forced circulation of hot air in order to keep a constant temperature (130°C).The catalyst sample (1g), previously sieved to 25÷45 mesh, was held in the middle of the reactor, between two sands beds (0.5 grams, 45÷60 mesh). The aqueous xylose solution (ca. 0.3M) was continuously fed into the catalytic bed reactor. The feed flow rate was kept constant at 0.1 $mL \cdot min^{-1}$ obtaining a contact time of 10 min $g \cdot mL^{-1}$. After starting the reaction, at least 100 mL of solution was left to flow before collecting samples for the analysis, so ensuring the stationary conditions to be obtained. The pressure in the reactor was kept between 10^3 and 2 10^3 kPa by means of a micrometric valve at the end of the reaction line. The products were analyzed in a liquid-chromatography apparatus (HPLC), consisting of a manual injector (Waters U6K), pump (water 510), heater (Water CHM) for the column and refractive index detector (Waters 410). A sugar Pack I column operating at 90ºC and eluted with an aqueous solution of Ca-EDTA (10^{-4} M) was used.

3. Results and discussion

3.1. Characterization of materials

The two catalysts prepared by deposition of niobia over silica-zirconia (Nb/SZ_i andNb/SZ_{sg}) were prepared starting from two different Nb precursors (ANBO and NBE) and employing two different preparation routes (impregnation and sol-gel, respectively). In both cases, calcination at 550°C ensured the formation of a oxide sample. The calcination temperature was chosen based on the results obtained from the thermogravimetric analysis performed on the dried samples (see Figure 7S1 in Supplementary Information section at the end of this chapter). Both the thermograms show at about 100°C losses of mass associated to the physical desorption of water. The most intense losses of mass centered around 250-300ºC, could be attributed to the decomposition of ANBO and NBE. Quantitative evaluation of the mass losses were in agreement with the calculated amounts of carbon and nitrogen of the Nb-precursor used.

X-ray powder diffraction (P-XRD) of the supported catalysts on SZ support (Nb/SZ_i and Nb/SZ_{sg}) showed an amorphous halo centered at 2θ=22°, typical of amorphous silica, indicating their main amorphous nature. Peaks related to the presence of Nb_2O_5 crystalline aggregates are detectable only for Nb/SZ_i (Figure 7.1). It could be then inferred a higher Nb-dispersion on Nb/SZ_{sg} than on Nb/SZ_i. P-XRD of pure NBO (see Figure 7S3 in Supplementary Information) showed the typical crystalline pattern in which monoclinic H-Nb_2O_5 and T: orthorhombic phases can be distinguished. On Nb/SZ_i catalyst, the SEM-EDX analyses detected surface amounts of Nb_2O_5 of

17 ± 5 wt.% with the different areal zones more or less covered by Nb (see Figure 7S2 in Supplementary Information).

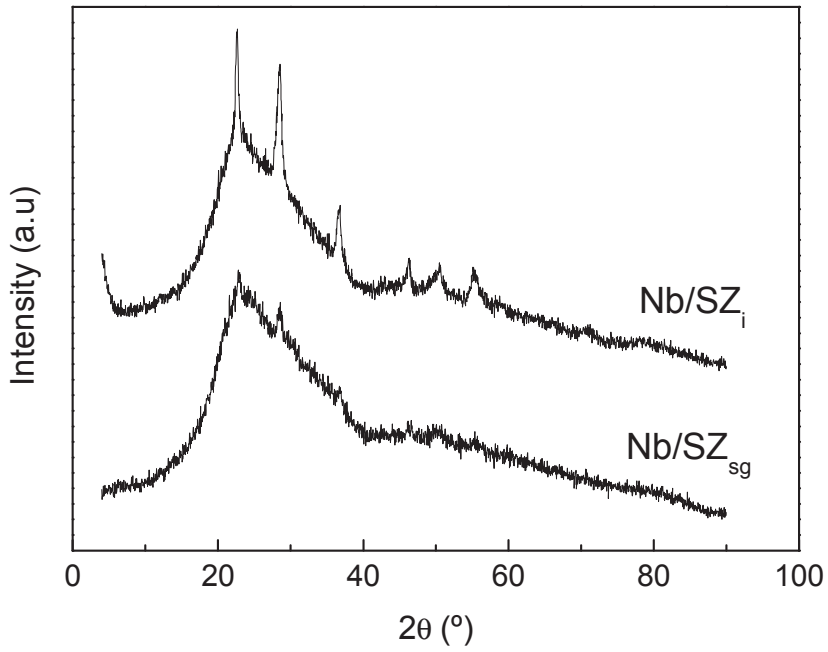

Figure 7.1. P-XRD of Nb/SZ_i and Nb/SZ_{sg} catalysts (P-XRD of NBO is shown in Supporting Information section, Fig. 3S).

The main textural properties of all catalysts and support have been studied. Figure 7.2 shows the N_2 adsorption-desorption isotherms of the two supported Nb-catalysts and bulk Nb_2O_5 (with graphite) and the silica-zirconia support. In Table 7.1, a summary of the main textural properties obtained is reported.SZ support shows type IV isotherm typical of the mesoporous solids: high specific surface area and pore volume with large pore diameter. The N_2

adsorption/desorption isotherms of Nb/SZ_{sg} are also typical of a mesoporous solid. Any significant variation of pore size compared with the SZ support has not been observed, suggesting a uniform Nb-distribution on the support matrix. The same happens with Nb/SZ_i, which has high surface area and pore volume but a significant decrease of pore size compared with SZ. The results suggest that niobium has been deposited at the external and internal surface of SZ. Concerning Nb_2O_5, the results confirm the already reported morphologic features with the presence of pores with small size.

Table 7.1. Main textural properties of the studied samples

Catalyst	BET surface area ($m^2 \cdot g^{-1}$)	Pore volume ($cm^3 \cdot g^{-1}$)	Average pore diameter (nm)
SZ	294	1.79	19.7
Nb/SZ_{sg}	217	1.21	18.1
Nb/SZ_i	262	0.95	13.6
NBO[a]	108	0.52	3.4

[a]niobia in pellets

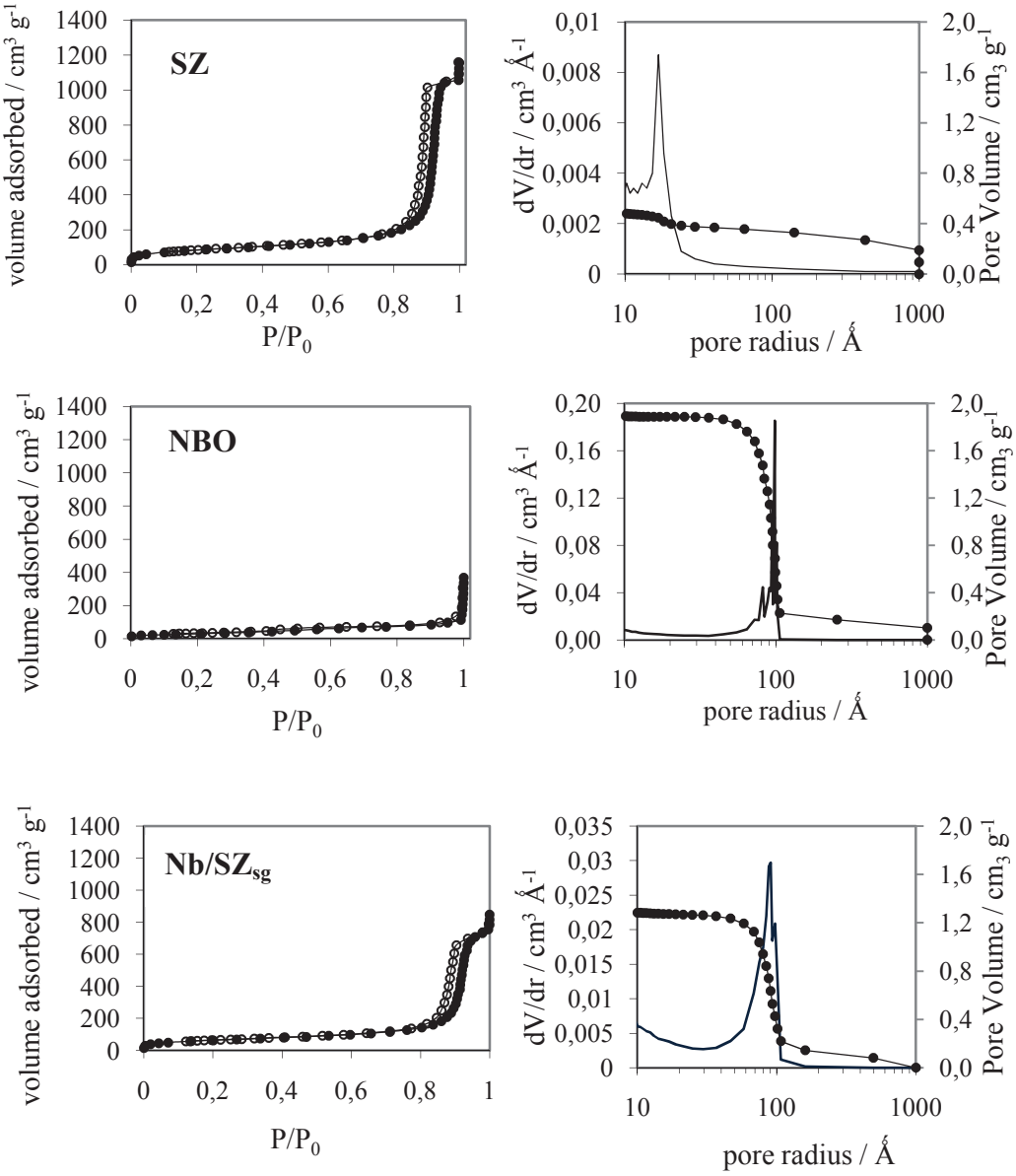

Figure 7.2. N2 adsorption-desorption isotherms (left side) and BJH pore volume distribution (right side) of all the catalysts sample

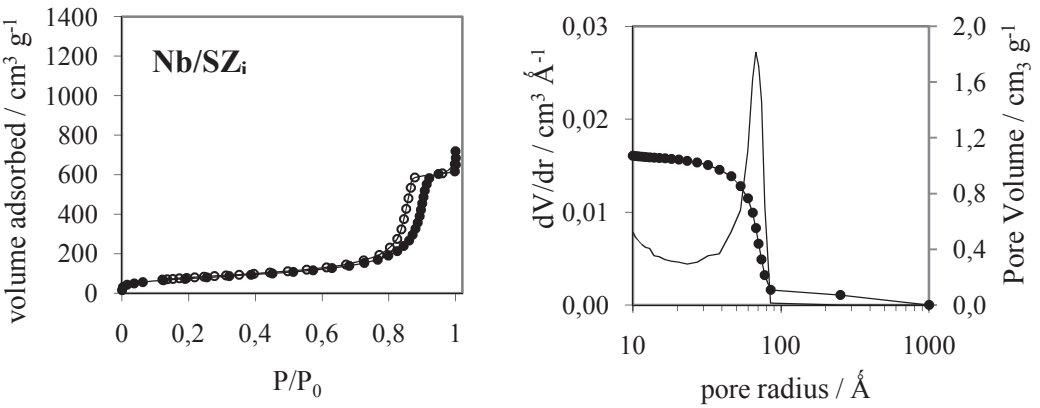

Figure 7.2. N2 adsorption-desorption isotherms (left side) and BJH pore volume distribution (right side) of all the catalysts sample (continuation)

The surface acidity developed by the support and the prepared catalysts is expected to direct the activity and selectivity in the dehydration reaction of xylose. In view of the importance of the acidity of the catalysts manifested in the reaction medium, we have measured the intrinsic and effective acidities [23] of the catalyst samples, by determining the amount and strength of the acid sites. Starting from the determination of the *intrinsic* acidity of the samples, determined in cyclohexane (an aprotic and apolar liquid), we moved to the *effective* acidities determined in water (a protic and polar solvent with high solvating ability). We have chosen water because the reaction takes place in pure water and in some water solutions (with γ-valerolactone and isopropanol). Also when the biphasic system water/CPME has been used, water, which has hydrophilic characteristics, is in contact with the catalyst oxide surfaces.

It is known that water with its polar, protic, and solvating properties can interact with the acid surfaces modifying the number and strength of the acid sites (in general decreasing it). Therefore, a given acid surface can reconstruct

itself in the presence of water. In order to find sound relations between the acid properties of the catalysts and their activity, the knowledge of the effective acidity seems more appropriate.

The *intrinsic* acidity of SZ is very high but only the half of the sites are strong acid sites (Table 7.2 and Figure 7.3). By covering part of SZ support with niobia phase, a decrease of surface acidity of the catalysts (Nb/SZ_{sg} and Nb/SZ_i) has been obtained. This was expected due to the lower surface area values of Nb/SZ compared with the SZ support (Table 7.1). Interestingly, the percent of the strong acid sites of Nb/SZ_{sg} and Nb/SZ_i increases compared with SZ, likely due to the dispersed Nb-centers which can be associated to new LAS sites created on the catalyst surfaces [32].

The determination of the *effective* acidity, measured in water, shows a different *scenario* (Table 7.2 and Figure 7.3). The catalyst prepared by sol-gel (Nb/SZ_{sg}) shows the highest amount of *effective* acid sites and it maintains, ca. 65% of its *intrinsic* acid sites in water. In water, the acidity of SZ deeply decreases as well as the acidity of Nb/SZ_i (only about 35% of acidity is retained in water for both the samples). In general, as known, the acid strength of the *effective* acid sites in water is low, the highest acid strength is associated to Nb/SZ_{sg} surface (0.042 mequiv/g corresponding to 14% of the titrated acid sites in water).

The acidity determination of NBO confirmed the already known water-tolerant acid properties; ca. 90% of the acid sites titrated in cyclohexane are maintained in water and high percent (66%) of the *effective* acid sites are strong. Considering the lower surface area of NBO than that of Nb/SZ_{sg} and Nb/SZ_i, the acid site density of NBO in water is very higher than that of the Nb/SZ catalysts.

Table 7.2. Summary of the *intrinsic* and *effective* acidities of the samples measured by PEA titration in cyclohexane (I.A.) and water (E.A.), respectively, at 30°C[a].

Catalyst	Intrinsic acidity (meq/g) in cyclohexane				Effective acidity (meq/g) in water			
	Total sites (meq/g)	**Weak sites** (meq/g)	**Strong sites** (meq/g)	**Strong sites (%)**	**Total sites** (meq/g)	**Weak sites** (meq/g)	**Strong sites** (meq/g)	**Strong sites (%)**
SZ	0.76	0.40	0.36	47	0.27	0.26	0.005	2
Nb/SZ_{sg}	0.47	0.16	0.31	66	0.30	0.25	0.042	14
Nb/SZ_{i}	0.59	0.12	0.47	80	0.22	0.20	0.013	6
NBO	0.21	0.07	0.14	66	0.19	0.07	0.12	64

[a]Total acid sites (determined from the I run isotherm), weak acid sites (determined from the II run isotherm) and strong acid sites (determined by difference); see Experimental section.

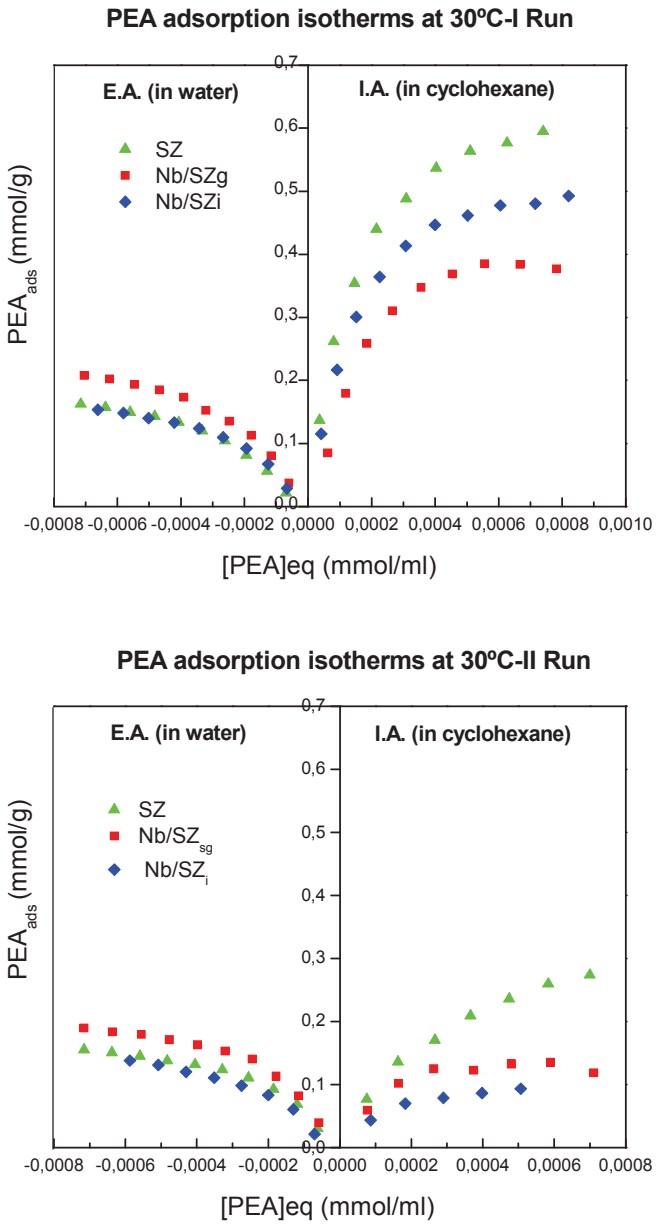

Figure 7.3. ***Intrinsic*** **(in cyclohexane) and** ***effective*** **(in water) acidities of the samples: adsorption isotherms of PEA at 30°C. I° run collected on fresh and activated sample and II° run collected on the previously sample saturated by PEA.**

3.2. Activity of xylose dehydration to furfural

Despite the apparent simplicity of the synthesis of furfural from xylose that consists only in a deep dehydration of the pentose, the reaction catalyzed by solid acids is far to be simple. Studies from literature have demonstrated that xylulose is a key intermediate that is formed from the xylose isomerization, by the catalytic action of LAS, and then it is dehydrated to furfural by BAS action [10]. However, excess of LAS on the catalyst surface causes side reactions to produce humins that decrease the furfural selectivity and yield and cause catalyst deactivation.

It has been previously demonstrated that [23, 33] that dispersed niobia systems on silica are more stable than bulk niobia in the dehydration of fructose to HMF, but conversion was low due to the inertness of silica surface. Taking into account these findings, for the xylose dehydration we have studied acid solid catalysts consisting of dispersed niobia phase onto an acidic oxide support. These systems might guarantee a convenient amount of acid sites with a balanced concentration of LAS and BAS sites [33, 34] for a high xylose conversion and its selectivity transformation to furfural, according with the mechanistic findings of the literature [10].

3.2.1 Catalytic tests of xylose dehydration at low temperatures with different solvents

First of all, all the catalysts were tested in batch experiments for dehydration of xylose to furfural in different reaction solvents at low temperature (130ºC). Besides water, a biphasic system, water/CPME, and two

aqueous solutions, water/γ-valerolatone and water/isopropanol, were employed. The goodness of CPME, a highly hydrophobic ether, as green solvent for carbohydrate biomass conversion has been already recognized [28]. γ-Valerolactone, too, is an interesting solvent as it can be produced from lignocellulose, it has been also used in dehydration of sugars with interesting performances [26, 27, 31, 35]. Also aqueous mixtures containing isopropanol could improve the stability of the catalyst by improving solubility of some of the condensation products formed during the reaction.

Figure 7.4 shows the results of xylose conversion and furfural yield obtained for both NBO and the two supported Nb-catalysts (Nb/SZ_i and Nb/SZ_{sg}). In all the solvents, NBO was more active than the other supported niobia catalysts; this was expected due to the lower amount of niobia on the supported catalysts and to the higher acid site density of NBO in comparison with the diluted Nb/SZ catalysts [23]. However, Nb/SZ_i and Nb/SZ_{sg} show similar catalytic behavior, disregarding the solvent used, it seems that the method of preparation does not have a crucial influence in the final catalytic activity but the solvent nature directs both xylose conversion and yield to furfural obtained. Comparing the results obtained in the different solvents, both xylose conversion and furfural yield are higher than those obtained when pure water was used, for all the catalysts. The biphasic system water/CPME appeared the best solvent by balancing the results obtained in terms of xylose conversion and selectivity. It is also worthy to mention that the supported niobia catalysts show the highest conversion in presence of γ-valerolactone compared with the other solvents.

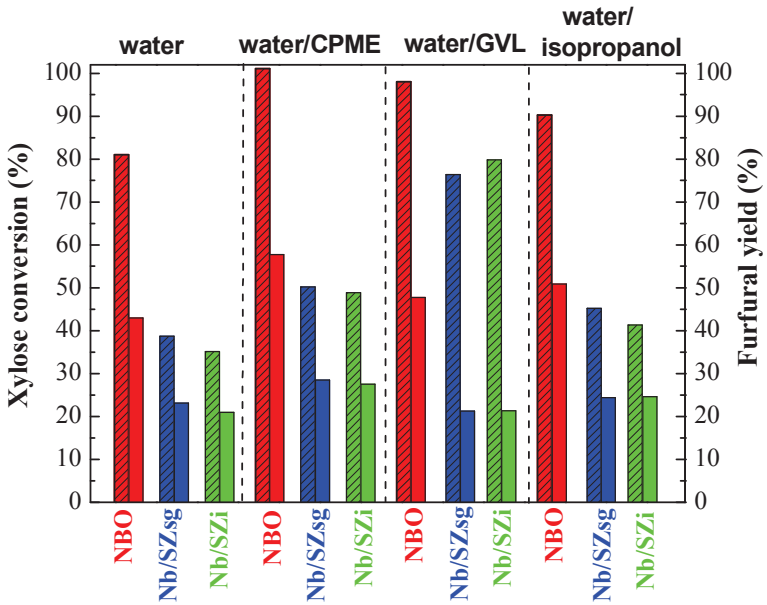

Figure 7.4. Xylose conversion (dashed bars) and furfural yield (filled bars) for the NBO and Nb/SZ catalysts in different reaction solvents. Reaction conditions: batch reactor; 4.5 wt.% xylose, 3 wt.% catalyst; 5 g total solution; γ-valerolactone (GVL)/aqueous mass ratio, 9;CPME/aqueous mass ratio, 2.33; water/isopropanol 20% v/v; reaction temperature, 130ºC; tos, 360 min.

Continuous catalytic tests in a flow fixed bed reactor have been made aimed to study the stability of the catalysts for long time on stream; we have chosen to compare water and isopropanol/water as solvents (Figure 7.5). The continuous tests showed that NBO was more active than the supported niobia catalysts in both the solvents tested, confirming what has been observed in batch reactor tests. Concerning the supported catalysts, even if initially less

active, they are more stable; only a little loss of activity was observed up to 60 h of activity. In addition, the presence of isopropanol in water improved the activity the catalysts, even if a certain degree of activity loss was still present.

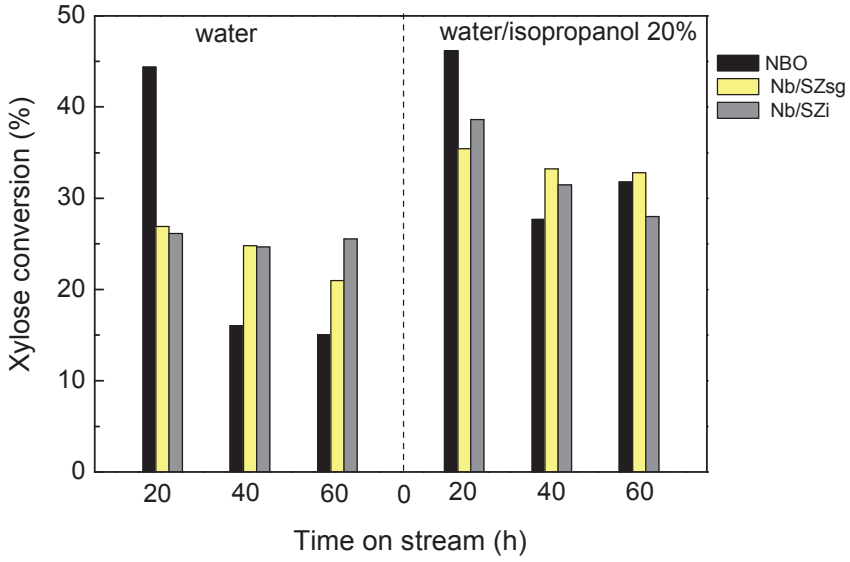

Figure 7.5. Xylose conversion for different time on stream for the NBO and Nb/SZ catalysts. Reaction conditions: fixed bed reactor; 4.5wt.% xylose, 3wt.% catalyst; contact time, 6-10 min·g·mL^{-1}; reaction temperature, 130ºC.

3.2.2. Catalytic tests of xylose dehydration at high temperatures with selected reaction solvents

On the basis of the results obtained from the tests of xylose dehydration at low temperatures (130ºC), emerged that the biphasic system water/CPME and the monophasic γ-valerolatone in mixture with water seemed to be the most

interesting solvents for the studied reaction. The key role of the solvent in the conversion of carbohydrate biomass has been recently pointed out also by Pérez and Fraga [36].Therefore, all the catalysts were tested again in the two selected solvents at higher temperatures (160°C for water/γ-valerolatone and 180ºC for water/CPME) and following the reaction as a function of time.

Figures 7.6 shows the results obtained in γ-valerolactone as solvent and Figure 7.7 those obtained in water/CPME biphasic system, in terms of xylose conversion and furfural yield, in comparison with the blank test carried out without catalyst. The results confirm the ranking of activity observed at low reaction temperature. Moreover, on all the catalysts xylose conversion and furfural yield can be described by increasing curves, suggesting that the activity loss is weak. Moreover, when plotting the selectivity to furfural against xylose conversion, exponential curves could be observed on all the catalysts, indicating that under the used experimental conditions, furfural is a final and stable product of reaction (see Figure 74S in Supplementary Information). The most interesting results (both conversion and furfural yield) have been observed in water/CPME system (Figure 7.7). In this solvent, Nb/SZsg had quite complete xylose conversion while yield to furfural was not higher than 40% after 240 min of reaction, with a poor increasing trend with reaction time. At this high temperature (180°C), resinification reactions could be very fast with high amount of by-product formation.

In water/CPME biphasic system, besides catalytic activity, also the stability of the NBO and Nb/SZ catalysts has been studied by performing recycling experiments at 180°C for various reaction times (60 min, 120 min, and 240 min of reaction time for NBO and 240 min for Nb/SZ catalysts). The

catalytic runs were carried out for short periods of time to facilitate the observation of any activity decline.

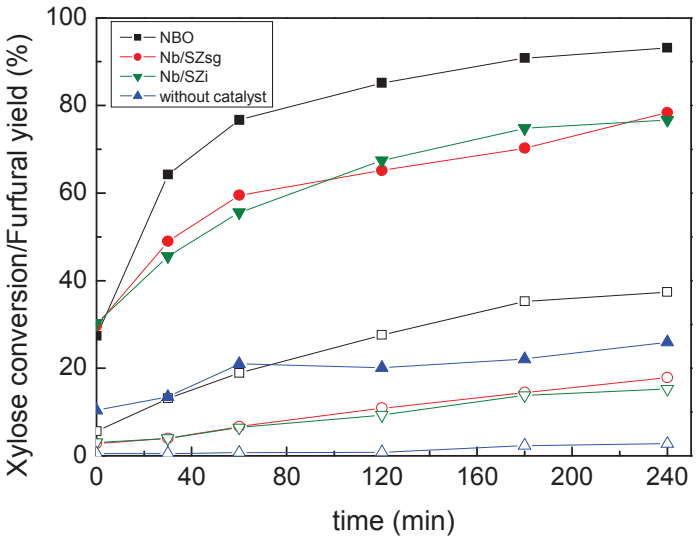

Figure 7.6. Comparison of the xylose conversion (filled markers) and furfural yield (empty markers) with reaction time on NBO and Nb/SZ catalysts and without catalyst (blank test). Reaction conditions: batch reactor; 2 wt.% xylose and 0.2 wt.% of catalyst; γ-valerolactone/aqueous mass ratio, 9; 50 g total solution; reaction temperature,160ºC.

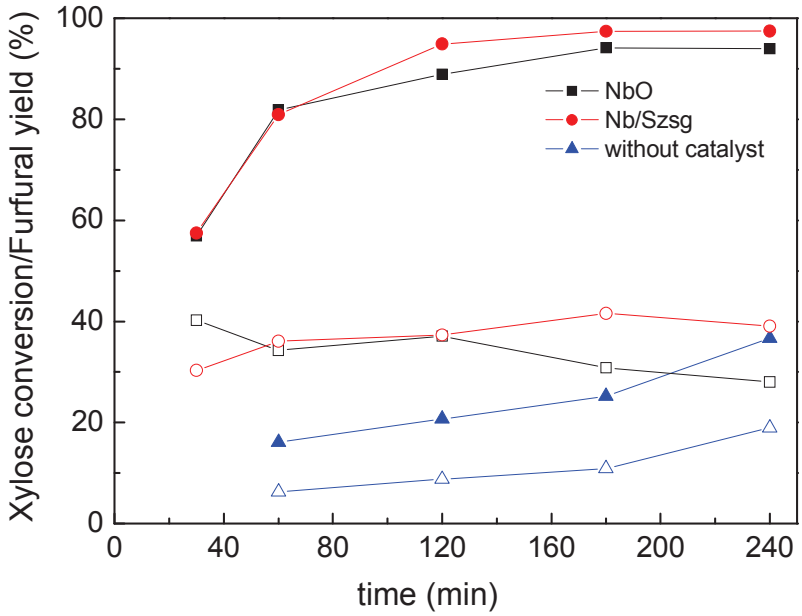

Figure 7.7. Comparison of the xylose conversion (filled markers) and furfural yield (empty markers) for NBO and Nb/SZ_{sg} catalysts and without catalyst (blank test) vs. reaction time. Reaction conditions: 10wt.% of xylose and 5 wt.% of catalyst in the aqueous phase, CPME/aqueous phase mass ratio, 2.33; 50 g total solution; reaction temperature, 180ºC.

Figure 7.8 shows the xylose conversion and furfural yield for several consecutive runs for each catalyst tested. Nb/SZ_{sg} and Nb/SZ_i have a quite stable production of furfural with yield around 45-50% and selectivity of almost 80% after 7 runs, while xylose conversion is roughly constant. This means that the presence of by-products also deposited on the catalyst surface do not

completely deactivate the catalyst surfaces. On the opposite, a regular deactivate trend of xylose conversion was observed on NBO, while once again, furfural yield production is more stable. By increasing the reaction time (recycling tests each 120 min and 240 min), the conversion and furfural yield increased suggesting that the NBO surface is not completely deactivated.

These results may suggest that the selective acid sites for the furfural formation, still lively in water and associated with the dispersed niobia phase, are not deactivated during the course of reaction, while the rest of the acid surface is mainly involved in the unselective conversion of xylose. Concerning the role of the reaction solvent, it clearly appears that water and water solutions can modulate the catalyst acidity decreasing the acid site density of the surfaces. This leads to a positive effect on the catalyst stability.

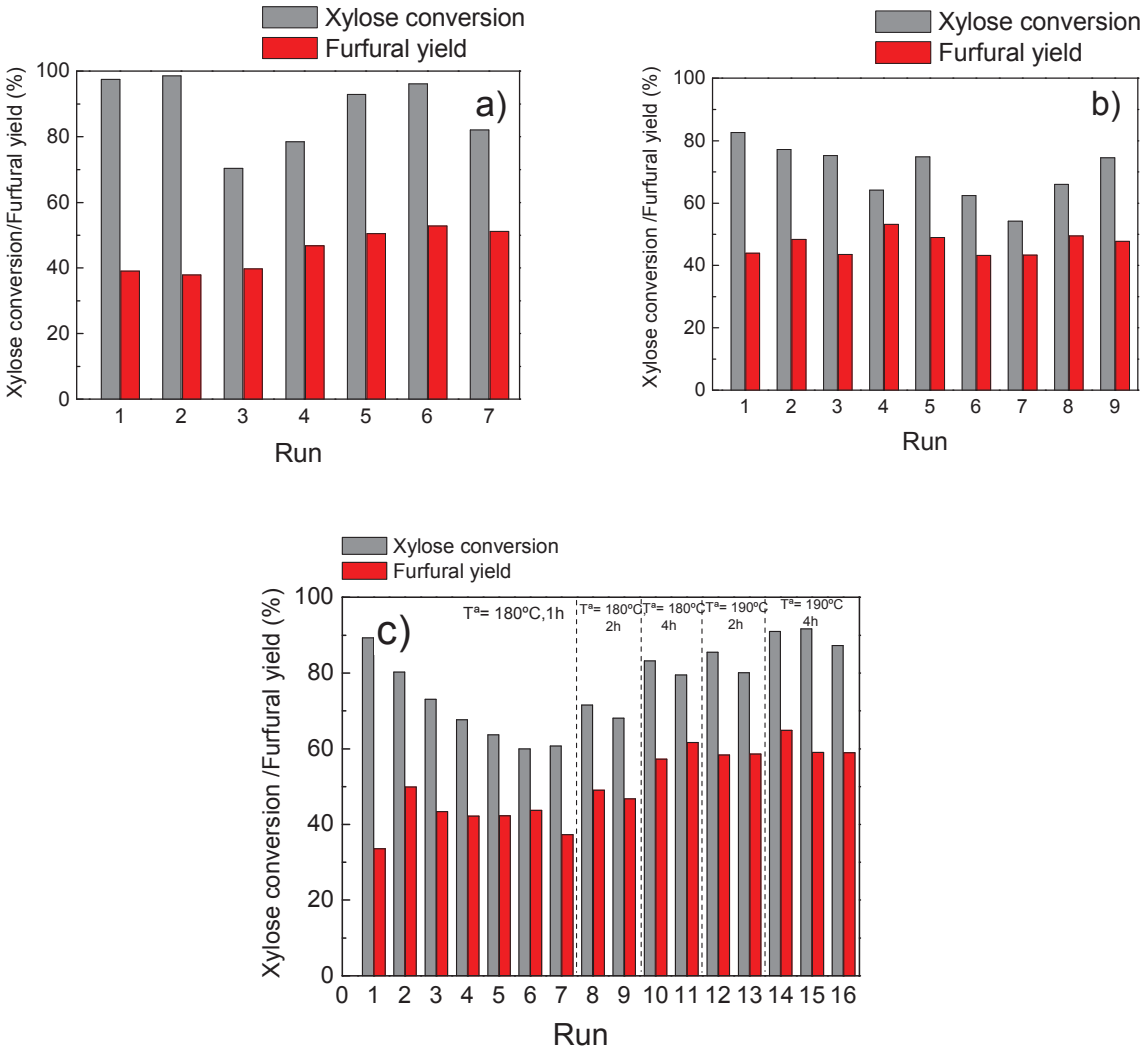

Figure 7.8. Recycling tests on NBO and Nb/SZ catalysts: a) Nb/SZ$_{sg}$, b)Nb/SZ$_{i}$,c) NBO. Reaction conditions: 10wt.% xylose and 5 wt.% catalyst in the aqueous phase, CPME/ aqueous phase mass ratio, 2.33; 50 g total solution, reaction temperature, 180°C, time of reaction, 240 min for the supported catalysts.

4. Conclusions

In this chapter, we have shown that niobia phase dispersed over an acid oxide support, like silica-zirconia, is effective for the acid conversion of xylose to furfural, due to the *water-tolerant* acid properties of the niobia phase, as proved by our acidity measurements carried out in water.

The niobia supported catalysts have lower activity than bulk niobia but higher stability during the reaction course, as proved by the recycling tests and continuous catalytic tests. The catalyst with the highest niobia dispersion (prepared by *sol-gel*) showed the most interesting performances, which can be associated with the highest amount of strong *effective* acid sites. Moreover, a crucial role of the reaction solvent has been enlightened; the wise choice of solvent prevents a severe catalyst deactivation and maintains the selective conversion of xylose to furfural. By using a biphasic system, it is possible extracting the final furfural product from aqueous phase and avoid side-reactions or/and lowering the formation of humins. It is also worth noticing that by using aqueous solutions (with alcohol or lactone), catalyst stability improves thanks to an increase of solubility of the formed humins, so avoiding that they can deposit on the catalyst surface and deactivate it.

A future activity could be directed towards the development of an optimized catalyst *plus* solvent system, in which there is a suitable ratio of Lewis and Brönsted acid sites on the catalyst surface and more solubility of the formed by-products. These are the two key factors to obtain a successful catalytic process in the sugar conversion.

5. Supplementary Information

This supported information includes: thermogravimetric profiles of the dried catalysts (Nb/SZ) (Figure 7S1); SEM image of Nb/SZi showing a morphology characterized by polyhedra of irregular shape (Figure 7S2); XRD patterns of fresh Nb_2O_5 (Figure 7S3) and trend of the selectivity to furfural vs. xylose conversion on the different Nb-catalysts in reaction carried out in γ-valerolactone:water monophasic system at 160°C in the batch reactor (Figure 7S4).

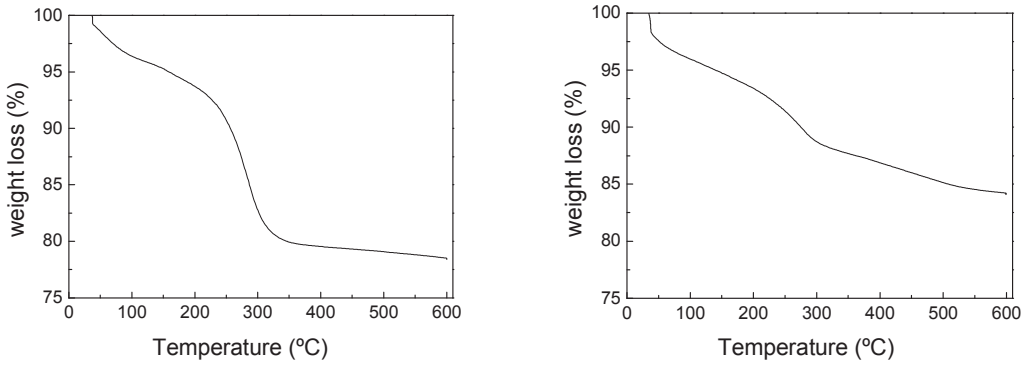

Figure 7S1.Thermogravimetric profiles of the dried catalysts prepared by impregnation, Nb/SZ_i (left side) and sol-gel Nb/SZ_{sg} (right side) method.

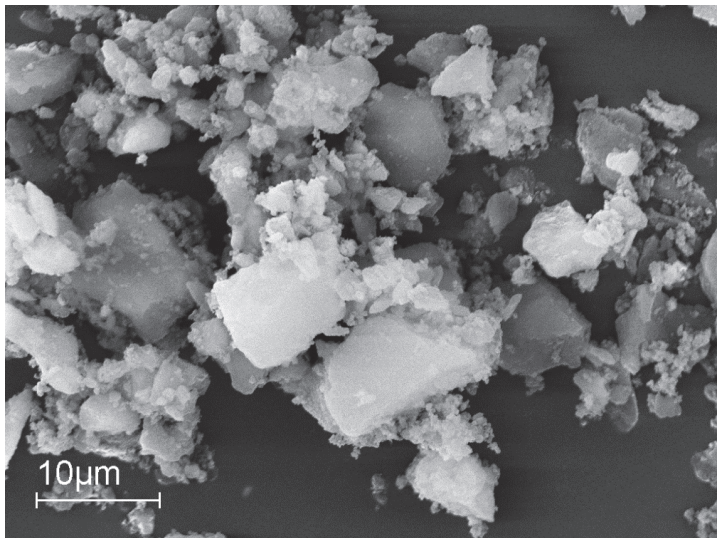

Figure 7S2.SEM image of Nb/SZ_i

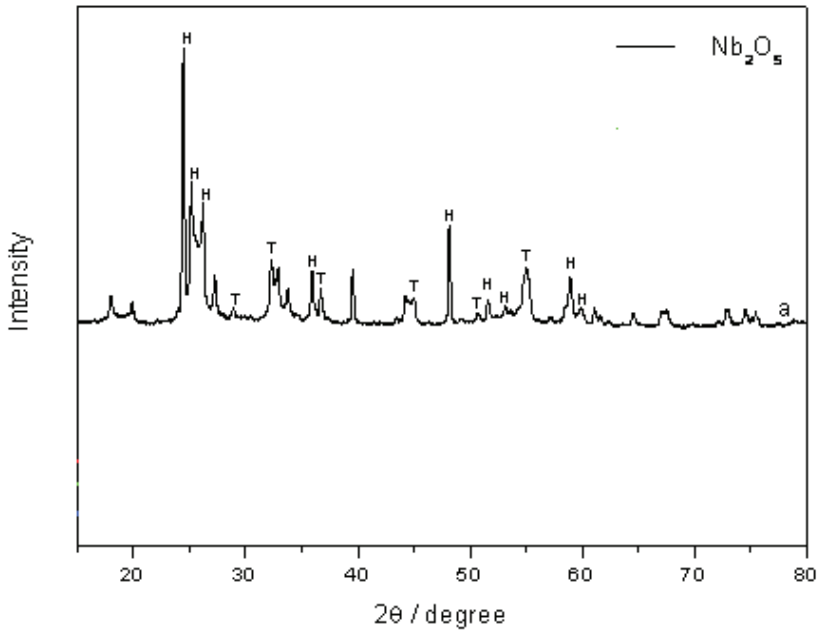

Figure 7S3. XRD patterns of Nb_2O_5 (H: monoclinic H-Nb_2O_5, T:orthorhombic T-Nb_2O_5).

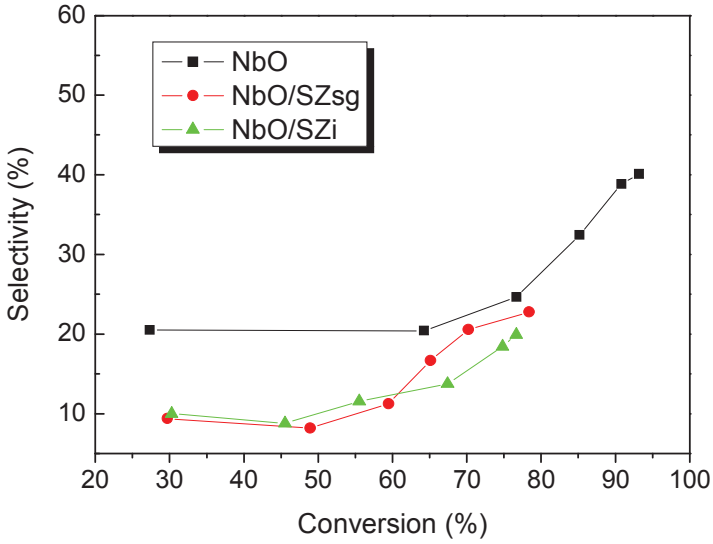

Figure 7S4. Selectivity to furfural *vs.* xylose conversion on different Nbcatalysts. Reaction conditions: batch reactor; 2 wt.% xylose and 0.2 wt.% of catalyst; γ-valerolactone:water, 9; total solution, 50 g; reaction temperature, 160ºC.

6. Bibliography

[1] A.S. Dias, M. Pillinger, A.A. Valente, Journal of Catalysis, 229 (2005) 414-423.
[2] J. Zhang, J. Zhuang, L. Lin, S. Liu, Z. Zhang, Biomass and Bioenergy, 39 (2012) 73.
[3] S. Lima, A. Fernandes, M.M. Antunes, M. Pillinger, F. Ribeiro, A.A. Valente, Catalysis Letters, 135 (2010) 41-47.
[4] X. Wang, S. Cheng, J.C.C. Chan, Journal of Physical Chemistry C, 111 (2007) 2156-2164.
[5] M.L. Granados, A.C. Alba-Rubio, I. Sádaba, R. Mariscal, I. Mateos-Aparicio, A. Heras, Green Chemistry, 13 (2011) 3203-3212.
[6] I. Sádaba, S. Lima, A.A. Valente, M. López Granados, Carbohydrate Research, 346 (2011) 2785.
[7] I. Sádaba, M. Ojeda, R. Mariscal, R. Richards, M.L. Granados, Catalysis Today, 167 (2010) 77-83.
[8] I. Agirrezabal-Telleria, J. Requies, M.B. Güemez, P.L. Arias, Applied Catalysis B: Environmental, 115-116 (2011) 169-178.
[9] P. Carniti, A. Gervasini, S. Biella, A. Auroux, Catalysis Today, 118 (2006) 373-378.
[10] B. Pholjaroen, N. Li, Z. Wang, A. Wang, T. Zhang, Journal of Energy Chemistry, 22 (2013) 826-832.
[11] C. García-Sancho, J.M. Rubio-Caballero, J.M. Mérida-Robles, R. Moreno-Tost, J. Santamaría-González, P. Maireles-Torres, Catalysis Today,152-153 (2014)1-10.
[12] T. Okuhara, Chemical Reviews, 102 (2002) 3641-3666.
[13] V.S. Braga, I.C.L. Barros, F.A.C. Garcia, S.C.L. Dias, J.A. Dias, Catalysis Today, 133-135 (2008) 106-112.
[14] K. Tanabe, Catalysis Today, 78 (2003) 65-67.
[15] I. Nowak, M. Ziolek, Chemical Reviews, 99 (1999) 3603-3624.
[16] K. Nakajima, Y. Baba, R. Noma, M. Kitano, J. N. Kondo, S. Hayashi, M. Hara, Journal of the American Chemical Society, 133 (2011) 4224-4227.
[17] C. Carlini, M. Giuttari, A.M.R. Galletti, G. Sbrana, T. Armaroli, G. Busca, Applied Catalysis A: General, 183 (1999) 295-302.
[18] F. Yang, Q. Liu, X. Bai, Y. Du, Bioresource Technology, 102 (2011) 3424-3429.
[19] S.K.R. Patil, C.R.F. Lund, Energy and Fuels, 25 (2011) 4745-4755.

[20] S.K.R. Patil, J. Heltzel, C.R.F. Lund, Energy and Fuels, 26 (2012) 5281-5293.
[21] I. Van Zandvoort, Y. Wang, C.B. Rasrendra, E.R.H. Van Eck, P.C.A. Bruijnincx, H.J. Heeres, B.M. Weckhuysen, ChemSusChem, 6 (2013) 1745-1758.
[22] M. Marzo, A. Gervasini, P. Carniti, Catalysis Today, 192 (2012) 89-95.
[23] P. Carniti, A. Gervasini, M. Marzo, Catalysis Today, 152 (2010) 42-47.
[24] C. García-Sancho, I. Agirrezabal-Telleria, M.B. Güemez, P. Maireles-Torres, Applied Catalysis B: Environmental, 152-153 (2014) 1-10.
[25] C. Sievers, I. Musin, T. Marzialetti, M.B.V. Olarte, P.K. Agrawal, C.W. Jones, ChemSusChem, 2 (2009) 665-671.
[26] L. Zhang, H. Yu, P. Wang, Y. Li, Bioresource Technology, 151 (2014) 355-360.
[27] E.I. Gürbüz, J.M.R. Gallo, D.M. Alonso, S.G. Wettstein, W.Y. Lim, J.A. Dumesic, Angewandte Chemie - International Edition, 52 (2013) 1270-1274.
[28] M.J. Campos Molina, R. Mariscal, M. Ojeda, M. López Granados, Bioresource Technology, 126 (2012) 321-327.
[29] R. Xing, W. Qi, G.W. Huber, Energy and Environmental Science, 4 (2011) 2193-2205.
[30] R. Weingarten, J. Cho, W.C. Conner Jr, G.W. Huber, Green Chemistry, 12 (2010) 1423-1429.
[31] D.M. Alonso, S.G. Wettstein, M.A. Mellmer, E.I. Gurbuz, J.A. Dumesic, Energy and Environmental Science, 6 (2012) 76-80.
[32] T. Onfroy, G. Clet, M. Houalla, Journal of Physical Chemistry B, 109 (2005) 14588-14594.
[33] P. Carniti, A. Gervasini, M. Marzo, Journal of Physical Chemistry C, 112 (2008) 14064-14074.
[34] A. Gervasini, C. Messi, D. Flahaut, C. Guimon, Applied Catalysis A: General, 367 (2009) 113-121.
[35] D.M. Alonso, J.M.R. Gallo, M.A. Mellmer, S.G. Wettstein, J.A. Dumesic, Catalysis Science and Technology, 3 (2012) 927-931.
[36] R.F. Perez, M.A. Fraga, Green Chemistry, 16 (2014) 3942-3950.

8. CONCLUSIONS

In the present manuscript a thorough study of the catalytic behavior of different catalysts used in the dehydration reaction of xylose to furfural has been carried out. Besides, the application of some of the prepared catalysts in the esterification reaction of free fatty acid to biodiesel has also carried out. Both reactions are of great interest in the context of biorefineries, allowing the development of new process to obtain chemicals and fuels based on renewable resources instead of fossil feedstock.

Despite the fact that in each chapter the particular conclusions have been explained, in this section a compilation of the **main general conclusions** deduced from the results described and discussed in this PhD dissertation are listed:

- First of all, concerning results package 1, devoted to the research on the dehydration of lignocellulosic biomass to furfural through homogeneous catalysis, it must be stressed that CPME was found to be a green solvent that allows the selective conversion of lignocellulosic pentoses into furfural using H_2SO_4 as acid catalyst (up to 100%). However, the presence of CPME did not have any effect on cellulose hydrolysis to glucose and its subsequent dehydration products. Furthermore, the addition of NaCl to the reaction medium combined with the effect of the solvent was found to accelerate notably the reaction rate of furfural formation from hemicellulosic pentoses.

- Regarding the second results package devoted to the research of solid acid catalysts which are active and stable in dehydration xylose to furfural, catalysts based on sulfonic acid polystyrene (silica-poly(styrene

sulphonic acid) nanocomposites) were prepared and tested in this reaction. Two different variable of synthesis were studied: synthesis temperature and initial S/N ratio. Besides, an exhaustive characterization of the fresh and used catalysts was carried out in order to unveil the composition of the catalysts and correlate it with the catalytic performance, especially during reutilisation. It was found that all these catalysts were active in xylose dehydration but they deactivate during the reutilisation cycles regardless of the synthesis temperature and the S/N at. ratio used in the synthesis, being the leaching of the polymer the primary cause of deactivation during the intense reaction conditions used in this reaction. However, an optimum synthesis temperature of 348 K and an initial S/N ratio between 4 and 8 was recommended.

Following in this package of results, the nanocomposites were also tested in esterification reaction of oleic acid to biodiesel and it was found that they were active and stable catalysts under the less severe conditions of this reaction. The leaching of the polymer was very limited and the catalyst deactivation could be caused by the deposition of hydrocarbonaceous residues but not by the loss of polymer during reaction.

- Finally, niobium based catalysts were also tested in xylose dehydration reaction to furfural and two different supported niobium catalysts over an oxide support (SZ) were synthesized through a sol-gel and impregnation methodology, respectively. It was found that both catalysts had lower activity than bulk niobia but higher stability during

the reaction course due to the water tolerant properties of the niobia phase. Additionally, the effect of the presence of a solvent different to water (in a biphasic or monophasic system) resulted in an improvement of both the activity and stability of the catalysts thanks to the increase of solubility of the formed solid humins that can deposit over catalyst surface and deactivate it.

PUBLICACIONES DERIVADAS DE LAS INVESTIGACIONES DE LA TESIS DOCTORAL

[1] **M.J. Campos**. R. Mariscal, M. Ojeda, M.L. Granados. Cyclopentyl methyl ether: a green co-solvent for the selective dehydration of lignocellulosic pentoses to furfural. *Bioresource Technology*, 126 (2012), 321-327. (DOI:10.1016/j.biortech.2012.09.049).

[2] **M.J. Campos**, R. Mariscal, M.L. Granados. Silica-poly(styrenesulphonic acid) nanocomposites as acid catalysts: effects of temperature and polymer concentration on their textural and chemical properties. *Enviada a Journal of Sol-Gel Science and Technology.*

[3] **M.J. Campos**, R. Mariscal, M.L. Granados. Silica-poly(styrenesulphonic acid) nanocomposites as promising acid catalysts. *Enviada a Polymer Composites.*

[4] **M.J. Campos**, M.L Granados, A. Gervasini, P. Carniti. Exploitment of niobium oxide effective acidity for xylose dehydration to furfural. *Aceptada para su publicación en Catalysis Today.*

OTRAS PUBLICACIONES DEL DOCTORANDO

[1] **M.J. Campos**, J.M. Rubio, M.C.G. Albuquerque, D.C.S Azevedo, C.L. Cavalcante, R. Moreno-Tost, J. Santamaría, J.M Mérida, P.J. Maireles. Base Catalysts Derived from Hydrocalumite for the Transesterification of Sunflower Oil. *Energy and Fuels* 2 (2010),979-984. (DOI: 10.1021/ef9009394).

CURRICULUM VITAE

Maria José Campos Molina obtuvo el título de Ingeniera Química por la Universidad de Málaga en el año 2008. Dos años más tarde consiguió una beca predoctoral FPI del Ministerio de Economía y Competitividad (MINECO) que le permitió iniciar su carrera investigadora en el Instituto de Catálisis y Petroleoquímica (CSIC) bajo la dirección del Dr. Manuel López Granados. En 2010 presentó y aprobó el trabajo de Iniciación a la Investigación (antiguo Diploma de Estudios Avanzados) en la Universidad Autónoma de Madrid en el Departamento de Química Física Aplicada y dentro del programa de doctorado en Química: Ciencia Interdisciplinar. En el año 2013, realizó una estancia predoctoral en la Universidad Degli Studi de Milán de 3 meses de duración bajo la supervisión del Profesor Paolo Carniti y la Profesora Antonella Gervasini.

Es coautora de 5 publicaciones científicas (4 derivadas de esta tesis doctoral), de las cuales 3 están publicadas en revistas SCI, y las otras 2 enviadas para su publicación próximamente.